
Plasma-assisted deposition of vegetable oil-based coatings for paper hydrophobization



TECHNISCHE
UNIVERSITÄT
DARMSTADT

Vom Fachbereich Chemie
der Technischen Universität Darmstadt

zur Erlangung des Grades

Doctor rerum naturalium

(Dr. rer. nat.)

genehmigte

Dissertation

von

Amelia Lösch-Zhang

Erstgutachter:

Prof. Dr. Markus Biesalski

Zweitgutachterin:

Prof. Dr. Annette Andrieu-Brunsen

Darmstadt 2024

Tag der Einreichung: 11. September 2024

Tag der mündlichen Prüfung: 28. Oktober 2024

Lösch-Zhang, Amelia: Plasma-assisted deposition of vegetable oil-based coatings for paper hydrophobization

Darmstadt, Technische Universität Darmstadt

Jahr der Veröffentlichung der Dissertation auf TUpriints: 2024

urn:nbn:de:tuda-tuprints-286144

Tag der mündlichen Prüfung: 28.10.2024

Veröffentlicht unter CC BY 4.0 International

<https://creativecommons.org/licenses/>

Acknowledgements – Danksagung

An dieser Stelle möchte ich mich bei allen bedanken, die mich während der Promotion begleitet und unterstützt haben.

Mein erster Dank gilt Prof. Dr. Markus Biesalski für die Ermöglichung der Promotion in seiner Arbeitsgruppe und das entgegengebrachte Vertrauen.

Bei Prof. Dr. Annette Andrieu-Brunsen möchte ich mich für die Übernahme des Koreferats bedanken, ebenso bei den Fachprüfern Prof. Dr. Christian Hess und Prof. Dr. Marcus Rose.

Mein ganz besonderer Dank geht an Dr. Andreas Geißler für die fachliche Betreuung meiner Arbeit. Danke insbesondere für dein Vertrauen, deine Unterstützung in allen Belangen, deine Verfügbarkeit wann immer Gesprächsbedarf bestand und deine pragmatische Herangehensweise an Probleme aller Art!

Ebenfalls bedanken möchte ich mich bei dem Projektteam BioPlas4Paper, Martin Bellmann, Dennis Möck und Dr. Jörn Appelt für die wunderbare Zusammenarbeit, gegenseitige fachliche Unterstützung und spannende Projekttreffen. Insbesondere bei Martin bedanke ich mich für die Hilfe bei allen technischen Fragen, das Korrekturlesen meiner Texte zum Thema Plasma und die vielen Stunden, die wir gemeinsam in Göttingen an der Plasmaanlage verbracht haben.

Ein herzlicher Dank allen aktuellen und ehemaligen Mitgliedern des Arbeitskreises Biesalski sowie des Arbeitskreises Andrieu-Brunsen für die fachliche und moralische Unterstützung und die vielen schönen gemeinsamen Erlebnisse. Mein besonderer Dank gilt Martina Ewald und Marion Trautmann für die Organisation und Hilfe bei allen Fragen innerhalb und außerhalb des Labors. Danke meinen Korrekturleserinnen und -lesern: Nele Link, Carina Breuer, Dr. Joanna Mikolei, Dr. Jan-Lukas Schäfer und Dr. Lucy Zhao. Danke Oliver Elle für deine guten Ideen und insbesondere für die Hilfe bei Datenauswertung und Statistik. Danke an PD Dr. Tobias Meckel für die Unterstützung bei der CLSM-Probenpräparation und Messung sowie an Dr. Dieter Spiehl für technische und analytische Unterstützung. Danke an meine Praktikantin Nele Link, meinen Bacheloranden Tobias Gaydoul sowie meine wissenschaftlichen Hilfskräfte Christopher Schilling und Antonia Streck. Danke den Kollegen in der Feinmechanik- und Elektrowerkstatt, insbesondere Matthias Guse, sowie unseren Assistentinnen Vanessa Schmidt, Bärbel Webert und Rama Aldada.

Zuletzt möchte ich meinen Eltern und meinem Mann danken – dafür, dass ihr immer für mich da seid, mich unterstützt und mir den Rücken freihaltet. Ohne euch wäre vieles nicht möglich gewesen.



The present work was carried out at the Ernst-Berl-Institute for Macromolecular and Technical Chemistry of the Technische Universität Darmstadt under the supervision of Prof. Dr. Markus Biesalski from July 2020 to June 2024.

Parts of this work have already been published or presented at conferences:

Scientific research articles as first author:

- (1) A. Loesch-Zhang, C. Cordt, A. Geissler, M. Biesalski, **A Solvent-Free Approach to Crosslinked Hydrophobic Polymeric Coatings on Paper Using Vegetable Oil**, *Polymers* **2022**, *14*, 1773.
- (2) A. Loesch-Zhang, T. Meckel, M. Biesalski, A. Geissler, **Enhancing Hydrophobic Properties in Olive Oil-Coated Papers through Thermal Treatment**, *Coatings* **2024**, *14*, 364.
- (3) M. Bellmann*, A. Loesch-Zhang*, D. M. J. Möck, J. Appelt, A. Geissler, W. Viöl, **Hydrophobic glass and paper coatings based on plasma-polymerized vegetable oils using a novel atmospheric pressure plasma concept**, *Plasma Process. Polym.* **2024**, *21*, e2300224.

*M.B. and A.L. contributed equally to this work
- (4) A. Loesch-Zhang, M. Bellmann, K. Lachmann, M. Biesalski, A. Geissler, **Plasma Polymerization of Vegetable Oils onto Paper Substrates of Varying Porosity for Improved Hydrophobicity**, *Adv. Mater. Interfaces* **2024**, 2400507.

Scientific review article as first author:

- (1) A. Loesch-Zhang, A. Geissler, M. Biesalski, **Plasma polymerization of biogenic precursors**, *Plasma Process. Polym.* **2023**, *20*, e2300016.

The paper was highlighted on the outside cover of the print version: *Plasma Process. Polym.* **2023**, *20*, e2370017.

Conference talks:

- (1) A. Loesch-Zhang, M. Bellmann, D. M. J. Möck, J. Appelt, A. Geissler, **Biobased hydrophobic glass and paper coatings obtained via plasma polymerization using a novel jet-induced sliding discharge method**, International Symposium on Wood, Fiber and Pulping Chemistry, Venice, Italy, **07/2023**.
- (2) A. Loesch-Zhang, M. Bellmann, D. M. J. Möck, J. Appelt, A. Geissler, **Plasma-polymerbeschichtungen auf Basis biogener Präkursoren**, 46. ak-adp Workshop, Dresden, Germany, **04/2024**.
- (3) A. Loesch-Zhang, M. Bellmann, D. M. J. Möck, J. Appelt, A. Geissler, **Biobasierte Plasmapolymerschichtungen zur Papierhydrophobierung**, 10. Partnerschafts-symposium Plasma For Life, Göttingen, Germany, **09/2024**.

Scientific poster as co-author:

- (1) M. Bellmann, A. Loesch-Zhang, D. M. J. Möck, A. Geißler, J. Appelt, K. Lachmann, W. Viöl, **Revolutionizing Surfaces: Unlock the Power of Hydrophobic Plasma-Polymerized Vegetable Oils**, Plasma Surface Engineering, Erfurt, Germany, **09/2024**.

Table of contents

1..... Introduction	1
2..... State of the art	3
2.1. Conventional strategies for paper finishing	3
2.2. Plasma-based strategies for surface modification	9
2.2.1. Plasma polymerization using biogenic precursors	9
2.2.2. Plasma-induced paper surface modification	34
2.2.3. Plasma polymerization for paper hydrophobization	39
3..... Aim and Strategy	43
4..... Methods	48
4.1. Cellulose fibers – the raw material for paper	48
4.2. Paper production and finishing	51
4.3. Vegetable oils	55
4.4. Atmospheric pressure plasma polymerization on sensitive 3D substrates	57
5..... Results and Discussion	62
5.1. Thiol-ene photocrosslinking as a conventional solvent-free method for hydrophobizing paper with vegetable oils	62
5.2. Covalently attached hydrophobic vegetable oil-based paper coatings through thermal treatment	78
5.3. Hydrophobic vegetable oil-based coatings deposited through plasma polymerization	95
5.4. Vegetable oil-based plasma polymer coatings on varying paper substrates	112
6..... Summary and outlook	128
7..... Zusammenfassung	132
8..... References	137
9..... Appendix	I
List of abbreviations	I
Declarations – Erklärungen	II



1. Introduction

In 1998, ANASTAS and WARNER formulated the 12 principles of green chemistry, a framework for reducing or eliminating the generation of hazardous substances during chemical activities.^[1] These principles include among others preventing waste, reducing consumption of hazardous chemicals, reducing the use of auxiliary chemicals and derivatives, enhancing energy efficiency and using renewable raw materials.^[1] Being a biobased material, paper is a promising replacement for plastics in manifold applications due to its good recyclability, low cost, easy availability and biocompatibility. It further features high specific strength, low thickness and weight as well as good flexibility and can be produced in-line at large length and width scales and with high throughput rates.^[2-4] In 2022, the worldwide production of paper and board was 420 million tons,^[5] and thus even higher than that of plastics with a production of 400 million tons.^[6] 65% of paper production are accounted for by the sector of packaging papers, 22% by graphic papers, 11% by hygiene papers and 2% by specialty papers (Figure 1).^[5]

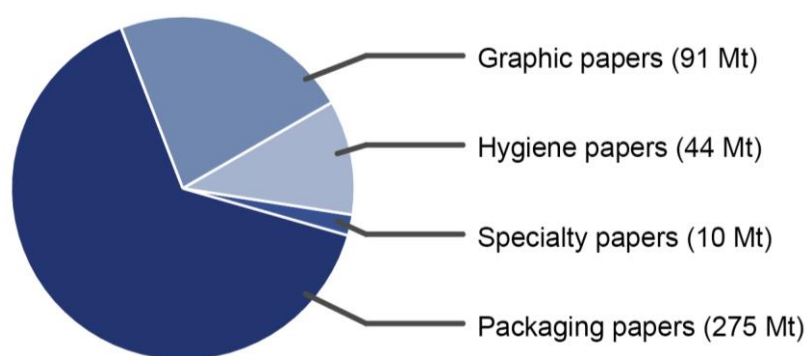


Figure 1: Worldwide production of the main varieties of paper and board in 2022.^[5]

Raw paper is an intrinsically hydrophilic and porous material and thus permeable to both gaseous and liquid media. This can be taken advantage of, for instance to develop materials with filtration characteristics such as coffee filters or laboratory filter paper, or to produce water-absorbent materials like paper tissues.^[2]

However, paper's susceptibility to water uptake is a great shortcoming for many other applications in which water resistance and durability are required. Considering the dominant sector of packaging, not only the penetration of humidity poses a problem with respect to protecting the content, but additionally the high porosity of paper allows easy transgression of gases and odors that may spoil the content or pollute the surrounding environment. With respect to graphic papers, the porosity can have adverse effects on printability and print image quality.^[2] Furthermore, hydrophilicity and porous structure facilitate the colonization with bacteria or fungi, leading to material loss and health hazards.^[7,8] Finally, the dimensional stability and tensile strength of paper deteriorate rapidly when the material becomes humid,

which for instance poses an issue for hygiene papers, as well as packaging papers and construction applications.^[4,9]

Hence, the paper industry has developed various sizing and coating strategies to endow paper with properties that directly reverse its original characteristics in terms of porosity and hydrophilicity. Whilst thus, good barriers against water, water vapor, grease and gases have been achieved, these processes are disadvantageous from the material-economic and energetic point of view, as current finishing strategies generally rely on wet-end processes.^[2,10] Not only can this lead to the application of excessive amounts of coating material, but the amount of generated solvent, which has to be recycled or discarded, is significant. Furthermore, this approach requires subsequent drying with a high energy demand, which is especially challenging as for instance in Germany the paper industry already suffers from high energy prices.^[11] Finally, durability, if it is not achieved through high coating amounts, needs to be attained through permanent attachment of the coating agent to, or around, the fiber. This is accomplished either through covalent bonding or post-coating crosslinking, which is challenging at industrial scale, especially considering the high process speeds characteristic for paper production.

Notwithstanding, in view of the sustainable development goals adopted by the United Nations in 2015^[12] and green chemistry principles that may help in achieving the former, the need to transform paper finishing and coating processes is evident. As such, reducing the amount of coating material and finding alternatives to solvent-based coating methods is crucial for reducing not only waste production, but also the use of auxiliary chemicals and excessive material consumption. Solvent-free processes are additionally needed to lower energy consumption. New approaches are required to enable replacement of hazardous substances with non-toxic biobased coating materials. In this frame, the present work suggests various strategies on the route towards more sustainable paper coatings using biobased coating materials in solvent-free processes.

2. State of the art

2.1. Conventional strategies for paper finishing

Paper applications are manifold and continuously expanding, especially with respect to the search for a more sustainable lifestyle, while specific usages also require specific properties. For instance, tissue and hygiene papers need to show high wet-strength.^[13] Microfluidic devices for medical applications require good fluid control and target-dependent adhesion properties,^[14] while biomedical applications such as wound dressings have to resist biofilm formation.^[15] Printing papers demand good ink printability, high smoothness and fine gloss.^[16] Construction papers require barriers against moisture and mold, while packaging papers similarly need to protect their content from any ingress of foreign substances, chemical modification, microbial colonization or damage through handling.^[17]

Paper features excellent qualities like high strength, low weight, low cost, good availability, recyclability and biodegradability. However, some properties, which can be advantageous in certain applications, are highly disadvantageous with respect to others. Especially, paper's hydrophilicity and porosity generate an excellent capillary system with a high absorbency capacity, that however makes for instance controlled printing impossible.^[18] On top of implementing water resistivity to overcome this issue, special requirements with respect to individual applications need to be taken into account. These challenges can be addressed either by using modified fibers, incorporating active agents during the sheet forming process or by different post-sheet formation finishing strategies, as will be discussed herein.

Sizing is a strategy for preventing liquid imbibition and uptake through paper.^[19] The first attempts to size writing paper after sheet formation were made in ancient China by using plant-based gelling paste that filled all pores and interfibrillar spaces on the surface and thus impeded capillary water uptake.^[18] After the papermaking technology reached Europe, bone and leather residues, which were more easily applicable on the pre-formed paper, were introduced as surface sizing agents.^[18] A significant improvement was the invention of internal sizing by ILLIG in 1806, which enabled performing paper production and sizing in one step on the newly patented paper machine.^[18,20] Herein, the sizing agent was added to the pulp prior to sheet formation and drying, and thus greatly simplified paper finishing. The process consisted of adding a saponified rosin dispersion to the pulp suspension and precipitating it onto the fibers using alum, which enabled obtaining a homogeneous sizing distribution throughout the pulp before sheet forming. Instead of the previous approach of closing the capillaries in paper through gelling agents, this new technique relied on partial hydrophobization of the paper surface.^[18,20] However, the overall acid character of the alum-based rosin sizing process reduced

the storage durability of the paper and complicated the incorporation of fillers. As an answer to those difficulties, alkaline and neutral sizing approaches were developed starting from the 1970ies.^[20] Today, apart from rosin, alkyl ketene dimers (AKD) and alkenyl succinic anhydride (ASA) are the most important sizing agents.^[20] AKD is based on a four-membered lactone ring as common functionality to which two aliphatic chains of C14 to C18 aliphatic fatty acids are attached. The lactone ring can form β -keto ester bonds with cellulose during the drying process. The hydrophobic tail accordingly orients away from the cellulose surface and thereby leads to hydrophobization.^[21,22] ASA is formed by reacting maleic anhydride with a mixture of C16 to C22 fatty acids, and can also attach covalently onto cellulose via esterification during the drying process.^[22] The exact extent of the attachment of sizing agents is however unclear, as recent research has for instance shown unbound ASA to contribute significantly to paper hydrophobization.^[23] Finally, polymeric materials have emerged as novel sizing agents in the second half of the 20th century.^[22] Both internal and surface sizing as well as accordingly used sizing agents have been extensively reviewed.^[22,24] Innovative sizing approaches using AKD and ASA on paper include vapor deposition^[25] and coatings from supercritical CO₂ solution,^[26] while novel biodegradable sizing agents are under development.^[27] Furthermore, attempts are made to produce existing sizing agents, especially ASA, at least partly from renewable resources using vegetable oils as feedstock for the fatty acid chain.^[28]

Whilst the initial goal of sizing was to improve paper writability, modern-day paper applications comprise a much larger scope of demands. Amongst those are printability, certain optical or tactile properties as well as durability and barrier properties. One shortcoming of sizing is its inability to maintain dimensional stability in paper independent of surrounding humidity conditions, as hydrophobization only takes place on the outer surface of fibers, but does not prevent water vapor from entering the fibers and making them swell. Thus, sized paper also loses its strength when soaked in water for a longer period of time.^[22] Considering these and other disadvantages with respect to certain applications, alternative surface modification approaches are required that endow paper with good barriers against liquid water and water vapor as well as all other target functionalities. This can for instance be achieved through lamination, sealing or impregnation. Also, various coating methods such as extrusion coating, bar coating, blade coating, curtain coating and spray coating are being used for paper surface modification. Coatings can be applied as solutions, emulsions or dispersions from aqueous media, but also from organic solvents.^[10,29,30]

In the construction and packaging sector, besides good durability, one crucial requirement is control over penetration of liquids, gases and other substances. Therefore, barrier properties against water vapor, oxygen, aromas, but also liquid water and grease have to be established.^[30]

Such barriers have until now mostly been produced from materials relying on fossil-based or synthetic materials. They often include, but are not restricted to, polymers like poly(ethylene), poly(vinylidene chloride), poly(ethylene terephthalate) and poly(butylene terephthalate).^[29,31] Polyfluorinated materials have found many applications due to their ability to repel both oil and water, combined with good mechanical properties, but give rise to great environmental and health concerns.^[32] Silicon-containing coatings, for instance based on tetraethoxysilane or (poly)dimethylsiloxane and silica particles, also result in superhydrophobic surfaces.^[33,34] Examples for manifold materials and approaches used to endow cellulose or paper with hydrophobic properties are shown in Figure 2.

Non-renewable products				Biobased products	
Vinyl	Polystyrene	Styrene-maleic anhydride	Ammonium salts	AKD	Fatty acids
PE	Styrene butadiene	Styrene-maleimide	Succinic anhydride	Rosin	Carnauba Wax
Hydroxypropyl	Hexanoate	Epoxy	Amines	ASA	Triglycerides (Vegetable oils)
Acrylate		Chemical modification - grafting from - grafting onto - layer-by-layer - solution treatment	Physico-chemical modification - plasma etching/ polymerization/patterning - (electro)spraying - laser - UV/Vis - electrowetting		Starch
	Acrylonitrile				Chitosan
Aliphatic Hydrocarbons		Surface coating - sol/gel - atomic layer deposition - magnetron sputtering - thermal flame			Cellulose whiskers
	Polyisoprene				Cellulose microfibrils
	Poly(carboxylic acid)				Alginate
	Poly(acrylic acid)		Kaoline	CaCO ₃	Wheat
	Poly(allyl)amine		Organoclay	Talc	Whey protein
	Poly(ethylene oxide)	Organic Nanoparticles	Montmorillonite		Poly lactide
	Poly(diallyldimethyl-ammonium chloride)		Silanes/Siloxane (derivatives)	Al ₂ O ₃ SiO ₂ ZnO ₂ TiO ₂ ZrO ₂	Polyhydroxyalkanoate
PTFE	Fluorine (derivatives)	Carbon Nanotubes	Polycaprolactam		Polyhydroxybutyrate

Figure 2: Methods and products for cellulose and paper hydrophobization. Adapted with permission from Springer Nature from work by SAMYN *et al.*^[35] © 2013, Springer Science Business Media New York.

With emerging new paper applications and an increased awareness of requirements for sustainability, the use of renewable raw materials for paper barriers, especially but not only with respect to food packaging applications, is gaining increasing interest and has been extensively reviewed.^[7,29,31,36] One approach for tuning cellulose's properties is the direct modification of cellulosic fibers or nanocelluloses,^[35,37,38] for example through crosslinking^[39] or through (trans)esterification reactions using vegetable oils or fatty acid chlorides.^[40]

Furthermore, a wide range of biobased materials for directly coating readily made paper has been investigated into, with each material showing distinct advantages and disadvantages with respect to processing, applications and degradability. For instance, the application of lignin, an important biopolymer and paper production byproduct, is challenging due to bad compatibility with polymers and aggregation.^[29] Polysaccharide-based coatings show good barriers against

grease, CO₂ and oxygen, but due to their hydrophilicity their ability to resist water and moisture is generally poor. Similar observations are made for protein-based coatings. Lipid-based coatings on the other hand are hydrophobic and therefore show good water and moisture repellency, but they are brittle and often inhomogeneous.^[29,41] Paperboards bar-coated with biodegradable poly(lactic acid), although displaying decreased water vapor permeability and water absorptivity as well as increased contact angles compared to uncoated paperboards, however still do not achieve actual surface hydrophobicity.^[42] Many approaches therefore combine the advantages of different biomaterials and biopolymers, for example as blends, fillers or through functionalization, to achieve both good processability and the desired functionality.

Derivatizing lignin through esterification not only makes it more easily applicable, but also results in hydrophobic coatings with water contact angles of 120°, using for instance linseed oil^[43] or oleic acid.^[44] A paperboard coating from lignin esterified with tall oil fatty acids and applied through bar coating showed reduced water vapor transmission rates and oxygen transmission rates. Even better barrier properties were obtained using a pure tall oil fatty acid coating, but its water contact angle decreased rapidly over time, contrary to that of the lignin ester coating. Overall, the oxygen transmission rate values were still unsatisfactorily high compared to established materials, which was attributed to insufficient coating homogeneity.^[45] Hydrophobicity of paper cationized with starch was improved through adsorption of lignin in the shape of granules.^[46] Blends of biodegradable polymers and bio-fillers are desirable for reducing production costs and improving mechanical and thermomechanical properties whilst maintaining biodegradability. For example, lignin was esterified with palmitoyl chloride to improve lignin dispersibility in a hydrophobic polymer matrix of biodegradable poly(butylene adipate-co-terephthalate) and applied onto paper through blade coating. Thus-obtained papers showed improved wet strength, decreased oxygen, water and oil permeability and an increased water contact angle (WCA).^[47]

Both plant- and animal-derived proteins have been used for paper coatings. Casein, a milk protein, both improved mechanical properties and water vapor barriers,^[48] while whey protein, incurring during cheese production, showed enhanced resistance against grease penetration^[49] and water vapor transmission when combined with beeswax.^[50] A wheat gluten coating simultaneously decreased water and oil wettability and absorption^[51] and enabled formation of oxygen barriers similar to those of conventional polymer-based coatings through application by compression molding.^[52] Soy protein and corn zein coatings led to grease barriers similar to those produced by poly(ethylene).^[53]

Amongst biobased polysaccharides, starch is commonly used as a sizing agent, but needs to undergo modification to be used as a coating material.^[31] Chitosan can show barrier properties

against lipids similar to those obtained by fluorocarbons when combined with alginate,^[54] as well as excellent oxygen barriers.^[52] Chemical modification enables chitosan's use as hydrophobic and even multifunctional coating. For instance, papers coated with chitosan-palmitic acid emulsions and palmitic acid-grafted chitosan were, despite showing either unchanged or decreased water vapor barriers, able to maintain liquid water resistivity whilst equally showing lipid barrier and antimicrobial properties.^[55] Native cellulose, unlike chitosan, has poor film-forming properties and therefore requires modification for use in coatings, which then can lead to hydrophobic or superhydrophobic surface properties. For instance, cellulose stearoyl ester (CSE) imparted different degrees of hydrophobicity on paper depending on the coating method. Dip coating from a solution of CSE in toluene led to WCAs above 120°, while spray coating of CSE nanoparticles resulted in surfaces with WCAs above 150° and self-cleaning character.^[56] Such nanostructured coatings were further enhanced through incorporation of ethylene glycol distearate (EGDS),^[57] based on which targeted introduction of hydrophilic domains shows potential for application in fog harvesting.^[58] The approach used to generate these superhydrophobic and superhydrophobic-hydrophilic hybrid surfaces is displayed in Figure 3.

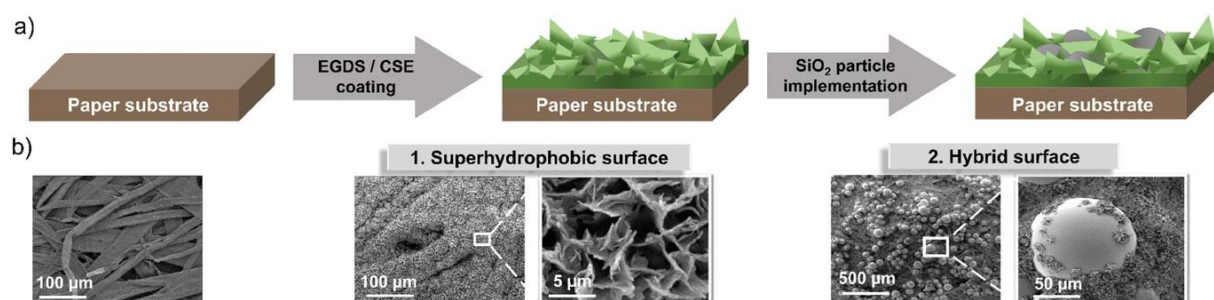


Figure 3: Generation of superhydrophobic and hybrid paper surfaces through a cellulose stearoyl ester (CSE)/ ethylene glycol distearate (EGDS) coating and introduction of hydrophilic particles. Reproduced from BREUER *et al.*^[58], which was published under CC BY 4.0 International open access license. © 2024 The Authors. *Advanced Materials Interfaces* published by Wiley-VCH GmbH.

Other approaches for imparting hydrophobicity directly onto paper using fatty acid-based materials include crosslinking reactions. For instance, *cis*-9,10-epoxy-18-hydroxyoctadecanoic acid, isolated from birch bark, was first polymerized using lipase as catalyst. The resulting polyester was mixed with curing agents tartaric or oxalic acid, applied to cotton linters cellulose by impregnation and cured through compression molding, which resulted in WCAs above 100°.^[59] Superhydrophobic and self-cleaning paper was prepared through thiol-ene click reaction between thiolated castor oil and 2,4,6,8-tetramethyl-2,4,6,8-tetravinylcyclotetrasiloxane by spray coating a solution of the reactants and modified SiO₂ nanoparticles, followed by crosslinking with ultraviolet (UV) light.^[60]

Waxes are also suitable for producing superhydrophobic surfaces. For instance, bar coating mixtures of carnauba wax and beeswax increased the water contact angle of sized copy paper from 110° to 167° through suitable choice of coating composition and annealing temperature.^[61] Superhydrophobic coatings were further obtained through spray coating of a hot solution of rice bran wax and candelilla wax. The coating showed good durability and repellency of a large variety of liquids such as honey, yoghurt and orange juice.^[62] Aqueous emulsions of beeswax using chitosan as emulsifier were applied to copy paper through bar coating to obtain both liquid water and water vapor barriers.^[63]

This large variety of examples is evidence of the high interest in coating papers with biobased precursors to improve barrier properties. However, the coating processes still show some shortcomings with respect to sustainability. Frequently, chemical derivatization is needed to obtain suitable coating materials, and coatings are deposited from organic solutions or emulsions. When coating is performed from aqueous solutions, an energy-intensive drying process is required, and water must be purified for re-use. A more sustainable way of modifying material surface properties is plasma-induced surface modification. Amongst these approaches, in view of the aim to deposit crosslinked coatings in a single step and without the use of supplementary chemicals, plasma-enhanced chemical vapor deposition, also known as plasma polymerization, is the method of choice to be examined within this work.

2.2. Plasma-based strategies for surface modification

2.2.1. Plasma polymerization using biogenic precursors

Plasma-enhanced chemical vapor deposition (PECVD), also known as plasma polymerization, is a promising coating technique for manifold applications. It bypasses many disadvantages of conventional coating methods, as it does in principle not require solvents and does not generate waste, but instead is highly versatile and applicable to a large variety of materials. Unlike other coating techniques, PECVD relies on the use of plasma, the fourth state of matter. Plasma is formed when a sufficient amount of energy is supplied to a gas. Collisions between electrons and gas atoms or molecules lead to the formation of radicals, ions and other metastable species, which are accordingly highly reactive.^[64,65] Thus, the coating precursor, which can be introduced into the reactive chamber in gaseous state, or as an aerosol carried by a neutral gas, is excited to the plasma state. The highly reactive plasma deposits on the substrate's surface, where reactions both among the coating molecules themselves and with the substrate surface take place.^[66] The result is a highly irregular, crosslinked structure covalently attached to the substrate, which would not be accessible by conventional coating chemistry. Although these structures are commonly referred to as "plasma polymers", it is important to note that, contrary to conventional polymers, plasma polymers do not have regular repeating units and are not accessible through typical polymerization reactions like chain-growth or step-growth polymerization.^[67] While plasma polymerization has been widely employed for depositing coatings using fossil-based or environmentally harmful precursors,^[68] depositing biobased precursors is of crucial importance for the strife towards a more sustainable world. The most recent developments in this field feature the plasma-assisted deposition of silk fibroin and chitosan, which widens the scope of biobased polymers applicable through PECVD, and has not yet been addressed in the present review article.^[69]

This section first gives an introduction to plasma technology and plasma-assisted surface modification and will then focus on the state of the art in plasma polymerization of biogenic precursors.

For this publication, I was responsible for literature research, conceptualization, writing and creating artwork. Andreas Geissler was involved in conceptualization and was responsible for proofreading and funding acquisition. Markus Biesalski was involved in proofreading.

The following review article has been published in *Plasma Processes and Polymers*.

A. Loesch-Zhang, A. Geissler, M. Biesalski, **Plasma polymerization of biogenic precursors**, *Plasma Process. Polym.* **2023**, *20*, e2300016.

Published by Wiley-VCH GmbH under Creative Commons Attribution 4.0 International (CC BY 4.0) License.

The online version of this article can be found under:

<https://onlinelibrary.wiley.com/doi/10.1002/ppap.202300016>.

REVIEW

Plasma polymerization of biogenic precursors

Amelia Loesch-Zhang¹ | Andreas Geissler^{1,2}  | Markus Biesalski¹

¹Macromolecular Chemistry and Paper Chemistry, Technical University Darmstadt, Darmstadt, Germany

²Papiertechnische Stiftung (PTS), Heidenau, Germany

Correspondence

Andreas Geissler, Macromolecular Chemistry and Paper Chemistry, Technical University Darmstadt, Peter-Gruenberg-Str. 8, Darmstadt 64287, Germany.

Email: andreas.geissler@tu-darmstadt.de

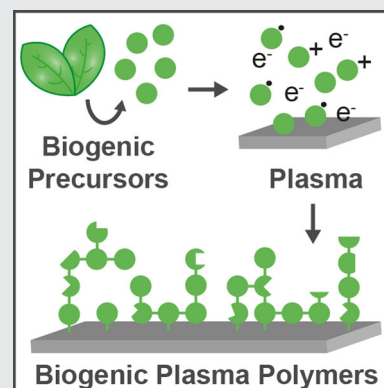
Funding information

Fachagentur Nachwachsende Rohstoffe, Grant/Award Number: 2220HV017A

Abstract

Plasma-enhanced chemical vapor deposition is a highly promising tool for coating deposition due to its versatility, tunability, low chemical consumption, and cost-effectiveness, with an increasing scope of deposition methods at both low and atmospheric pressure. Adhering to green chemistry principles, biobased precursors have recently shifted into the focus of research interests. This review gives an overview of the main biogenic substance classes that have been used for the deposition of plasma polymer coatings, including natural oils, terpenes, enzymes, and lactic acid-based precursors.

The common feature of these precursors is not only their biogenic origin, but additionally the manifold properties of the resulting plasma-deposited thin films, ranging from antimicrobial properties to tunable surface-wetting characteristics, electrical conductivity, or biodegradability. This combination of unique features makes plasma-derived polymers based on natural precursors immensely attractive for manifold applications.



KEYWORDS

coatings, enzymes, extractives, nonthermal plasma, plasma-enhanced chemical vapor deposition (PECVD)

Abbreviations: AA-PECVD, aerosol-assisted plasma-enhanced chemical vapor deposition; ac, alternating current; AFM, atomic force microscopy; AP, atmospheric pressure; APPJ, atmospheric pressure plasma jet; CVD, chemical vapor deposition; DBD, dielectric barrier discharge; dc, direct current; MS, mass spectrometry; MW, microwave; OES, optical emission spectroscopy; PAVTD, plasma-assisted vapor thermal deposition; PECVD, plasma-enhanced chemical vapor deposition; PET, poly(ethylene terephthalate); PLA, poly(lactic acid); RF, radio frequency; ToF-SIMS, Time-of-Flight Secondary Ion Mass Spectrometry; XPS, X-ray photoelectron spectroscopy.

This is an open access article under the terms of the Creative Commons Attribution License, which permits use, distribution and reproduction in any medium, provided the original work is properly cited.

© 2023 The Authors. *Plasma Processes and Polymers* published by Wiley-VCH GmbH.

1 | PLASMA

The term “plasma” was first used by Langmuir et al. in the 1920s to describe the central region of an electrical gas discharge.^[1] Plasma is formed when gases are supplied with such a high level of energy that their outer electrons overcome their orbital binding energy. The resulting ionized gas condition is nowadays often considered to be the fourth state of matter. It is assumed that ~99% of the universe consists of plasma.^[2] In addition to stars, such as our sun, which are entirely in the state of plasma, ionized gas with much lower density also fills the space between all celestial objects.^[3] Furthermore, plasma formation can be observed with *aurora borealis*, when charged particles of the solar winds interact with Earth's atmosphere and become trapped near the poles, as well as at the moment of a lightning strike.^[4]

Prerequisite for plasma formation is the sufficient supply of energy to a neutral gas.^[5] Methods for generating plasmas in a laboratory environment include the supply of mechanical (adiabatic compression), thermal, chemical, radiant, nuclear, or electrical energy. The most common method for producing plasmas on a lab scale is the use of electrical fields.^[6] Highly energetic electrons and photons collide with neutral gas species in both elastic and inelastic collisions. Elastic collisions only change the kinetic, but not the internal energy of the neutral species. Through the inelastic collision, the electronic structure of the neutral gas particles can be modified. If the colliding electrons or photons have sufficiently high energy, electrons, ions and neutrals (atoms, molecules, and radicals) are formed in fundamental and excited states.^[7,8] A plasma therefore contains free charge carriers and is electrically conductive, while at the same time showing both collective behavior and quasi-neutrality.^[9]

Due to their significantly lower mass, electrons are accelerated much faster than ions or neutral gas species. This may lead to disparate temperatures for the various species contained in plasma, so that two basic types of plasma can be distinguished. Thermal plasmas, or “hot plasmas,” which include solar plasma, are characterized by the kinetic energy and temperature of the heavier plasma particles reaching that of the high-energy electrons. Energy and degrees of freedom are therefore equally distributed between the particles, giving rise to the term of local thermal equilibrium (LTE) plasmas.^[10,11] Opposed to this are nonthermal plasmas or “cold plasmas,” also referred to as non-LTE plasmas. In this case, the electrons and part of the ions have a much higher kinetic energy than the main gas fraction. Consequently, the electron temperature (up to

10,000 K) is significantly higher than the overall gas temperature, which may well still be at room temperature. Ionization and chemical processes are therefore determined by the electron temperature. Nonthermal plasmas are less powerful but more easily controllable than thermal plasmas.^[10,12] Due to their low heat generation they are well suitable for processing organic compounds.^[13] Decisive for the formation of LTE and non-LTE plasmas is the efficiency of energy exchange induced by frequent collisions between electrons and heavier particles, which is enabled by a low mean free path with respect to the discharge length. High pressures and high plasma powers therefore enhance LTE plasma formation, while non-LTE plasmas are preferentially induced by lower pressures or low energy input.^[14] Nevertheless, various methods exist to generate non-LTE plasmas even at atmospheric pressure.

1.1 | Plasma generation

For nonthermal plasmas, various categories exist for classification depending on their generation mechanism (direct current [dc] vs. alternating current [ac], radio frequency [RF] versus microwave frequency [MW]), pressure range (low pressure vs. atmospheric pressure) or electrode geometry.^[10] Eliasson et al. suggested the categorization displayed in Figure 1, whose four main constituents will be briefly described in the following.^[10] However, it should be noted that due to ongoing research in plasma generation, nowadays manifold combinations of these discharge types under varying conditions exist.^[4] Nonetheless, this scheme is very useful to describe the basic functioning of these methods.

1.1.1 | Glow discharge

The term glow discharge is derived from the glow that can be observed during radiation emission of excited species that are formed in the plasma. The ions generated by inelastic collisions are accelerated toward the cathode, where an ion-induced secondary electron emission occurs on impact. The electrons released in this process can then in turn initiate further ionization. These processes of ionization and electron emission sustain the glow discharge plasma. The potential difference and resulting electric field strength are unevenly distributed in the discharge area, leading to the identification of different spatial regions (e.g., cathode dark space, negative glow, and anode zone) within the discharge. A prerequisite for sustaining dc glow discharges is the presence of two conducting electrodes. In the case of

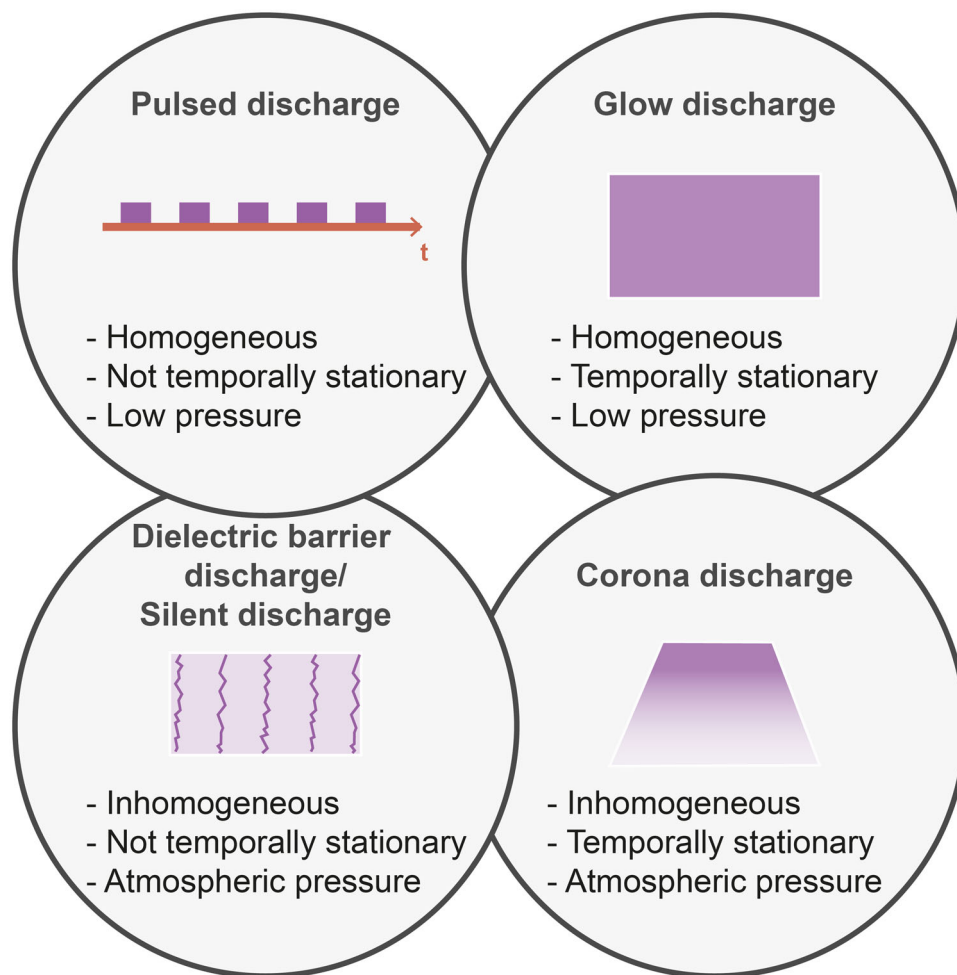


FIGURE 1 Categorization of discharge types depending on their temporal behavior, pressure, and appearance as proposed by Eliasson et al.^[10]

nonconducting electrodes or in the presence of a dielectric layer, an alternating current is applied to avoid excessive electrode charging and extinction of the glow discharge. Usually, radio frequencies are used to generate alternating voltages. Pulsed glow discharges can be considered as very short dc glow discharges with a long afterglow time. They have the advantages of facilitating the generation of non-LTE plasmas and allowing higher peak voltages and currents, while achieving better efficiencies and avoiding excessive sample heating. Atmospheric pressure glow discharges face the challenge of excessive cathode and gas heating and arcing due to high pressure. This can be overcome by changing the device dimensions as well as by covering at least one of the electrodes with a dielectric and operating at alternating voltages. Operation is possible both in homogeneous and filamentary mode, respectively. Processing at atmospheric pressure is technologically less challenging than operating at vacuum conditions and allows treatment of a wider range of materials.^[14]

1.1.2 | Dielectric barrier discharge

Dielectric barrier discharges (DBDs), also called “silent discharges” are very similar to atmospheric pressure glow discharges.^[14] DBDs were first introduced by Siemens in 1857 for the ozonation of air.^[15] DBD devices consist of two planar or cylindrical electrodes with a discharge gap width between 0.1 mm (or even smaller) and up to 100 mm. The characteristic feature is the presence of one or two insulating layers (dielectric barriers) in contact with the discharge in the gap (Figure 2a). Materials for the insulating layer include glass, quartz, ceramics as well as thin coatings from enamel or polymer on the electrode itself. For the subsequent plasma treatment, the substrate in question is placed on top of the insulation layer unless it acts itself as a dielectric layer.^[16] As direct current cannot pass the insulating layer, alternating current has to be used.^[17] When an electrical field is applied to a DBD device, electron avalanches develop and initiate streamers,

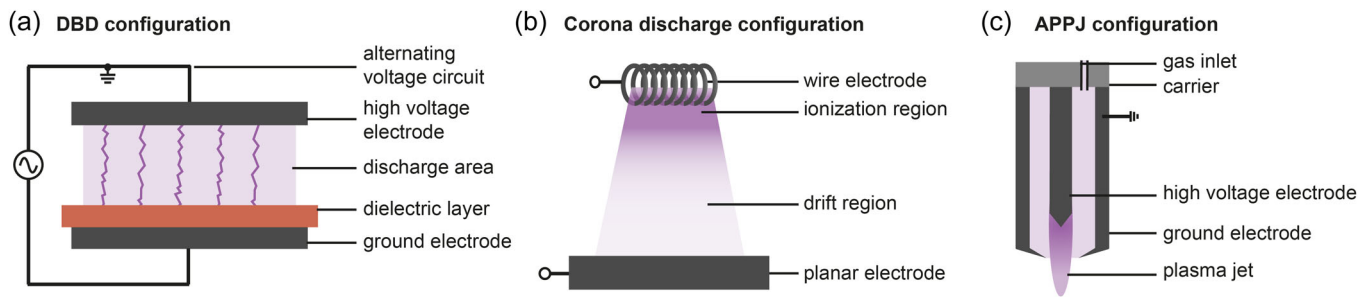


FIGURE 2 Examples of device configurations for (a) dielectric barrier discharge (DBD), (b) corona discharge, and (c) atmospheric pressure plasma jet (APPJ).

leading to the formation of a conducting channel of weakly ionized plasma and allowing the flow of an electron current.^[18] Charge accumulates on the dielectric layer until the voltage polarity (and thereby anode and cathode) reverses, leading to the formation of new avalanches and streamers on that spot. These can macroscopically be observed as filament or micro-discharge.^[12] Because of the charge accumulation this local electric field eventually breaks down and the micro-discharge stops.^[19] The filaments formed during the discharge are nearly cylindrical plasma columns with a lifetime in the range of several nanoseconds.^[20] The dielectric barrier prevents arc formation by limiting the current flow through restriction of the amount of energy in a single micro-discharge and distribution of the micro-discharges across the electrode area.^[10] However, the filamentary character of the discharge makes the plasma inhomogeneous, which limits the DBD applicability in deposition and etching to smooth surfaces.^[21] Under certain conditions, an alternative approach is therefore using the more homogeneous glow discharge for surface treatment or thin film deposition.^[4]

1.1.3 | Corona discharge

Corona discharges differ from the previously named setups by the cathode, which is shaped like a wire, sharp tip or rough edge, while different anode geometries exist.^[22] An example is given in Figure 2b. The discharge mechanism is like that of a dc glow discharge. Corona discharges operate at atmospheric pressure at dc and in nonequilibrium state in pulsed form.^[14] The ionization is controlled by the electrode geometries and its zone is confined to a very small space around the cathode (ionization zone). In contrast to other plasma generation methods, there is a large low-field drift region of low conductivity between the cathode and the anode (low-field zone). The discharge is therefore highly inhomogeneous. Yet, this array stabilizes the discharge

and prevents arc formation. Due to the high number of inelastic collisions occurring in the ionization zone, the species reaching the drift region have energies lower than ionization energies, so the drift region is characterized by neutral chemistry. Depending on the electrode polarity, positive and negative coronas are differentiated, although some other types also exist.^[6,10,13,21]

1.1.4 | Device configurations

For industrial applications, atmospheric pressure plasmas are more suitable than low-pressure plasmas due to the simplicity of device setup, cost-effectiveness, controllability, and in-line applicability.^[23] Corona discharges, atmospheric pressure glow discharges and DBD are frequently used for atmospheric pressure plasma processing.^[24] The challenge of treating complex 3D objects is addressed by atmospheric pressure plasma jets (APPJ).^[25] They consist of an inner needle-shaped electrode connected to the power source and a grounded outer electrode (Figure 2c). Frequently, the outer electrode is covered on the inside by an insulating layer. Carrier and reactive gases at atmospheric pressure and room temperature flow between the electrodes and become ionized. The plasma exits the device through a nozzle and is directed onto the substrate.^[26] The plasma is most commonly generated via DBD, as neither corona discharges are suitable due to their discharge heterogeneity, nor glow discharges because of the low pressure required.^[27] A high variety of different device setups, component materials, and potential applications exist.^[20,28] The main advantages of APPJs are their ability to create a homogeneous high plasma flux and the possibility of using compact, low-cost plasma sources. A downside of this design is the pronounced point discharge characteristic which requires scanning or array mounting for treatment of larger areas.^[27] As the plasma is not generated directly at the substrate surface, high processing speeds are possible, however, plasma species

can react with their surroundings on their way to the surface, causing a decrease in efficiency. The high process gas consumption, the relatively low treatable surface area and the need for cooling limits the profitability of APPJ.^[29] Other setups have been recently designed to address such challenges, such as the disc jet developed by Bellmann et al.^[29]

1.2 | Plasma-assisted surface processing

Plasma is an increasingly important tool for surface processing to tune chemical and physical properties of various materials ranging from metals and glasses to polymers, which this review is concerned with. An enormous range of applications from agriculture to medicine, smart surfaces, electronics, optics, and so on arises therefrom.^[30,31] Depending on their impact on the substrate surface, plasma processing methods can be divided into different categories (Figure 3).

Plasma cleaning and plasma etching both refer to plasma treatment techniques in which material is removed from a substrate surface, only differing by the extent of the removal.^[31,32] Plasma cleaning refers to the removal of contaminants such as oil, dust, oxides, or even bacteria from a substrate surface. Plasma etching describes the gradual removal of exposed surface layers of a bulk material. As only the material surface is exposed, the influence of etching on the physical and chemical properties of the substrate is limited, especially since UV light and the resulting radicals have a limited penetration depth.^[7,33,34] Plasma etching enables for instance targeted surface roughening to generate nanostructures.^[35]

Plasma functionalization or activation is used to modify substrate surface functionalities via reaction of the plasma species with the substrate surface.^[36] The resulting functionalities and properties depend on the nature of the plasma, which makes this method highly useful both for tuning of surface properties and for surface pretreatment followed for instance by grafting approaches.^[34,37] Typically used gases include noble gases such as Ar and He, but also O₂, N₂, NH₃, and CF₄.^[37,38] For instance, an oxygen treatment leads to an increase in oxygen-containing functionalities and thereby to improved surface hydrophilicity, while hydrophobicity can be enhanced by using fluorinated compounds like CF₄ or SF₆ as reactive gas.^[39] Nonreactive gases do not introduce functional groups but induce radical formation and thereby create reactive sites that can induce cross-linking (crosslinking via activated species of inert gases, CASING),^[32] lead to activation or ablation, or be used for posttreatment functionalization. Upon exposure to air or oxygen, autoxidation reactions form (hydro)peroxides, which can be used for subsequent conventional grafting from polymerization.^[37,40]

Alternatively, monomer adsorption to the substrate can be combined with plasma treatment if the precursor is not volatile enough to be transferred to the gas phase. In this case, the coating is performed via conventional methods, while surface binding is ensured with plasma treatment.

In the context of biogenic precursors, plasma treatment approaches have been used with copaiba oil,^[41] oleic acid,^[42] lavender and tea tree oil,^[43] and limonene and myrcene.^[44]

In the following, this review will focus on plasma polymer deposition. During plasma polymer deposition,

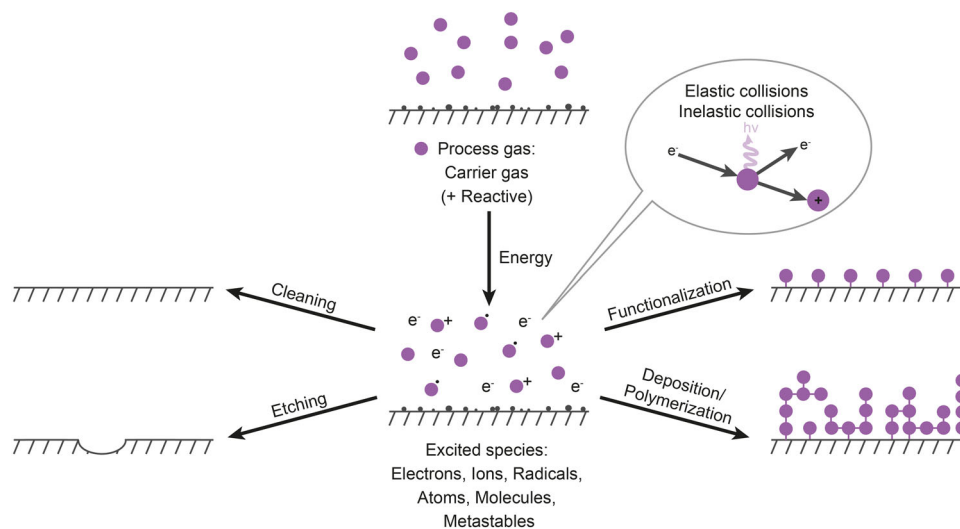


FIGURE 3 Plasma-assisted surface processing methods include plasma cleaning, etching, functionalization, and deposition.

single molecules do not only react with and attach to the substrate surface, but they also react with each other, creating an entire material layer. Plasma polymer deposition is therefore a process in which the application of a coating completely changes the surface properties while leaving the characteristics of the base material unaffected. Various methods using plasma exist, the best known among which is plasma polymerization.^[34] The term is derived from the occurrence of successive plasma-activated radical initiation, propagation, and termination reactions that lead to the deposition of a polymeric coating. Contrasting with conventional polymers, plasma polymers do not comprise regular repeating units, but form irregular, highly crosslinked networks of monomer fragments.^[45] Another term is “plasma-enhanced chemical vapor deposition” (PECVD). Just like in conventional chemical vapor deposition (CVD), a gaseous precursor reacts with a solid substrate surface forming a solid reaction product while simultaneously releasing gaseous byproducts.

Early research on the formation of polymeric structures in plasmas was conducted in the first half of the 20th century^[46,47] and intensified starting from the 1950ies.^[48–51] It was found that when gaseous compounds are subjected to plasma, insoluble solids are formed in the gas phase^[47] and films can be deposited.^[49] The resulting structure only partly corresponds to that of the precursor,^[51] while crosslinking is usually observed. Different rates for film formation were observed for different precursors.^[50] Yasuda et al. examined the effect of pulsed discharge on plasma polymer formation, showing that during plasma off-periods addition polymerization occurs exclusively, while competing with delamination processes during plasma on-periods.^[52]

Due to the high energy input, the polymers formed during plasma polymerization are partially fragmented and thus deposition and ablation continuously compete with each other. The process can be tuned by many parameters, such as the nature of the plasma, the energy generation and device geometry and the deposition conditions including flow rate, use of a carrier gas, pressure, and plasma power as well as the substrate material, roughness, and temperature.^[2,25,52–55] Initially plasma polymerizations were described by these partly interdependent parameters, which do not allow comparing different polymerization systems or monomers. Indeed, up to now it is difficult to reproduce plasma polymers if not exactly similar deposition conditions are used. To address these challenges, in the 1970ies Yasuda et al. developed a new parameter for describing the conditions of plasma formation, depending on (1) the power input W , which is highly dependent of the monomer chosen, (2) the monomer flow rate F , which

correlates to the pressure in a closed system, and (3) the monomer molecular weight M . The W/FM parameter, or Yasuda parameter, therefore describes the energy input per mass unit of monomer transferred to the monomer molecule crossing the active plasma zone and governs the formation of reactive intermediates.^[56] However, the Yasuda parameter can only be applied under limited circumstances, as it does not take into account the type of discharge, possible precursor dilution in inert gases or varying precursor reactivity.^[57]

Yasuda et al. also produced important findings with respect to the mechanism of plasma polymer formation, showing that certain precursor functionalities favor decomposition, such as oxygen-containing groups, chlorine atoms, and aliphatic or cyclic hydrocarbons, while other functionalities, such as aromatics, C=C double bonds, amine, and Si-containing groups favor polymer deposition.^[58] Polymerization was found to occur via radical formation, either by hydrogen abstraction or opening of multiple bonds or cyclic structures.^[59]

Much further research has been conducted into the mechanism of plasma polymerization, frequently confirming these observations. Plasma fragmentation generally follows bond dissociation energies, with the weakest bonds breaking most readily.^[60] Therefore, the presence of double bonds leads to increased retention of other precursor functionalities in the resulting polymer, since the π -component of C=C double bonds possesses a relatively low binding energy.^[61] Using mass spectroscopy, Mertens et al. showed that the presence of double bonds leads to formation of rather large fragments and even oligomerization via double bond opening, while homologous monomers containing no double bonds show very strong fragmentation into small molecules.^[53] Double bond opening has been ascribed to the formation of biradicals with a strong recombination tendency.^[52,62] Nisol et al. conducted manifold investigations into the energetics and mechanistic processes of a wide range of monomers such as esters, hydrocarbons, and so on.^[63] Friedrich et al. reviewed the mechanisms of plasma polymerization, identifying the main reaction pathways taking place following fragmentation such as chemical chain-growth polymerization (radical or ionic), ion-molecule reactions, and (poly-)recombination leading to linearly or irregularly structured materials and copolymers. Plasma polymerization processes performed in continuous wave mode are the least similar to conventional polymerization mechanisms and can best be described with a fragmentation-(poly)recombination mechanism. Due to the immense energy input, precursor molecules are strongly fragmented, with subsequent fragment (poly)recombination creating a structurally inhomogeneous product.^[62]

For tailoring applications, retaining precursor functionalities has gained increased attention in recent years. Functional group preservation has been obtained, for instance, by maintaining a low substrate temperature, using low plasma powers, or pulsing the plasma discharges.^[64]

Pulsing plasma has various advantages: The plasma can be operated at higher instantaneous power and peak voltages, while the average power is unchanged. The process can be more easily controlled and film inhomogeneity can be reduced.^[5] At atmospheric pressure, the formation of thermal equilibrium, overheating, and arc/spark formation can be prevented.^[7] Pulsed discharges can be produced with different device configurations and include radio frequency (RF) and microwave frequency (MW) discharges mostly operating at 13.56 MHz and 2.54 GHz respectively.^[19]

The key parameter in pulsed plasma polymerizations is the duty cycle, which is defined as the plasma on-time t_{on} divided by the total pulse duration (t_{on} and plasma off-time t_{off}) (Equation 1):

$$\text{Duty cycle} = \frac{t_{\text{on}}}{t_{\text{on}} + t_{\text{off}}}. \quad (1)$$

During t_{on} , electrons, photons, radicals, ions, and metastable states are created and initiate reactions, but most of them react quickly during t_{off} . Radicals are more stable and can at atmospheric pressure induce free radical polymerization during t_{off} . Long t_{off} periods therefore result in better monomer and polymer structural retention.^[65] For instance, in this way the preservation of hydroxyl-functionalities was tunable during PECVD of allyl alcohol, which allowed tailoring of surface properties.^[66]

Advantages of PECVD over CVD include processing at much lower temperatures and allowing use of more sensitive precursors and substrates such as cellulose.^[23,67] PECVD can be performed using low frequency, corona, DBD, radio frequency and microwave frequency plasma sources at both low and atmospheric pressure.^[68] Atmospheric pressure PECVD (AP-PECVD) is gaining increasing attention as its advantages are manifold, such as the enablement of continuous processing using open systems. No expensive vacuum pumping systems are required, which reduces cost and energy consumption. A large variety of precursors are accessible. The method is suitable for homogeneous treatment of large surfaces as well as for deposition of micro- and nanoscale structures.^[25,69] However, AP-PECVD also faces some downsides caused by the relatively short mean free paths and resulting high gas phase reaction rates induced by atmospheric pressure. Secondary reactions occur in the gas phase and mass transport is limited, which leads to

the formation of powder contaminating the substrate surface as well as poor film uniformity and properties.^[24]

AP-PECVD can be operated in direct or remote mode. In direct mode, the substrate is placed between the electrodes and the active species are created in the discharge area, leading to full precursor decomposition and requiring precise control of process parameters. In remote mode (APPJ), the precursor is injected downstream from the discharge area in the post-glow, yielding larger precursor fragments. This process extends the possible substrate selection to complex 3D substrates, but increases difficulty in achieving a uniform layer distribution.^[25,68,70] Examples of AP-PECVD include deposition of silicon compounds such as hexamethyl disiloxane (HMDSO) and tetraethoxy silane (TEOS)^[71] as well as deposition of fluorine compounds such as C_2F_4 , C_3F_6 , or C_3F_8 ^[72] for instance with the aim of substrate hydrophobization. Another example is the use of hexamethyl disilane (HMDS) and tris(trimethoxysilyloxy)vinylsilane (TTMSVS) as antireflective coating layer for poly(ethylene terephthalate) (PET).^[73] Even superconductive films have already been deposited.^[74]

Plasma polymerization is also receiving great attention in the biomedical field. Tetraglyme has been deposited with an atmospheric plasma torch for obtaining protein-repellent coatings,^[75] while biocompatible coatings were produced from tetraethylene glycol dimethyl ether and lactic acid.^[76] Various reviews on the use of PECVD at both low and atmospheric pressure for manifold applications have been published.^[69,77]

With the focus of research interests shifting toward sustainability, the implementation of green chemistry in coating strategies has become of primordial importance. PECVD is expected to play a key role because of its low coating material consumption, no solvent use, cost-effectiveness, adjustability, and possibility to apply complex multi-layered systems. Biogenic precursors are of key relevance in replacing fossil-based resources, while at the same time offering exciting new features for functional materials. Of special interest are precursors that not only occur in nature, but additionally show inherent special properties to be transferred to the coating, such as biodegradability or bioactivity. Other biogenic precursors have already been plasma polymerized for their electrical properties, making them suitable for organic electronic devices. However, the structures of biogenic precursors are often very complex, which increases the difficulty in tuning plasma deposition conditions to ensure structural and functionality retention as well as film stability to suit the desired applications. Post-deposition auto-oxidation processes must equally be taken into account concerning both short-term and long-term property analysis.

Obviously, the number of chemical substances that can be found in nature is extremely vast and greatly exceeds the scope of this work. In the following chapter, we will therefore focus on the most prominent biogenic chemical substance classes that have been plasma polymerized to obtain specific functionalities. An initial focus will be placed on essential oils, which are the first biobased precursors to have been plasma polymerized, followed by plant-based extractives such as terpenes, equally being essential oils' main constituents, which allow clear attribution of plasma polymer properties to individual chemical components. A second class of plasma polymerized materials are amino acids and enzymes. Here, the preservation of the required bioactive center is especially challenging. Finally, the plasma polymerization of lactic acid and its derivatives is reviewed, as these polymers are of interest due to expected ease of biodegradability.

2 | PECVD OF BIOGENIC PRECURSORS

2.1 | PECVD of essential oils

Essential oils, formed as secondary metabolites by many plants, have been extracted from natural compounds for centuries and used for example for their antiseptic properties as well as their fragrance. In modern industry, they are used in cosmetics, sanitary and medical products as well as in agriculture and food industry.^[78–80] While about 3000 different essential oils are known, only 10% are of commercial relevance. Essential oils are mixtures of about 20–60 different components, with the main groups being (1) terpenes and terpenoids as well as (2) aromatics and aliphatics, which all possess different biological properties.^[78–80] In nature, essential oils protect plants against bacteria, viruses, fungi, insects, and herbivores. They are easily available from biological sources, at low cost and in commercial quantities. On the other hand, they show very low human toxicity (i.e., harmful potential for humans).^[78–80] These factors make essential oils very interesting starting materials for new “green” functional coatings, as can be obtained through plasma polymerization (Figure 4).

The first to plasma polymerize essential oils were Sakthi Kumar et al., using **lemongrass oil** and **eucalyptus oil**. Polymerization was performed at radio frequency under reduced pressure to obtain metal-insulator-metal structures and analytics were focused on the electrical properties and conduction mechanism of the resulting thin films, which was found to be of the Schottky type in both cases.^[81,82] The eucalyptus oil plasma polymer was further examined after deposition



FIGURE 4 Examples of plants serving as sources for essential oils that have already been used for plasma polymerization.

on glass substrates using IR spectroscopy where reduction or lack of C–H and C–C bending modes indicated the formation of highly crosslinked structures. The optical band gap was found to be at 1.53 eV.^[82]

Jacob et al. initiated a wide range of investigations on the plasma polymerization of essential oils at RF power and reduced pressure with the goal of obtaining new materials for organic electronical and optical applications by plasma polymerizing **lavender oil**. Deposition times of 5–90 min at 25 W RF power enabled the preparation of transparent, very smooth films with thicknesses in the range of 200–2400 nm characterized by an energy gap of 2.93 eV, a refractive index of 1.565 (500 nm) and an extinction coefficient of 0.01 (500 nm).^[83]

Extensive research on plasma polymerized thin films from lavender oil was continued by Easton et al., wherein the influence of plasma power on the resulting films was examined. The films were deposited on precleaned glass substrates in a glow discharge at reduced pressure and at RF plasma powers ranging from 10 to 75 W. The retention of the precursor structure, especially of C=C double bonds, decreased with plasma power, while fragmentation increased.^[84] Except for the optical band gap, which was slightly higher than that observed by Jacob et al., optical parameters were found to be independent from the plasma power.^[85] Solubility tests showed the plasma polymer's insolubility in various solvents. Water contact angles ranged between 82° and 91° increasing with RF power.^[86] Aging effects were associated to oxidation and etching processes.^[87]

Al-Jumaili et al. examined the properties of plasma polymerized **geranium oil** thin films as a function of plasma power. Refractive index, extinction coefficient, and optical band gap were generally independent from the plasma power, while the surface roughness, hardness, elastic modulus, wettability, and solubility resistance increased with plasma power. A higher degree of cross-linking resulting from higher plasma powers impedes the reorientation of functionalities at the interface and increases the film rigidity, resulting in more stable contact angles over time. The authors examined the biofilm formation of *Staphylococcus aureus*, *Pseudomonas aeruginosa*, and *Escherichia coli* on films deposited at 10 and 50 W. Decreased bacterial attachment and biofilm formation on plasma polymer films deposited at 10 W as opposed to those deposited at 50 W was attributed to the combined effects of retention of the structural integrity of the bioactive precursor, surface morphology and chemistry (especially the presence of hydroxyl groups).^[88] Electrical properties were investigated by incorporating plasma polymer thin films derived from geranium oil into metal-insulator-metal sandwich structures with aluminum electrodes. The conductivity values were typical for insulating materials. The optical band gap decreased slightly from 3.67 to 3.60 eV for higher plasma powers, which was explained by the increased presence of dangling chains that might lead to formation of additional intermediate energy levels and/or defects decreasing the optical band gap.^[89]

Hennekam et al. analyzed the fragmentation occurring in the plasma phase during PECVD of **sandalwood oil** at reduced pressure and 2–50 W RF power. The gas phase was characterized using mass spectrometry (MS) and optical emission spectroscopy (OES), while the resulting films were characterized with X-ray photoelectron spectroscopy (XPS), Time-of-flight Secondary Ion MS (ToF-SIMS) and atomic force microscopy (AFM). Oligomers were formed at low plasma powers, with a relatively good stability being assigned to the bridged cyclic ring structure of santalol. With increasing RF power, hydrogen abstraction, and crosslinking were enhanced, while the incorporation of oxygen-containing groups was reduced. At the same time, an increased formation of smaller fragments was observed, which were detected for example in the form of carbon monoxide and ethylene in the plasma.^[90]

Mol et al. examined the optical absorption and emission properties of plasma polymer films made from **tea tree oil**. Depending on the irradiation wavelength, photoluminescence emissions occurred in the yellow spectral region (465–695 nm) and IR region (850–1090 nm) and were attributed to the presence of chromophore units and polaronic transitions as well as interchain emission respectively. UV-Vis absorption signals at 332 and 558 nm were attributed to C=O groups

inducing π - π^* -transitions of the aromatic ring as well as interchain π - π stacking interactions respectively. IR spectroscopy showed that band maxima shifted depending on the substrate used, indicating a variation in bond lengths depending on the substrate and showing that amorphous glass substrates are better scaffolds for plasma polymer growth than crystalline silicon substrates.^[91] Bazaka et al. were the first to examine the effects of plasma treatment with Ar APPJ on thin films from tea tree oil plasma polymers upon PET substrates. Compared to as-deposited plasma polymers, APPJ-treated plasma polymers showed increased surface oxidation, with three potential oxygen sources being: fragments of oxygen moieties from retained precursor molecules, coating exposure to ambient air and reactions between Ar plasma and ambient air. Slight changes in surface roughness were observed and primarily attributed to the removal of loosely attached low molecular weight fragments by the plasma. Contact angles decreased nonlinearly with plasma treatment from $>70^\circ$ to $\sim 57^\circ$ after 5 s and $<40^\circ$ after 60 s due to surface oxidation. The bioactivity against *S. aureus* was partially and temporarily improved due to easy release of antimicrobial low molecular weight fragments.^[92] Jacob et al. are among the researchers using PECVD for deposition of graphene from natural substances, focusing on tea tree oil as a carbon source. They produced multilayered graphene by introducing volatile tea tree oil vapors into an H_2 gas-filled plasma chamber, inside which precursor dissociation and deposition occurred at 0.2 mbar, $800^\circ C$ and 500 W RF power. The resulting films were nearly free of structural defects and mainly consisted of sp^2 - and some sp^3 -hybridized C atoms as well as some C–O bonds. The contact angle was 135° due to combined effects of material hydrophobicity and nanoscale surface morphology. Suitable electrical properties also showed the possibility to use the films as functional component in memristors.^[93]

Romo-Rico et al. compared plasma polymerization of **oregano oil** onto glass slides at reduced pressure in continuous wave and pulsed mode. Water contact angles of 45° and 7° were obtained respectively. The plasma polymers showed antibacterial activity against *S. aureus* and *P. aeruginosa* whilst supporting human dermal fibroblast adhesion.^[94]

Considering essential oil-based plasma polymers, it is important to remember that essential oils are natural products whose composition may vary from batch to batch. Results from different research works can therefore not be easily compared and may not always be entirely reproducible with materials from different suppliers or batches.

Table 1 gives an overview of frequently analyzed parameters of plasma polymerized essential oils.

TABLE 1 Plasma polymerized essential oils and commonly analyzed properties.

Precursor	Optical properties			Surface properties			Mechanical properties			Electrical properties			Water contact angle (°)	Antimicrobial properties	Literature
	Refractive index	Band gap (eV)	Extinction coefficient	Roughness average (nm)	Roughness RMS (nm)	Hardness (GPa)	Elastic modulus (GPa)	Dielectric constant	Conductivity ($\Omega^{-1}\text{m}^{-1}$)	Water contact angle (°)					
Eucalyptus oil	1.55	3.66; 1.53	0.006	-	0.2	-	-	-	-	-	-	-	-	-	[82, 95]
Geranium oil	-	3.67–3.60	-	0.23–0.60	0.30–0.77	0.63–0.85	9.39–20.61	4.40–2.10	10^{-16} – 10^{-17}	54.0–65.6	Staphylococcus aureus, Escherichia coli, Pseudomonas aeruginosa	-	-	[88, 89]	
Lavender oil	1.53–1.57	2.93–2.34	0.001	0.41–0.37	-	-	-	-	-	81–92	-	-	-	[83–85]	
Orange oil	1.55	3.60	-	0.62–1.14	0.79–1.51	0.50–0.78	-	-	-	-	-	-	-	[96]	
Oregano oil	-	-	-	-	-	-	-	-	-	45°/7°	S. aureus, P. aeruginosa	-	-	[94]	
Sandalwood oil	-	-	-	-	1.35–0.64	-	-	-	-	-	-	-	-	[90]	
Tea tree oil	-	3.19	-	-	-	-	-	-	-	-	-	-	S. aureus	[91, 92, 97]	

Note: For detailed results and deposition conditions, please be referred to the cited literature.

2.2 | PECVD of extractives

In contrast to the use of essential oils, the functionality and structure of plasma polymer thin films obtained from pure extractives can be attributed to defined precursor molecular patterns. Extensive research has been performed on the plasma polymerization of terpenes (Figure 5), which constitute 90% of the components in essential oils, and many of which are known to be antimicrobial agents.^[78,80] They can be extracted from crude essential oils and are therefore relatively easily accessible.

Very early research was performed by Linder et al. in 1931, who examined the effect of a glow discharge on 57 different hydrocarbons in the gas phase, amongst them being the terpenes limonene and pinene. Analysis of the evolution of the formation of gaseous and solid species and their chemical composition showed very similar gas compositions regardless of the original feedstock. The comparatively high amount of unsaturated species contained in most of the formed gases was attributed to relatively mild discharge conditions compared to other works of the time.^[47]

Bazaka et al. plasma polymerized **terpinen-4-ol**, a key component of tea tree oil, using a glow discharge device with RF power at reduced pressure. In agreement with comparable studies, the film thickness was found to increase with deposition time.^[98] Continuing these investigations, Kumar et al. found that the chemical structure of the films depends on the substrate temperature, because it affects the balance between adsorption and desorption on the surface, leading to the formation of different chemical functionalities and surface morphologies.^[99]

The fragmentation behavior of terpinen-4-ol in plasma was examined by Grant et al. using residual gas analysis and positive ion mode mass spectroscopy. Both techniques showed precursor fragmentation to increase

with RF power, with a significant amount of precursor being retained at relatively low plasma power up to 10 W (Figure 6).^[97]

Accordingly, the optical, physical, and chemical properties of terpinen-4-ol thin films, such as optical band gap, refractive index, extinction coefficient, hardness, chemical stability and contact angle, are tunable with plasma power. Films deposited at higher RF power showed a surface with more, narrower and sharper peaks, while there was no significant change in surface roughness parameters R_a , R_q , and R_{max} .^[55] AFM further showed the surface to be smooth and pinhole-free, indicating the polymerization to have occurred directly on the substrate surface and not in the gas phase, which would result in “dust” on the surface.^[98]

Samples were stored in ambient conditions for almost 50 days to examine the effects of aging. Refractive index measurements showed the main material property degradation to take place within the first week after deposition. Its origin was found in oxidation processes as well as volumetric relaxation in the material.^[100] Due to their relatively good retention of the precursor chemistry during the deposition process, films deposited at 10 W showed antimicrobial properties against *S. aureus* and *P. aeruginosa*, contrary to those deposited at higher plasma power.^[101] Kumar et al. were additionally able to demonstrate antifouling properties of these coatings in the marine environment for a limited period of 1 week.^[102] Jacob et al. examined the suitability of terpinen-4-ol thin films for use in flexible organic electronics by incorporating them as insulating layer in metal-insulator-metal structures and organic field-effect transistors.^[103] In this context, the films' ability to simultaneously block the transport of electrons and enable the transport of holes, which is of interest for organic light-emitting diode applications, was demonstrated.^[104]

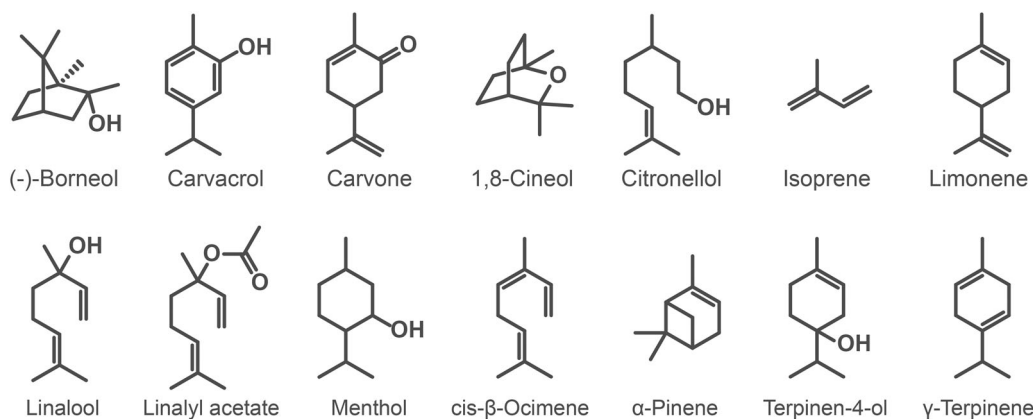


FIGURE 5 Examples of terpenes deposited via plasma-enhanced chemical vapor deposition.

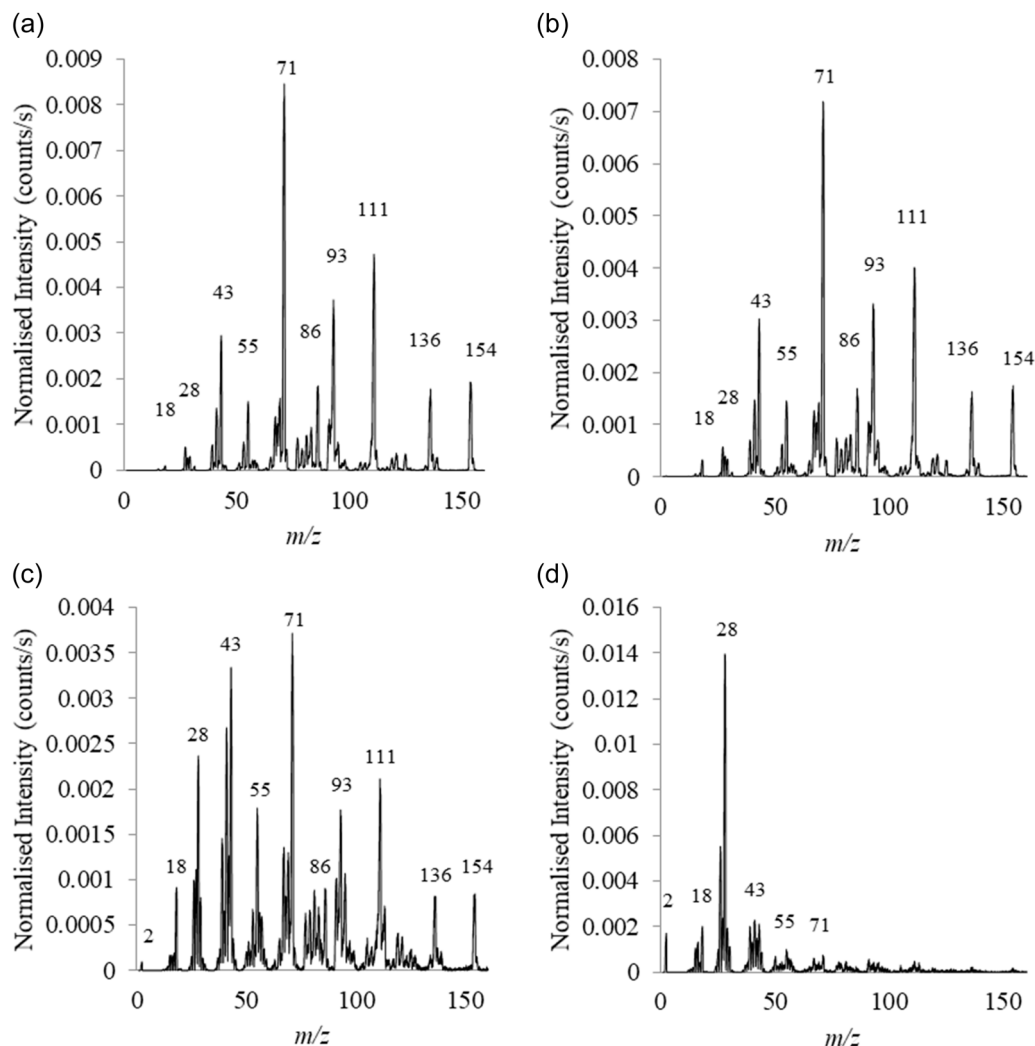


FIGURE 6 Electron impact ionization residual gas analysis mass spectra of (a) neutral terpinen-4-ol species and the plasma phase at (b) 5 W, (c) 25 W, and (d) 50 W show increased fragmentation for higher plasma powers, the peak at $m/z = 154$ representing the terpinen-4-ol monomer.^[97] Reproduced from Grant et al.^[97] (CC BY 4.0). Copyright 2021 by the authors.

While continuous wave deposition had been used previously for producing films from terpinen-4-ol, Kumar et al. used pulsed plasma deposition to decrease precursor fragmentation and functionality loss with the aim of retaining the precursor's antimicrobial activity. To this end, plasma polymers were deposited at a peak power of 10 W and four different duty cycles (10%, 20%, 40%, 100%, resulting in effective plasma power of 1 W, 2 W, 4 W, and 10 W) and a total deposition time of 15 min at reduced pressure with a pulse repetition frequency of 500 Hz. Chemical radical chain reactions were found to dominate at lower duty cycles and plasma polymerization at higher duty cycles. As a result, films deposited at higher duty cycles showed a higher degree of precursor fragmentation and crosslinking, making them more stable in contact with water. Both the highest bacterial attachment of *P. aeruginosa* due to the highest

hydrophobicity as well as the highest antimicrobial activity were detected on films deposited at 40% duty cycle.^[105]

A far more mechanistic approach was chosen by Ahmad et al., in which the fragmentation and oligomerization behavior of γ -terpinene during plasma polymerization was analyzed by gas phase MS. Precursor fragmentation was augmented with increasing plasma power, as shown by the decrease in higher molecular weight fraction peak intensities and increase in lower molecular weight fraction peak intensities. It is interesting to note that oligomeric species $[M + H]^+$ and $[2M + H]^+$ (M being the precursor molecule) were observed, with equally decreasing intensity at increasing plasma power. Ion deposition was an important part of film formation at all plasma powers, but a small amount of unfragmented precursor was also incorporated. The authors identified a

number of fragments and suggested fragmentation pathways (Figure 7).^[106]

To evaluate the suitability of plasma polymers from plant-derived secondary metabolites as encapsulation materials for organic photovoltaics, γ -terpinene was plasma polymerized at different deposition rates onto glass substrates and onto organic solar cells, respectively, followed by investigation of the stability of the resulting films under UV irradiation. Encapsulation of the solar cell with plasma-deposited γ -terpinene led to a significantly slower decrease in device efficiency. UV irradiation-induced degradation of the plasma polymer thin films manifested itself in photooxidation of the films with the degradation pathway and velocity depending on the UV light wavelength and dose.^[107]

Getnet et al. examined the suitability of **carvacrol**-based plasma polymers deposited in atmospheric pressure dielectric barrier discharge as antimicrobial coatings for stainless steel, which is frequently used as an implant and prosthetics material in underdeveloped countries. They observed antibacterial activity against *E. coli*, *S. aureus*, *P. aeruginosa*, and *C. albicans*. Good antimicrobial activity was attributed to high hydroxyl content, surface roughness, and hydrophilicity. The coatings were further stable under UV light irradiation for 1 h and to air exposure for 120 days and reduced the corrosion rate of the underlying steel substrate.^[108,109]

Antibacterial properties of **1,8-cineole** plasma polymer films deposited at reduced pressure and 20 W RF power were examined by Pegalajar-Jurado et al. *S. aureus* and *E. coli* attachment to 1,8-cineole plasma polymer coated glass slides were reduced by 63% and 98% respectively compared to hydrophilic glass slides. No leaching of bioactive substances from the films into the media was observed. Preliminary experiments also indicated that neither the plasma polymer films nor potential leachables were harmful to mammalian cells.^[110]

Mann et al. closely correlated surface properties and antibacterial activity of plasma polymerized 1,8-cineole films while varying plasma power (50–150 W) and pressure (15–100 mTorr). The plasma phase was analyzed with OES, while the film surface chemistry

was examined with XPS and IR spectroscopy. Increasing pressure leads to less oxygen incorporation in form of alcohol/ether/carbonyl functionalities. Water contact angles correspondingly ranged from $(54.3 \pm 4.1)^\circ$ to $(85.6 \pm 1.1)^\circ$. Bacterial attachment assays showed decreased bacterial attachment and growth for *E. coli* after 24 h incubation and 5-day incubation compared to reference samples (Figure 8).^[111]

By plasma polymerization of **carvone**, Chan et al. deposited films with an average surface roughness R_a of 0.11 nm and a water contact angle of 78.8° on glass substrates. IR spectroscopy indicated that the ring structure of the precursor was destroyed by fragmentation. Bacterial adherence of *E. coli* and *S. aureus* was decreased compared to untreated glass coverslips, along with bacterial growth which was reduced by over 80%. No cytotoxicity toward human cells was observed.^[112]

Tone et al. compared the suitability of different plasma polymerized terpenes, namely **L-menthol**, **(S)-(-)- β -citronellol**, **(1S)-(-)-borneol**, and **R-limonene** for ultrafiltration membranes made from cellulose acetate for separation of racemic amino acids. They found that the coating deposition not only depends on deposition time, but also on the precursor structure and reactivity, with ring tension and double bonds leading to increased deposition rates. All membranes showed similar partition coefficients toward separation of racemic amino acid mixtures. When comparing membranes with the same degree of coating fixation at the same volume flux, those with citronellol-based coatings showed the highest separation factor.^[113]

Research toward production of synthetic rubber thin films has been performed by Gürsoy et al. by plasma polymerizing **isoprene** at reduced pressure and 5–35 W RF power. The characterization of the obtained films showed a basically good preservation of the precursor structure together with a decrease of the C=C double bond content. The stretching resistance of plasma polymerized isoprene deposited on an elastomer was evaluated using contact angle measurements and the material was shown to withstand up to 1000 stretching cycles of 25% elongation and showed only small contact angle decreases at 125% elongation. Plasma polymerized

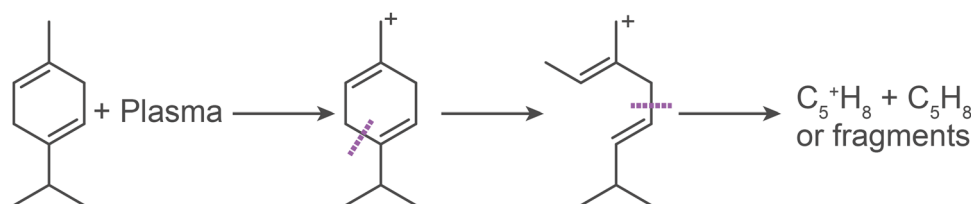


FIGURE 7 One exemplary step of the fragmentation pathway for γ -terpinene during plasma polymerization as suggested by Ahmad et al. Reproduced and adapted with permission from Ahmad et al.^[106] © 2015 WILEY-VCH Verlag GmbH & Co. KGaA, Weinheim.

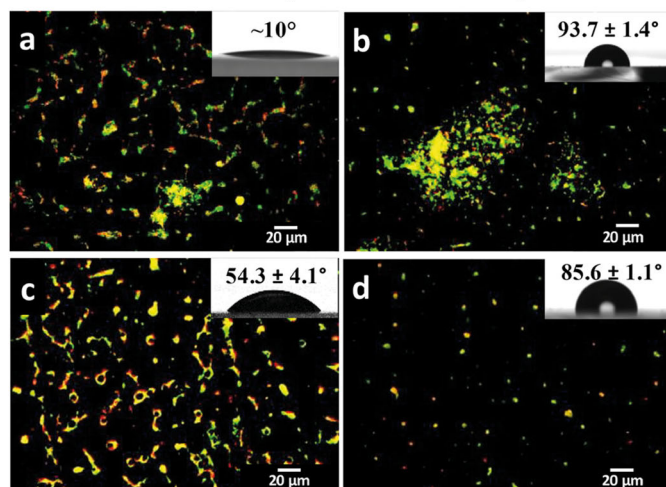
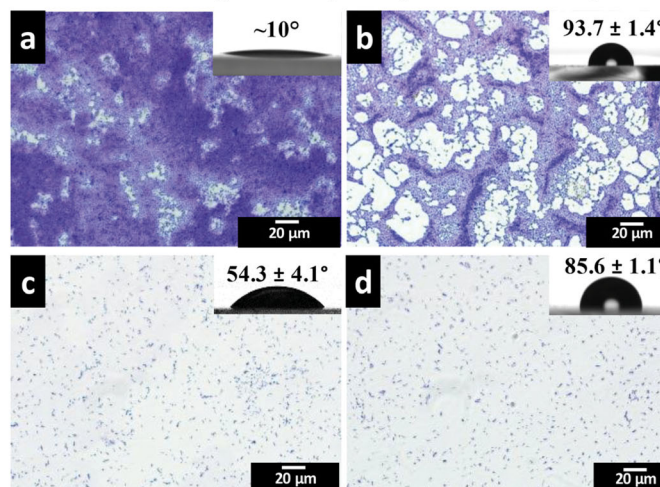
E. coli attachment (24 h incubation)*E. coli* biofilm growth (5 days incubation)

FIGURE 8 Fluorescence microscopy images (left, viable attached bacteria depicted in green, dead ones in red) and bright field microscopy images (right, samples stained with crystal violet) presented by Mann et al. show the attachment of *Escherichia coli* after 24 h and 5 days respectively on (a) control glass slides, (b) reference glass slides coated with plasma polymerized 1,8-octadiene, (c, d) plasma polymerized 1,8-cineole (low and high pressure and plasma power). Adapted with permission from Mann and Fisher.^[111] Copyright 2017 American Chemical Society.

isoprene deposited on bamboo fibers showed contact angles of up to 146.8° that could be maintained after three washing cycles with liquid detergent for 30 min each.^[114]

Further terpenes that have been used for plasma deposition are linalool,^[115] cis- β -ocimene,^[116] D-limonene,^[117] and linalyl acetate.^[118] Table 2 presents an overview of plasma polymerized terpenes and their commonly examined properties.

To the best of our knowledge, the only nonterpene extractive that has been plasma polymerized so far is **eugenol**. In line with their research of antimicrobial coatings based on carvacrol for steel-based implants, Getnet et al. plasma polymerized eugenol on a stainless steel substrate in an atmospheric pressure dielectric barrier discharge at effective discharge powers of around 1.2 W. At these conditions, the electron temperature was 1.5 eV assuming LTE. Initially, the film thickness increased with the applied voltage until ablation processes eventually dominated over deposition. No significant precursor fragmentation was observed in OES. IR spectroscopy of the plasma polymer film revealed that the aromatic and hydroxyl functions were retained, but the vinyl groups disappeared, and ketone groups were formed, the latter possibly due to oxidation processes after deposition. By means of IR spectroscopy, it was further demonstrated that the films are resistant to aging for 120 days in air and under UV irradiation. *S. aureus* and *E. coli* adhesion was reduced by 78% and 65% on these surfaces.^[125] Antibacterial properties were equally

observed for *P. aeruginosa* and *C. albicans*, as were anticorrosive effects.^[109]

2.3 | PECVD of amino acids

Contrary to essential oils, which only occur in plants, amino acids can be found in all living beings. Apart from plasma-assisted two-step functionalization approaches in which suitable anchor groups are first placed on the surface and the amino acids are subsequently grafted on, direct deposition is possible, even if it results in less defined layers. Alongside some work that has used sputtering techniques for direct deposition of amino acids,^[126] PECVD of histidine and tyrosine has already been described.

For biometallization, Anderson et al. used PECVD to deposit coatings from **tyrosine** on silicon wafers, PET, and cellulose nitrate substrates. Tyrosine was chosen for its ability to reduce noble metal nanoparticles such as gold from solution and bind them onto surfaces. The precursor was transferred into the gas phase via sublimation at up to 300°C in the PECVD chamber at reduced pressure followed by deposition at 60 W RF power. The obtained plasma polymer films were optically transparent in the visible wavelength range, resistant to mechanical stress and tolerated immersion in the aqueous gold chloride solution. IR spectroscopy confirmed crosslinking with high retention of tyrosine monomer functionality required for gold reduction. The

TABLE 2 Plasma polymerized terpenes and commonly analyzed properties.

Precursor	Optical properties			Surface properties		Mechanical properties			Electrical properties			Water contact angle (°)	Antimicrobial properties	Literature
	Refractive index	Band gap (eV)	Extinction coefficient	Roughness average (nm)	Roughness RMS (nm)	Hardness (GPa)	Elastic modulus (GPa)	Dielectric constant	Conductivity ($\Omega^{-1}\text{m}^{-1}$)					
1,8-Cineole	1.543	2.83	0.001	0.39	≤50	-	-	-	-	-	77–90	<i>Escherichia coli</i> , <i>Staphylococcus aureus</i>	[110, 111, 119]	
Carvacrol	-	-	-	200–800	-	-	-	-	-	-	25–55	<i>E. coli</i> , <i>S. aureus</i> , <i>Pseudomonas aeruginosa</i> , <i>Candida albicans</i>	[108, 109]	
Carvone	-	-	-	0.11	0.14	-	-	-	-	-	78.8	<i>E. coli</i> , <i>S. aureus</i>	[112]	
Cis- β -ocimene	1.58	2.85	-	-	<1	-	-	3.5–3.6	10^{-12} – 10^{-11}	-	94.14	-	[116, 120]	
Limonene	-	-	-	0.48	-	-	-	-	-	-	-	-	[117]	
Linalool	1.55	2.64–2.82	0.001	0.44	-	-	-	-	-	-	76–80	-	[115, 121]	
Linalyl acetate	ca. 1.56	2.95–3.02	-	0.19–0.21	-	0.30–0.44	-	2.39–2.43; 3–3.5	10^{-11}	-	85.7	-	[118, 120, 122]	
Terpinen-4-ol	1.55	2.67	0.0007	0.33–0.44	0.42–0.56	0.33–0.51	-	3.4	-	-	63–69	<i>P. aeruginosa</i> , <i>S. aureus</i>	[55, 98, 100, 101, 103, 123]	
γ -Terpinene	1.57–1.58	3	-	0.21–0.30	0.30–0.39	0.40–0.58	4.22–5.69	3.24–3.69	10^{-13} – 10^{-12}	-	61–81	-	[124]	

Note: For detailed results and deposition conditions, please refer to the cited literature.

deposition of a patterned tyrosine PECVD coating was achieved successfully as well and enabled the selective growth of gold nanoparticles on the substrate surface.^[127] Tyrosine was also used to investigate the plasma “copolymerization” of amino acids with other organic and inorganic monomers frequently used in synthetic materials, showing the possibility to obtain biologically active coatings by incorporating biomolecules into organic or inorganic matrices with the help of plasma deposition methods.^[128]

Histidine was plasma polymerized by Anderson et al. onto single crystal Si wafers and 3D substrates as a precursor for enabling titania reduction and nanoparticle growth directly on the substrate. Histidine was transferred into the gas phase by sublimation at 200°C at reduced pressure, followed by plasma deposition at 50 W RF power. Immersion of the resulting film in water lead to partial dissolution, whilst the remainder of the coating was sufficient for titania reduction. IR spectroscopy showed sufficient monomer structure retention to enable titania nanoparticle formation. The latter was successful on Si wafers with a surface coverage of ~75% as well as on 3D substrates, indicating a potential use in tailoring photonic structures and creating hybrid organic-inorganic multilayer systems with highly varying refractive indexes.^[129]

2.4 | PECVD of proteins

When it comes to the matter of functionality retention across the plasma polymerization process, there is one class of biogenic substances posing even more challenges than those discussed previously: Proteins and enzymes are biological macromolecules consisting of amino acids linked by peptide bonds which possess highly specific functionalities closely linked to their structure. This leads to the double challenge of not only preserving functional

groups, but also the bonding sites and cavities linked to biological functionality.

Heyse et al. investigated the deposition of sprayed liquid precursors at very mild plasma conditions and atmospheric pressure to obtain maximum retention of the precursor structure and functionality for protein plasma deposition.^[130] By dissolving the precursors in an aqueous carrier solution followed by atomization, they were able to deposit precursors within a polymer matrix produced by the carrier gas (C_2H_2 or pyrrole), a method referred to as aerosol-assisted PECVD (AA-PECVD) (Figure 9). The water shell formed around the precursors makes the droplets act as shuttles while serving as protection against reactions with the plasma. This enables deposition of intact proteins within the growing polymer network, and for enzymes additionally preserves their catalytic activity.^[131]

Using this method, the authors were the first who immobilized proteins in organic coatings in a single-step procedure, by simultaneously polymerizing proteins and acetylene in an atmospheric pressure dielectric barrier discharge. They used fluorescein-isothiocyanate labeled **bovine serum albumin** (BSA-FTIC) and **allophycocyanin**, an auto-fluorescent protein found in cyanobacteria and red algae. Confocal and fluorescence microscopy proved a homogeneous fluorescence distribution, contrary to aggregate formation observed by conventional protein immobilization procedures. The autofluorescence of allophycocyanin further enabled proving successful intact molecule entrapment as its fluorescence emission is strongly dependent on retention of its quaternary structure (Figure 10).^[132] Apart from the allophycocyanin protein, the authors further deposited **glucose oxidase**, **lipase**, and **alkaline phosphatase** enzymes using plasma.^[131]

Alkaline phosphatase was also embedded into plasma polymer matrices from acetylene and pyrrole by Ortore et al., using an enzyme buffer solution aerosol and

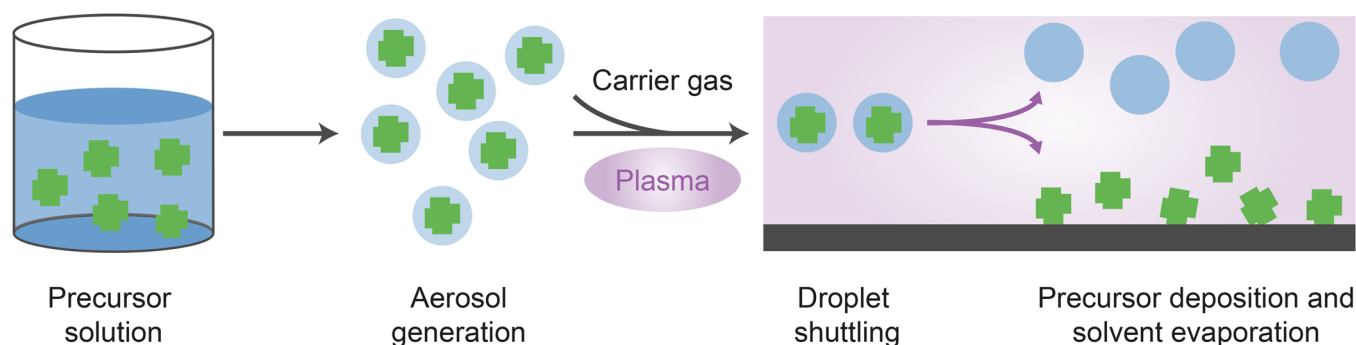


FIGURE 9 Illustration of the principle of aerosol-assisted plasma-enhanced chemical vapor deposition showing the water droplets functioning as shuttles protecting the proteins during plasma deposition.

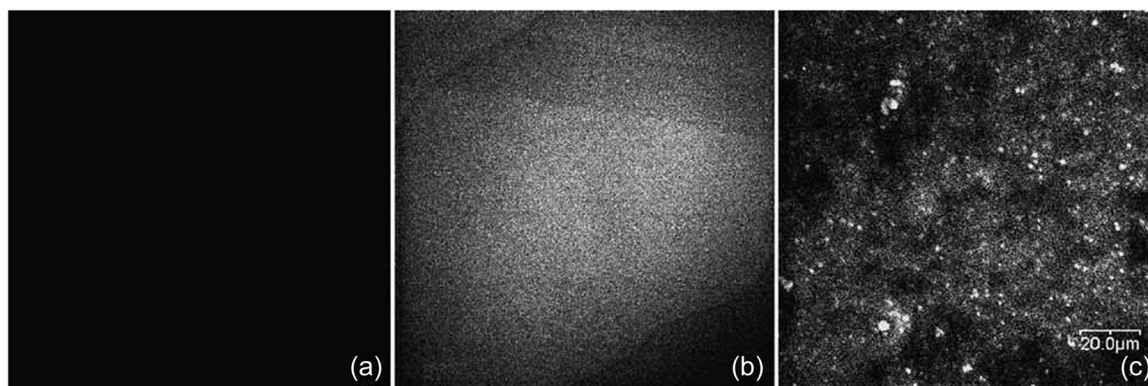


FIGURE 10 Fluorescence microscopy images prove the preservation of the fluorescent structure of BSA-FITC after plasma deposition by showing (a) pure plasma polymerized acetylene coating, (b) plasma polymerized BSA-FITC with acetylene, and (c) covalently immobilized BSA-FITC on glass as reference. Reproduced with permission from Heyse et al.^[132] © 2008 WILEY-VCH Verlag GmbH & Co. KGaA, Weinheim.

atmospheric pressure DBD plasma polymerization. Grazing-incidence small X-ray scattering (GISAXS) was established as a new method to analyze the scattering patterns of the plasma polymer taking into account the various contributions from the polymer matrix and the embedded enzyme. This new technique enabled proving the protein incorporation and determining their concentration as well as the microdomain size.^[133]

Palumbo et al. used the AA-PECVD technique to deposit films consisting of a plasma polymerized ethylene matrix with incorporated aqueous **lysozyme** solution using a DBD reactor. The authors were the first to examine the integrity of the embedded enzymes and the potential damage occurring during plasma deposition using Matrix-Assisted Laser Desorption/Ionization Time-of-Flight (MALDI-ToF), using α -cyano-4-hydroxycinnamic acid as matrix, and high-pressure liquid chromatography (HPLC) release monitoring. Both analytical methods indicated the absence of smaller peptide/protein fractions, meaning no substantial damage took place during plasma polymerization. The peaks for the intact lysozyme molecule were present, although somewhat widened compared to the reference, indicating that on individual lysozyme amino acids some limited degradation or modification reactions occurred in the plasma phase. The retention of the lysozyme biological activity could nevertheless be confirmed by the agar diffusion test. The release from the coating into water was found to occur within 1 day, making the material interesting for applications in drug delivery.^[134]

The principle of AA-PECVD was combined with an APPJ producing corona discharge by Malinowski et al. to deposit **laccase**, an oxidoreductase enzyme forming part of the biosynthesis in plants, insects, fungi, and bacteria. Bioactivity was found to be retained to a greater extent

than in coatings deposited by conventional methods, due to monomer crosslinking and covalent binding to the glass surface. Reduction of bioactivity compared to the untreated laccase enzyme was attributed to the fragmentation of monomers during the plasma process. It was found that reactions with the plasma mainly occur in the outer region of the protein while the center of the molecule remains unaffected.^[135] The applicability of this method for producing laccase-based biosensors from corona discharge was found to be promising, as it could greatly decrease biosensor construction times compared to conventional methods while maintaining comparability of analytical parameters.^[136] The authors further examined the binding mechanism of laccase during corona jet plasma deposition onto graphene. They demonstrated that laccase is both polymerized and simultaneously bound to solid substrates. Preservation of the molecule's active center allowed the coating to retain its bioactivity.^[137]

Further enzymes and proteins polymerized via AA-PECVD in DBD include **lipase**,^[138] **elastin**,^[139] and **collagen**.^[140,141] An overview of plasma polymerization of proteins and enzymes is given in Table 3.

2.5 | PECVD of lactic acid-based precursors

Besides the large groups of essential oils and their components as well as proteins and their components, there is a great variety of other biogenic molecules that have been used for plasma polymerization, which cannot all be cited here. The most prominent group, and therefore the only one that we will focus on, is certainly that of lactic acid and its derivatives. Poly(lactic acid) has

TABLE 3 Plasma-polymerized proteins and (potential) applications thereof.

Precursor	Deposition device	Carrier gas/matrix gas	(Potential) Applications	Literature
Alkaline phosphatase	Dielectric barrier discharge (DBD)	He/Acetylene, pyrrol	Analytics	[133]
Allophycocyanine	DBD	He/Acetylene	Protein immobilization	[132]
BSA	DBD	He/Acetylene	Protein immobilization	[132]
	DBD	He/Ethylene	Biosensors	[142]
Collagen	Custom-built	He	Polystyrene labware	[140]
	Custom-built	He	Wound treatment	[141]
Elastin	DBD	He, N ₂ /Lactic acid solution	Bioactive biodegradable surfaces	[139]
Laccase	Atmospheric pressure plasma jet	He	Biocoatings, biosensors	[135–137]
Lipase	DBD	He/Ethylene	Protein immobilization	[138]
Lysozyme	DBD	He/Ethylene	Drug delivery	[134]
	DBD		Protein immobilization	[143]

recently been of great interest to the scientific community due to its biogenic origin, biocompatibility in application and biodegradability.

Pistillo et al. deposited **L-lactic acid** at reduced pressure in a radio frequency discharge by sublimating the precursor at 110°C, with plasma power from 2 to 150 W and deposition times of 2–80 min. Plasma power was the key parameter influencing the chemical structure, as shown by previously mentioned studies. Successful deposition of COOH-rich coatings at low plasma power that were stable in water showed the material's potential for use as a platform for cell cultures.^[144]

Another method, plasma-assisted vapor thermal deposition (PAVTD) was used by Krtous et al. for depositing thin films from **poly(lactic acid)** (PLA). A polymer is used as a precursor and heated at reduced pressure to its chain decomposition temperature. The resulting species are then activated and fragmented by a plasma initiating polymerization. PAVTD is considered to yield polymers with properties intermediate between those of a conventional polymer and those of a plasma polymer obtained by PECVD. In agreement with studies already mentioned, it was found for PLA that the structural integrity of the precursor decreases with increasing deposition power, as films deposited at higher plasma powers showed a decreased oxygen and increased methyl and ether group content. The average amount of intact PLA chain units was up to 4 for films deposited at low powers. At increasing powers, the PLA unit chain length decreases down to almost monomeric lactic acid units that are statistically separated by CH₃/CH₂ or other groups. The resulting polymer network can be described as a statistical block-copolymer network from PLA, hydrocarbon units, and poly(ethylene-oxide)-like units,

which confirms the ability of PAVTD to combine both characteristics of conventional polymerization and PECVD.^[145] Plasma polymerized poly(lactic acid) coatings further showed controlled drug release properties and biodegradability, making the material highly interesting as a platform for biomedical devices. The drug release was studied using nisin, an antibacterial peptide, showing a clear relationship with the discharge power. At low powers, nisin passed through micro-scale pores, and drug release was delayed for hours or days, while at high powers, the drug was released within minutes through buckling instabilities. Bactericidal activities against *M. luteus* correlated with the observed drug release kinetics.^[146]

Ligot et al. found that plasma power has the greatest influence among plasma deposition parameters on **ethyl lactate** plasma polymers deposited at reduced pressure. XPS and chemical derivatization experiments showed that higher power leads to increased fragmentation of the precursor and a consequential decrease in COOX functionalities. At the same time, ToF-SIMS and mechanical profilometry demonstrated a higher degree of crosslinking for polymers deposited under these conditions. Tuning the degree of crosslinking, the water/gas diffusion rate and the amount of ester bonds via controlling the plasma parameters shows the potential to enable the precise design of (bio)degradable barrier coatings.^[147] Moreover, films with a higher degree of crosslinking show improved mechanical properties such as hardness, viscoelastic recovery (i.e., self-healing ability), creep, wear, and fracture resistance since plastic contributions (e.g., viscoplasticity) decrease.^[148] In addition, the ester content within the plasma phase was examined by combining residual gas analysis mass

spectroscopy with in situ FTIR spectroscopy and Density Functional Theory calculations. It was shown that an increase in plasma power generally leads to a decrease in ester species in both the plasma and the resulting polymer.^[149]

Furthermore, Nisol et al. investigated the energetic parameters of atmospheric PECVD of ethyl lactate in a DBD reactor. Plasma polymers with energies per molecule ranging from 21 to 42 eV/molecule and varying amounts of ester functionalities and crosslinking were observed. The degradation rate of these polymers in aqueous media could likewise be predicted from employed flow rates and resulting energies per molecule.^[150]

The influence of the carrier gas on the resulting plasma polymer was shown by Laurent et al. in a study on plasma polymerized ethyl lactate deposited in an atmospheric pressure dielectric barrier discharge using either N₂ or Ar as carrier gas. They found that polymers deposited with N₂ carrier gas mainly contain isolated hydrophilic functionalities leading to fast degradation in aqueous environments. Polymers deposited with Ar carrier gas not only degrade more slowly, corresponding more closely to the behavior of conventional lactide-based polymers, but additionally show a greater structural retention of the ethyl lactate precursor and are mainly composed of a hydrocarbon structure containing comparably low amounts of ester moieties.^[151]

Different dielectric barrier discharge modes at atmospheric pressure have been examined by Milaniak et al., who compared the deposition characteristics of ethyl lactate in PECVD in the glow and filamentary dielectric barrier discharge using FTIR spectroscopy. The degree of polymerization, homogeneity, and competition between deposition and etching depend on the discharge mode. The deposition further depends on bond dissociation energies and fragment stability, as stable fragments and bonds with high dissociation energies are best preserved.^[152]

Overall, the precise inquiry into the process of plasma polymerization of lactic acid derivatives may lead toward new functional polymers with both tunable ester content and biodegradability.

3 | CONCLUSION AND FUTURE CHALLENGES

Plasma polymer coatings derived from natural precursors show exciting potential for application in biomedicine, organic electronics, packaging, and many more areas. Fundamental research has proven basic applicability and properties in laboratory conditions and at small scales.

However, for real-life use, process adaption to industrial scales remains a challenge, as many devices still operate at low pressures or can only treat small areas. To make use of PECVD's low chemical consumption, molecules need sufficient volatility for easy transfer into the gas phase, which greatly restricts the precursor choice. For biomedical applications, further insight into compatibility with human organisms is required, while for packaging solutions, biodegradability and barrier properties need to be explored in more detail. At the same time, model substrates must be replaced by scaffolds relevant to applications, which is often challenging due to manifold interactions between substrates and plasma. Further, to date results obtained by plasma polymerization strongly depend on the choice of plasma device and can hardly be considered universally applicable. Better chemically defined deposition could be achieved by combining plasma polymerization by techniques suitable for separation into single molecules such as electrospraying. While proof of concept experiments focusing on applications have been performed, there is still little insight into the actual processes occurring in the plasma phase and during the polymerization process. The influence of individual plasma parameters, precursor functionality, and polymerization mechanisms are poorly understood and polymer structural characterization remains an unsolved challenge. Gas phase analysis and structural elucidation combining conventional or inventing new analytical methods therefore is imperative to understanding structure–property relationships and to selecting the most suitable precursors with respect to the desired applications. In-depth examination of the auto-oxidation process and the resulting matter of long-term consistency of physicochemical properties additionally needs to be conducted. In the field of biogenic precursors, these challenges are intensified by the natural variance in the already complex material composition and properties. Nonetheless, biogenic precursors remain of indispensable importance for replacing non-regenerative, fossil-based resources. Ultimately, low material consumption of plasma deposition is a key factor in the implementation of sustainable, green chemistry processes. Plasma polymerization of biogenic precursors can therefore be expected to play a leading part in future coating applications.

AUTHOR CONTRIBUTIONS

Amelia Loesch-Zhang was involved in investigation and writing—original draft. Amelia Loesch-Zhang and Andreas Geissler were involved in conceptualization. All authors were involved in writing—reviewing and editing. Andreas Geissler and Markus Biesalski were involved in supervision.

ACKNOWLEDGMENTS

This study was funded as part of the BioPlas4Paper project by Agency for Renewable Resources (Fachagentur Nachwachsende Rohstoffe e.V.—FNR), grant number 2220HV017A. The authors would like to thank Martin Bellmann, Dennis Marvin Janek Moeck, and Joern Appelt for fruitful discussions. Open Access funding enabled and organized by Projekt DEAL.

CONFLICT OF INTEREST STATEMENT

The authors declare no conflict of interest.

DATA AVAILABILITY STATEMENT

Not applicable.

ORCID

Andreas Geissler  <http://orcid.org/0000-0002-4284-7942>

REFERENCES

- [1] L. Tonks, *Am. J. Phys.* **1967**, 35, 857.
- [2] R. Jafari, S. Asadollahi, M. Farzaneh, *Plasma Chem. Plasma Process.* **2013**, 33, 177.
- [3] U. Stroth, *Plasmaphysik*, Springer, Berlin, Heidelberg, **2018**.
- [4] A. Fridman, A. Chirokov, A. Gutsol, *J. Phys. D Appl. Phys.* **2005**, 38, R1.
- [5] H. Conrads, M. Schmidt, *Plasma Sources Sci. Technol.* **2000**, 9, 441.
- [6] F. Dene, *Prog. Polym. Sci.* **2004**, 29, 815.
- [7] C. Tendero, C. Tixier, P. Tristant, J. Desmaison, P. Leprince, *Spectrochim. Acta Part B* **2006**, 61, 2.
- [8] (a) A. Rutscher, H. Deutsch, *Plasmatechnik. Grundlagen und Anwendungen; eine Einführung*, Hanser, München **1984**; (b) N. S. J. Braithwaite, *Plasma Sources Sci. Technol.* **2000**, 9, 517.
- [9] H. V. Boenig, *Plasma Sci. Technol.*, **1982**, 16.
- [10] B. Eliasson, U. Kogelschatz, *IEEE Trans. Plasma Sci.* **1991**, 19, 1063.
- [11] L. Bárdos, H. Baránková, *Thin Solid Films* **2010**, 518, 6705.
- [12] A. A. Fridman, *Plasma Chemistry*, Cambridge University Press, Cambridge, **2012**.
- [13] U. Kogelschatz, *Plasma Phys. Control. Fusion* **2004**, 46, B63.
- [14] A. Bogaerts, E. Neyts, R. Gijbels, J. van der Mullen, *Spectrochim. Acta Part B* **2002**, 57, 609.
- [15] W. Siemens, *Annalen der Physik und Chemie* **1857**, 178, 66.
- [16] U. Kogelschatz, *IEEE Trans. Plasma Sci.* **2002**, 30, 1400.
- [17] U. Kogelschatz, *Contrib. Plasma Phys.* **2007**, 47, 80.
- [18] U. Kogelschatz, *Plasma Chem. Plasma Process.* **2003**, 23, 1.
- [19] B. Eliasson, U. Kogelschatz, *IEEE Trans. Plasma Sci.* **1991**, 19, 309.
- [20] M. Laroussi, T. Akan, *Plasma Process. Polym.* **2007**, 4, 777.
- [21] A. Schutze, J. Y. Jeong, S. E. Babayan, P. Jaeyoung Park, G. S. Selwyn, R. F. Hicks, *IEEE Trans. Plasma Sci.* **1998**, 26, 1685.
- [22] D. D. Pappas, *J. Vac. Sci. Technol. A* **2011**, 29, 20801.
- [23] D. Merche, N. Vandencastele, F. Reniers, *Thin Solid Films* **2012**, 520, 4219.
- [24] H. Kakiuchi, H. Ohmi, K. Yasutake, *J. Vac. Sci. Technol. A* **2014**, 32, 30801.
- [25] F. Massines, C. Sarra-Bournet, F. Fanelli, N. Naudé, N. Gherardi, *Plasma Process. Polym.* **2012**, 9, 1041.
- [26] J. Y. Jeong, S. E. Babayan, V. J. Tu, J. Park, I. Henins, R. F. Hicks, G. S. Selwyn, *Plasma Sources Sci. Technol.* **1998**, 7, 282.
- [27] O. V. Penkov, M. Khadem, W.-S. Lim, D.-E. Kim, *J. Coat. Technol. Res.* **2015**, 12, 225.
- [28] (a) S. Förster, C. Mohr, W. Viöl, *Surf. Coat. Technol.* **2005**, 200, 827; (b) H. Koinuma, H. Ohkubo, T. Hashimoto, K. Inomata, T. Shiraishi, A. Miyana, S. Hayashi, *Appl. Phys. Lett.* **1992**, 60, 816; (c) M. Laroussi, X. Lu, *Appl. Phys. Lett.* **2005**, 87, 113902; (d) C. Cheng, Z. Liye, R.-J. Zhan, *Surface Coat. Technol.* **2006**, 200, 6659.
- [29] M. Bellmann, C. Ochs, M. Harms, W. Viöl, *DE102016209097A1*, **2016**.
- [30] (a) S. Bekeschus, P. Favia, E. Robert, T. von Woedtke, *Plasma Process. Polym.* **2019**, 16, 1800033; (b) R. Brandenburg, A. Bogaerts, W. Bongers, A. Fridman, G. Fridman, B. R. Locke, V. Miller, S. Reuter, M. Schiorlin, T. Verreycken, K. Ostrikov, *Plasma Process. Polym.* **2019**, 16, 1700238; (c) U. Cvelbar, J. L. Walsh, M. Černák, H. W. de Vries, S. Reuter, T. Belmonte, C. Corbella, C. Miron, N. Hojnik, A. Jurov, H. Puliyalil, M. Gorjanc, S. Portal, R. Laurita, V. Colombo, J. Schäfer, A. Nikiforov, M. Modic, O. Kylian, M. Polak, C. Labay, J. M. Canal, C. Canal, M. Gherardi, K. Bazaka, P. Sonar, K. K. Ostrikov, D. Cameron, S. Thomas, K. Weltmann, *Plasma Process. Polym.* **2019**, 16, 1700228; (d) M. Šimek, M. Černák, O. Kylián, R. Foest, D. Hegemann, R. Martini, *Plasma Process. Polym.* **2019**, 16, 1700250.
- [31] R. d'Agostino, P. Favia, C. Oehr, M. R. Wertheimer, *Plasma Process. Polym.* **2005**, 2, 7.
- [32] E. M. Liston, L. Martinu, M. R. Wertheimer, *J. Adhes. Sci. Technol.* **1993**, 7, 1091.
- [33] (a) A. Holländer, R. Wilken, J. Behnisch, *Surf. Coat. Technol.* **1999**, 116-119, 788; (b) J. Katz, S. Gershman, A. Belkind, *Plasma Med.* **2015**, 5, 223.
- [34] P. Chu, *Mater. Sci. Eng. R Rep.* **2002**, 36, 143.
- [35] (a) D. Mariotti, A. C. Bose, K. Ostrikov, *IEEE Trans. Plasma Sci.* **2009**, 37, 1027; (b) H. Puliyalil, U. Cvelbar, *Nanomaterials*, **2016**, 6, 108.
- [36] (a) A. Vesel, M. Mozetic, *J. Phys. D Appl. Phys.* **2017**, 50, 293001; (b) J. M. Grace, L. J. Gerenser, *J. Dispers. Sci. Technol.* **2003**, 24, 304; (c) C.-M. Chan, T.-M. Ko, H. Hiraoka, *Surf. Sci. Reports.* **1996**, 24, 1.
- [37] T. Desmet, R. Morent, N. de Geyter, C. Leys, E. Schacht, P. Dubruel, *Biomacromolecules* **2009**, 10, 2351.
- [38] (a) K. Schröder, A. Meyer-Plath, D. Keller, W. Besch, G. Babucke, A. Ohl, *Contrib. Plasma Phys.* **2001**, 41, 562; (b) J. Friedrich, *Rev. Adhes. Adhes.* **2018**, 6, 253.
- [39] (a) S.-H. Gao, M.-K. Lei, Y. Liu, L.-S. Wen, *Appl. Surf. Sci.* **2009**, 255, 6017; (b) R. Barni, C. Riccardi, E. Selli, M. R. Massafra, B. Marcandalli, F. Orsini, G. Poletti, L. Meda, *Plasma Process. Polym.* **2005**, 2, 64; (c) M. R. Sanchis, V. Blanes, M. Blanes, D. Garcia, R. Balart, *Eur. Polym. J.* **2006**, 42, 1558.

- [40] K. Bazaka, M. V. Jacob, R. J. Crawford, E. P. Ivanova, *Acta Biomater.* **2011**, 7, 2015.
- [41] Y. Ferreira da Silva, V. M. Queiroz, I. C. S. Kling, B. S. Archanjo, R. N. Oliveira, R. A. Simao, *Plasma Process. Polym.* **2020**, 17, 2000035.
- [42] (a) M.-C. Popescu, M. Totolin, C. M. Tibirna, A. Sdrobis, T. Stevanovic, C. Vasile, *Int. J. Biol. Macromol.* **2011**, 48, 326; (b) L. Cabrales, N. Abidi, *Appl. Surf. Sci.* **2012**, 258, 4636.
- [43] S. Sousa, C. Gaiolas, A. P. Costa, C. Baptista, M. E. Amaral, *Cell. Chem. Technol.* **2016**, 50, 711.
- [44] C. Gaiolas, M. N. Belgacem, L. Silva, W. Thielemans, A. P. Costa, M. Nunes, M. J. Santos Silva, *J. Colloid Interface Sci.* **2009**, 330, 298.
- [45] H. Biederman, *Plasma Polymer Films*, Imperial College Press, London, **2004**.
- [46] G. S. Schoepfle, L. H. Connell, *Indust. Eng. Chem.* **1929**, 21, 529.
- [47] E. G. Linder, A. P. Davis, *J. Phys. Chem.* **1931**, 35, 3649.
- [48] (a) H. König, G. Helwig, *Zeitschrift für Physik.* **1951**, 129, 491-503; (b) R. H. Hansen, H. Schonhorn, *J. Polym. Sci. Part B Polym. Lett.* **1966**, 4, 203; (c) T. Williams, M. W. Hayes, *Nature* **1966**, 209, 769; (d) A. R. Denaro, P. A. Owens, A. Crawshaw, *Eur. Polym. J.* **1968**, 4, 93; (e) A. R. Westwood, *Eur. Polym. J.* **1971**, 7, 363; (f) H. Yasuda, *J. Polym. Sci., Part D Macromol. Rev.* **1981**, 16, 199; (g) H. Kobayashi, A. T. Bell, M. Shen, *Macromolecules* **1974**, 7, 277.
- [49] J. Goodman, *J. Polym. Sci.* **1960**, 44, 551.
- [50] A. Bradley, J. P. Hammes, *J. Electrochem. Soc.* **1963**, 110, 15.
- [51] K. Jesch, J. E. Bloor, P. L. Kronick, *J. Polym. Sci., Part A-1 Polym. Chem.* **1966**, 4, 1487.
- [52] H. Yasuda, T. Hsu, *J. Polym. Sci. Polym. Chem. Ed.* **1977**, 15, 81.
- [53] J. Mertens, J. Baneton, A. Ozkan, E. Pospisilova, B. Nysten, A. Delcorte, F. Reniers, *Thin Solid Films* **2019**, 671, 64.
- [54] J. Mertens, B. Nisol, J. Hubert, F. Reniers, *Plasma Process. Polym.* **2020**, 17, 1900250.
- [55] K. Bazaka, M. V. Jacob, B. F. Bowden, *J. Mater. Res.* **2011**, 26, 1018.
- [56] H. Yasuda, T. Hirotsu, *J. Polym. Sci. Polym. Chem. Ed.* **1978**, 16, 743.
- [57] (a) B. Nisol, S. Watson, S. Lerouge, M. R. Wertheimer, *Plasma Process. Polym.* **2016**, 13, 900; (b) A. Kakaroglou, B. Nisol, K. Baert, I. de Graeve, F. Reniers, G. van Assche, H. Terryn, *RSC Adv.* **2015**, 5, 27449.
- [58] (a) H. Yasuda, C. E. Lamaze, *J. Appl. Polym. Sci.* **1973**, 17, 1519; (b) H. Yasuda, C. E. Lamaze, *J. Appl. Polym. Sci.* **1973**, 17, 1533.
- [59] H. Yasuda, M. O. Bumgarner, J. J. Hillman, *J. Appl. Polym. Sci.* **1975**, 19, 531.
- [60] F. Huang, L. Chen, H. Wang, Z. Yan, *Chem. Eng. J.* **2010**, 162, 250.
- [61] (a) A. Batan, B. Nisol, A. Kakaroglou, I. de Graeve, G. van Assche, B. van Mele, H. Terryn, F. Reniers, *Plasma Process. Polym.* **2013**, 10, 857; (b) B. Nisol, G. Arnoult, T. Bieber, A. Kakaroglou, I. de Graeve, G. van Assche, H. Terryn, F. Reniers, *Plasma Process. Polym.* **2014**, 11, 335.
- [62] J. Friedrich, *Plasma Process. Polym.* **2011**, 8, 783.
- [63] (a) B. Nisol, S. Watson, S. Lerouge, M. R. Wertheimer, *Plasma Process. Polym.* **2016**, 13, 557; (b) B. Nisol, S. Watson, S. Lerouge, M. R. Wertheimer, *Plasma Process. Polym.* **2017**, 14, 1600191; (c) B. Nisol, S. Watson, A. Meunier, D. Juncker, S. Lerouge, M. R. Wertheimer, *Plasma Process. Polym.* **2018**, 15, 1700132.
- [64] (a) M. Moreno-Couranjou, J. Guillot, J.-N. Audinot, J. Bour, E. Prouvé, M.-C. Durrieu, P. Choquet, C. Detrembleur, *Plasma Process. Polym.* **2020**, 17, 1900187; (b) G. P. Lopez, B. D. Ratner, *Langmuir* **1991**, 7, 766; (c) F. Hilt, D. Duday, N. Gherardi, G. Frache, J. Didierjean, P. Choquet, *RSC Adv.* **2015**, 5, 4277.
- [65] N. D. Boscher, F. Hilt, D. Duday, G. Frache, T. Fouquet, P. Choquet, *Plasma Process. Polym.* **2015**, 12, 66.
- [66] C. L. Rinsch, X. Chen, V. Panchalingam, R. C. Eberhart, J. H. Wang, R. B. Timmons, *Langmuir* **1996**, 12, 2995.
- [67] (a) C. Gaiolas, A. P. Costa, M. Nunes, M. J. S. Silva, M. N. Belgacem, *Plasma Process. Polym.* **2008**, 5, 444-452; (b) A. Grüniger, P. Rudolf von Rohr, *Surf. Coat. Technol.* **2003**, 174-175, 1043.
- [68] S. E. Alexandrov, M. L. Hitchman, *Chem. Vap. Deposition* **2005**, 11, 457.
- [69] T. Belmonte, G. Henrion, T. Gries, *J. Therm. Spray Technol.* **2011**, 20, 744.
- [70] R. A. Wolf, *Atmospheric Pressure Plasma for Surface Modification*, John Wiley & Sons, Hoboken, N.J., **2013**.
- [71] (a) Y. Sawada, S. Ogawa, M. Kogoma, *J. Phys. D Appl. Phys.* **1995**, 28, 1661; (b) K. Schmidt-Szalowski, Z. Rżanek-Boroch, J. Sentek, Z. Rymuza, Z. Kusznerewicz, M. Misiak, *Plasma Polym.* **2000**, 5, 173; (c) M. C. Kim, C.-P. Klages, *Surf. Coat. Technol.* **2009**, 204, 428.
- [72] (a) I. Vinogradov, A. Lunk, *Plasma Process. Polym.* **2005**, 2, 201; (b) R. Prat, Y.J. Koh, Y. Babukutty, M. Kogoma, S. Okazaki, M. Kodama, *Polymer* **2000**, 41, 7355.
- [73] H.-R. Lee, D. Kim, K.-H. Lee, *Surf. Coat. Technol.* **2001**, 142-144, 468.
- [74] A. Shah, S. Patel, E. Narumi, D. T. Shaw, *Appl. Phys. Lett.* **1990**, 57, 1452.
- [75] B. Nisol, C. Poleunis, P. Bertrand, F. Reniers, *Plasma Process. Polym.* **2010**, 7, 715.
- [76] G. Da Ponte, E. Sardella, F. Fanelli, A. van Hoeck, R. d'Agostino, S. Paulussen, P. Favia, *Surf. Coat. Technol.* **2011**, 205, 525.
- [77] (a) M. C. Vasudev, K. D. Anderson, T. J. Bunning, V. V. Tsukruk, R. R. Naik, *ACS Appl. Mater. Interfaces* **2013**, 5, 3983; (b) G. Ozaydin-Ince, A. M. Coclite, K. K. Gleason, *Rep. Prog. Phys.* **2012**, 75, 016501; (c) S. Bhatt, J. Pulpytel, F. Arefi-Khonsari, *Surf. Innovat.* **2015**, 3, 63; (d) J. Ibrahim, S. A. Al-Bataineh, A. Michelmoré, J. D. Whittle, *Plasma Chem. Plasma Process.* **2021**, 41, 47; (e) K. Vasilev, S. S. Griesser, H. J. Griesser, *Plasma Process. Polym.* **2011**, 8, 1010; (f) F. Fanelli, *Surface Coat. Technol.* **2010**, 205, 1536; (g) F. F. Shi, *Surface Coat. Technol.* **1996**, 82, 1.
- [78] F. Bakkali, S. Averbeck, D. Averbeck, M. Idaomar, *Food Chem. Toxicol.* **2008**, 46, 446.
- [79] S. Burt, *Int. J. Food Microbiol.* **2004**, 94, 223.
- [80] F. Nazzaro, F. Fratianni, R. Coppola, V. D. Feo, *Pharmaceuticals* **2017**, 10, 86.
- [81] D. Sakthi Kumar, M. G. Krishna Pillai, *Thin Solid Films* **1999**, 353, 249.

- [82] D. Sakthi Kumar, K. Nakamura, S. Nishiyama, H. Noguchi, S. Ishii, K. Kashiwagi, Y. Yoshida, *J. Appl. Polym. Sci.* **2003**, *90*, 1102.
- [83] M. V. Jacob, C. D. Easton, G. S. Woods, C. C. Berndt, *Thin Solid Films* **2008**, *516*, 3884.
- [84] C. D. Easton, M. V. Jacob, R. A. Shanks, B. F. Bowden, *Chem. Vap. Deposit.* **2009**, *15*, 179.
- [85] C. D. Easton, M. V. Jacob, *Thin Solid Films* **2009**, *517*, 4402.
- [86] C. D. Easton, M. V. Jacob, *J. Appl. Polym. Sci.* **2010**, *115*, 404.
- [87] C. D. Easton, M. V. Jacob, *Polym. Degrad. Stab.* **2009**, *94*, 597.
- [88] A. Al-Jumaili, K. Bazaka, M. Jacob, *Nanomaterials* **2017**, *7*, 270.
- [89] A. Al-Jumaili, S. Alancherry, K. Bazaka, M. Jacob, *Electronics* **2017**, *6*, 86.
- [90] B. E. Hennekam, S. A. Al-Bataineh, A. Michelmores, *J. Appl. Polym. Sci.* **2020**, *137*, 49288.
- [91] B. Mol, J. James, C. Joseph, M. R. Anantharaman, M. J. Bushiri, *SN Appl. Sci.* **2020**, *2*, 801.
- [92] O. Bazaka, K. Prasad, I. Levchenko, M. V. Jacob, K. Bazaka, P. Kingshott, R. J. Crawford, E. P. Ivanova, *Molecules* **2021**, *26*, 7133.
- [93] M. V. Jacob, R. S. Rawat, B. Ouyang, K. Bazaka, D. S. Kumar, D. Taguchi, M. Iwamoto, R. Neupane, O. K. Varghese, *Nano Lett.* **2015**, *15*, 5702.
- [94] J. Romo-Rico, S. Murali Krishna, J. Golledge, A. Hayles, K. Vasilev, M. V. Jacob, *Plasma Process. Polym.* **2022**, *19*, 2100220.
- [95] B. Mol, J. James, K. K. Anoop, I. Sulaniya, C. Joseph, M. R. Anantharaman, M. J. Bushiri, *J. Mater. Sci. Mater. Electron.* **2019**, *30*, 12603.
- [96] S. Alancherry, K. Bazaka, M. V. Jacob, *J. Polym. Environ.* **2018**, *26*, 2925.
- [97] D. S. Grant, J. Ahmed, J. D. Whittle, A. Michelmores, K. Vasilev, K. Bazaka, M. V. Jacob, *Molecules* **2021**, *26*, 4762.
- [98] K. Bazaka, M. V. Jacob, *Mater. Lett.* **2009**, *63*, 1594.
- [99] A. Kumar, D. S. Grant, K. Bazaka, M. V. Jacob, *J. Appl. Polym. Sci.* **2018**, *135*, 45771.
- [100] K. Bazaka, M. V. Jacob, *Polym. Degrad. Stab.* **2010**, *95*, 1123.
- [101] K. Bazaka, M. Jacob, V. K. Truong, R. J. Crawford, E. P. Ivanova, *Polymers* **2011**, *3*, 388.
- [102] A. Kumar, S. Mills, K. Bazaka, N. Bajema, I. Atkinson, M. V. Jacob, *Surf. Coat. Technol.* **2018**, *349*, 426.
- [103] M. V. Jacob, K. Bazaka, M. Weis, D. Taguchi, T. Manaka, M. Iwamoto, *Thin Solid Films* **2010**, *518*, 6123.
- [104] M. V. Jacob, K. Bazaka, D. Taguchi, T. Manaka, M. Iwamoto, *Chem. Phys. Lett.* **2012**, *528*, 26.
- [105] A. Kumar, A. Al-Jumaili, K. Prasad, K. Bazaka, P. Mulvey, J. Warner, M. V. Jacob, *Plasma Chem. Plasma Process.* **2020**, *40*, 339.
- [106] J. Ahmad, K. Bazaka, J. D. Whittle, A. Michelmores, M. V. Jacob, *Plasma Process. Polym.* **2015**, *12*, 1085.
- [107] K. Bazaka, J. Ahmad, M. Oelgemöller, A. Uddin, M. V. Jacob, *Sci. Rep.* **2017**, *7*, 45599.
- [108] T. G. Getnet, G. F. da Silva, I. S. Duarte, M. E. Kayama, E. C. Rangel, N. C. Cruz, *Materials* **2020**, *13*, 3166.
- [109] T. G. Getnet, M. E. Kayama, E. C. Rangel, I. C. S. Duarte, G. F. da Silva, N. C. Cruz, *J. Mater. Res. Technol.* **2022**, *18*, 2217.
- [110] A. Pegalajar-Jurado, C. D. Easton, K. E. Styan, S. L. McArthur, *J. Mater. Chem. B* **2014**, *2*, 4993.
- [111] M. N. Mann, E. R. Fisher, *ACS Appl. Mater. Interfaces* **2017**, *9*, 36548.
- [112] Y. W. Chan, K. S. Siow, P. Y. Ng, U. Gires, B. Yeop Majlis, *Mater. Sci. Eng. C* **2016**, *68*, 861.
- [113] S. Tone, T. Masawaki, K. Eguchi, *J. Membr. Sci.* **1996**, *118*, 31.
- [114] M. Gürsoy, *J. Appl. Polym. Sci.* **2021**, *138*, 49722.
- [115] M. V. Jacob, N. S. Olsen, L. J. Anderson, K. Bazaka, R. A. Shanks, *Thin Solid Films* **2013**, *546*, 167.
- [116] K. Bazaka, R. Destefani, M. V. Jacob, *Sci. Rep.* **2016**, *6*, 38571.
- [117] D. Gerchman, B. Bones, M. B. Pereira, A. S. Takimi, *Prog. Org. Coat.* **2019**, *129*, 133.
- [118] L. J. Anderson, M. V. Jacob, *Appl. Surf. Sci.* **2010**, *256*, 3293.
- [119] C. D. Easton, M. V. Jacob, R. A. Shanks, *Polymer* **2009**, *50*, 3465.
- [120] M. V. Jacob, C. D. Easton, L. J. Anderson, K. Bazaka, *Int. J. Modern Phys. Conf. Ser.* **2014**, *32*, 1460319.
- [121] K. Bazaka, M. V. Jacob, R. A. Shanks, *Adv. Mater. Res.* **2010**, *123-125*, 323.
- [122] (a) L. J. Anderson, M. V. Jacob, *Mater. Sci. Eng. B.* **2012**, *177*, 311; (b) L. J. Anderson, M. V. Jacob, *Thin Solid Films* **2013**, *534*, 452.
- [123] K. Bazaka, M. V. Jacob, *J. Mater. Res.* **2011**, *26*, 2952.
- [124] (a) J. Ahmad, K. Bazaka, M. Jacob, *Electronics* **2014**, *3*, 266; (b) J. Ahmad, K. Bazaka, M. Oelgemöller, M. Jacob, *Coatings* **2014**, *4*, 527; (c) I. Ahmad, M. I. Khan, H. Khan, M. Ishaq, R. Tariq, K. Gul, W. Ahmad *J. Appl. Polym. Sci.* **2015**, *132*, 42318.
- [125] (a) T. G. Getnet, M. E. Kayama, E. C. Rangel, N. C. Cruz, *Polymers* **2020**, *12*, 2692; (b) T. G. Getnet, M. E. Kayama, E. C. Rangel, I. C. S. Duarte, G. F. da Silva, N. C. Cruz, *Thin Solid Films* **2021**, *734*, 138833.
- [126] (a) I. Sugimoto, M. Nakamura, H. Kuwano, *Anal. Chem.* **1994**, *66*, 4316; (b) I. Sugimoto, M. Nakamura, H. Kuwano, *Sens. Actuat. Chem* **1996**, *36*, 342; (c) M. Seyama, Y. Iwasaki, S. Ogawa, I. Sugimoto, A. Tate, O. Niwa, *Analyt. Chem.* **2005**, *77*, 4228.
- [127] K. D. Anderson, J. M. Slocik, M. E. McConney, J. O. Enlow, R. Jakubiak, T. J. Bunning, R. R. Naik, V. V. Tsukruk, *Small* **2009**, *5*, 741.
- [128] K. D. Anderson, S. L. Young, H. Jiang, R. Jakubiak, T. J. Bunning, R. R. Naik, V. V. Tsukruk, *Langmuir* **2012**, *28*, 1833.
- [129] K. D. Anderson, K. Marczewski, S. Singamaneni, J. M. Slocik, R. Jakubiak, R. R. Naik, T. J. Bunning, V. V. Tsukruk, *ACS Appl. Mater. Interfaces* **2010**, *2*, 2269.
- [130] P. Heyse, R. Dams, S. Paulussen, K. Houthoofd, K. Janssen, P. A. Jacobs, B. F. Sels, *Plasma Process. Polym.* **2007**, *4*, 145.
- [131] P. Heyse, A. van Hoeck, M. B. J. Roeyfaers, J.-P. Raffin, A. Steinbüchel, T. Stöveken, J. Lammertyn, P. Verboven, P. A. Jacobs, J. Hofkens, S. Paulussen, B. F. Sels, *Plasma Process. Polym.* **2011**, *8*, 965.
- [132] P. Heyse, M. B. J. Roeyfaers, S. Paulussen, J. Hofkens, P. A. Jacobs, B. F. Sels, *Plasma Process. Polym.* **2008**, *5*, 186.

- [133] M. G. Ortore, R. Sinibaldi, P. Heyse, S. Paulussen, S. Bernstorff, B. Sels, P. Mariani, F. Rustichelli, F. Spinozzi, *Appl. Surf. Sci.* **2008**, *254*, 5557.
- [134] F. Palumbo, G. Camporeale, Y.-W. Yang, J.-S. Wu, E. Sardella, G. Dilecce, C. D. Calvano, L. Quintieri, L. Caputo, F. Baruzzi, P. Favia, *Plasma Process. Polym.* **2015**, *12*, 1302.
- [135] S. Malinowski, P. Herbert, J. Rogalski, J. Jaroszyńska-Wolińska, *Polymers* **2018**, *10*, 532.
- [136] S. Malinowski, C. Wardak, J. Jaroszyńska-Wolińska, P. Herbert, R. Panek, *Sensors* **2018**, *18*, 4086.
- [137] S. Malinowski, J. Jaroszyńska-Wolińska, P. A. F. Herbert, *J. Mater. Sci.* **2019**, *54*, 10746.
- [138] Y.-C. Cheng, C.-P. Hsiao, Y.-H. Liu, C.-H. Yang, C.-Y. Chiang, T.-R. Lin, Y.-W. Yang, J.-S. Wu, *Plasma Process. Polym.* **2018**, *15*, 1700173.
- [139] G. Da Ponte, E. Sardella, F. Fanelli, S. Paulussen, P. Favia, *Plasma Process. Polym.* **2014**, *11*, 345.
- [140] D. O'Sullivan, H. McArdle, J.-A. O'Reilly, R. J. O'Kennedy, R. Forster, L. O'Neill, *Plasma Process. Polym.* **2020**, *17*, 1900147.
- [141] L. O'Neill, P. Dobbyn, M. Kulkarni, A. Pandit, *Clin. Plasma Med.* **2018**, *12*, 23.
- [142] D. Liu, T. He, Z. Liu, S. Wang, Z. Liu, M. Rong, M. G. Kong, *Plasma Process. Polym.* **2018**, *15*, 1870022.
- [143] C.-P. Hsiao, C.-C. Wu, Y.-H. Liu, Y.-W. Yang, Y.-C. Cheng, F. Palumbo, G. Camporeale, P. Favia, J.-S. Wu, *IEEE Trans. Plasma Sci.* **2016**, *44*, 3091.
- [144] B. R. Pistillo, L. Detomaso, E. Sardella, P. Favia, R. d'Agostino, *Plasma Process. Polym.* **2007**, *4*, S817.
- [145] Z. Krtouš, L. Hanyková, I. Krakovský, D. Nikitin, P. Pleskunov, O. Kylián, J. Sedlaříková, J. Kousal, *Materials* **2021**, *14*, 459.
- [146] Z. Krtouš, J. Kousal, J. Sedlaříková, Z. Kolářová Rašková, L. Kučerová, I. Krakovský, J. Kučera, S. Ali-Ogly, P. Pleskunov, A. Choukourov, *Surf. Coat. Technol.* **2021**, *421*, 127402.
- [147] S. Ligot, F. Renaux, L. Denis, D. Cossement, N. Nuns, P. Dubois, R. Snyders, *Plasma Process. Polym.* **2013**, *10*, 999.
- [148] S. Ligot, E. Bousser, D. Cossement, J. Klemberg-Sapieha, P. Viville, P. Dubois, R. Snyders, *Plasma Process. Polym.* **2015**, *12*, 508.
- [149] S. Ligot, M. Guillaume, P. Raynaud, D. Thiry, V. Lemaure, T. Silva, N. Britun, J. Cornil, P. Dubois, R. Snyders, *Plasma Process. Polym.* **2015**, *12*, 405.
- [150] B. Nisol, S. Watson, S. Lerouge, M. R. Wertheimer, *Plasma Process. Polym.* **2016**, *13*, 965.
- [151] M. Laurent, J. Koehler, G. Sabbatier, C. A. Hoesli, N. Gherardi, G. Laroche, *Plasma Process. Polym.* **2016**, *13*, 711.
- [152] N. Milaniak, G. Laroche, F. Massines, *Plasma Process. Polym.* **2021**, *18*, 2000248.

How to cite this article: A. Loesch-Zhang, A. Geissler, M. Biesalski, *Plasma Process Polym.* **2023**;20:e2300016.
<https://doi.org/10.1002/ppap.202300016>

2.2.2. Plasma-induced paper surface modification

Both plasma polymerization and plasma modification have been used to tailor the properties of cellulosic surfaces to specific needs. While plasma polymerization provides entire coatings with a wide range of functionalities, plasma modification is used to modify functional groups at the substrate surface or incorporate functional groups from the plasma into the surface.^[64] Unlike conventional cellulose functionalization strategies, the use of plasma enables the functionalization not only of the hydroxyl group, but of all carbon and oxygen species present in cellulose.^[70] Such modifications in functionality can be initiated by simple radical generation through the use of so-called inert process gases, such as noble gases, O₂ or N₂. Those then may lead to subsequent grafting of further species either through post-treatment functionalization or exposure to ambient air. Alternatively, functionalization can be performed directly through so-called reactive gases like NH₃, SiCl₄, CF₄ or SF₆.^[71,72]

Plasma surface treatment shows prospects for use in a wide range of applications, from paper restoration, where the possibility to clean surfaces, deactivate bacteria and increase paper stability^[73] is of importance, to paper-based microfluidic devices, where selective surface hydrophobization and etching are required.^[74,75] This chapter first focuses on the plasma-induced modification of lignocellulosic materials in general and then specifically on the modification of paper surfaces through plasma treatment with inert gases that do not introduce novel chemical species into the paper, but rather modify the existing ones. Finally, an outlook into the possibilities of modifying finished paper through plasma modification using either inert or reactive gases will be given.

Plasma treatment has been performed to modify the properties not only of paper but of manifold lignocellulosic materials.^[70,76] Examples of natural cellulose-containing fibers that have been submitted to plasma treatment are cotton,^[77,78,79–82] linen^[83] and jute.^[84] Furthermore, pulps and handsheets produced from a wide range of woods including eucalyptus, aspen and spruce, as well as bleached and unbleached variants have been examined.^[73,85–90] The influence of plasma treatment on bulk properties depends on the respective material. For instance, no bulk degradation was observed for treatment of different pulps derived from cotton, flax and several kinds of wood.^[90] In the case of cotton fibers, plasma treatment only affected the top surface layer, the cuticle and the primary cell wall, while the secondary cell wall remained unaltered.^[82]

In some cases, however, changes in the bulk properties have been observed after plasma treatment. For instance, one group demonstrated the tunability of cotton fabric's degree of crystallinity by argon plasma treatment and the influence thereof on cellulosic crystal unit cell parameters. Formation of strains in the glycosidic linkages of the cellulose and in hydrogen

bonds were observed. The changes in crystallinity as well as fiber etching and smoothing showed good accordance with changes in wetting properties. Different sets of parameters varying input power, plasma exposure time and gas pressure were found to interact with each other in their influence on wicking height through a Design of Experiments approach (Figure 4).^[80]

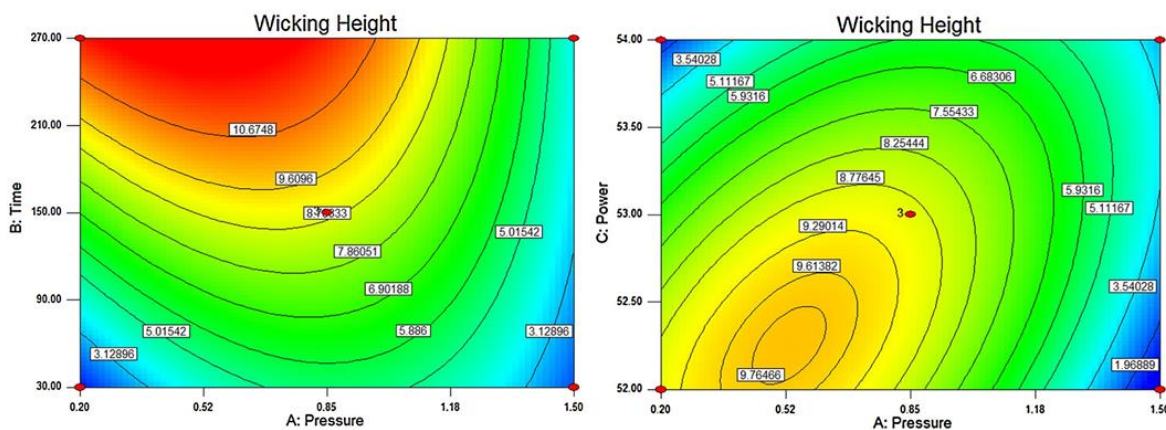


Figure 4: Argon microwave plasma treatment of cotton fabric was studied using a Design of Experiments approach, where different combinations of input power, exposure time and gas pressure were found to affect the wicking height. Reprinted and adapted from work by PRABHU *et al.*^[80], Copyright (2016), with permission from Elsevier.

Air plasma treatment decreased the degree of polymerization from 200 to 120 for microcrystalline cellulose and from 1,000 to 160 for α -cellulose.^[91] Initially, plasma treatment was assumed to cause a reaction between cellulosic water and OH radicals, leading to depolymerization by cleavage of the glycosidic bonds. When the cellulose water content was sufficiently low, the thus formed fragments reassembled into branched glucans.^[92] However, other studies also hypothesized the cellulosic water to react with NO_x species formed inside the plasma,^[93] leading to acid formation and resulting in acidic cellulose hydrolysis.^[76]

Treatment with plasma from noble gases, air or O_2 often leads to surface oxidation resulting in an increase in O/C ratio and hydrophilicity. This has been observed for the substrates mentioned above,^[79,81,82,85,89] but also for pure cellulosic materials such as argon-treated α -cellulose, helium-treated cellulose nanofibrils and air-treated nanocellulose sheets.^[94,95] It was hypothesized that these changes might be caused by post-treatment oxidation reactions.^[94] On the other hand, increased hydrophobicity was reported for N_2 plasma treatment of bacterial cellulose.^[96]

Being based on the same materials, the observations made during plasma modification of lignocellulosics are generally well in accordance with those made after modifying paper surfaces with plasma. As such materials usually contain significant amounts of hemicelluloses and lignin, it is important to note these are primarily removed by plasma treatment, as indicated by X-ray

photoelectron spectroscopy (XPS). This results in increased surface porosity and increased fibrillation.^[86,89] The dependence of the paper surface properties on the choice of plasma gas has been shown in a study of plasma treatment on filter paper. In this example, H₂ plasma decreased the amount of hydroxyl groups and thereby decreased water absorption, with WCAs of 115° after 8 min treatment time, while O₂ plasma both oxidized and reduced the surface, leading to presumed cellulose degradation as well as oxygen incorporation into carboxylic acid groups.^[97]

Similarly, low pressure oxygen plasma treatment of sheets from different chemical pulps at 200 W improved water sorption. The amount of extractives had a strong influence on water permeation, with a somewhat smaller contribution from lignin. Both lignin and extractives were oxidized by plasma treatment. Oxidation reactions also occurred on cellulose itself. However, even more prolonged treatment times again led to O=C–O decomposition.^[85] The surface properties of papers from bleached softwood chemical pulp treated with an atmospheric pressure dielectric barrier discharge (DBD) at 0, 1 and 5 W·min·m⁻² were shown to depend on the power input. Papers treated at low power showed increased wetting and surface energy, while higher treatment power led to decreased wetting and surface energy. O/C ratios increased with plasma power due to oxidation reactions resulting in carbonyl and carboxyl formation.^[86] Another study examined the surface properties of air plasma-treated handsheets from spruce, aspen, bleached and unbleached kraft pulp. Contrary to sheets made from kraft pulp, aspen and spruce fiber-based sheets displayed a strong increase in O/C ratio as well as in oxidation reactions and a decrease in surface lignin and extractives content.^[89]

Furthermore, plasma treatment can influence the macroscopic properties of paper. For instance, wet- and dry-strength can be improved by plasma treatment due to crosslinking, as observed on various paper sheets after air plasma treatment.^[86–89] On papers from bleached softwood chemical pulp, wet-tensile and wet-stiffness indices increased with higher treatment power and were associated to covalent crosslinking. Contrastingly, low treatment intensities primarily led to oxidation and surface cleaning effects.^[86] A comparison between bleached kraft pulp and unbleached softwood thermomechanical pulp papers showed different tensile properties depending on the selected substrate. For handsheets from bleached kraft pulp, enhanced wet tensile indices are accompanied by a decrease of Young's modulus and wet strain and attributed to fiber crosslinking. For handsheets from unbleached thermomechanical pulp, wet strain remained constant while Young's modulus increased, which was attributed to fiber surface lignin protecting fiber-to-fiber bonds.^[87] Improved wet-tensile strength has also been observed for eucalyptus handsheets after DBD treatment^[88] as well as after air plasma treatment^[89] on aspen, spruce, bleached and unbleached kraft pulp handsheets.^[89]

Finally, plasma treatment can also be used to modify sized papers with respect to a target application, like to tune wetting properties. For instance, hydrophobic AKD coated ink-jet paper was rendered hydrophilic under oxygen plasma treatment at 200 W and 1 s to 200 s treatment time, which was attributed to degradation of the AKD sizing agent and its subsequent removal through vaporization.^[98] Hence, plasma treatment enables creating hydrophobic-hydrophilic structures, which may be applicable in paper-based microfluidic analytical devices.^[74,75] For example, microfluidic channel structures in paper were produced making use of locally confined DBD microdischarges within the paper pores. Herein, hydrophilic and hydrophobic patterns were generated in two approaches, either by etching hydrophobic AKD-sized paper or by depositing a C₄F₈-based plasma polymer onto hydrophilic paper.^[99]

Furthermore, the effect of aging on pigment coated and surface sized papers submitted to plasma treatment has been examined. Plasma treatment was shown to directly increase the surface energy and oxidation level. However, aging for 3 months led to a decrease in surface energy, especially of its polar component and most prominently during the first weeks of storage, while the oxidation level did not change significantly. Thus, this aging effect was not attributed to ongoing chemical reactions, but rather to the rotation of polar groups back into the material and re-contamination of the plasma-cleaned surface.^[100] An extensive study on the surface composition and wetting properties of security paper treated with SiCl₄, O₂ and CF₄ plasma was conducted using XPS and WCA measurements, including statistical evaluation of the parameters pressure, power and treatment time. Decisive effects however varied depending on the selected treatment gas. Both for SiCl₄ and O₂, short treatment times and low plasma power led to high wettability.^[72]

Other works on modification of cellulosic substrates rely on combined strategies of plasma activation or treatment before or after applying hydrophobizing agents through conventional coating methods, most frequently impregnation or spray coating.^[77,101,102] Using this approach, some biobased precursors have been applied to improve durability of cellulosic materials.^[103,104] For instance, eucalyptus paper sheets were coated with limonene and myrcene using plasma treatment. Three different methods were used to apply the coating. To this end, the two crucial steps, plasma activation or treatment and impregnating the paper by immersing it in the precursor solution, were performed in different order, namely (1) impregnation – plasma activation, (2) plasma activation – impregnation and (3) impregnation – activation – impregnation. These were followed by Soxhlet extraction performed to remove any unbound residues. Successful precursor attachment was confirmed through XPS. Best results concerning hydrophobization were achieved with the impregnation – activation – impregnation method, yielding WCAs of 105° and 107° for limonene and myrcene respectively. Water penetration was

greatly decreased and the polar contribution to the surface energy was close to zero.^[105] Cotton fabric was likewise hydrophobized using oleic acid in an activation – immersion – treatment approach, wherein cotton fabric was first activated with argon microwave frequency plasma at reduced pressure, then immersed into an ethanolic solution of oleic acid and treated again with argon plasma afterwards. The concentration of the oleic acid solution and thus the amount of grafted material greatly influenced the resulting water penetration into the fabric as monitored through WCA measurement. Relatively stable contact angles over time with values over 150° were obtained at oleic acid concentrations between 0.1 M and 0.2 M.^[106] Similarly, oleic acid was grafted onto unbleached and bleached kraft pulp fibers through immersion into a solution of oleic acid in acetone followed by plasma treatment and Soxhlet extraction. Successful oleic acid grafting was proven through XPS by an increase in the C1 and C4 peak intensities (indicating C–C/C–H and O–C=O bonds respectively), which are characteristic for the fatty acid, relative to the C2 and C3 peak intensities (indicating C–O and C=O/O–C–O bonds respectively), which are present in cellulose (Figure 5).^[104]

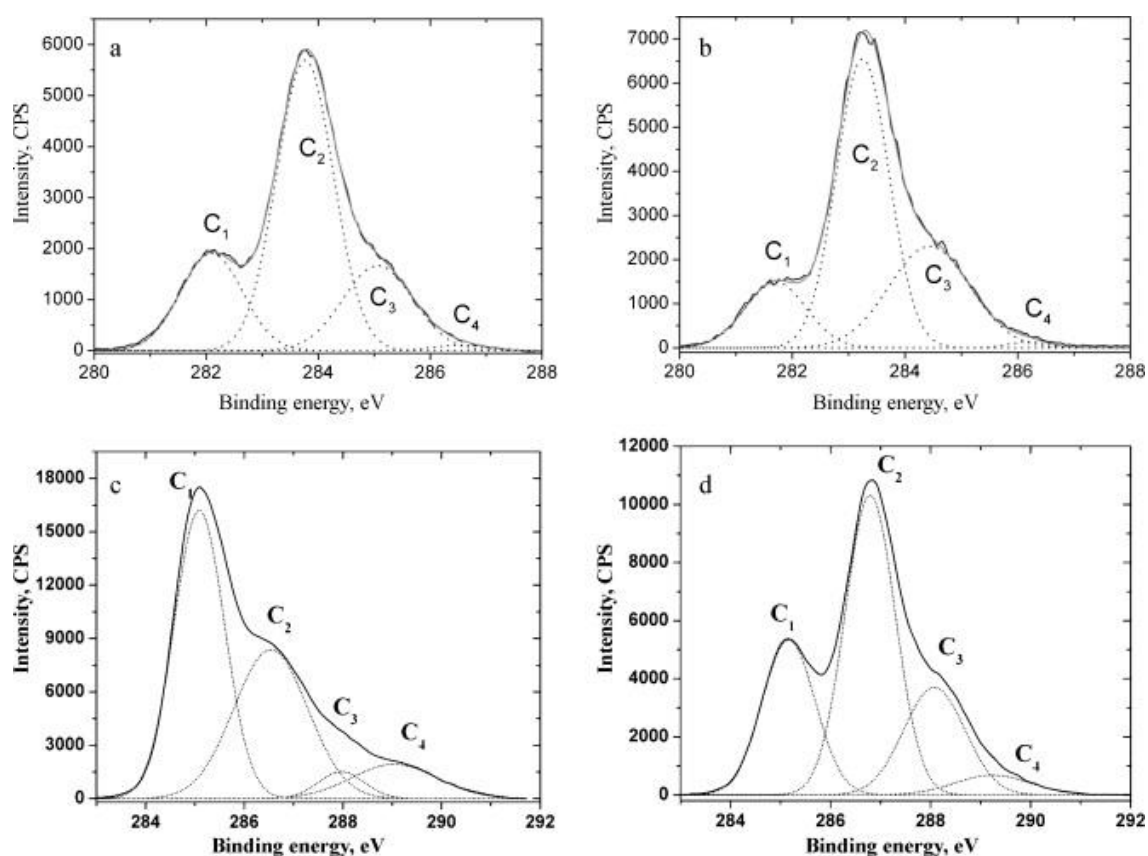


Figure 5: XPS spectra, recorded on (a) untreated unbleached kraft pulp fibers, (b) untreated bleached kraft pulp fibers, (c) oleic acid-treated unbleached kraft pulp fibers and (d) oleic acid-treated bleached kraft pulp fibers, prove successful oleic acid grafting through an increase in C1 and C4 peak intensities relative to C2 and C3 intensities. Reprinted from work by POPESCU *et al.*^[104], Copyright (2011), with permission from Elsevier.

These strategies combining plasma treatment and conventional coating techniques however still have the disadvantage of being multi-step processes and frequently containing excessive coating amounts that are often removed through extraction. A more material-economic approach is the direct introduction of the coating material within the coating process through plasma-enhanced chemical vapor deposition.

2.2.3. Plasma polymerization for paper hydrophobization

Besides the possibility to modify the outmost paper surface by introducing new functional groups or to modify already present ones with the help of plasma, it is equally possible to deposit thin polymer-like coatings using plasma polymerization.

In 1971, LIEPINS *et al.* examined the suitability of sixteen monomers to produce water vapor barriers on filter paper, notably aromatic hydrocarbons, nitriles, chlorine-containing compounds, isoprene, hexane and a silane, using a radio frequency low pressure glow discharge at 80–300 W and varying deposition times. Water vapor barriers depended on treatment time and reached a plateau after 20 min. The highest barriers were achieved with the precursors styrene and toluene. For certain materials, higher power levels or prolonged treatment times led to a deterioration of barrier properties. All coatings were proven resistant to rubbing as well as water and silicone oil penetration during 6 h of testing. A decrease in dry tensile strength was attributed to either dehydration of the sample in plasma or to partial cellulose oxidation or degradation. Wet strength, however, increased. Staining experiments showed the coating penetration depth to range between 5 and 25 μm .^[107] In a two-step process, a gas and water vapor barrier coating was achieved on a kraft fiber mat, while at the same time preserving combustibility. First, surface pores were covered through spray coating with a colloidal solution that did not provide barrier properties itself but served to avoid penetration of the actual barrier material into the paper pores. Second, a nonporous barrier layer was applied through low pressure glow discharge plasma polymerization of styrene.^[108]

Nowadays, with respect to endowing paper with barrier properties, most precursors deposited through PECVD are based on fluorine- and silicon-containing compounds. For instance, permanent hydrophobization of paper with C_3F_8 and C_4F_8 in a DBD at reduced pressure was achieved through 200 nm thick coatings, while the WCA decreased within 30 min at lower coating thickness. WCAs ranged between 117° and 128° and showed no clear dependency on plasma power in the examined range of 25 W to 1000 W. In contrast, using C_2F_2 narrowly failed to create a hydrophobic surface, with WCAs ranging between 83° and 89° .^[109] Plasma polymer coatings from 1H,1H,2H,2H-perfluorodecyl acrylate endowed filter papers with a WCA of 129°

to 151° as well as oleophobic and antifouling properties. Field emission scanning electron microscopy images showed the conformal coating on the substrate, wherein the fibrous structure was maintained, but fiber coverage with the coating was clearly visible.^[110] Another study took advantage of the ability of plasma to perform surface roughness modification through etching, taking into account that not only surface chemistry but also surface roughness has a decisive influence on wetting behavior. Low pressure PECVD of pentafluoroethane for 2 min at 120 W using argon carrier gas produced sticky, near superhydrophobic surfaces on laboratory handsheets with a WCA of 145° and hysteresis of 79°. However, preliminary creation of nanoroughness by removal of amorphous cellulose domains through exposure to oxygen plasma at 150 W for 30 min, combined with paper's inherent microscale roughness, resulted in roll-off superhydrophobic surfaces with a WCA of 167° and hysteresis of 3.4°.^[111] In another approach, hierarchical structuring on sized paper was created through helium-oxygen plasma etching at atmospheric pressure, which removed cellulosic material and left calcite filler particles behind. Subsequent fluorocarbon coating with octafluorocyclobutane resulted in superhydrophobic properties.^[112] A further study examined the penetration depth of a glow discharge-based PECVD of perfluoromethoxycyclohexane on a stack of five filter papers through water absorption time measurements on the top and bottom of each paper in the stack. The plasma penetrated more deeply into the stack with increasing treatment time. While after 2 min only the outmost surface was hydrophobized, after 15 min the entire stack showed hydrophobic behavior. Fluorine presence was further evidenced in all layers and at varying content using XPS.^[113]

Amongst silicon-based precursors, hexamethyldisiloxane (HMDSO) has received a lot of attention, not only as paper coating,^[114] but also for instance in wood finishing.^[115] An early study examined the deposition of HMDSO onto filter paper through microwave frequency low-pressure plasma at 0.1 W·cm⁻³ power density and deposition times between 5 s and 120 s, resulting in a coating thickness between 0.17 μm and 1.59 μm. The coating was applied on the fiber and fibril surface, so at increasing coating amount, the fiber diameter increased and interfibrillar spaces were filled, whereby further coating penetration into the bulk material was prevented. No coating was deposited within the fibers or in the bulk material.^[116] Another study analyzed the penetration depth and the influence of the substrate position with respect to the helium gas flow inlet for plasma-polymerized (pp) HMDSO deposited in a DBD at atmospheric pressure. Fourier-transform infrared (FTIR) spectroscopy bands indicating coating presence, as well as increased hydrophobicity were observed on all four layers of a stack of bleached kraft laboratory papers. However, the water absorption time was highest for the paper on top of the stack and when measured on the position placed closest to the gas inlet.^[117] Paper coatings

based on pp(HMDSO) were further examined with respect to their suitability for packaging applications using model liquids, notably water, acetic acid, ethanol and heptane, as food simulants. The hydrophobicity of the paper sheets was not significantly changed by immersion into these liquids for up to 24 h except for immersion in heptane.^[118] Films of fibrillated cellulose coated with pp(HMDSO) were highly hydrophobic, but showed no improvement in water vapor and oxygen transmission rate compared to an uncoated substrate. Coating with a bilayer of carboxymethyl cellulose (applied through spray coating) and pp(HMDSO) not only generated hydrophobicity, but additionally decreased the water absorbency by 98%, oxygen transmission rate by 95% and water vapor transmission rate by 66%.^[119]

In a similar setup, a stack of four layers of bleached unrefined kraft paper was coated with pp(2,4,6,8-tetramethylcyclotetrasiloxane). Hydrophobization was achieved throughout the stack and both at the top (F) and on the bottom (B) of each paper sheet with all WCAs ranging above 125° (Figure 6). Those sheets covered by a thick coating layer showed good stability after immersion in water for 20 h.^[120]

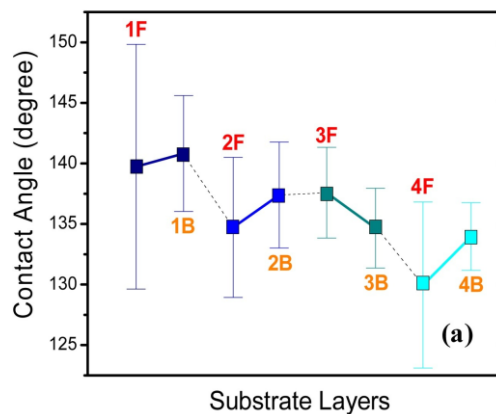


Figure 6: Water contact angles measured on bleached unrefined kraft paper after dielectric barrier charge plasma deposition of 2,4,6,8-tetramethylcyclotetrasiloxane. Four papers were stacked on top of each other within the plasma chamber and WCAs were measured on the top (F) and bottom (B) of each of the four (1-4) sheets. Reprinted from work by PROFILI *et al.*^[120], Copyright (2020), with permission from Elsevier.

Hexamethyldisilazane-based plasma polymer coatings deposited on filter paper were conformal with WCAs above 100° and showed good stability against strong acids and bases as well as exposition to UV light.^[121] A coating from pp(octamethylcyclotetrasiloxane) on spruce bleached kraft paper reduced water absorptivity by 44% and air permeability by 41%. Scanning electron microscopy (SEM) images showed varying morphology depending on applied wattage, from smooth covering to increased particle deposition at higher plasma powers (Figure 7).^[122]

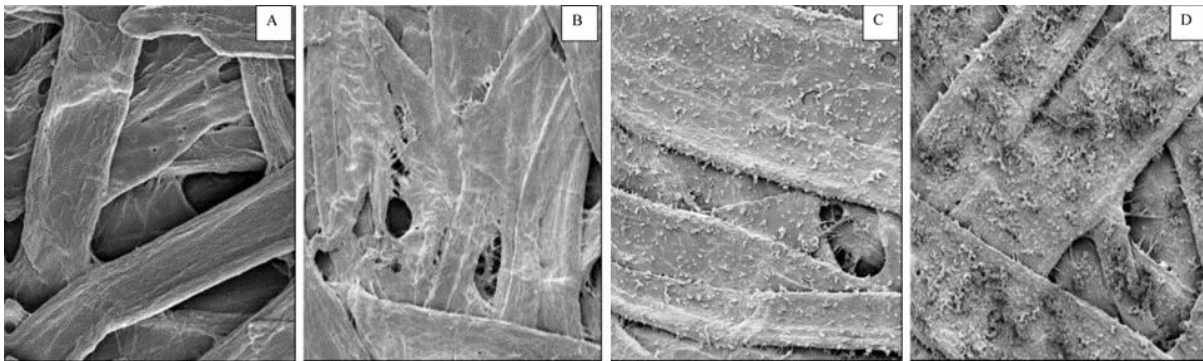


Figure 7: SEM images of pp(octamethylcyclotetrasiloxane) deposits on bleached kraft paper reveal a clear influence on the surface morphology. Comparative images show (a) the plain substrate and (b-d) the paper coated at 10 W, 25 W and 100 W plasma power. The change from smooth coatings to increased particle deposition at higher power is clearly visible. Unfortunately, the authors only provide the magnification ($1000\times$), but no scale bars. Reprinted and adapted from work by SAHIN *et al.*^[122], Copyright (2013), with permission from Elsevier.

Comparison of different plasma modification approaches with respect to hydrophobization of paper using γ -methacryloxypropyltrimethoxysilane showed differences in WCAs depending on the selected method: PECVD at reduced pressure led to a WCA of 82° , while plasma activation followed by immersion into the precursor resulted in 76° and impregnation with precursor followed by plasma treatment led to 100° .^[102] The authors do however not give any information on the amount of coating deposited in either case.

Despite the research on paper hydrophobization using PECVD, biobased precursors have not yet been used for paper hydrophobization in this material-effective approach of directly depositing the precursor material during the plasma polymerization process. Vegetable oils as intrinsically hydrophobic materials have never been directly plasma-polymerized in PECVD at all. Therefore, the plasma polymerization of vegetable oils in general and for paper hydrophobization in particular are promising novel approaches for obtaining more sustainable coatings.

3. Aim and Strategy

Sustainably produced, durable, moisture-proof paper-based materials are urgently needed to replace conventional plastics in manifold applications. Thus, the aim of this work is to establish hydrophobic paper coatings based on vegetable oils, with a focus on coating strategies foregoing solvent- and drying energy-intensive processes, and consuming a minimal amount of supplementary chemicals.

The initial focus is placed on established coating strategies to increase paper hydrophobicity with vegetable oils as main coating component, considering either the use of crosslinking agents or covalent coating attachment onto cellulose. Subsequently, vegetable oil-based coatings that are both crosslinked and covalently attached to the substrate are to be applied through plasma-enhanced chemical vapor deposition (PECVD), also known as plasma polymerization. This process is equally solvent-free and will first be studied on glass slides as simple hydrophilic model surfaces and then transferred to porous paper substrates.

Focusing on the aim of achieving hydrophobic paper coatings based on vegetable oils, the following questions are addressed:

- I Is it possible to hydrophobize paper through crosslinked vegetable oil-based coatings using a conventional coating technique while maintaining a solvent-free single-step process?**
- II Can elevated temperatures induce covalent attachment of vegetable oils onto paper to achieve hydrophobization?**
- III Is atmospheric pressure plasma polymerization able to produce crosslinked, covalently attached hydrophobic coatings using vegetable oils?**
- IV To what extent do vegetable oil-based plasma polymer coating properties depend on the paper substrate properties?**

The approaches for addressing these questions will be presented in the following and are schematically displayed in Figure 8.

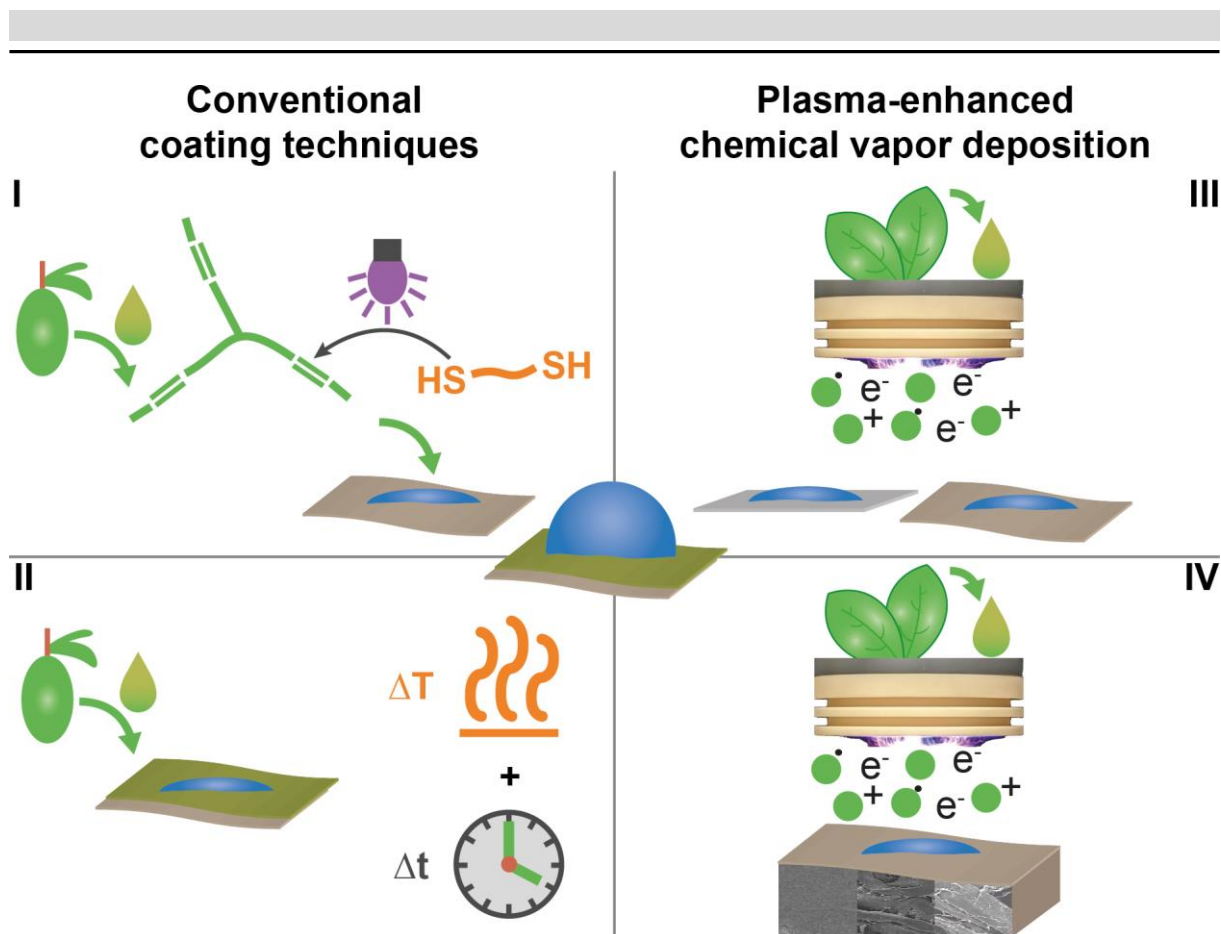


Figure 8: Approaches for enhancing paper hydrophobicity using vegetable oils. (I) Photoinduced crosslinking of dithiols with vegetable oil; (II) Covalent attachment of vegetable oil through thermal treatment; (III) Plasma polymerization of vegetable oils on glass and smooth paper substrates; (IV) Plasma polymerization of vegetable oils on papers with different porosity. (III) and (IV) adapted from reference^[123], which was published under Creative Commons License CC BY 4.0, Attribution 4.0 International; © 2024 The Author(s). *Advanced Materials Interfaces* published by Wiley-VCH GmbH.

I Thiol-ene photocrosslinking as a conventional solvent-free method for hydrophobizing paper with vegetable oils

When crosslinked coatings are targeted, the challenge consists in the deposition and subsequent crosslinking of the individual components, as fully crosslinked coatings can generally not be directly deposited from solution due to their insolubility in organic solvents and water. Instead, the coating material, possibly pre-functionalized with a suitable crosslinkable moiety, is first deposited, and crosslinks are introduced after coating deposition, for instance using light or heat as stimulus to initiate the crosslinking reaction. Inherent disadvantages of such processes are the need for solvents and the necessity to introduce crosslinking agents or crosslinkable moieties, often through multiple chemical derivatization steps performed prior to coating.

This work targets providing crosslinked vegetable oil-based hydrophobic coatings in a single-step solvent-free process. Based on the principle of in-situ crosslinking, the first research question is:

Is it possible to hydrophobize paper through crosslinked vegetable oil-based coatings using a conventional coating technique while maintaining a solvent-free single-step process?

To investigate the possibility to hydrophobize paper with a crosslinked vegetable oil-based coating without prior derivatization steps, using the thiol-ene click reaction is a promising approach considering the presence of unsaturated carbon-carbon bonds in many vegetable oils. The coating consists of a commercial dithiol mixed with olive oil, which are then deposited through dip coating and crosslinked by UV light, thereby fulfilling the requirements of a solvent-free process without further derivatization steps (Figure 8a). Reaction monitoring through observation of carbon-carbon double bond conversion enables establishment of suitable conditions for paper hydrophobization.

II Covalently attached hydrophobic vegetable oil-based paper coatings through thermal treatment

Sizing is the traditional technique for increasing paper's water resistivity through covalent or electrostatic attachment of the hydrophobizing agent. However, it does not endow paper with durable water resistance and moreover, the synthesis of sizing agents relies on non-renewable and non-environmentally friendly materials. Despite attempts to replace at least part of the raw materials with renewable feedstock such as vegetable oils, the need to functionalize the latter is still disadvantageous for green chemistry-based approaches. Ideally, the coating agent would be able to react with the cellulose by itself without the need for prior derivatization. It is known from literature that cellulose can undergo transesterification reactions with vegetable oils when exposed to elevated temperatures. Considering that such a process might possibly also impart paper with hydrophobic properties, the second question is:

Can elevated temperatures induce covalent attachment of vegetable oils onto paper to achieve hydrophobization?

A simple process of impregnating paper with olive oil by dip coating, followed by thermal treatment at 70 °C for one month and subsequent Soxhlet extraction, shows the potential to obtain covalently attached hydrophobic coatings without the use of additional chemicals during

the coating step. Substrate storage under different conditions enables elucidation of the processes occurring during aging of vegetable oil-coated paper (Figure 8b).

III Hydrophobic vegetable oil-based coatings deposited through plasma polymerization

Compared to conventional coating techniques, plasma-enhanced chemical vapor deposition (PECVD), also known as plasma polymerization, has several advantages. It is versatile with respect to the selected coating material and substrate and allows deposition of highly crosslinked coatings. Simultaneously, the coating is covalently attached to the substrate. PECVD consumes very small amounts of chemicals and can be operated without generating waste. It is cost-effective and industrial scale-up is considered possible when plasmas are operated at atmospheric pressure. In view of the large amounts of generated waste and drying energy required for conventional coating processes, plasma-assisted coating application shows a great potential for process improvement within the paper industry.

With respect to green chemistry principles, PECVD is a highly interesting approach for avoiding the use of solvents, additional chemicals, multi-step reactions and extraction processes. It therefore promises a truly single-step, waste-free process from deposition to end-use, with minimum consumption of chemicals. So far, vegetable oils have not been used for direct aerosol-based deposition at atmospheric pressure in a PECVD process. Accordingly, the third research question is:

Is atmospheric pressure plasma polymerization able to produce crosslinked, covalently attached hydrophobic coatings using vegetable oils?

PECVD, performed operating a jet-induced sliding discharge device (DiscJet) at atmospheric pressure, enables deposition of vegetable oil-based plasma polymer coatings by means of an aerosol. Initial studies use chia oil and tung oil as precursors, and glass slides as simple model substrates, to examine the influence of the plasma power on the coating properties. Thus-obtained parameters are used for coating deposition onto smooth glassine paper substrates (Figure 8c).

IV Vegetable oil-based plasma polymer coatings on varying paper substrates

One advantage of performing PECVD using a jet-induced sliding discharge device at atmospheric pressure is its suitability for coating sensitive, rough substrates such as paper. Having proven the basic suitability of plasma-polymerized vegetable oil for hydrophobization

of smooth paper substrates, further enquiries into the coating of porous papers are needed for gaining insight into the scope of applicability. Accordingly, the fourth research question is:

To what extent do vegetable oil-based plasma polymer coating properties depend on the paper substrate properties?

To examine the influence of substrate porosity, three cotton linter papers calendered with different line pressures are compared, using glassine paper as relatively smooth reference substrate. The influence of mere paper surface modification through plasma treatment is examined, followed by PECVD of chia oil at constant plasma parameters but different coating amounts. Finally, proof of concept examinations of the suitability of other plasma-polymerized vegetable oils for paper hydrophobization are conducted (Figure 8d).

4. Methods

4.1. Cellulose fibers – the raw material for paper

Cellulose is the most abundant biopolymer on earth, as it is the main constituent of the plant secondary cell wall, binding about 40% of the world's plant-based carbon and amounting to approximately 265 billion tons.^[124] Its molecular structure was determined by PAYEN in 1838,^[125] while its polymeric characteristic was described by STAUDINGER in 1920.^[126] Cellulose is composed of linearly bound β -(1,4)-linked D-anhydroglucose units which, due to the stereochemistry of the 1,4-glycosidic bond, are rotated 180° in plane with respect to their neighbors. Two adjacent anhydroglucose units form a cellobiose unit, which is considered the repeating unit of the cellulose polymer (Figure 9a).^[127] The degree of polymerization of cellulose depends on its origin and is strongly influenced by the applied pulping method. For wood-based cellulose, the degree of polymerization can range between 300 and 1,700 while that of cotton, plant fibers and bacterial cellulose ranges between 800 and 10,000.^[125]

Linear cellulose chains are the smallest building blocks of the hierarchical structure forming cellulose fibers. The chains are arranged into elementary fibrils of 1.5–3.5 nm diameter, that in turn form microfibrils of 10–30 nm diameter, which are arranged into macrofibrils that constitute part of the cell wall of the plant fiber (Figure 9a).^[35,128]

The architecture of plant fibers depends on their origin, as for instance wood fibers differ from cotton fibers (Figure 9b and c). They have in common their concentric multilayered structure, wherein the cellulose microfibrils vary in orientation in each layer of the cell wall. The microfibrillar arrangement depends on the plant origin and endows each material with its characteristic properties like strength and elasticity.^[125,129] Wood can be considered a composite material made from cellulose, hemicellulose and lignin. Fibers are glued together by the middle lamella (ML), which is rich in lignin but barely contains any cellulose. This is followed by the primary wall (P), the secondary walls 1 and 2 (S1 and S2), with the latter containing the largest amount of cellulose, the tertiary wall (T), also referred to as secondary wall 3, and sometimes a coverage of the luminal surface with warts (W).^[124] The secondary wall 2 is the thickest and responsible for tensile resistance due to the steep fibril arrangement, while the fibrils in the secondary wall 1 are sloped more gently and thus induce compression resistance.^[124]

Raw cotton linter fibers feature an intrinsically high cellulose content of 73%, while the components of the fiber's protective cuticle (C), waxes and pectins, as well as fats, proteins and ash are to be named amongst the most important impurities.^[130] The primary wall (P) below the cuticle is very thin (below 1 μ m) and contains mainly pectins and waxes with only 5% cellulose. In the secondary wall 1 (S1), the cellulose is arranged in a criss-cross helical way,

while it is more directed in the secondary wall 2 (S2).^[129] The combination of the network-like arrangement of the cellulose fibrils in the primary wall with the more regular orientation of the fibrils in the secondary wall has a decisive influence on the fibers' swelling behavior.^[129]

The supramolecular structure of cellulose is characterized by an extensive hydrogen bonding network, in which intramolecular hydrogen bonds stabilize the linear chain conformation and intermolecular hydrogen bonds link individual cellulose chains (Figure 9d).^[38] This hydrogen bonding network, combined with the high degree of chain linearity, enables formation of highly ordered, crystalline regions, which are surrounded by amorphous regions, an arrangement which HEARLE described by the *fringed fibril model*.^[131] Out of five crystalline allomorphs known,^[38] naturally occurring cellulose only features two distinct crystalline cellulose modifications. Their proportion depends on the cellulose's origin, as cellulose I_α is primarily produced by lower forms such as bacteria and algae, while cellulose I_β is produced by higher plants such as cotton and therefore relevant for paper production.^[132]

The fiber is held together by comparatively long cellulose chains that form part of several crystalline regions. The strong intermolecular chain bonding in the crystalline areas leads to high fiber strength and bad solubility in most solvents. As the hydrogen bonding is weaker in amorphous areas, these are more easily accessible to water, which is the reason for paper swelling through penetration of moisture. However, this also allows access for solvents and chemical reagents, which is a requirement for certain chemical modifications that enable paper to be used in manifold applications.^[38,129,133] Additionally, fiber-fiber interactions contribute to paper strength. While for a long time these interactions were thought to be hydrogen bonds,^[134] it is now assumed that many different forces interact thereupon.^[135]

The choice of raw material to be used for paper production depends largely on the desired properties.^[3] This work uses cotton linter fibers, refined at 100 kWh·t⁻¹ specific refining energy to a refining degree of 21.5 °SR. Cotton linters cellulose mainly consists of α-cellulose and is therefore highly crystalline.^[130,136] It features a high degree of polymerization and a fiber length of 3.5–5 mm, which is well suitable for papermaking and results in high paper strength and good resistance to aging.^[10] Raw cotton linter fibers contain about 80% cellulose, while after bleaching, the cellulose content reaches up to 99%.^[130] Thus, it is especially interesting for research in which a low degree of contamination from other constituents such as hemicellulose and lignin is required. With respect to the plasma polymer coatings and staining experiments targeted in this work, it was of key importance to use very pure cellulose in order to obtain reliable results and reduce the risk of contamination-induced artefacts.

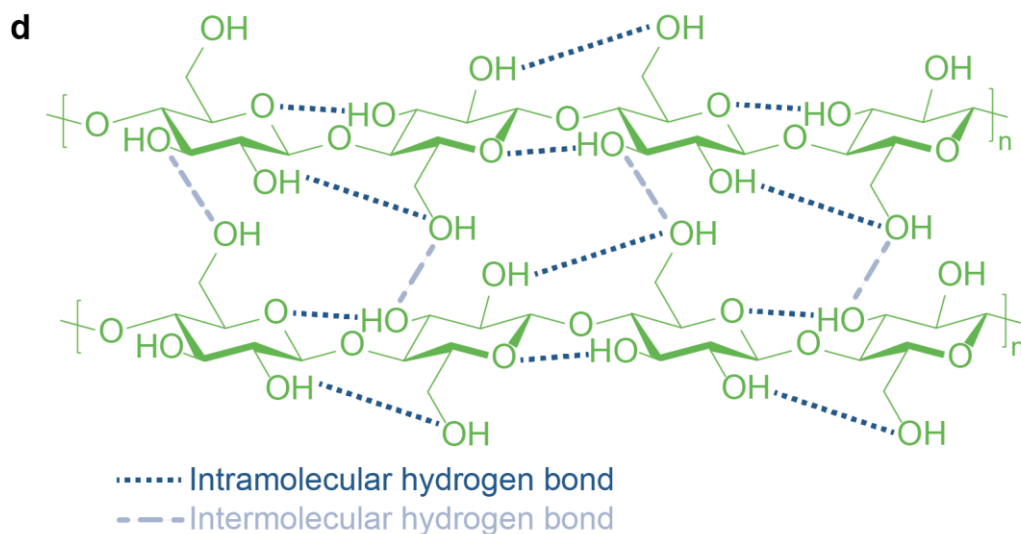
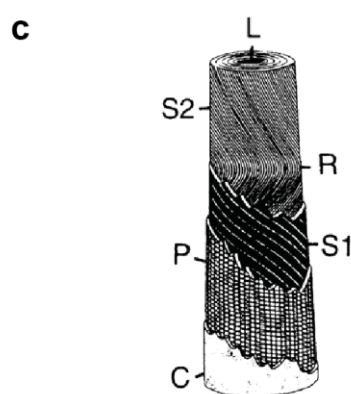
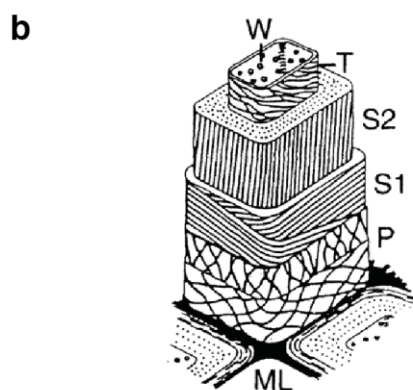
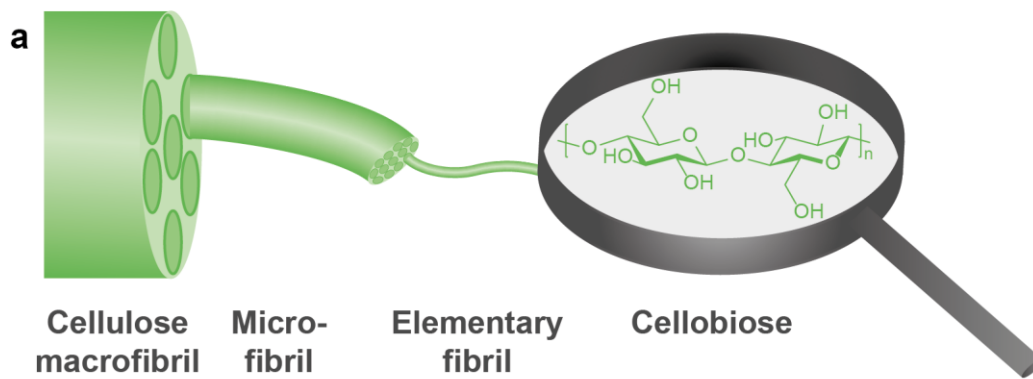


Figure 9: (a) Hierarchical structure of cellulose ranging from the cellulose macrofibril to cellobiose as monomeric building block; (b) Wood fiber,^[124] and (c) Cotton linter fiber^[129,137] showing the characteristic fiber structure (C = cuticle, L = lumen, ML = middle lamella, P = primary wall, R = reversal of the fibril spiral, S1 = secondary wall 1, S2 = secondary wall 2, T = tertiary wall, W = wart layer); (d) Supramolecular structure of cellulose with hydrogen bonding network.^[38]

4.2. Paper production and finishing

The first cellulose-based substrate humankind used to write on was papyrus produced in ancient Egypt in about 3,000 B.C. To make papyrus sheets, two layers of thin papyrus plant stripes were positioned perpendicular to each other and fastened through beating, using the leaking sap as binder.^[138] Despite being its namesake, papyrus was actually different from today's paper, being more similar to a plant stripe-based mat and not made from fiber suspension.^[139] The first sheet forming process based on pulp was developed in China in the second century A.D. and has been the basis of paper production to this day. Both the first paper-based newspaper and the first use of sizing agents were seen in China during the fourth century A.D.^[138] From there, the papermaking technique was spread over the world, first reaching Japan, then Arabia, from where it was brought to Europe in the eighth century A.D. The invention of movable type printing in the 15th century by GUTENBERG greatly increased the demand for paper. This led to novel developments with respect to the scale-up of paper production. For example, rags as material stock got replaced by wood-based fibers. In 1799 ROBERT invented the first paper machine, known as FOURDRINIER machine after its patent owners, thus forming the basis of today's papermaking process.^[138,139] Since then, paper consumption and application fields have continuously increased, with an annual paper production of 420 million tons worldwide in 2022.^[5]

Today, wood is the main raw material for paper, making up around 94% of industrial paper production. Depending on their origin, however, the suitability of wood materials for paper production varies. The length of the fibers is one amongst many relevant factors, as the use of longer fibers leads to higher paper strength. Therefore, softwood, which has fibers of 2–5 mm length, is generally preferred to hardwood, with fibers of 1–2 mm length. Furthermore, the wood's composition equally influences its suitability for paper production. Amongst softwoods, spruce and pine are the materials of choice, while birch, beech, poplar, aspen and eucalypt are the most suitable hardwood-based materials. Besides wood, annual plants such as straw, sugar cane bagasse, bamboo, cotton linters, flax and hemp are also used.^[10]

With regard to the production of pulp for paper manufacturing, a basic distinction can be made between chemical and mechanical pulping, with several hybrid processes combining certain features thereof. Chemical pulping aims at isolating the cellulose from the lignin matrix, while keeping the fibrillar structure intact. The sulfate or kraft process and the sulfite process are the two predominant processes for chemical pulping. Contrastingly, during mechanical pulping, the wood is defibrated by means of grinding or refining. Unlike during chemical pulping, lignin is temporarily softened to enable fiber disintegration, but remains in the pulp. This leads to lower paper strength and restricts the applicability of thus-obtained papers compared to those made

from chemical pulp. Furthermore, grinding or refining reduces the pulp's long fiber content. However, the overall yield (including lignin) is much higher than for chemical pulping.^[2,10] Both the raw material and the pulping process are selected according to the targeted paper application. Following pulping, pulp fibers are fibrillated in the refiner through mechanical treatment, again in view of the desired paper properties. In the approach flow section, the pulp is degassed and diluted to the desired concentration, contaminants are removed and a uniform suspension flow into the wet section of the paper machine is ensured.^[2]

The paper machine itself consists of several components and processing steps (Figure 10), wherein only the most central ones to sheet formation will be described here. The initial wet section consists of the headbox, the wire section and the press section. In the headbox, the suspension is delivered onto the wire with a uniform distribution across the machine width. Subsequently, the fiber web formation from suspension takes place in the wire section, where the first water removal step is performed.^[2] For dewatering, the paper suspension is poured onto a sieve. Drainage occurs through the continuously growing filter cake and the wire and is driven by gravity, foils, and finally vacuum.^[2] After sheet forming, the sheet dry content is 16–22% and is increased to 40–55% by mechanical pressing in the press section. The sheet then reaches the final dryer section, where the dry content is further increased to 90–96%.^[2] Drying is usually performed through contact drying, where the paper passes over a series of steam heated cylinders. Drying felts ensure transportation and press the paper against the cylinders. Alternatives to contact drying are convection drying and infrared drying.^[10] This last step is also the most energy-intensive one, requiring 20 times the energy needed for the sheet forming step, mostly in the form of steam energy.^[2] Herein, in addition to water removal by evaporation, the hydrogen bonds are formed that endow paper with its high strength.^[2] Finally, the paper is rolled up in the reel section.^[2] Sheet forming is the decisive process for many bulk properties of paper. Although paper is of homogenous thickness, stiffness and porosity vary across the transverse section due to different drying velocities across the machine width.^[10] Furthermore, because of the high processing speeds, the fibers are aligned along the machine direction, which leads to anisotropic properties that differ between machine direction and cross direction.^[2] Additionally, the sieve structure is “imprinted” on the paper.^[10] Industrial-scale paper production from pulp is a highly sophisticated process, wherein process speeds of 2000 m·min⁻¹ and sheet widths of 11 m can be achieved.^[140]

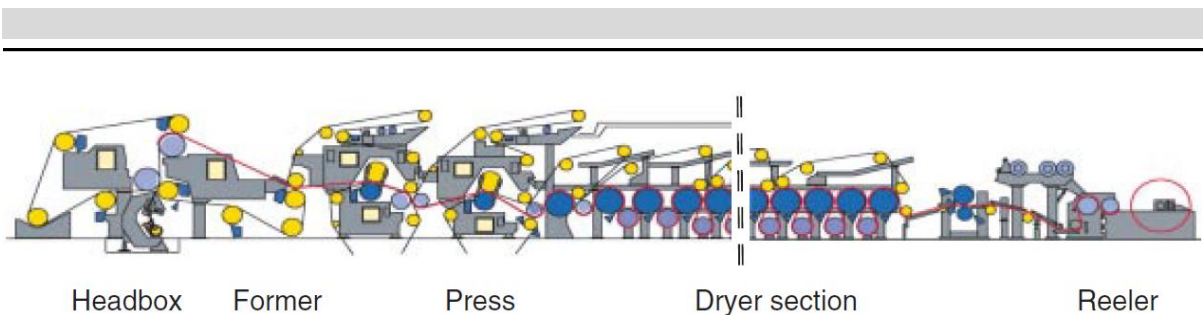


Figure 10: Schematic display of the most important sections of an exemplary paper machine.^[2]

Paper production on a laboratory sheet former consists of the same steps as on a paper machine and is performed in accordance with DIN EN ISO 5269-2.^[141] First, the pulp dispersion is diluted to the desired concentration and stirred continuously for 30 min to avoid fiber entanglement. The pulp (this work using 2 L of 0.16 wt% cotton linter fiber dispersion for sheets with a grammage of 100 g·m⁻²) is transferred into the sheet forming column, while water (4 L) is injected from below. The mixture is swirled for 5 s, then the water drops to the level of the filter cake followed by vacuum suction for 10 s. Through couching, the paper is transferred onto a couching board. To this end, the couching board is placed onto the sheet and couched twice using a couch roll. The wet sheet is then removed from the sieve by knocking it against a rubber base. Afterwards, the wet sheet is covered by a cover sheet and dried under reduced pressure (93 °C, 10 min). Immediately after drying, the grammage is determined by the bone dried paper weight. In contrast to machine paper, the fiber orientation and thus also the mechanical characteristics of laboratory hand sheets are isotropic in the sheet plane.

While on the laboratory scale, paper production, calendering and finishing are usually performed as separate steps, paper machines can be equipped to further modify the paper directly on the machine before reeling.^[140]

After sheet formation, paper finishing endows paper with the desired properties. Surface sizing aims at improving paper's resistivity to water intake and thus printability without significantly modifying the surface itself. Coating covers the surface and smoothens its texture.^[19,140] Its aim is to improve optical properties, tactile properties and printability or to form barriers against fluids and gases, and finally to functionalize paper for specific applications.^[30,142,143] After surface sizing or coating, papers are again submitted to a subsequent drying step.^[2] In this work, dip coating and size press coating have been used to apply coating material onto paper, and will therefore be described in more detail.

Size press coating is used to coat paper on both surfaces, contrary to film press coating, which can cover either one or both sides, with the film being applied via a pre-metered roll.^[142] During size press coating, the paper is transported through a pond of sizing solution, passing between two rolls that press the liquid from the pond into the paper. The sizing agent thus penetrates

into the paper due to a combined effect of capillary forces and hydraulic pressure.^[140] The distance between the rolls as well as the paper transportation speed are decisive for the amount of coating applied. An advantage of size press coating is its relatively easy incorporation into the paper production line.^[10]

Contrarily to traditional paper coating and sizing techniques that have been adapted for large-scale and in-line processing such as size pressing, dip coating allows for coating of comparatively small substrates. It is a helpful alternative in the laboratory, when the available amount of coating material is not sufficient for large-scale processing. Herein, the substrate is immersed into the coating liquid at controlled speed, kept in the liquid for a defined time and then withdrawn at controlled speed. Thus, immersion time and withdrawal speed, concentration of the coating solution as well as paper properties and finally temperature are decisive for coating thickness and morphology.^[144] Dip coating has been used previously for coating paper at small scale using different silica-based precursors.^[33,145]

Finally, different finishing approaches modify the surface quality of paper, such as smoothness, gloss or density. One of those is the calendering approach used in this work. The paper is transported between two rolls made of steel or elastic material (paper, cotton or plastics such as rubber or resin), whereby pressure and temperature compact the paper and plastically level the surface, while the interior remains elastic.^[10] The smoothening effect of calendering is determined by many factors. Increasing the temperature of the rolls and the paper as well as the pressure exerted by the rolls leads to higher smoothness, while increasing the calendering speed leads to lower smoothness. Elasticity and surface quality of the rolls as well as the paper humidity are equally relevant.^[146] The polymeric properties and especially the glass temperature (T_g) of cellulose are decisive for the calendering process. The paper's T_g depends on the humidity, which acts as plasticizer, and can be modified through heating, applying pressure or modifying the humidity distribution. Such T_g gradients are created during the calendering process and allow for smoothening the paper surface whilst maintaining the bulk volume of the paper.^[146] However, calendering may also intensify inhomogeneities – such as areas of increased flocculation – present in the paper. As such, thicker parts of the paper are subjected to higher pressure and will therefore become denser, which is observable by increased gloss and even blackening.^[146]

Similar effects are observed when calendering round laboratory handsheets. In this case, the paper sheets are smaller than the calendering rollers, which has the same effect as thickness inhomogeneity, especially around the paper edge. Therefore, the handsheets are denser, more glossy and appear darker around the edge than in the center. This has to be taken into account

for experimental design and interpretation. As a consequence, usage of the outer parts should be avoided.^[146]

4.3. Vegetable oils

Vegetable oils can be obtained from the fruit, seeds or kernel of manifold plants such as olives, safflower, chia, rapeseed, soy beans and coconuts.^[147,148] They are not only used in human diet, but additionally are highly relevant for example in the cosmetics industry, such as in skincare, in the pharmaceutical industry, like as laxative or for transporting lipophilic active agents, in binders, for example in wood varnish, as well as in lubricant and biodiesel production.^[147-149] The most important vegetable oils worldwide in the trading year 2023/2024 were palm oil, soybean oil, rapeseed oil and sunflowerseed oil.^[150]

Vegetable oils are triesters of glycerol and fatty acids, and thus also known as triacylglycerols.^[149,151] The fatty acids differ in their respective chain length, which can range from 4 to 26 carbon atoms, and degree of saturation, both of which are decisive for the oils physical properties and scope of application. For instance, depending on their degree of saturation, oils can be solid or liquid at room temperature.^[151] Beyond that, minor components, such as antioxidants, also have a great influence on the vegetable oil's final properties.^[151] Note that vegetable oils are a natural product and thus their composition varies depending on growth and harvesting time and location.^[152]

Humankind has been exploiting vegetable oils for around 6,000 years, with the to date oldest findings originating from Egypt and Babylonia. Even in ancient times, different methods were used to obtain olive oil, that epoch's most important vegetable oil. The oil was cold-pressed using the olives' own weight, or with the help of a stone or a wooden beam, which resulted in oils of the best quality. Pouring hot water over the olives also enabled producing high quality oils. Finally, by first pressing the olives, then adding hot water followed by another pressing step, several oil batches with decreasing quality were obtained.^[148]

Nowadays, vegetable oil can be produced either through mechanical pressing, chemical extraction or combination thereof, preceded by precleaning and crushing. The process is selected depending on the desired properties and applications.^[148] Pressing refers to application of mechanical pressure to remove the liquid, while preserving the properties of the oil and its constituents, without use of other chemicals.^[153] The use of the thus-obtained cake as animal feedstock constitutes an additional valorization of the residual material.^[148] To improve yields, several pressing steps can be performed subsequently. The first cold pressing produces oil with the highest quality, also known as virgin oil, while subsequent pressing steps can be performed

at higher temperature to improve rupture of the oil cell walls, which results in inferior oil quality but higher yields.^[148]

Extraction refers to the removal of liquids with the help of a solvent. Compared to pressing, the yields are higher,^[153] but the cake cannot be used as animal feedstock anymore.^[148] The oil quality is often inferior as many valuable extractives may also be removed through extraction,^[148] but it can be preserved for a longer period of time.^[153] Extraction is nowadays mostly performed using hexane.^[147]

Afterwards, unwanted substances and contaminants can be removed through refining. Amongst these are for example phospholipids, which can be converted into lecithin, free fatty acids, pesticides, mycotoxins, pro-oxidative substances and finally unwanted coloration, odors and flavors.^[147]

Extensive encyclopedias summarize the characteristics of an enormous variety of vegetable oils. The following descriptions of the oils central to this work are based on the encyclopedias by KRIST^[151] as well as ROTH and KORMANN.^[148]

The chia plant (*Salvia hispanica*) was widespread in Mesoamerica before the Spanish conquest and valued as staple food, probably with similar importance as corn. Chia requires an arid, frost-free climate and is nowadays grown in Central and South America. Both the seeds and the plant itself contain a high amount of α -linolenic acid. With respect to the plant, it has however been found that the α -linolenic acid content decreases as the plant becomes older. The oil can be extracted from chia seeds through pressing, solvent extraction or extraction with supercritical carbon dioxide. Chia oil can be used as drying oil, in paints and varnish and for food consumption. Interestingly, it has been found to increase the content of unsaturated fatty acids in meat after the corresponding animals had been fed therewith.^[151]

Olive oil is obtained through pressing of olives, the fruits of the olive tree (*Olea europaea*). Olive trees grow best in Mediterranean climate and can survive heat, but dislike frost and extreme climate in general. Most of the worldwide olive production is located around the Mediterranean Sea. The variety of olive oil quality grades is vast, with the best quality one being virgin olive oil. Note that not all quality grades are fit for human consumption. Like many other oils, olive oil can also be used for pharmacological applications, in cosmetics or as lubricant.^[151]

Safflower (*Carthamus tinctorius*) was mainly used to produce a red dye during the Medieval Age and even in Ancient Egypt, until natural dyes were replaced by synthetic dyes in the 19th century. Today, safflowers for oil production mostly grow in the USA, Australia, Greece, Turkey and India, where the weather is warm and not too humid. Safflower oil is produced from safflower seeds through pressing or extraction, which is usually followed by refining.

Although the fatty acid composition is subject to variation, safflower oil generally features an extraordinarily high content in linoleic acid. It is rather stable despite its high degree of unsaturation. However, it is not very resistant to heat. It is used in medicine against high cholesterol levels and arteriosclerosis, but can also for instance be used to replace linseed oil in linoleum production or in varnishes.^[148,151]

Tung oil is obtained from the tung tree (*Aleurites ssp.*), which originates from China and Southeast Asia. The seeds are separated from the peel and afterwards, the oil is extracted through hot or warm pressing. It features a characteristic smell of lard oil.^[148,151] Its main component is α -elaeostearic acid, which results in extremely fast drying properties and thus makes tung oil an excellent drying oil for wood varnish. On heating, its viscosity rapidly increases until gelation.^[149,151]

All four vegetable oils used in this work feature C18 fatty acid chains as main component and were selected based on the degree of unsaturation. Olive oil, safflower oil and chia oil are characterized by especially high contents in oleic acid, linoleic acid and α -linolenic acid respectively. Oleic acid contains one, linoleic acid contains two and α -linolenic acid contains three isolated carbon-carbon double bonds. Contrarily to these three oils, tung oil mainly features α -elaeostearic acid with three conjugated carbon-carbon double bonds.

Olive oil, with its main component oleic acid, promised to be a good research subject for understanding the processes involved in conventional paper hydrophobization, as not only the oil but also the constituting fatty acid is well available for use in simplified model systems. Contrarily, chia oil's α -linolenic acid can only be purchased at high costs and was therefore not considered for extensive studies. However, chia oil, featuring three unsaturated carbon-carbon double bonds, was regarded as a promising precursor for plasma polymerization with the potential for interesting comparisons to more saturated safflower and olive oil as well as the constitutional isomer tung oil.

4.4. Atmospheric pressure plasma polymerization on sensitive 3D substrates

Compared to substrates commonly used for plasma-assisted surface modification, paper is rather challenging. It is not only far more sensitive than glass or silica wafers with respect to disintegration, breaking or surface property modification, its surface is also characterized by its high roughness, which makes depositing a homogeneous coating more difficult. Established paper coating techniques are used in-line, even often directly integrated into the paper production line and proceed at extremely high speeds. For large-scale industrial application, a PECVD device should ideally be adapted to this process. Therefore, low temperature plasma-

based coating processes at atmospheric pressure that are applicable across large substrate surface areas, ideally the entire width of the paper roll, are needed.

Unfortunately, the most commonly used volume dielectric barrier discharge (DBD) devices are disadvantageous when it comes to treating larger surfaces. Usually, the space in the discharge gap between the electrodes is limited and so is the thickness of the substrate to be placed between the electrodes. In the case of thicker substrates, rather high voltages are a prerequisite for a successful discharge, leading to working safety issues.^[154] Additionally, microdischarges tend to form in the same channels as the footpoint of previously ignited microdischarges, which leads to inhomogeneous surface treatment and ultimately to material damage.^[155] Further development of DBD has led to the invention of the surface DBD, where the electrodes cover two sides of a planar dielectric, as well as coplanar arrangements frequently seen in plasma displays, both of which do no longer impose volume restrictions.^[156] The persisting problem of discharge stability and homogeneity as well as the desire to treat larger surfaces has been further addressed by the introduction of the diffuse coplanar surface barrier discharge (DCSBD).^[157] DCSBD devices comprise parallel electrodes embedded in an alumina dielectric layer (Figure 11a).^[157] The electric current and the plasma are not generated between the electrodes, but in a 0.3 mm thin layer between the electrodes and the substrate surface.^[158] The plasma is highly homogeneous and therefore ideal for the treatment of and coating deposition onto larger flat surfaces.^[157,158,159] However, the width of the discharge gap, in this case between the dielectric layer and the substrate, is restricted by the need to maintain discharge stability, which calls for extremely precise process conduction and may be challenging with inherently rough substrates such as paper.

Another method for generating uniform plasmas at low temperatures for material processing is the atmospheric pressure plasma jet (APPJ), which features a large variety of different device setups, component materials and potential applications.^[160] Usually, the plasma is generated in an open electrode arrangement and the plasma is expelled onto the substrate surface through the process gas flow (Figure 11b).^[161] The source geometry with both electrodes arranged above the substrate enables coating of thick materials and tolerates relatively large discharge gaps, but the point-discharge characteristic limits the treatable surface, requiring surface scanning or array mounting of electrodes to treat larger areas.^[162]

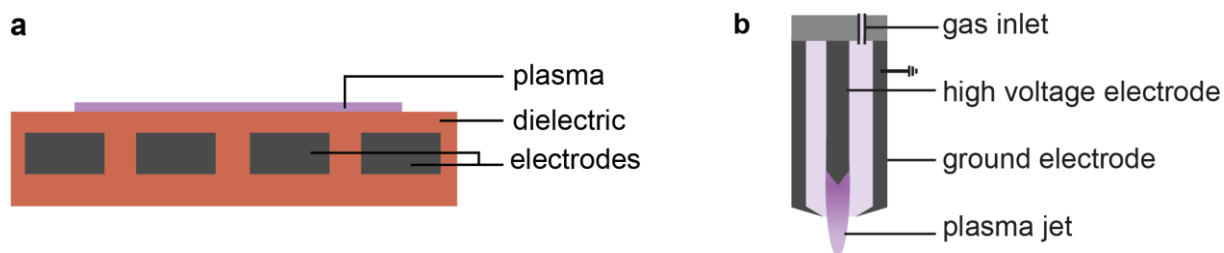


Figure 11: (a) Schematic display of the DCSBD based on reference^[158]; (b) Schematic display of the APPJ, adapted from reference^[163], published under Creative Commons License CC BY 4.0, Attribution 4.0 International; <https://creativecommons.org/licenses/by/4.0/>; © 2023 The Authors. *Plasma Processes and Polymers* published by Wiley-VCH GmbH.

Besides the necessity to coat large surface areas at atmospheric pressure, the high process speeds during paper production remain an issue due to a significant influence of drag air. This can induce turbulences, which may lead to heterogeneous coating deposition and impair coating properties. Therefore, a plasma polymerization device that is able to coat large areas homogeneously and at the same time insensitive to drag air is required.

A device that combines both the advantages of DCSBDs and APPJs and tries to address the issue of drag air is the jet-induced sliding discharge device, called DiscJet, developed by VIÖL *et al.*^[164] (Figure 12), which enables both surface modification and PECVD on flat as well as rough surfaces. The DiscJet is a rotationally symmetrical device wherein the high voltage electrode, 3D-printed from titanium, is placed in the center of the discharge chamber, and the mass electrode, made from copper, concentrically surrounds it (Figure 12a). The mass electrode is covered by a dielectric made from aluminum oxide ceramic, which creates a dielectric barrier. Besides plasma generation, the high voltage electrode further functions as gas mixing device. The process gas is fed into a space between the inner and the outer shell of the electrode and flows into the discharge gap through tangential bores in the outer shell, which equip the process gas with a spin. The high voltage electrode further contains a second gas inlet for the carrier gas transporting the precursor. The carrier gas passes through the space generated by the inner shell of the electrode and only encounters the plasma when exiting the electrode into the discharge zone. This arrangement avoids premature plasma polymerization within the electrode, as plasma and precursor only mix directly before reaching the substrate surface. The process gas, flowing out of the electrode with a spin, takes up the carrier gas emerging from the center of the electrode. This rotating gas flow ensures uniform transportation to the substrate and coating deposition across the entire device width. Additionally, it leads to the formation of a gas cushion between the substrate and the plasma source that enables working under almost full exclusion of ambient air. When the plasma encounters the surface of a nonconductive substrate, a floating potential is generated, offering a counter-potential to the mass electrode

and thereby closing the discharge circuit. The discharges slide across the surface to return to the mass electrode, which is why this concept is referred to as a sliding discharge concept. Combining APPJ and DCSBD features thus enables coating thick nonconductive, sensitive substrates independent of their geometry. Furthermore, the DiscJet can operate at substrate-source distances of several centimeters and coat surfaces in the width of several centimeters. Additionally, the gas cushion has the potential to reduce the effects of drag air at elevated process speeds.^[164,165]

The DiscJet may be used both for plasma-assisted surface treatment and plasma-enhanced chemical vapor deposition. The system used in this work relies on liquid precursors, which are introduced into the system as aerosol produced by the carrier gas flowing through a nebulizer unit, which is connected to the high voltage electrode by tubes (Figure 12b). Precursors with higher vapor pressure can also be introduced by bubbling the carrier gas through a gas washing bottle containing the liquid precursors instead of using a nebulizer unit. Finally, the whole device can be moved across the substrate surface by a portal system to coat larger areas or to perform multiple coating runs.

Many parameters can be varied to modify plasma characteristics and surface properties and it is important to note that numerous aspects of such variations have not yet been fully explored and understood. Amongst these are for example the interactions of plasma power, substrate-source distance, the choice and flow rate of plasma and carrier gas as well as the speed and multiplicity of transportation across the substrate.^[165,166] Within the frame of this work, focus is placed on examining the influence of plasma power, carrier gas flow rate as well as the number of transportation and thus coating runs.

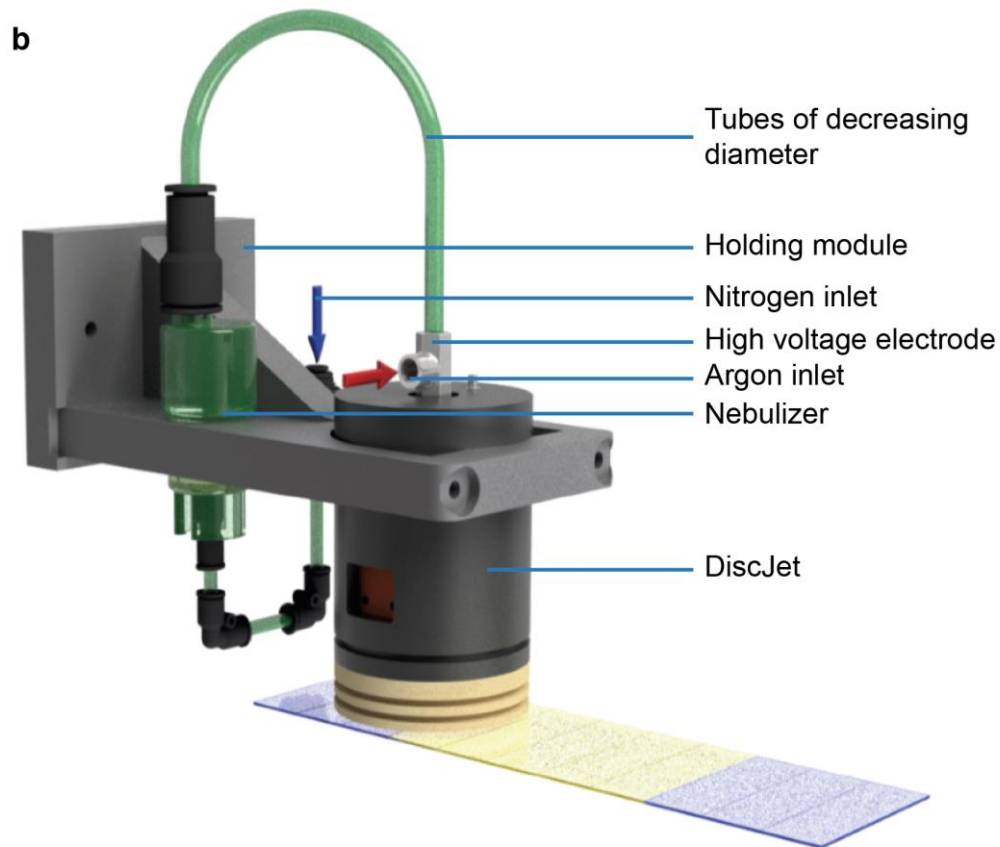
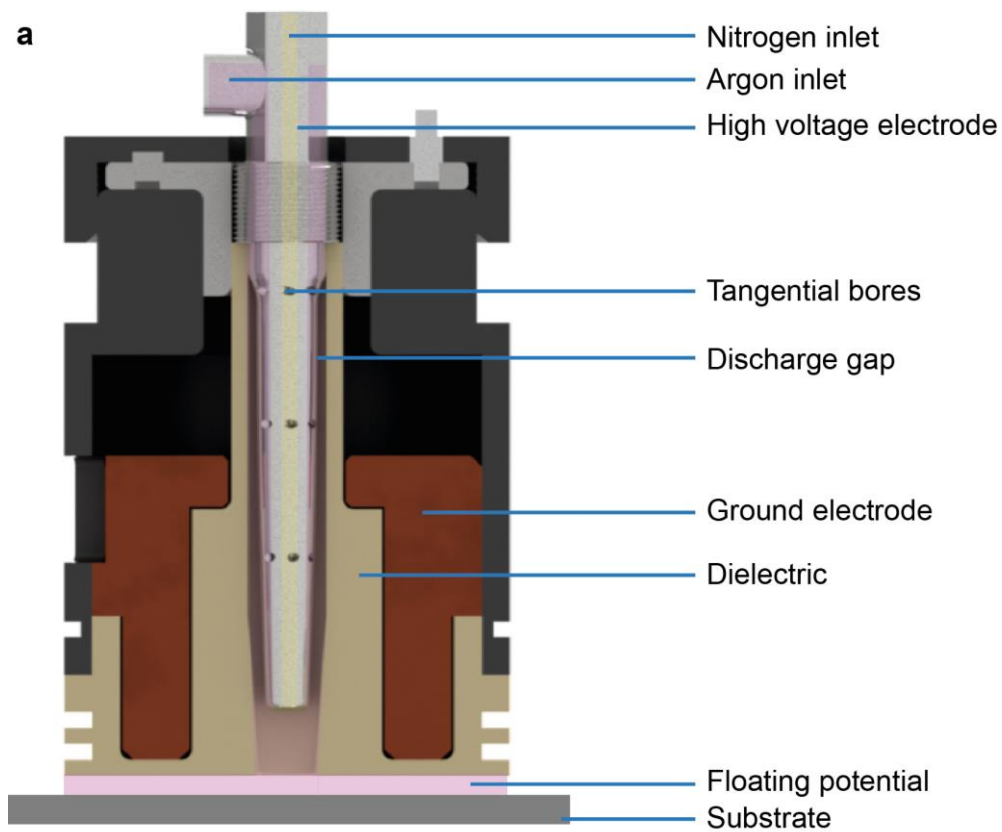


Figure 12: (a) Cross-section of the DiscJet device; (b) Setup of the DiscJet during operation. (a) and (b) are adapted from reference^[167], which was published under Creative Commons License CC BY 4.0, Attribution 4.0 International; © 2024 The Authors. *Plasma Processes and Polymers* published by Wiley-VCH GmbH.

5. Results and Discussion

5.1. Thiol-ene photocrosslinking as a conventional solvent-free method for hydrophobizing paper with vegetable oils

Application of crosslinkable materials is one approach for obtaining durable paper coatings. Generally, the coating formulation – frequently containing materials derivatized with a crosslinkable moiety, as well as a crosslinking agent – is deposited in a wet-end process, followed by applying a stimulus that induces the actual crosslinking reaction.

In an initial step, this traditional approach was to be modified with the aim of achieving a greener process, focusing on waste prevention and reduction of derivatives. Thus, a solvent-free system achieving paper hydrophobization through crosslinked coatings without performing prior derivatization steps was examined. Herein, vegetable oils represented a suitable starting material due to their intrinsic hydrophobicity and functionalization potential at the carbon-carbon double bond.

Several previous works have crosslinked vegetable oils after derivatizing the carbon-carbon double bonds.^[168] Yet, to forego the need for derivatization reactions, the ability of unsaturated vegetable oils to undergo photopolymerization at the carbon-carbon double bond^[169,170] can be considered a promising starting point. For instance, ZHAO *et al.* have shown that in a system containing solely linseed oil and 1,6-hexanedithiol, photocrosslinking was possible at wavelengths below 275 nm without the use of neither photoinitiator nor solvent.^[170]

Based on these findings, a thiol-ene photocrosslinking system was selected to examine the suitability of conventional, crosslinked vegetable oil-based coatings for paper hydrophobization. Thiol-ene photocrosslinking was conducted through ultraviolet (UV) irradiation at a wavelength of 254 nm and without the use of photoinitiator or solvent. Olive oil was chosen as vegetable oil component, because both the triglyceride and its main constituent, oleic acid, are easily available and thus enable in-depth examination of the selected system. 1,8-octanedithiol (1,8-ODT) was selected as crosslinking agent due to its good miscibility with olive oil. To determine optimal irradiation conditions, hydrophobized glass slides were used as model substrates, while cotton linter laboratory handsheets were used as paper-based substrates.

Initially, oleic acid and 1,8-ODT were linked on hydrophobized glass slides to find suitable reaction conditions, as the resulting dimer was still soluble in solvents for ¹H-nuclear magnetic resonance (NMR) spectroscopy and therefore enabled reaction monitoring. Varying the irradiation dose from 5 J·cm⁻² to 50 J·cm⁻² revealed a maximum carbon-carbon double bond conversion of (85.2 ± 1.2)% at an irradiation dose of 20 J·cm⁻². Water contact angles (WCAs) on paper increased significantly to (80.2 ± 1.8)° at 20 J·cm⁻², contrary to immediate absorption

on uncoated paper, and did not show any further significant increase at even higher irradiation dose. The successful thiol-ene reaction was confirmed by attenuated total reflectance-Fourier transform infrared (ATR-FTIR) spectroscopy through the disappearance of the signal associated with the carbon-carbon double bond. Furthermore, ATR-FTIR spectra demonstrated that the oleic acid-1,8-ODT dimer was not covalently attached to the paper, as the characteristic bands vanished after Soxhlet extraction.

In accordance with these observations, the optimized irradiation dose of $20 \text{ J}\cdot\text{cm}^{-2}$ was used for crosslinking olive oil and 1,8-ODT. To facilitate analytics using simple model substrates, the mixture was again applied to glass slides through dip coating. After UV irradiation, the coating was insoluble in various organic solvents, which is a good indicator for successful crosslinking. ATR-FTIR spectra again showed consumption of the carbon-carbon double bond. Differential scanning calorimetry (DSC) measurements displayed changes in the original olive oil melting peak at $-10 \text{ }^\circ\text{C}$, notably peak broadening and a peak maximum shift to higher temperatures. This, as well as the appearance of a second melting transition around $11 \text{ }^\circ\text{C}$, was indicative of the formation of olive oil-thiol compounds, dimers and oligomers. The decreased overall melting enthalpy revealed the formation of a crosslinked network that did not melt in the examined range up to $100 \text{ }^\circ\text{C}$.

Based on the thus-obtained understanding of the crosslinking process, cotton linter papers were size press coated with the olive oil-1,8-ODT mixture and irradiated with UV light. While the surface roughness did not change significantly, hydrophobicity was greatly enhanced from $(62.7 \pm 2.9)^\circ$ for a purely olive oil-coated paper to $(120.7 \pm 2.1)^\circ$ for papers covered with the crosslinked coating.

Thus, thiol-ene photocrosslinking proved to be a successful approach for hydrophobizing paper using olive oil without the use of solvents or subsequent derivatization steps.

In the frame of this work, I was involved in conceptualization, data acquisition and interpretation (glass hydrophobization, paper production, dip coating and size press coating, WCA measurements, ATR-FTIR spectroscopy, SEM imaging and optical profilometry, all performed by myself, as well as ¹H-NMR spectroscopy, which was measured by the NMR service department of TU Darmstadt), writing and creating artwork. Cynthia Cordt was involved in DSC measurements and results discussion. Andreas Geissler was involved in optical microscopy images, conceptualization and interpretation, supervision and funding acquisition. Markus Biesalski was involved in supervision. All authors were involved in proof-reading.

The following article has been published in *Polymers*.

A. Loesch-Zhang, C. Cordt, A. Geissler, M. Biesalski, A solvent-free approach to crosslinked hydrophobic polymeric coatings on paper using vegetable oil, *Polymers* 2022, 14, 1773.

Published by MDPI, Basel, Switzerland under Creative Commons Attribution 4.0 International (CC BY 4.0) License.

The supporting information has not been reprinted here, but can be accessed via the online version of this article: <https://www.mdpi.com/2073-4360/14/9/1773>.

Article

A Solvent-Free Approach to Crosslinked Hydrophobic Polymeric Coatings on Paper Using Vegetable Oil

Amelia Loesch-Zhang¹, Cynthia Cordt¹, Andreas Geissler^{1,2,*} and Markus Biesalski^{1,*}

¹ Macromolecular and Paper Chemistry, Technical University Darmstadt, Alarich-Weiss-Str. 8, 64287 Darmstadt, Germany; amelia.loesch-zhang@tu-darmstadt.de (A.L.-Z.); cordt@cellulose.tu-darmstadt.de (C.C.)

² Papiertechnische Stiftung (PTS), Pirnaer Str. 37, 01809 Heidenau, Germany

* Correspondence: andreas.geissler@tu-darmstadt.de (A.G.); markus.biesalski@tu-darmstadt.de (M.B.); Tel.: +49-61511623727 (A.G.); +49-61511623721 (M.B.)

Abstract: Hydrophobic coatings are of utmost importance for many applications of paper-based materials. However, to date, most coating methods demand vast amounts of chemicals and solvents. Frequently, fossil-based coating materials are being used and multiple derivatization reactions are often required to obtain desired performances. In this work, we present a solvent-free paper-coating process, where olive oil as the main biogenic component is being used to obtain a hydrophobic barrier on paper. UV-induced thiol-ene photocrosslinking of olive oil was pursued in a solvent-free state at a wavelength of 254 nm without addition of photoinitiator. Optimum reaction conditions were determined in advance using oleic acid as a model compound. Paper coatings based on olive oil crosslinked by thiol-ene reaction reach water contact angles of up to 120°. By means of Fourier transform infrared spectroscopy and differential scanning calorimetry, a successful reaction and the formation of a polymer network within the coating can be proven. These results show that click-chemistry strategies can be used to achieve hydrophobic polymeric paper coatings while keeping the amount of non-biobased chemicals and reaction steps at a minimum.

Keywords: vegetable oil; coatings; paper; thiol-ene; hydrophobicity; barrier; food packaging



Citation: Loesch-Zhang, A.;

Cordt, C.; Geissler, A.; Biesalski, M.

A Solvent-Free Approach to Crosslinked Hydrophobic Polymeric Coatings on Paper Using Vegetable Oil. *Polymers* **2022**, *14*, 1773. <https://doi.org/10.3390/polym14091773>

Academic Editor: Mariaenrica Frigione

Received: 30 March 2022

Accepted: 22 April 2022

Published: 27 April 2022

Publisher's Note: MDPI stays neutral with regard to jurisdictional claims in published maps and institutional affiliations.



Copyright: © 2022 by the authors. Licensee MDPI, Basel, Switzerland. This article is an open access article distributed under the terms and conditions of the Creative Commons Attribution (CC BY) license (<https://creativecommons.org/licenses/by/4.0/>).

1. Introduction

Due to the increasing importance and demand of circular and sustainable materials, paper has gained increased attention as a packaging and versatile light-weight construction material. The advantages of paper in such applications include high specific mechanical strength, the possibility to add further properties by simple coatings, the availability from renewable resources, and finally technologically well-developed recycling processes. However, with paper, some important challenges exist, such as a lack of protection against water penetration and associated changes in dimension and strength, potential damages by microorganisms, permeability to gases, absorption of odors, and sensitivity to abrasion under continuous mechanical loads. While some of these challenges can be addressed using functional additives already during paper sheet production, other aspects are tackled by subsequent finishing of readily prepared paper.

There are already several reports addressing this highly complex set of demands for paper applications. Some have focused on applying vegetable oil-based precursors onto cellulose materials using various methods for obtaining increased hydrophobicity. For instance, cotton with low water absorbance and increased contact angle (up to 80°) was obtained via deposition of soybean oil from an organic solvent followed by thermal treatment [1]. In jute and sisal fibers coated with an emulsion of rice bran or neem oil and a phenolic resin, transesterification reactions between the triglycerides and cellulose were induced by thermal curing, resulting in increased hydrophobicity, tensile strength and durability of the fibers [2]. Chemical reactions were employed for direct covalent

attachment of fatty acids to cellulosic materials via transesterification reactions using fatty acyl chlorides [3–5]. Ring-opening polymerization enabled crosslinking of epoxidized soybean oil onto filter paper with the cellulose hydroxyl groups acting as initiators, resulting in contact angles of up to 145° [6]. In a very interesting work, Onwukamike et al. directly grafted sunflower oil onto cellulose without any supplementary activation or derivatization steps using a 1,8-diazabicyclo[5.4.0]undec-7-ene (DBU)-CO₂ solvent system [7]. Samyn et al. applied dispersions of different vegetable oils incorporated into poly(styrene-maleic anhydride) particles onto paper and paperboard substrates, obtaining porous coatings chemically stable against water and exhibiting static contact angles above 90° [8]. Entirely new structures can be obtained by plasma treatment, which was used by Cabrales et al. to graft oleic acid from ethanolic solution onto cotton fabric, obtaining contact angles above 150° with long-term stability [9].

Apart from covalent attachment to or physical deposition onto substrates, intensive research has recently been focused on using fatty acids or vegetable oils as sustainable resources for polymer production through crosslinking reactions [10–16]. Altuna et al. produced a network from epoxidized soybean oil crosslinked with an aqueous citric acid solution without the use of additional solvents or catalysts [17]. Wuzella et al. photocured acrylated epoxidized linseed oil with three different photoinitiators using a polychromatic ultraviolet (UV) lamp with a maximum light intensity at 365 nm, correlating resulting properties to cure evolution and double bond conversion [18]. Wang et al. esterified castor oil with 3-mercaptopropionic acid, which in the following allowed crosslinking of the derivatized oil films deposited on glass substrates without further addition of solvent or initiator using UV light [19].

To date, most of these strategies require various reaction steps, which again renders them rather sophisticated. Hence, more simple one-step procedures are increasingly in focus. An example for the latter is the well-known thiol-ene click reaction, as it can be performed on unsaturated fatty acids and vegetable oils without further derivatization. Thiol-ene reactions enjoy high popularity due to their good uniformity, controllability and insensitivity towards oxygen inhibition [20]. Thiol-ene polymerizations proceed via step-growth radical polymerization (Figure 1). The olefin structure has a decisive influence on the kinetics and conversion rates. While terminal double bonds react rapidly and quantitatively, internal enes react more slowly and without full conversion, which is due to steric effects induced by 1,3 interactions of the substituents. Internal cis-configured double bonds first isomerize to trans bonds in an insertion–isomerization–elimination process, while in the following the thiyl radical adds on the trans-configured double bond [21]. The rate-determining step of the thiol-ene-reaction is the hydrogen transfer from the thiol to the carbon-centered radical leading to product formation [22].

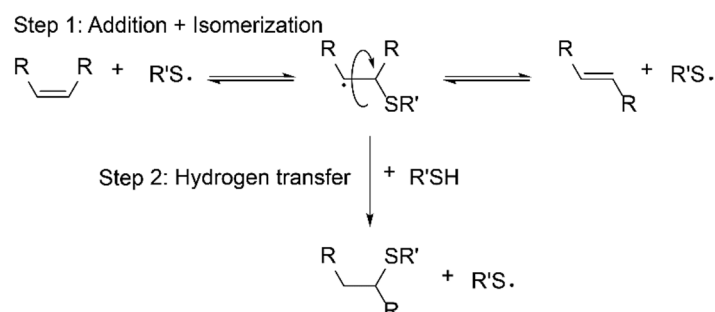


Figure 1. Propagation steps of the thiol-ene reaction, the first step including thiol addition via cis–trans isomerization comprising an addition–isomerization–elimination process, the second step being the rate-determining hydrogen abstraction from another thiol molecule.

Due to their good controllability and simplicity, thiol-ene reactions often serve for introducing new, sometimes complex, functionalities into vegetable oils [23,24]. Several authors made use of thiol-functionalized vegetable oils to produce organic–inorganic hy-

brid crosslinked coatings for wood, paper and cotton textiles with (super-)hydrophobic or flame-retardant properties [25–28]. Because of the high reaction rates for terminal olefins, vegetable oils used as biobased materials for thiol-ene chemistry have frequently been functionalized with terminal double bond-containing moieties (e.g., acrylates) to allow for easier crosslinking [29–31]. Other research, however, has been directed towards producing crosslinked networks directly from fatty acids or vegetable oils without additional derivatization. Moser et al. synthesized linear aliphatic poly(thioether-esters) based on fatty acids by connecting C10 fatty acids and alcohols via ester chemistry followed by photoinitiator-catalyzed thiol-ene crosslinking at the unsaturated chain ends [32]. Samuelsson et al. compared reactivities and reaction rates of two different trithiols with the olefinic double bonds in methyl oleate and methyl linoleate in the presence of a photoinitiator. They found that the addition to methyl oleate occurs more quickly, which was attributed to higher *cis*–*trans* isomerization rates due to less restricted rotation, and higher reactivity of the resulting *trans* unsaturation compared to *cis* unsaturation [33]. According to Bouaziz et al., who monitored photopolymerization of olive oil with and without the presence of a thiol crosslinker, under UV irradiation thiol-ene photocrosslinking occurs much faster than oxopolymerization (under ambient air), enabling the formation of crosslinked films within only 20 s [34]. Zhao et al. produced films from linseed oil applied onto glass and metal substrates and photocrosslinked them with different thiols (both miscible and immiscible with linseed oil). Interestingly, neither photoinitiator nor solvent were required for crosslinking at irradiation wavelengths below 275 nm, with a ratio of 0.5 equivalents of thiol per double bond being sufficient for successful crosslinking [35].

The latter examples in particular show that thiol-ene chemistry has been evolved to produce networks from fatty acid or vegetable oil precursors without the use of solvents or supplementary chemicals. To date, however, the focus was mostly on the organic reactions themselves, while only in rare cases paper has been used as substrate. Coatings on paper using fatty acids or vegetable oils without the use of further derivatization or supplementary components and applying thiol-ene crosslinking reactions in solvent/catalyst-free states have yet not been reported. The latter is of great interest as by such a strategy hydrophobic surface properties can be implemented in paper with a high degree of sustainability.

Given this motivation, in this contribution, we focus on a fundamental understanding of the thiol-ene crosslinking process and its applicability with respect to biobased paper coatings. In a first step, oleic acid-based thiol-ene reactions will be examined as a model system to establish suitable crosslinking parameters. In a second part of our presented work, olive oil, containing primarily oleic acid chains, will be used to obtain polymeric hydrophobic paper coatings, and the resulting surface properties will be analyzed.

2. Materials and Methods

2.1. Materials

1,8-Octanedithiol (1,8-ODT) (99%) was purchased from Acros Organics (Geel, Belgium). Oleic acid ($\geq 99\%$) was obtained from Carl Roth (Karlsruhe, Germany). 1,1,1,3,3,3-Hexamethyldisilazane ($\geq 98\%$) was obtained from Merck Schuchardt (Hohenbrunn, Germany), and isopropanol and chloroform ($\geq 99\%$) from Fisher Scientific (Loughborough, UK). Deuterated acetone (99.8%) was purchased from Deutero (Kastellaun, Germany). Olive oil was purchased from Oelmuehle Solling (Boffzen, Germany).

2.2. Methods

2.2.1. Glass Wafer Hydrophobization

The glass substrate hydrophobization procedure was adapted from a procedure by Xiao et al. [36]. Glass substrates were precleaned with dish soap and distilled water followed by rinsing with isopropanol. Glass substrates were then cleaned in an ultrasonic bath by immersion into isopropanol and chloroform (7.5 min each). They were then treated by ultrasonication in a solution of 1,1,1,3,3,3-hexamethyldisilazane in chloroform (5 wt%) (15 min).

2.2.2. Paper Making

Paper sheets with a grammage of 100 g/m² were produced from aqueous cotton linters dispersion (2.2 wt%) using a HAAGE sheet former BBS (Haage, Peissenberg, Germany), compliant with DIN EN ISO 52692. Prior to sheet forming, the cotton linters dispersion was diluted to 0.16 wt% and stirred for 30 min to avoid entanglement of the long cotton linter fibers and obtain homogeneous paper sheets. After drying at 93 °C under reduced pressure for 10 min, grammage was determined by the bone dried paper weight. Papers were stored at norm climate conditions (23 °C, 50% relative humidity) at least for another 24 h prior to further use. This equilibration procedure is important for paper sheets to reach equilibrium water content in the sheet at the given norm climate condition.

2.2.3. Coating Preparation and Crosslinking

Coatings were prepared by mixing oleic acid (10.0 g, 35.4 mmol) with 1,8-ODT (3.16 g, 17.7 mmol, 0.5 eq., corresponding to a stoichiometric C=C to SH ratio) and stirring for 30 min. Similarly, olive oil coatings were prepared from olive oil (12.0 g, 8.68 mmol) and 1,8-ODT (2.37 g, 13.2 mmol, 1.5 eq., corresponding to a stoichiometric C=C to SH ratio). Glass substrates and paper substrates used for reaction progress monitoring were coated via dip coating (home-built device) with a withdrawal speed of 2 mm/s. Paper substrates for surface analytics were impregnated with a Mathis SP 6513 size press (Mathis, Oberhasli, Switzerland) at 2 m/min speed and 0.5 bar, resulting in a final oil pick-up of (50.9 ± 0.8) wt%. UV crosslinking was performed in a Bio-Link 254 (Vilber Lourmat, Eberhardzell, Germany) at 254 nm wavelength and an irradiation dose of 20 J/cm². Samples were stored overnight at ambient conditions before further analytics to ensure uniform reaction completion.

2.2.4. ¹H-NMR Spectroscopy

NMR measurements were conducted on a Bruker DRX 500 NMR spectrometer at 500 MHz, apart from measurements shown in the supporting information, which were performed on a Bruker Avance II NMR spectrometer at 300 MHz (Bruker BioSpin GmbH, Rheinstetten, Germany). Crosslinked samples were removed from the glass substrate. Samples were dissolved in deuterated acetone. Chemical shifts were calibrated to the deuterated solvent signal. Data processing was performed using MestReNova 11.0 software (Mestrelab Research S. L., Santiago de Compostela, Spain). Double bond conversions were calculated from the mean values of integrals at $\delta = 0.88$ ppm (m, 3H, CH₃) and $\delta = 5.39$ ppm (m, 2H, CH=CH), integrated from three different samples. Errors were calculated from standard deviations.

2.2.5. FTIR Spectroscopy

FTIR measurements were performed on Perkin Elmer Spectrum One FTIR spectrometer (PerkinElmer Instruments, Waltham, USA) in the spectral region of 650 to 4000 cm⁻¹, using 4 scans with a nominal resolution of 4 cm⁻¹. Spectra were recorded directly from the paper substrate or from coating material removed from the glass substrate. Data processing and background correction were performed using PerkinElmer Spectrum software.

2.2.6. DSC Measurement

For DSC measurements, sample material was removed from the glass substrate and placed into 40 μ L aluminum crucibles closed with a perforated lid. DSC measurements were performed using a Mettler Toledo DSC 3 apparatus (Mettler Toledo, Gießen, Germany) and data evaluation was performed using STARe software. Two heating cycles were carried out under nitrogen atmosphere in a temperature range between -75 °C and 150 °C at a heating and cooling rate of 10 K/min, with the second heating cycle being used for data evaluation.

2.2.7. Contact Angle Measurement

Coated paper samples were stored at norm climate conditions for at least 24 h prior to contact angle measurement. Static contact angle measurements were performed using a Dataphysics OCA35 device (Dataphysics, Filderstadt, Germany) at standard climate conditions with 2 μL droplets of ultrapure water (Milli-Q-, Advantage A10, Millipak Express 20, (Merck Millipore, Billerica, MA, USA)). Drop shape fittings were performed using Dataphysics SCA20 software and applying the Young–Laplace fitting mode. A total of 10 measurements were performed for mean value determination for each sample, with a total of 3 samples per data point. Time-dependent contact angles were determined for a total of five measurements. Errors were calculated from the standard deviation from the mean for each sample followed by Gaussian error propagation.

2.2.8. Surface Roughness Measurements

Tactile profilometry was performed on a DektakXT stylus profiler by Bruker (Bruker Nano Surfaces Business, Tucson, AZ, USA) with a 2.5 μm -diameter stylus and a stylus force of 3 mg. Measurements were performed over a z-scan range of 65.5 μm , a length of 1000 μm and a resolution of 0.111 $\mu\text{m}/\text{pt}$. A total of 10 measurements were performed per sample in two perpendicular directions to exclude any potential effects caused by sample preparation. Roughness parameters R_a , R_q and R_z were calculated by the software according to ISO 4287 standard. Three samples were measured in total, with the mean value and the standard deviation from the mean being determined for each sample, followed by Gaussian error propagation to determine the overall error.

Optical profilometry was performed on a Sensofar PLu neox optical profiler (Sensofar-Tech, Terrassa, Spain) using a Nikon EPI 20 \times objective, a 850.08 \times 709.35 μm scan area, a resolution of 0.69 $\mu\text{m}/\text{pixel}$, a z-scan range of 160 μm and 3 images per measurement. Surface roughness parameters S_a , S_q and S_z were determined according to ISO 25178 standard. A total of 5 measurements were taken per sample for a total of 3 samples. The mean value and the standard deviation from the mean were determined for each sample, resulting from which the overall mean value and error, using Gaussian error propagation, were calculated.

2.2.9. Optical Microscopy

Images of paper samples were obtained with a Keyence digital microscope VHX-1000 (Keyence GmbH, Neu-Isenburg, Germany) equipped with an objective VH-Z250R. Depending on the reflectivity of the specimens, a selection was made between the ring light and coaxial light modes as optimal illumination.

2.2.10. SEM

For SEM measurements, samples were sputtercoated with a Pd/Pt (20/80) layer of 10 nm thickness using a Cressington Turbo 208HR sputter coater (Tescan GmbH, Dortmund, Germany). Measurements were performed on a Philips XL 30 FEG scanning electron microscope at 2 kV beam voltage, 66 μA current and 250 \times magnification.

3. Results and Discussion

In a first step, the crosslinking efficiency of dithiol linking agent 1,8-octanedithiol (1,8-ODT) for fatty acid chains was examined. Oleic acid, being the most common monounsaturated fatty acid, was chosen as a model compound, as it can at maximum form dimers when undergoing thiol-ene reactions with dithiols. This enables monitoring effects such as double bond conversion while retaining access to a higher range of analytical methods due to maintaining the solubility of the resulting compounds. The model system of oleic acid and 1,8-ODT helped to determine suitable crosslinking conditions and highlighted the significance of the thiol-component as compared to using the pure monomer at identical conditions. Secondly, the crosslinking of olive oil, a vegetable oil containing mainly oleic acid triglycerides, with 1,8-ODT was examined. The coating was applied to handsheets

made from cotton linter fibers and the resulting surface morphology and water contact angles were analyzed.

1,8-ODT was chosen as thiol for its good miscibility with both oleic acid and olive oil, contrary to various commercially available tri- and tetrathiols used in preliminary experiments, while still allowing for network formation when combined with olive oil. A stoichiometric ratio of thiol functionalities to double bonds was used to ensure maximum double bond conversion. Preliminary experiments have shown that 254 nm is a suitable irradiation wavelength for crosslinking without requiring the use of curing agents or solvents, in accordance with observations made by Zhao et al. [35].

In the first part, a mixture of oleic acid and 1,8-ODT was applied onto both glass substrates and cotton linters paper and photocrosslinked at varying irradiation intensities (Figure 2a) in order to examine optimum reaction conditions and analyze the thiol-ene reaction process in detail.

¹H-NMR spectroscopy (Figure 2b) allowed the quantitative examination of the double bond conversion during irradiation, as the integral associated to the two olefinic protons at 5.29–5.47 ppm decreases relative to the integral associated to the terminal methyl group at 0.80–0.92 ppm following double bond conversion. Further, the isomerization from cis double bonds (centered at 5.35 ppm), primarily present in oleic acid, to trans double bonds (centered at 5.41 ppm) can be observed as described in the literature. The latter is caused by reversible addition of thiol radicals to the double bond and results in the majority of non-reacted double bonds showing trans character [21–23]. ¹H-NMR spectra of coatings deposited on glass substrates showed increasing double bond conversion with irradiation intensity, reaching a maximum of $(85.2 \pm 1.2)\%$ at an irradiation intensity of 20 J/cm^2 without significant changes at higher irradiation doses (Figure 2c), indicating that with this energy input, almost all accessible double bonds have reacted and no further crosslinking occurs at higher irradiation doses. Water contact angle (WCA) measurements of coatings deposited on cotton linters paper show similar behavior, with an augmentation of WCA values from $(72.8 \pm 2.5)^\circ$ at 5 J/cm^2 to $(80.2 \pm 1.8)^\circ$ at 20 J/cm^2 and insignificant increase at higher irradiation intensities (Figure 2d). This confirms the results obtained by ¹H-NMR spectroscopy and indicates that the main part of the reaction including a rise of the fluid's viscosity takes place until this point. A value of 20 J/cm^2 was therefore selected as irradiation intensity for all future experiments.

FTIR spectroscopy was used to qualitatively assess the thiol-ene reaction (Figure 3a). The bands of main interest (Table S1) are those characterizing the double bonds, in particular the C=C_{cis} stretching mode at 3009 cm^{-1} , which disappears after the thiol-ene reaction, as well as the newly appearing C=C_{trans} bending mode at 967 cm^{-1} caused by cis–trans isomerization during the reaction, and the disappearing C=C_{cis} bending modes at 722 cm^{-1} , 934 cm^{-1} and 1412 cm^{-1} [23,37]. A low amount of conjugated C=C bonds is also observed for the crosslinked sample at 998 cm^{-1} [33]. Theoretically, the observation of the diminishing S–H bond and forming C–S bond could also be expected, but can in reality not be observed due to its low intensity [23].

Comparison of the FTIR spectra of coated cotton linters paper before and after Soxhlet extraction shows that the coating was not covalently bound to the paper sheet. (Figure 3b). After extraction no signals are present that can be assigned to oleic acid. The latter is not unexpected as there are no double bonds in the pure cotton linters paper that would allow for direct reaction and the dimers are most likely too small to physically anchor in the paper fiber network.

The decisive relevance of the thiol as radical initiator for the oleic acid double bond conversion was also proven, as pure oleic acid coatings on glass submitted to the same irradiation conditions showed only $(2.2 \pm 0.5)\%$ double bond conversion as opposed to $(82.5 \pm 1.2)\%$ for the mixture. This confirms that oxidation reactions with air oxygen radicals play no significant role during the irradiation process, but may occur to a very low degree, as previously described by Zhao et al. [35]. Corresponding observations were made during WCA measurements of pure oleic acid coatings on linters paper, with a

slight contact angle increase from $(22.9 \pm 3.0)^\circ$ for untreated paper coatings to $(41.3 \pm 1.9)^\circ$ after UV treatment, whilst a significant increase into the almost hydrophobic range at $(80.2 \pm 1.8)^\circ$ took place after and due to UV treatment of the oleic acid/thiol mixture coating. Performing the photoinitiated thiol-ene reaction between oleic acid and 1,8-ODT allowed using a simple scaffold for determining suitable reaction conditions and ruling out significant environmental influences on the reaction.

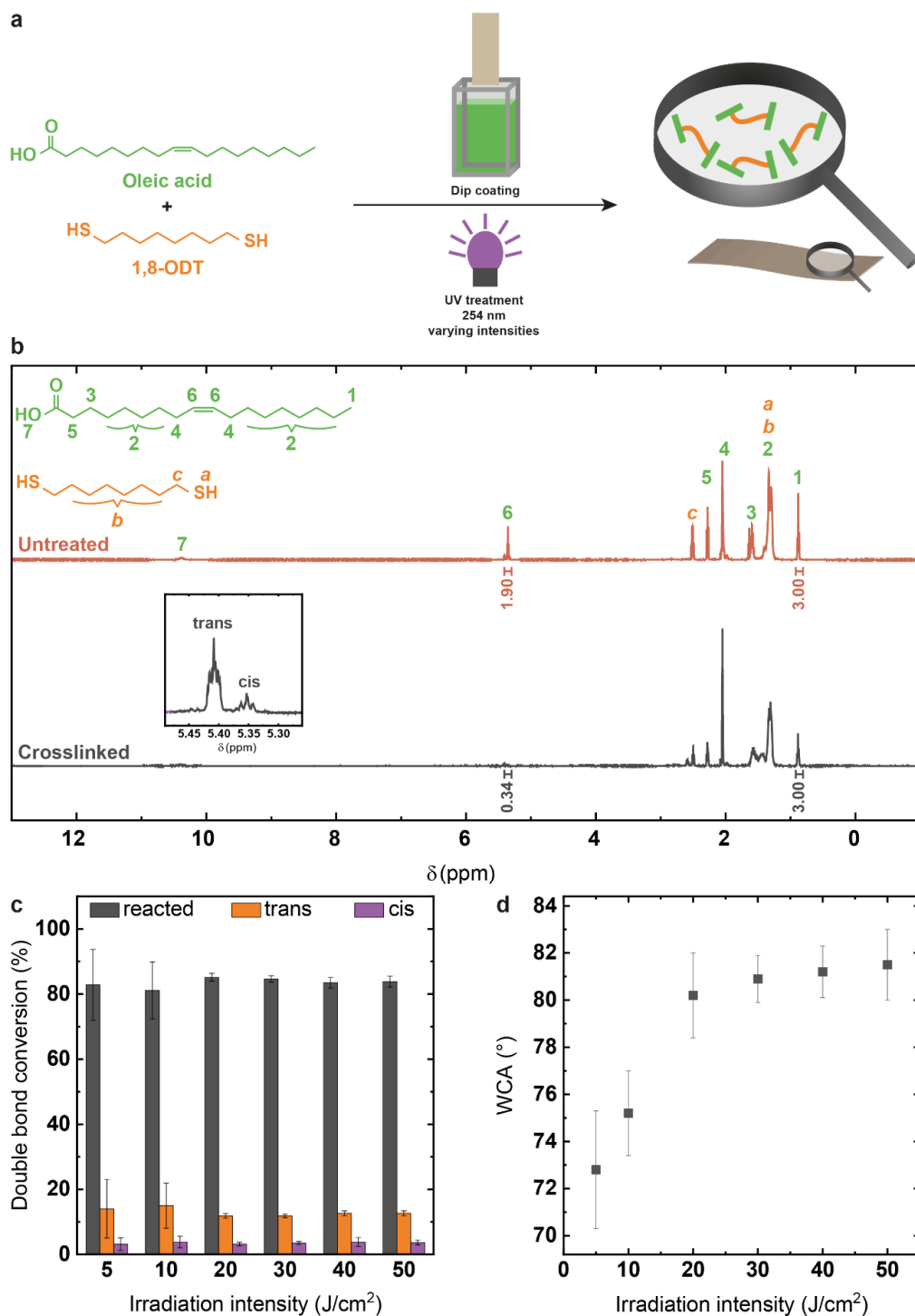


Figure 2. (a) Reaction scheme for crosslinking oleic acid with 1,8-octanedithiol and coating application; (b) 1H -NMR spectrum for untreated and crosslinked reactant mixtures as basis for calculating the double bond conversion; (c) double bond conversions at different irradiation intensities; (d) water contact angles on paper correlating to different irradiation intensities.

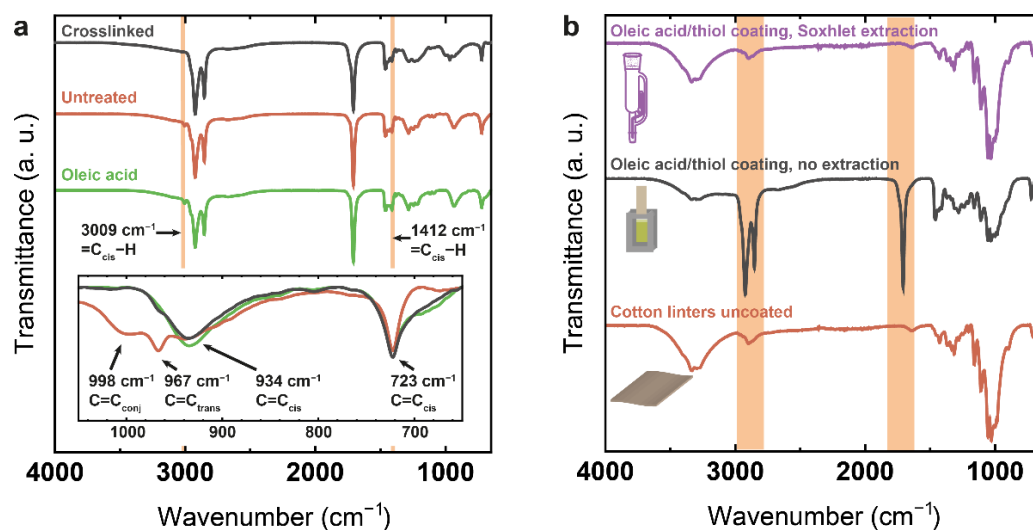


Figure 3. (a) FTIR spectra of pure oleic acid, the untreated oleic acid/thiol mixture and the crosslinked coating highlighting the transformations characterized by double bond conversion; (b) FTIR spectra of uncoated cotton linters paper, cotton linters paper coated with crosslinked oleic acid/thiol mixture and the same after Soxhlet extraction show that the coating is not permanently linked to substrate.

The resulting knowledge was used in a second step for producing crosslinked polymer networks based on olive oil and 1,8-ODT and examining the surface properties of such coatings applied to cotton linters sheets (Figure 4a).

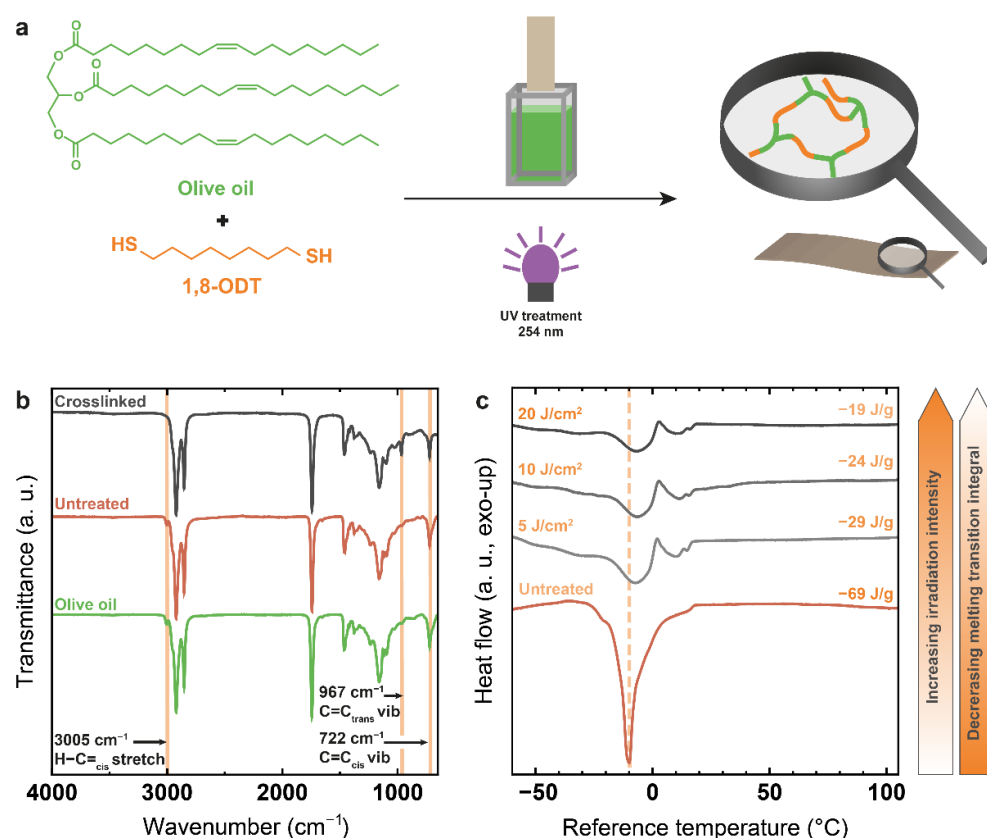


Figure 4. (a) Reaction scheme for thiol-ene reaction of olive oil with 1,8-ODT; (b) comparison of the FTIR spectra of fresh olive oil, the untreated olive oil/1,8-ODT mixture and the crosslinked mixture; (c) DSC curves of the olive oil/1,8-ODT mixture before and after crosslinking with different UV intensities showing decreasing integrals for the combined melting transitions.

$^1\text{H-NMR}$ spectroscopy (Figure S1) revealed the olive oil batch used contained 3.03 C=C double bonds per triglyceride, as calculated from olefinic and methyl proton signal integrals, and thereby allowed calculation of the required amount of thiol to obtain a precise stoichiometric functionality ratio.

Following UV irradiation, the resulting coatings on glass substrates proved insoluble in a wide range of organic solvents, so successful network formation can be assumed. Qualitative proof of thiol-ene reaction is given by FTIR spectra (Figure 4b) of the crosslinked coating after removal from the glass substrate, as compared to pure olive oil and to the untreated olive oil/thiol mixture, showing the disappearance of the C=C band at 3005 cm^{-1} as well as trans bond formation caused by reversible thiol addition at 967 cm^{-1} . DSC measurements (Figure 4c) equally point towards a successful crosslinking reaction. The thermograms show the melting peak of the untreated olive oil/thiol mixture at $-10\text{ }^\circ\text{C}$ prior to the crosslinking reaction. This very sharp peak represents the structurally uniform olive oil triglycerides with their rather defined melting temperature, as 1,8-ODT shows no thermal transition in the examined temperature range. After crosslinking, a strong broadening of the melting peak is observed combined with a slight shift of the maximum to $-7\text{ }^\circ\text{C}$, while a second melting transition at $10\text{--}11\text{ }^\circ\text{C}$ becomes visible. These changes originate from the formation of triglyceride dimers and oligomers not yet integrated into the polymeric network. The peak intensity and sum of the integrals of both melting transitions decreases with increasing irradiation intensity from -69 J/g for the untreated mixture to -19 J/g after 20 J/cm^2 UV treatment. The decreasing integral proves that the amount of liquid low molecular weight monomer and oligomer molecules decreases. More and more olive oil molecules become integrated into the solidified crosslinked polymer network, which accordingly does not have a melting point. The main part of the reaction occurs already after submission to very low irradiation intensities below 5 J/cm^2 , as indicated by the melting transition integral, which shows the strongest decrease in that area. This corresponds to the observation made during $^1\text{H-NMR}$ analysis of the oleic acid-based model system. Reference experiments of UV treatment of pure olive oil confirmed the necessity of thiol presence for successful double bond consumption reactions as equally observed in the case of oleic acid.

Following the chemical characterization, the surface properties of olive oil/1,8-ODT coatings applied onto cotton linters sheets using size pressing were examined. Optical microscopy (Figure 5a,d) and scanning electron microscopy (SEM, Figure 5b,e) allowed comparison of the sheet surface before and after coating. For uncoated cotton linters paper, individual fibers and the characteristic porous structures of the paper sheet are clearly visible and well defined both in optical microscopy and SEM, respectively. Imaging of the coated samples shows complete coverage of individual fibers with coating material, and levelling out of the entire substrate surface due to pore filling. The optical profilometry images (Figure 5c,f) show that although the fiber structure gets less distinct, the overall maxima and minima do not significantly change. Measuring roughness parameters using both tactile and optical profilometry showed that interestingly, there was no significant difference between coated and uncoated substrates, with an average roughness (R_a) of approximately $6\text{ }\mu\text{m}$, a root mean square roughness (R_q) of approximately $8\text{ }\mu\text{m}$ and a z-scale roughness (R_z) of approximately $40\text{ }\mu\text{m}$. The surface roughness parameters (S_a , S_q and S_z) were generally slightly higher, with the most prominent difference in the z-scale area roughness that amounts to approximately $125\text{ }\mu\text{m}$ (Table 1) due to the inherent roughness of the paper surface.

Static water contact angle measurements were performed in sessile drop configuration both on coated hydrophobized glass and cotton linters paper (Figure 6). Due to the high hydrophilicity and porosity of uncoated cotton linters paper, the water droplet is immediately absorbed and does not allow for contact angle investigation. Although coating with olive oil and crosslinking already lead to a significant increase in contact angles, hydrophobicity was only observed after coating with and crosslinking of the thiol-oil

mixture, with the contact angle finally increasing to approximately 120° . The contact angle remained stable for at least two minutes, showing good absorption inhibition (Figure S2).

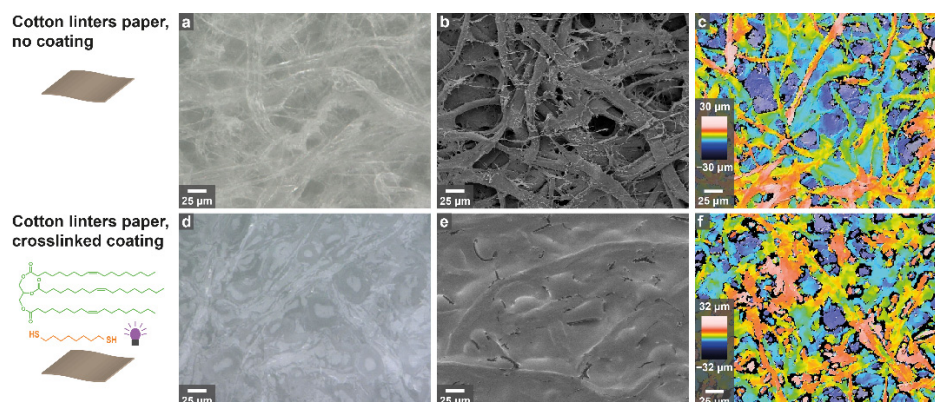


Figure 5. Surface characterization of uncoated (a–c) cotton linters paper and (d–f) cotton linters paper coated with olive oil/1,8-ODT using (a,d) optical microscopy, (b,e) SEM and (c,f) optical profilometry.

Table 1. Roughness parameters determined from tactile profilometry (profile roughness values) and optical profilometry (surface roughness values).

	R_a (μm)	R_q (μm)	R_z (μm)	S_a (μm)	S_q (μm)	S_z (μm)
Cotton linters paper, uncoated	6.3 ± 0.7	8.0 ± 0.9	39.8 ± 4.8	7.6 ± 0.6	10.0 ± 0.7	124.2 ± 12.0
Cotton linters paper, olive oil coating	6.1 ± 0.6	7.8 ± 0.8	40.8 ± 5.5	6.8 ± 0.6	9.3 ± 1.0	126.3 ± 10.8

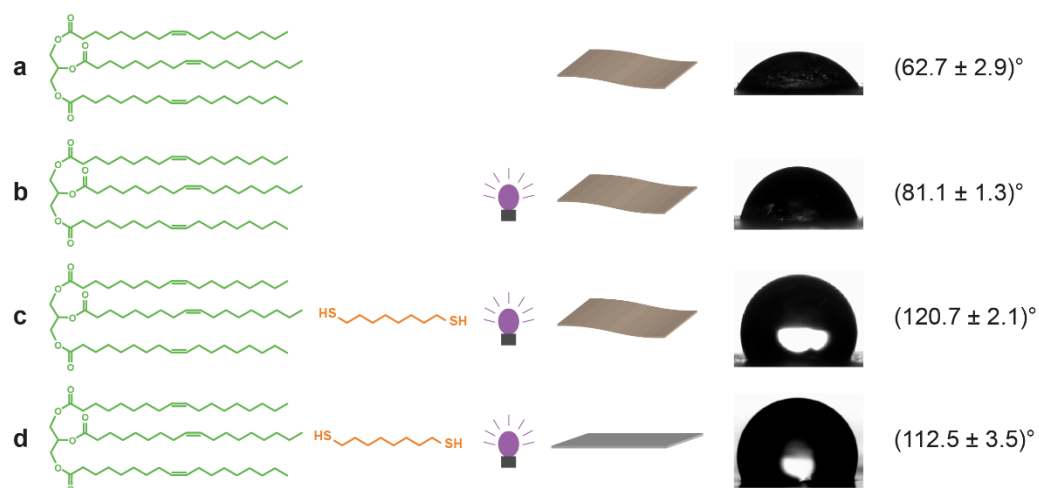


Figure 6. Static water contact angles (sessile drop) measured on (a) cotton linters paper coated with pure olive oil; (b) cotton linters paper coated with pure olive oil and submitted to UV irradiation; (c) cotton linters paper coated with the olive oil/thiol mixture and submitted to UV crosslinking; (d) glass coated with the olive oil/thiol mixture and submitted to UV crosslinking as a smooth reference substrate for comparison.

As a smooth reference substrate, coated glass showed a contact angle increase from $(82.5 \pm 1.1)^\circ$ to $(112.5 \pm 3.5)^\circ$. This is significantly higher than for instance the contact angle below 90° observed for a crosslinked glass coating based on tung oil and a dithiolated isosorbide [38]. However, the superhydrophobic contact angles, approximately 160° , observed for hybrid organic–inorganic coatings are far from being attainable [25]. Covalent attachment of fatty acids or oils onto cellulosic substrates lead to similar or lower contact

angles, with the exception being the metathesis polymerization resulting in contact angles of up to 145° [1,3–6].

As the surface roughness did not change significantly after coating, the increase in hydrophobicity can be attributed solely to the modification of the cellulose surface chemistry by thiol-ene photocrosslinking. These results clearly demonstrate the potential of polymer networks based on vegetable oils for use in hydrophobic paper coatings.

4. Conclusions and Outlook

Our report shows that it is possible to generate hydrophobic barriers on paper by applying a coating based on natural olive oil and a dithiol followed by UV-induced photocrosslinking polymerization in bulk without prior derivatization of any of the components nor the addition of a photoinitiator. The latter conclusions have been drawn from model studies using 1,8-octanedithiol as crosslinker for the natural oil. Crosslinking of the olive oil results in smooth films that exhibit contact angles well above 100° and therefore show water-repellent properties.

Avoiding the use of solvents and photoinitiators allows reducing the consumption of supplementary chemicals to an absolute minimum. Yet in our model studies, the crosslinker is not a biobased precursor. In upcoming steps, the latter will be replaced by natural, ideally low-odor or odorless, biogenic thiols. In addition, future steps will also account for investigations into material-efficient applications, barrier properties, ageing effects, recyclability and biodegradability, in order to assess a possible transfer of these model barrier films into barriers useful for packaging or construction materials.

Supplementary Materials: The following supporting information can be downloaded at: <https://www.mdpi.com/article/10.3390/polym14091773/s1>, Table S1: Attribution of IR spectral bands of oleic acid/thiol mixture to functional groups; Figure S1: ¹H-NMR spectrum of olive oil; Figure S2: Time-dependent evolution of contact angles on cotton linters paper coated with crosslinked olive oil/1,8-ODT mixture.

Author Contributions: Conceptualization, A.L.-Z. and A.G.; investigation, A.L.-Z., C.C. and A.G.; visualization and writing—original draft preparation, A.L.-Z.; writing—review and editing, all authors; supervision, A.G. and M.B. All authors have read and agreed to the published version of the manuscript.

Funding: This research was funded as part of the BioPlas4Paper project by Agency for Renewable Resources (Fachagentur Nachwachsende Rohstoffe e.V.—FNR), grant number 2220HV017A.

Institutional Review Board Statement: Not applicable.

Informed Consent Statement: Not applicable.

Data Availability Statement: The data presented in this study are available on request from the corresponding authors.

Acknowledgments: The authors thank the NMR service-group at the Department of Chemistry, TU Darmstadt for service NMR measurements.

Conflicts of Interest: The authors declare no conflict of interest.

References

1. Dankovich, T.A.; Hsieh, Y.L. Surface modification of cellulose with plant triglycerides for hydrophobicity. *Cellulose* **2007**, *14*, 469–480. [[CrossRef](#)]
2. Saha, P.; Manna, S.; Sen, R.; Roy, D.; Adhikari, B. Durability of lignocellulosic fibers treated with vegetable oil–phenolic resin. *Carbohydr. Polym.* **2012**, *87*, 1628–1636. [[CrossRef](#)]
3. Crépy, L.; Chaveriat, L.; Banoub, J.; Martin, P.; Joly, N. Synthesis of cellulose fatty esters as plastics-influence of the degree of substitution and the fatty chain length on mechanical properties. *ChemSusChem* **2009**, *2*, 165–170. [[CrossRef](#)]
4. Freire, C.S.R.; Silvestre, A.J.D.; Neto, C.P.; Belgacem, M.N.; Gandini, A. Controlled heterogeneous modification of cellulose fibers with fatty acids: Effect of reaction conditions on the extent of esterification and fiber properties. *J. Appl. Polym. Sci.* **2006**, *100*, 1093–1102. [[CrossRef](#)]

5. Geissler, A.; Bonaccorso, E.; Heim, L.O.; Heinze, T.; Zhang, K. Temperature-responsive thin films from cellulose stearyl triester. *J. Phys. Chem. C* **2014**, *118*, 2408–2417. [[CrossRef](#)]
6. Huang, X.; Wang, A.; Xu, X.; Liu, H.; Shang, S. Enhancement of hydrophobic properties of cellulose fibers via grafting with polymeric epoxidized soybean oil. *ACS Sustain. Chem. Eng.* **2017**, *5*, 1619–1627. [[CrossRef](#)]
7. Onwukamike, K.N.; Grelier, S.; Grau, E.; Cramail, H.; Meier, M.A.R. Sustainable transesterification of cellulose with high oleic sunflower oil in a DBU-CO₂ switchable solvent. *ACS Sustain. Chem. Eng.* **2018**, *6*, 8826–8835. [[CrossRef](#)]
8. Samyn, P.; Schoukens, G.; Stanssens, D.; Vonck, L.; van den Abbeele, H. Hydrophobic waterborne coating for cellulose containing hybrid organic nanoparticle pigments with vegetable oils. *Cellulose* **2013**, *20*, 2625–2646. [[CrossRef](#)]
9. Cabrales, L.; Abidi, N. Microwave plasma induced grafting of oleic acid on cotton fabric surfaces. *Appl. Surf. Sci.* **2012**, *258*, 4636–4641. [[CrossRef](#)]
10. Sharmin, E.; Zafar, F.; Akram, D.; Alam, M.; Ahmad, S. Recent advances in vegetable oils based environment friendly coatings: A review. *Ind. Crops Prod.* **2015**, *76*, 215–229. [[CrossRef](#)]
11. Montero de Espinosa, L.; Meier, M.A.R. Plant oils: The perfect renewable resource for polymer science?! *Eur. Pol. J.* **2011**, *47*, 837–852. [[CrossRef](#)]
12. Miao, S.; Wang, P.; Su, Z.; Zhang, S. Vegetable-oil-based polymers as future polymeric biomaterials. *Acta Biomater.* **2014**, *10*, 1692–1704. [[CrossRef](#)] [[PubMed](#)]
13. Zhang, C.; Garrison, T.F.; Madbouly, S.A.; Kessler, M.R. Recent advances in vegetable oil-based polymers and their composites. *Prog. Polym. Sci.* **2017**, *71*, 91–143. [[CrossRef](#)]
14. Hong, J.; Shah, B.K.; Petrović, Z.S. Vegetable oil cast resins via click chemistry: Effects of cross-linkers. *Eur. J. Lipid Sci. Technol.* **2013**, *115*, 55–60. [[CrossRef](#)]
15. Kreye, O.; Tóth, T.; Meier, M.A.R. Copolymers derived from rapeseed derivatives via ADMET and thiol-ene addition. *Eur. Pol. J.* **2011**, *47*, 1804–1816. [[CrossRef](#)]
16. Lomège, J.; Lapinte, V.; Negrell, C.; Robin, J.J.; Caillol, S. Fatty acid-based radically polymerizable monomers: From novel poly(meth)acrylates to cutting-edge properties. *Biomacromolecules* **2019**, *20*, 4–26. [[CrossRef](#)] [[PubMed](#)]
17. Altuna, F.I.; Pettarin, V.; Williams, R.J.J. Self-healable polymer networks based on the cross-linking of epoxidised soybean oil by an aqueous citric acid solution. *Green Chem.* **2013**, *15*, 3360. [[CrossRef](#)]
18. Wuzella, G.; Mahendran, A.R.; Müller, U.; Kandelbauer, A.; Teischinger, A. Photocrosslinking of an acrylated epoxidized linseed oil: Kinetics and its application for optimized wood coatings. *J. Polym. Environ.* **2012**, *20*, 1063–1074. [[CrossRef](#)]
19. Wang, Q.; Chen, G.; Cui, Y.; Tian, J.; He, M.; Yang, J.W. Castor oil based biothiol as a highly stable and self-initiated oligomer for photoinitiator-free UV coatings. *ACS Sustain. Chem. Eng.* **2017**, *5*, 376–381. [[CrossRef](#)]
20. Hoyle, C.E.; Bowman, C.N. Thiol-ene click chemistry. *Angew. Chem. Int. Ed. Engl.* **2010**, *49*, 1540–1573. [[CrossRef](#)]
21. Roper, T.M.; Guymon, C.A.; Jönsson, E.S.; Hoyle, C.E. Influence of the alkene structure on the mechanism and kinetics of thiol-alkene photopolymerizations with real-time infrared spectroscopy. *J. Polym. Sci. A Polym. Chem.* **2004**, *42*, 6283–6298. [[CrossRef](#)]
22. Claudino, M.; Johansson, M.; Jonsson, M. Thiol-ene coupling of 1,2-disubstituted alkene monomers: The kinetic effect of cis/trans-isomer structures. *Eur. Pol. J.* **2010**, *46*, 2321–2332. [[CrossRef](#)]
23. Desroches, M.; Caillol, S.; Lapinte, V.; Auvergne, R.; Boutevin, B. Synthesis of biobased polyols by thiol-ene coupling from vegetable oils. *Macromolecules* **2011**, *44*, 2489–2500. [[CrossRef](#)]
24. Zhao, Y.H.; Vuluga, D.; Lecamp, L.; Burel, F. Photoinitiated thiol-epoxy addition for the preparation of photoinduced self-healing fatty coatings. *RSC Adv.* **2016**, *6*, 32098–32105. [[CrossRef](#)]
25. Shang, Q.; Chen, J.; Liu, C.; Hu, Y.; Hu, L.; Yang, X.; Zhou, Y. Facile fabrication of environmentally friendly bio-based superhydrophobic surfaces via UV-polymerization for self-cleaning and high efficient oil/water separation. *Prog. Org. Coat.* **2019**, *137*, 105346. [[CrossRef](#)]
26. Shang, Q.; Liu, C.; Chen, J.; Yang, X.; Hu, Y.; Hu, L.; Zhou, Y.; Ren, X. Sustainable and robust superhydrophobic cotton fabrics coated with castor oil-based nanocomposites for effective oil-water separation. *ACS Sustain. Chem. Eng.* **2020**, *8*, 7423–7435. [[CrossRef](#)]
27. Wang, T.; Li, L.; Cao, Y.; Wang, Q.; Guo, C. Preparation and flame retardancy of castor oil based UV-cured flame retardant coating containing P/Si/S on wood surface. *Ind. Crops Prod.* **2019**, *130*, 562–570. [[CrossRef](#)]
28. Meng, L.; Qiu, H.; Wang, D.; Feng, B.; Di, M.; Shi, J.; Wei, S. Castor-oil-based waterborne acrylate/SiO₂ hybrid coatings prepared via sol-gel and thiol-ene reactions. *Prog. Org. Coat.* **2020**, *140*, 105492. [[CrossRef](#)]
29. Black, M.; Rawlins, J.W. Thiol-ene UV-curable coatings using vegetable oil macromonomers. *Eur. Polym. J.* **2009**, *45*, 1433–1441. [[CrossRef](#)]
30. Türünc, O.; Meier, M.A.R. The thiol-ene (click) reaction for the synthesis of plant oil derived polymers. *Eur. J. Lipid Sci. Technol.* **2013**, *115*, 41–54. [[CrossRef](#)]
31. Resetco, C.; Hendriks, B.; Badi, N.; Du Prez, F. Thiol-ene chemistry for polymer coatings and surface modification—Building in sustainability and performance. *Mater. Horiz.* **2017**, *4*, 1041–1053. [[CrossRef](#)]
32. Moser, B.R.; Doll, K.M.; Peterson, S.C. Renewable poly(thioether-ester)s from fatty acid derivatives via thiol-ene photopolymerization. *J. Am. Oil Chem. Soc.* **2019**, *96*, 825–837. [[CrossRef](#)]

33. Samuelsson, J.; Jonsson, M.; Brinck, T.; Johansson, M. Thiol-ene coupling reaction of fatty acid monomers. *J. Polym. Sci. A Polym. Chem.* **2004**, *42*, 6346–6352. [[CrossRef](#)]
34. Bouaziz, K.; Ayadi, M.; Allouche, N.; Chemtob, A. Renewable photopolymer films derived from low-grade lampante and pomace olive oils. *Eur. J. Lipid Sci. Technol.* **2017**, *119*, 1700003. [[CrossRef](#)]
35. Zhao, Y.H.; Vuluga, D.; Lecamp, L.; Burel, F. A rapid, eco- and environmental friendly alternative to oil oxidation for the preparation of fatty coatings using photoinitiated thiol-ene chemistry. *Prog. Org. Coat.* **2016**, *101*, 216–224. [[CrossRef](#)]
36. Xiao, Y.; Ritcey, A.M. Phase Transitions in Spread Monolayers of Cellulose Ethers. *Langmuir* **2000**, *16*, 4252–4258. [[CrossRef](#)]
37. Zhang, Q.; Liu, C.; Sun, Z.; Hu, X.; Shen, Q.; Wu, J. Authentication of edible vegetable oils adulterated with used frying oil by fourier transform infrared spectroscopy. *Food Chem.* **2012**, *132*, 1607–1613. [[CrossRef](#)]
38. Şeker, H.; Çakmakçı, E. Fully bio-based thiol-ene photocured thermosets from isosorbide and tung oil. *J. Polym. Sci.* **2020**, *58*, 1105–1114. [[CrossRef](#)]

5.2. Covalently attached hydrophobic vegetable oil-based paper coatings through thermal treatment

Well-established strategies for covalent attachment of hydrophobization agents to paper have been used at industrial scale for many decades. The most prominent materials used therein are alkyl ketene dimer and alkenyl succinic anhydride, which feature fatty acid chains as characteristic hydrophobic moiety. However, their raw materials mostly originate from fossil-based resources. Covalent attachment of fully biobased hydrophobizing agents, like vegetable oils, to paper, however remains a challenge.

A system where the interaction of vegetable oils and paper has been well-examined are transformers, which use paper as insulation and vegetable oil as insulation and coolant.^[171] During prolonged use in transformers, paper and oil undergo transesterification reactions, whereby fatty acids are covalently attached to the cellulose. These processes have also been simulated through long-term immersion of paper into vegetable oils at elevated temperatures.^[171,172] Beyond that, vegetable oil has previously proven favorable for enhancing cotton fabric hydrophobicity.^[173] Hence, this section aims at exploring the possibility to hydrophobize vegetable oil-coated paper through simple exposure to high temperature and at understanding the mechanisms thereof. Besides, the changes taking place in coated papers both at elevated and room temperature are of crucial importance with respect to long-term stability of such coatings.

Samples were prepared by dip coating cotton linter laboratory handsheets into olive oil and subsequent storage under defined conditions (at 70 °C or under norm climate or under argon at room temperature) for four weeks followed by Soxhlet extraction. The papers were analyzed both prior to and after extraction, as was the extracted oil.

While freshly olive oil-coated papers only showed a WCA of 66°, the WCA increased to 97° after storage at 70 °C for four weeks. Soxhlet extraction even resulted in a WCA of 138°, indicating covalent attachment of the oil onto cellulose. This assumption was supported by ATR-FTIR spectra weakly depicting the carbonyl band at 1736 cm⁻¹, which hinted at the presence of an ester bond that was neither observed on uncoated nor on freshly coated and extracted paper. Further proof was delivered through fluorescence imaging, where coated, extracted paper showed fluorescence of a fat-selective dye after staining, which indicated oil presence and was not at all detected on a stained uncoated paper.

In order to understand the aging processes in olive oil, to which both temperature and oxygen accessibility contribute, the storage of the olive oil coated papers for four weeks at 70 °C was compared to storage at norm climate or under argon. While the papers' WCAs increased after storage at all conditions, the highest values were obtained for storage at 70 °C. Further, water

droplet absorption times increased from 6 s for freshly coated paper to 11 s for paper stored under argon, to 35 s for paper stored at norm climate and to 240 s for paper stored at 70 °C. Surface roughness measurements showed that these differences were not due to a change in wetting regime, as the surface roughness did not change significantly during storage at any examined condition. It was instead dominated by the intrinsic paper roughness. Confocal laser scanning microscopy (CLSM) of coated papers, stained with a cellulose-selective and an oil-selective staining agent, showed a comparative increase in the cellulose staining agent's fluorescence intensity, which possibly indicated oil migration from the surface of the fiber into the fiber wall.

Chemical analytics provided various clues that finally enabled an insight into processes taking place in the olive oil coating itself during aging. For instance, ¹H-NMR spectra of oil coatings stored at 70 °C showed a decrease in integrals of all hydrogens in close vicinity to carbon-carbon double bonds, indicating the consumption of the latter, while the integrals of aliphatic hydrogens and those neighboring ester groups increased. These changes were observed to a very small extent after storage at norm climate and not at all after storage under argon. Size exclusion chromatography (SEC) revealed an increase in low molecular weight fractions for all storage methods and of high molecular weight fractions for storage at 70 °C, as well as to a very small extent after storage at norm climate. ATR-FTIR spectra showed the disappearance of the =C_{cis}-H bond at 3005 cm⁻¹ and formation of a C=O_{acid} shoulder at 1709 cm⁻¹ after storage at 70 °C, but no such modification for storage at room temperature. DSC cooling curves evidenced no changes after storage under argon. Yet, after storage at room temperature, the characteristic crystallization peak of unsaturated triacylglycerols was replaced by an extended crystallization range, which shifted to higher temperatures after storage at 70 °C. Further, a decrease in crystallization enthalpy reflected the hindrance in crystallization through smaller or larger molecules.

Together, chemical and morphological analytics permitted drawing conclusions on the aging processes of olive oil coated paper stored under different conditions. No chemical or morphological changes were observed after storage under argon, making the slight WCA increase the exclusive product of coating penetration into the paper. Thus, oxygen accessibility was found to be strictly necessary for chemical aging reactions that led to significant hydrophobization. Oxidation reactions occurred to a low extent during storage at norm climate and led to the formation of a small number of species with higher and lower molecular weight than the original olive oil. These inhibit crystallization, but are not evident in less sensitive characterization methods such as ATR-FTIR spectroscopy. However, after storage at 70 °C, the full consumption of the carbon-carbon double bond, as well as the products of these oxidation,

di- and oligomerization or crosslinking processes were clearly visible across the selected analytical methods. In addition, an interplay of heat and paper-intrinsic moisture led to transesterification reactions liberating fatty acids that became covalently attached to the cellulose and thus caused permanent hydrophobization.

Finally, different storage times were examined to improve understanding of the time scales at which the observed changes took place. Water droplet absorption times increased with storage time both at norm climate and at 70 °C, accompanied by an increase in oxidized species content, displayed through DSC curves. However, water repellency developed more slowly when papers were stored at norm climate. Therein, a paper storage time of three months resulted in a water droplet absorption time around 100 s, which was also reached after one week of paper storage at 70 °C. The latter paper showed a stable WCA around 130° after Soxhlet extraction, thus achieving similar properties as the paper stored for four weeks and showing the potential of good paper hydrophobization through extremely low amounts of covalently attached vegetable oil.

In the frame of this work, I was involved in conceptualization, data acquisition and interpretation (paper making, dip coating, WCA measurements, sample staining, fluorescence imaging, optical profilometry, ATR-FTIR spectroscopy and DSC, all performed by myself, as well as ¹H-NMR spectroscopy, SEC and GC-MS/FID, measured by NMR service department of TU Darmstadt, by Marion Trautmann and by Silke Radtke, respectively), writing and creating artwork. Tobias Meckel recorded CLSM images and was involved in results discussion. Andreas Geissler was involved in conceptualization, interpretation, supervision and funding acquisition. Markus Biesalski was involved in supervision. All authors were involved in proof-reading.

The following article has been published in *Coatings*.

A. Loesch-Zhang, T. Meckel, M. Biesalski, A. Geissler, *Enhancing Hydrophobic Properties in Olive Oil-Coated Papers through Thermal Treatment*, *Coatings* **2024, *14*, 364.**

Published by MDPI, Basel, Switzerland under Creative Commons Attribution 4.0 International (CC BY 4.0) License.

The supporting information has not been reprinted here, but can be accessed via the online version of this article: <https://www.mdpi.com/2079-6412/14/3/364>.

Article

Enhancing Hydrophobic Properties in Olive Oil-Coated Papers through Thermal Treatment

Amelia Loesch-Zhang ¹, Tobias Meckel ¹ , Markus Biesalski ¹  and Andreas Geissler ^{1,2,*} 

¹ Macromolecular and Paper Chemistry, Technical University Darmstadt, Peter-Grünberg-Str. 8, 64287 Darmstadt, Germany; amelia.loesch-zhang@tu-darmstadt.de (A.L.-Z.); tobias.meckel@tu-darmstadt.de (T.M.); markus.biesalski@tu-darmstadt.de (M.B.)

² Papiertechnische Stiftung (PTS), Pirnaer Str. 37, 01809 Heidenau, Germany

* Correspondence: andreas.geissler@tu-darmstadt.de

Abstract: Enhancing paper hydrophobicity is of key importance for many paper-based applications. Fatty acids or vegetable oils and their derivatives replace environmentally harmful conventional coating materials but still require challenging chemical reactions for covalent attachment onto paper. Here, we show that simple storage of olive oil-coated cotton linter paper at 70 °C and subsequent Soxhlet extraction is able to endow paper with hydrophobic properties, reaching water contact angles above 130°. In-depth chemical and morphological analytics show the relevance of temperature and air accessibility during the aging process compared with aging at ambient temperature and under the exclusion of oxygen, underlining the importance of assessing a coating's long-term performance and stability under diverse storage conditions. Simple storage of vegetable oil-coated paper at elevated temperatures followed by extraction proves to be an easy way to produce stable covalently attached hydrophobic paper coatings with exceptionally low coating amounts.

Keywords: aging; dip coating; hydrophobicity; olive oil; paper; water contact angle



Citation: Loesch-Zhang, A.; Meckel, T.; Biesalski, M.; Geissler, A. Enhancing Hydrophobic Properties in Olive Oil-Coated Papers through Thermal Treatment. *Coatings* **2024**, *14*, 364. <https://doi.org/10.3390/coatings14030364>

Academic Editor: Fábio Ferreira

Received: 12 February 2024

Revised: 8 March 2024

Accepted: 16 March 2024

Published: 20 March 2024



Copyright: © 2024 by the authors. Licensee MDPI, Basel, Switzerland. This article is an open access article distributed under the terms and conditions of the Creative Commons Attribution (CC BY) license (<https://creativecommons.org/licenses/by/4.0/>).

1. Introduction

In view of the global challenge to reduce consumption of fossil-based resources, plant-based materials have shifted into focus, e.g., for the application of (super)hydrophobic paper coatings. (Super)hydrophobic coatings are required in manifold applications such as packaging, biosensing, textiles and membranes. As such, fatty acids and plant-based oils have shown great potential for improving surface hydrophobicity [1]. Fatty acid-derivative-based hydrophobization approaches for cellulosic materials include esterification reactions based on fatty acyl chlorides such as stearoyl chloride, oleoyl chloride and palmitoyl chloride [2–4], which even give access to superhydrophobic coatings [5–7]. Transesterification can also be performed under supercritical solvent conditions, e.g., using sunflower oil [8]. Further approaches include grafting processes such as ring-opening polymerization [9], crosslinking processes [10–12], plasma polymerization [13] or application as part of hybrid organic nanoparticles [14] using a large variety of oils such as derivatives of soybean, castor, chia oil and olive oil. A simple process of immersing cotton substrates in organic solutions of soybean oil and subsequent heating to 120 °C for 1 h followed by acetone rinsing imparted water contact angles (WCAs) of up to 80°, while fully hydrophobic properties could not be achieved despite the use of a rather rough substrate [15].

In consideration of their importance in food industry, the aging process of fatty acids and vegetable oils has been extensively examined [16–22]. It is well known that vegetable oils undergo oxidation and hydrolysis processes during storage and that air accessibility, light exposure and high temperature accelerate this process [16–18]. Oxidation processes are induced by radical mechanisms wherein initially, a hydrogen radical is abstracted from the vicinity of a C=C double bond [23,24]. Concurrently, hydrolysis leads to the liberation of free fatty acids that in turn autocatalyze hydrolytic reactions [23–25]. Aging processes in paper

equally have been extensively examined and reviewed [26], but the work focused on the aging of the fibers rather than the coatings. To the best of our knowledge, the only research conducted on the aging of paper in combination with vegetable oils so far has focused on cellulosic materials used as insulators in transformers [24,27–30]. In this context, cellulosic materials, such as pressboard immersed in vegetable oil, were found to depolymerize during aging due to the presence and liberation of water, as indicated by an increase in 2-furfuraldehyde content [23,24,31]. The vegetable oil showed hydrolysis, oxidation and oxidative polymerization processes, resulting in increased viscosity and increased acid number that can, among others, be attributed to ester scission and polymerization [23,30]. Finally, a transesterification reaction occurs, in which free fatty acids formed as hydrolysis products react with cellulosic hydroxyl groups to form covalent ester bonds [24,29,32].

Not only the processes required to produce (super)hydrophobic paper coatings are still relatively complicated, but especially, the modifications occurring in coatings subjected to thermal stress or aging processes are still poorly understood—despite their relevance with respect to long-term performance and stability. In this work, we show that it is possible to obtain hydrophobic coatings with WCAs above 130° through the simple process of thermal storage of olive oil-coated paper followed by Soxhlet extraction. To elucidate the underlying mechanisms, we further examine aging processes at norm climate and under argon for comparison using chemical and surface analytics.

2. Materials and Methods

2.1. Materials

Olive oil was purchased from Oehlmuehle Solling (Boffzen, Germany) and determined to contain 77% oleic acid, 13% palmitic acid and 5% linoleic acid as well as some minor component fatty acids by GC-MS/FID (for the procedure, see Supplementary Information). Acetone and ethanol (analytical grade) were purchased from Merck (Darmstadt, Germany), Fluorescent Brightener 28 (Calcofluor White) from Sigma-Aldrich (St. Louis, MO, USA), Sudan III powder (dye content $\geq 75\%$) from Carl Roth (Karlsruhe, Germany) and Sudan III staining solution (2.5 g/L in ethanol (99.0%, denatured)) from Morphisto (Offenbach, Germany). Argon (99.999%) was obtained from Westfalen (Muenster, Germany).

2.2. Methods

- Cotton linter handsheet production

Cotton linter laboratory handsheets (100 g/m²) were produced from aqueous cotton linter dispersion (2.2 wt%, diluted to 0.16 wt%) after stirring for 30 min to avoid fiber entanglement. Sheets were formed on a Haage sheet-former BBS (Haage, Preissenberg, Germany) in accordance with ISO 5269-2 [33]. The sheets were dried under reduced pressure (93 °C, 10 min), and sheet grammage was determined by bone-dried paper weight. To allow for the papers to reach equilibrium water content, the sheets were stored at norm climate conditions (23 °C, 50% relative humidity) for 24 h before use.

- Coating preparation and aging

Cotton linter handsheets were cut into stripes of 7.5 × 2.5 cm and dip-coated with olive oil on a custom-built device at a withdrawal speed of 2 mm/s.

For aging experiments performed at norm climate, samples were stored in an open Petri dish under controlled climate (23 °C, 50% relative humidity). For thermal aging, samples were stored in an open petri dish at 70 °C in a Heraeus function line T12 incubator (Heraeus, Hanau, Germany). For aging under argon, samples were stored in Schlenk vials from which air was removed by triple application of vacuum to 10^{−3} mbar followed by argon purging. The storage time was 4 weeks unless stated otherwise.

Soxhlet extractions were performed with acetone (300 mL) for 6 h.

- Staining with Calcofluor White and Sudan III

To examine the coating penetration into the paper during aging using confocal laser scanning microscopy (CLSM), the cotton linter papers were first immersed into an aqueous

Calcofluor White solution (100 μM , 15 min), after which excess dye was removed by gentle shaking in distilled H_2O (15 min). The stained papers were dried under reduced pressure at (40 $^\circ\text{C}$, 1.5 h). The papers were then dip-coated with olive oil, which was mixed with Sudan III (25 $\mu\text{g}/\text{g}$ oil) for staining.

For the fluorescence imaging of the extracted papers, Calcofluor White staining was performed as described. For Sudan III staining, the papers were first immersed in ethanol (10 s) and then immersed in an alcoholic Sudan III solution (10 vol% in ethanol, 5 min), after which excess dye was removed by gentle stirring in ethanol (3 \times , 15 min). The stained papers were dried under reduced pressure (40 $^\circ\text{C}$, 1.5 h). Reference papers were equally extracted prior to staining.

- Attenuated total reflectance–Fourier transformation infrared (ATR-FTIR) spectroscopy

ATR-FTIR spectra were recorded with a Spectrum 3 spectrometer (PerkinElmer, Waltham, MA, USA) between 4000 cm^{-1} and 650 cm^{-1} at a nominal resolution of 4 cm^{-1} and 10 scans directly on the paper substrate. Background correction was performed using Spectrum software (Version 10.7.2).

- Confocal laser scanning microscopy (CLSM)

CLSM images were taken on a Leica TCS SP8 microscope (Leica Microsystems, Mannheim, Germany) with an HC PL APO CS2 20 \times /0.75 DRY objective. The samples were fixed in the sample holder without the use of coverslips and marked to reproduce the measurement position before and after aging. CFW fluorescence was excited at 405 nm, and emission was detected between 424 nm and 496 nm. Sudan III fluorescence was excited in a separate channel at 552 nm, and emission was detected between 561 nm and 681 nm. At each marked position, 3D image stacks were recorded with a plane-to-plane distance of 2 μm to capture the entire depth of said position. For presentation, maximum intensity projections were generated from the 3D stacks using ImageJ2 (Version 1.54b) [34].

- Differential scanning calorimetry (DSC)

DSC curves were measured both on coated paper and extracted oils using a Mettler Toledo DSC 3 calorimeter (Mettler Toledo, Gießen, Germany), and the data was evaluated using STARe software (Version 16.30a). Two cooling and heating cycles from 25 $^\circ\text{C}$ to -90 $^\circ\text{C}$, and vice versa, were carried out at a cooling and heating rate of 5 K/min under nitrogen atmosphere (30 mL/min). The second cooling cycle was used for data evaluation. Crystallization enthalpies were determined for olive oil extracted from paper from the integral between -60 $^\circ\text{C}$ and -10 $^\circ\text{C}$ (5 $^\circ\text{C}$ for the thermally aged sample).

- Fluorescence imaging

Fluorescence images were recorded on a Vilber Fusion FX7 Edge Imager (Vilber, Eberhardzell, Germany) using (365 \pm 20) nm and (530 \pm 20) nm illumination combined with UV and orange emission filters, respectively. Due to its low depth discrimination (in contrast to CLSM imaging), this device is well suited to compare the emission intensities between samples.

- ^1H -Nuclear magnetic resonance (NMR) spectroscopy

NMR spectra were measured on a Bruker Avance II NMR spectrometer at 300 MHz, (Bruker BioSpin GmbH, Rheinstetten, Germany) in deuterated chloroform. Chemical shifts were calibrated to the deuterated solvent signal. MestReNova 11.0 software (Mestrelab Research S. L., Santiago de Compostela, Spain) was used to process the spectra.

- Optical profilometry

Surface roughness data was obtained by optical profilometry using a Sensofar PLu neox optical profiler (Sensofar-Tech, Terrassa, Spain) equipped with a Nikon EPI 20 \times objective ((850.08 \times 709.35) μm scan area, 0.69 $\mu\text{m}/\text{pixel}$) using a 140 μm z-scan range. Measurements were repeated in triplicate, and surface roughness parameters S_a , S_q and S_z

were determined according to ISO 25178 [35]. Errors were calculated based on the standard deviation of the mean.

- Size exclusion chromatography (SEC)

Size exclusion chromatography (SEC) was performed using an Agilent Technologies system (Agilent Technologies, Santa Clara, CA, USA) equipped with an Agilent Technologies 1260 Infinity II G7129A autosampler, an Agilent Technologies 1260 Infinity II G7110B pump, an Agilent Technologies 1260 Infinity G1362A RI detector and a HP 1050 series UV detector and a PSS SDV 5 μm column. THF was used as a mobile phase at a flow rate of 1 mL/min and with an analyte concentration of (1.5–2) g/L.

- Water contact angle measurement

The coated papers were stored at norm climate conditions overnight before water contact angle measurements. Contact angles were measured on a Dataphysics OCA35 device (Dataphysics, Filderstadt, Germany) at norm climate conditions using the sessile drop method with 2 μL droplets of ultrapure water. Drop shape fittings were performed using Dataphysics SCA20 software and applying the Young–Laplace fitting mode. Individual data points were based on five different measurements, while time-dependent measurement series were repeated in triplicate. Advancing and receding contact angles were calculated as mean values of water contact angles measured during an increase of a 2 μL droplet by 10 μL at a speed of 1 $\mu\text{L}/\text{s}$ and the subsequent decrease in that same droplet with the same parameters, also performed in triplicate. Errors were calculated from the standard deviation of the mean.

3. Results

In this work, we applied olive oil onto cotton linter laboratory handsheets via dip-coating and stored them for 4 weeks at either 70 $^{\circ}\text{C}$, under norm climate (23 $^{\circ}\text{C}$, 50% relative humidity) or at room temperature under argon (Figure 1). Afterward, excess oil was removed by Soxhlet extraction. Both the coated and extracted papers as well as the extracted oils were analyzed.

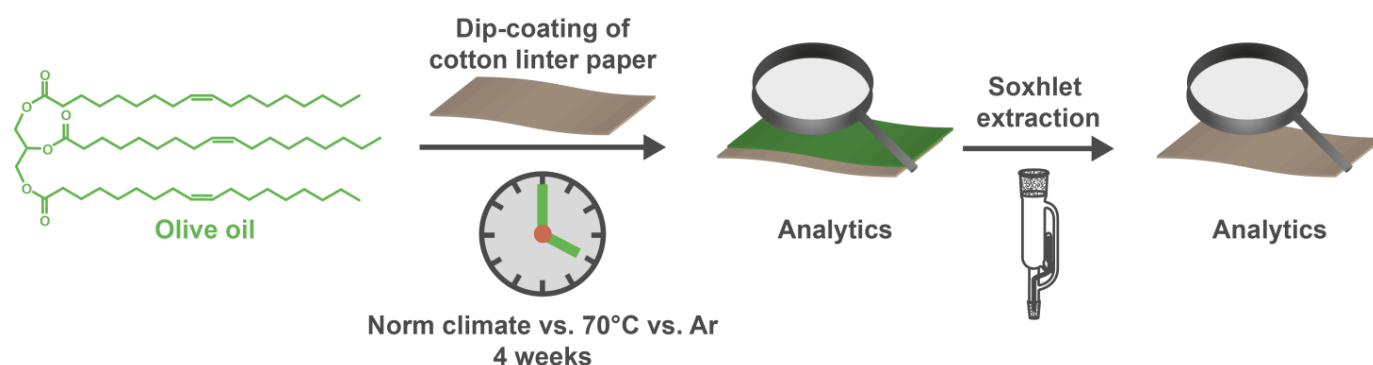


Figure 1. The approach used to examine the aging processes with olive oil as a coating material. Coated papers were stored for 4 weeks at norm climate, at 70 $^{\circ}\text{C}$ or under argon.

The olive oil-coated paper aged at 70 $^{\circ}\text{C}$ for 4 weeks shows a significantly enhanced water contact angle (WCA) of $(97.4 \pm 1.6)^{\circ}$ compared with $(66.0 \pm 0.7)^{\circ}$ for coated surfaces measured the day after coating. Soxhlet extraction leads to an even higher static water contact angle of $(137.7 \pm 1.2)^{\circ}$, which is stable for at least 5 min (Figure 2a), as well as advancing and receding WCAs of $(137.9 \pm 6.4)^{\circ}$ and $(122.9 \pm 23.8)^{\circ}$, respectively. This is a strong indication that olive oil has in some way been covalently attached to the paper surface. Contrastingly, both the uncoated cotton linter paper and freshly coated paper submitted to subsequent Soxhlet extraction absorb water immediately, so WCA measurement is not possible. While the possibly covalently attached coating amount is too low to be detected in differential scanning calorimetry (DSC) measurements, attenuated

total reflectance–Fourier transformation infrared (ATR-FTIR) spectroscopy shows a weak signal at 1736 cm^{-1} that is not present in the cotton linter paper or in the freshly olive oil-coated extracted paper (Figure 2b, full spectrum in Figure S1). This band is indicative of C=O ester bonds [36] and indicates that transesterification has taken place, covalently linking a fatty acid chain of the oil to the cellulose hydroxyl groups, as has previously been observed [24,29,32]. Due to an overlap of the CH_2 vibration modes of fatty acids and cellulose in the region between 3000 cm^{-1} and 2800 cm^{-1} [36], this area cannot be taken into consideration for the current discussion. The low intensity of the characteristic olive oil bands compared with the cellulosic bands shows that the retained coating amount is very low. Furthermore, both the olive oil-coated and uncoated cotton linter papers were stained with Calcofluor White, a fluorescent dye that has a high affinity for cellulose, and Sudan III, a fat-soluble staining agent. Fluorescent imaging of the stained papers and an unstained reference proves the presence of fat in the aged paper after Soxhlet extraction, as Sudan III excitation yields much brighter images for the coated paper than for those not supposed to contain aliphatic species (Figure 2c). Notably, Calcofluor White emission is lower in the presence of either olive oil or Sudan III than without the hydrophobic coating.

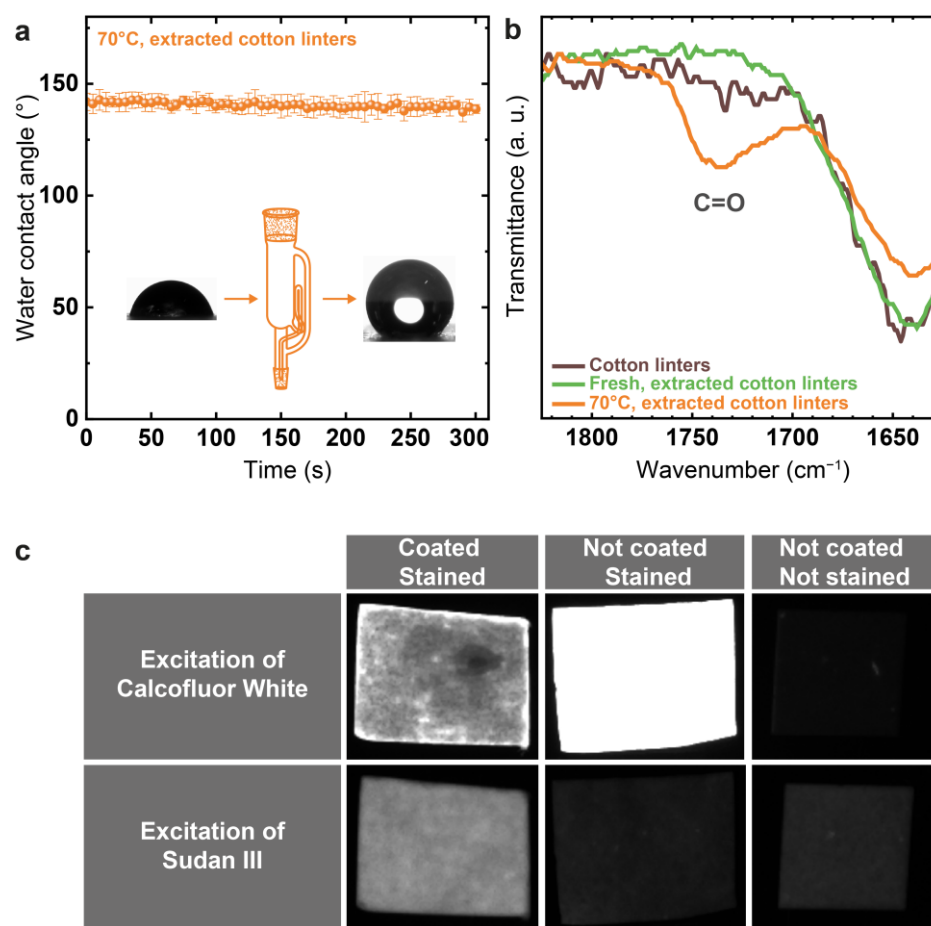


Figure 2. (a) WCA evolution for extracted thermally aged cotton linter paper over 5 min showing permanent hydrophobization. (b) Excerpt of FTIR spectra from 1625 cm^{-1} to 1825 cm^{-1} measured on extracted cotton linters after varying aging processes and showing a small C=O band indicating esterification exclusively after thermal aging. (c) Fluorescence images comparing coated stained, uncoated stained and uncoated unstained papers exciting either Calcofluor White or Sudan III. While CFW is observed in both stained samples, Sudan III is only present in the coated ones, proving the presence of fatty acids. All images of one channel were taken simultaneously and cropped for better display without further modification, original size of approximately (7×10) mm.

While these observations are convincing proof that transesterification leading to the covalent attachment of fatty acids onto cellulose occurs when paper ages at 70 °C, further inquiries into the aging process would deepen the understanding thereof and accordingly help to explain the increase in the WCA after thermal aging and Soxhlet extraction. As it is well known that both temperature and oxygen accessibility influence the aging of olive oil, we compared the aging processes occurring at 70 °C to those occurring during storage at norm climate and under argon.

Initially, we compared surface properties for the three aging processes. The water contact angles increase under all aging conditions, from $(66 \pm 0.7)^\circ$ for the fresh sample to $(77.8 \pm 0.6)^\circ$ after aging under argon atmosphere and to $(82.9 \pm 1.4)^\circ$ after aging at norm climate, even to the aforementioned hydrophobic range with $(97.4 \pm 1.6)^\circ$ after aging at 70 °C (Figure 3a). Complete water droplet absorption into the paper is slowed down compared with the uncoated paper and takes place within 15 s after deposition for the fresh and argon-aged samples, within 30 s for the samples aged at norm climate and around 4 min for samples aged at 70 °C (Figure 3b). Surface roughness measurements show no significant change in roughness parameters independent of the aging conditions, indicating that the water contact angle modification is not caused by a change in the wetting regime. Instead, the paper roughness is defined by the roughness of the cotton linter paper substrate and is not significantly modified by the vegetable oil coating (Figure 3c).

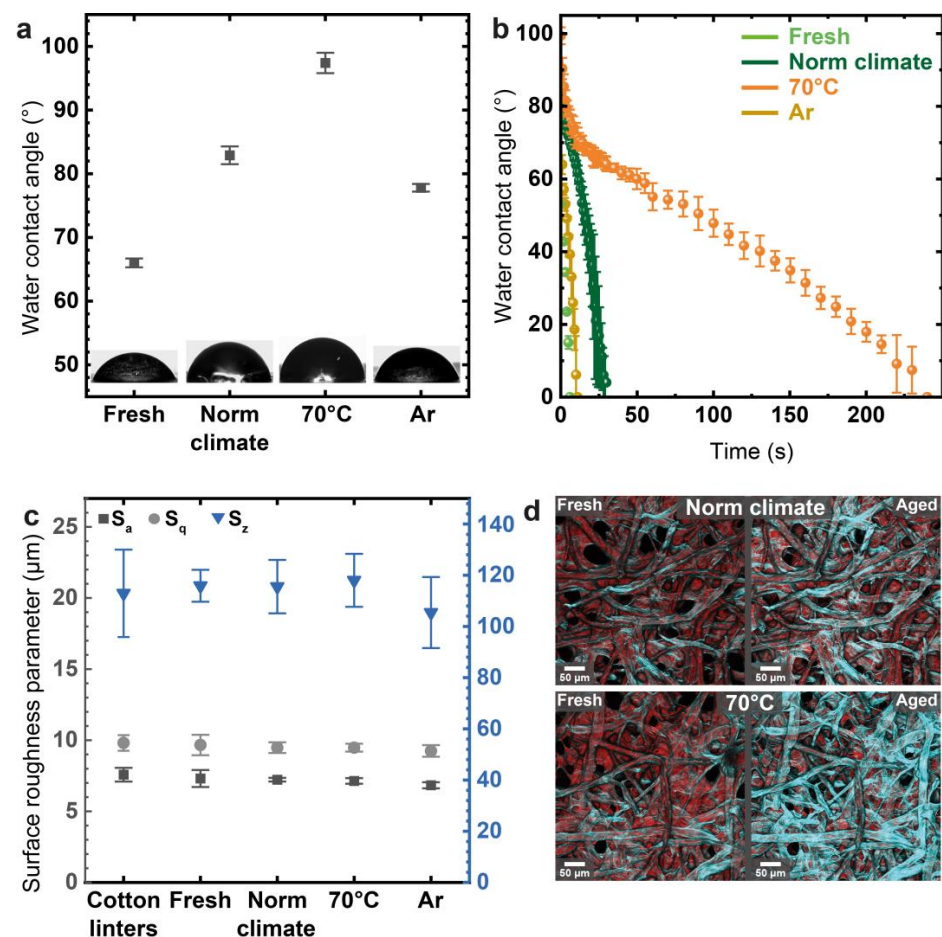


Figure 3. (a) Static and (b) time-dependent static WCA measurements showing increasing WCAs with air accessibility and temperature. (c) Surface roughness parameters show no significant modification with aging. (d) CLSM images showing the comparison between fresh and aged samples indicating a migration of oil from the fiber surface into the fiber wall, especially at 70 °C (cellulose stain in cyan, oil stain in red). Images were recorded with the same settings for excitation and emission (power and detector gain) and at the same position between fresh and aged samples.

The same fluorescent dyes for cellulose and oil, which were used above for fluorescence intensity imaging, were also used for confocal microscopic examinations. Images were taken at the very same positions on each paper sample before and after aging. The comparison between these time points reveals a marked increase in the Calcofluor White fluorescence intensity after storage (Figure 3d). An increased intensity of the Calcofluor White fluorescence in the absence of a Sudan III-stained oil coating was similarly observed in the aforementioned analysis with the fluorescent imager (Figure 2c). It is therefore reasonable to assume that the proximity of the coating and Calcofluor White on the fiber surface right after staining and dip coating—and before aging—causes the latter dye to fluoresce less. More importantly, the increase during aging then strongly points to a separation between Calcofluor White and the coating. This separation could be the result of a progressing migration of the oil from the fiber surface into the fiber wall. The observation that the increase in Calcofluor White fluorescence intensity is even stronger for paper aged at 70 °C supports this migration hypothesis, as temperature decreases the oil's viscosity, which facilitates migration.

Chemical analytics show the processes occurring within the coating during aging. To perform ¹H-nuclear magnetic resonance (NMR) spectroscopy and size exclusion chromatography (SEC), unbound coating material was extracted from the paper through Soxhlet extraction, and the oil residue obtained after solvent removal was analyzed. When performing ATR-FTIR spectroscopy and differential scanning calorimetry, both the coated paper and the extracted oil were examined, and the results were in good agreement with each other. The data shown is that of the coated paper.

¹H-NMR spectroscopy shows strong modifications for the samples stored at 70 °C. Integrals of all peaks indicating hydrogens in vicinity to double bonds decrease, namely, those at (5.50–5.30) ppm (R-CH=CH, decrease to ~2% of its original value), (2.10–1.93) ppm (CH₂-CH=CH, decrease to ~4% of its original value) and (2.85–2.70) ppm (CH=CH-CH₂-CH=CH, complete disappearance). Simultaneously, the integral of the peak indicating aliphatic chains at (1.45–1.15) ppm increases, as do all peaks indicating hydrogen groups in the vicinity of oxygen-containing groups, namely, those at (5.30–5.20) ppm (CH-O-CO-R), (4.35–4.10) ppm (CH₂-O-CO-R), (2.40–2.25) ppm (CH₂-CO-O-R/H) and (1.70–1.15) ppm (CH₂-CH₂-CO-O-R/H). Peak attribution was in good accordance with the literature [37]. These changes indicate that oxidative processes take place during thermal aging. For the coatings aged at norm climate, similar changes are observed, but to a lower extent, with, for instance, the integral at (5.50–5.30) ppm decreasing by ~6%. No changes are observed for samples aged under argon atmosphere, whereby these results indicate that both the presence of oxygen and temperature is crucial to the chemical aging process (Figure 4a, all spectra shown in Figure S2).

SEC curves show the main peak for fresh olive oil at ~1300 Da relative to the calibration standard polystyrene. The intensity of a tiny shoulder at ~400 Da increases during aging in the order argon < norm climate < 70 °C. An additional peak appears at ~2600 Da after norm climate aging but not after argon aging, and reaches almost the same intensity as the fresh olive oil peak after aging at 70 °C. An overall widespread content of higher molecular weight fractions is observed for the thermally aged sample, indicating that di-/oligomerization and other intermolecular reactions such as crosslinking lead to molecular weight increase. However, reactions that lead to lower molecular weight fractions occur under all aging conditions (Figure 4b). Note that the values given for SEC-based molecular weights are not absolute due to the use of polystyrene standards and can only be compared relative to each other, which nonetheless allows for qualitative molecular weight evolution assessment.

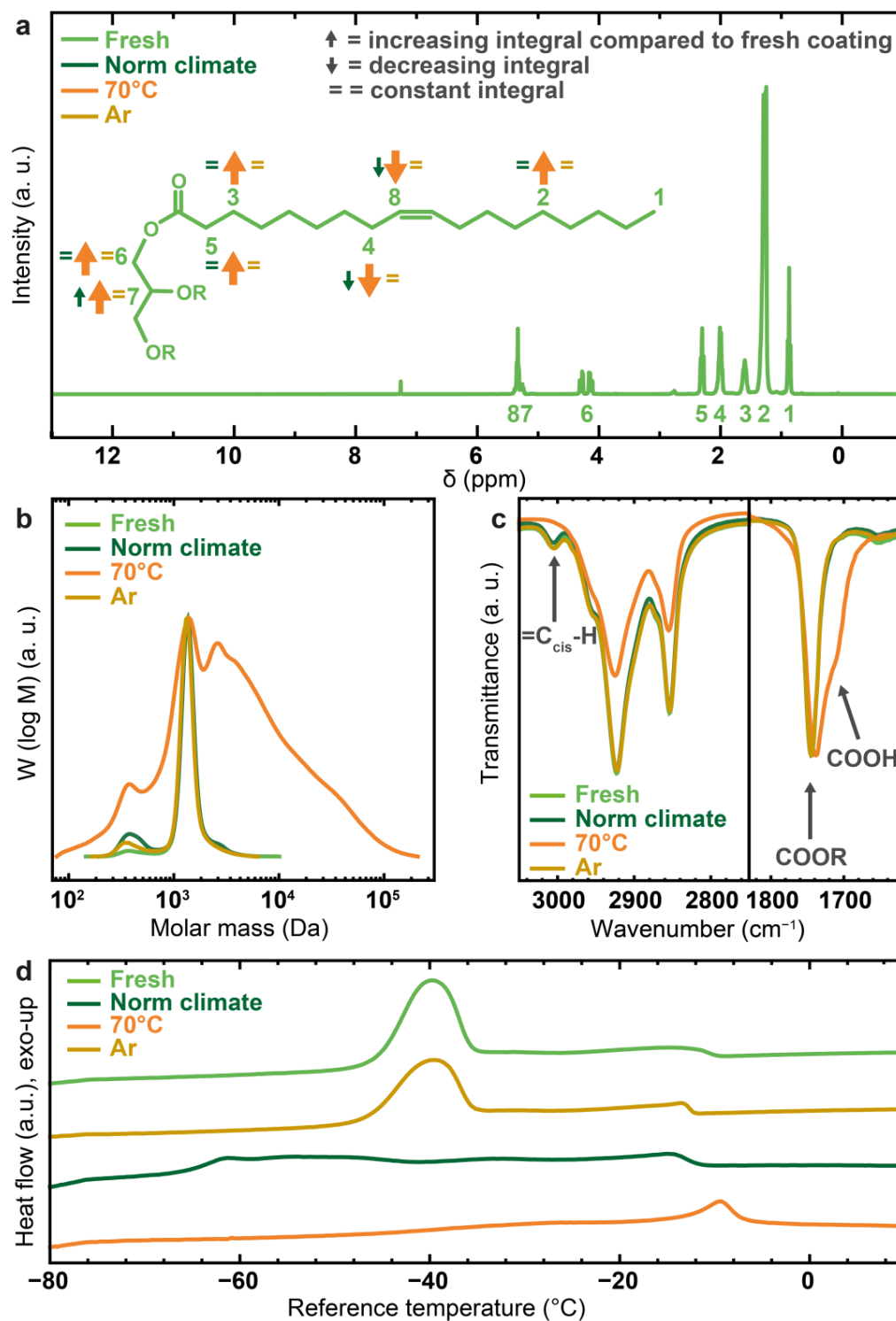


Figure 4. (a) ^1H -NMR spectrum of olive oil, inset indicating trends after aging for individual hydrogen integrals. (b) Normalized SEC curves show the formation of lower molecular weight compounds and of higher molecular weight compounds especially after thermal aging. (c) Excerpts of FTIR spectra normalized to $\text{C}=\text{O}$ peak intensity showing the disappearance of $=\text{C}_{\text{cis}}-\text{H}$ bond in the spectral area from 2775 cm^{-1} to 3025 cm^{-1} and $\text{C}=\text{O}_{\text{acid}}$ shoulder formation in the spectral area from 1625 cm^{-1} to 1825 cm^{-1} after aging at 70°C . (d) DSC cooling curves showing the disappearance of the original triglyceride peak and the emergence of higher and lower molecular weight species. (a,b) were measured on oil after its extraction from paper; (c,d) were measured directly on paper, and the results were in accordance with those measured on oil after extraction.

ATR-FTIR spectroscopy highlights interesting properties in the areas of aliphatic and carbonyl vibration bands. While no modifications are observed for the coated samples aged at ambient temperature, the samples aged at 70 °C show several changes. The band indicating =C_{cis}-H vibrations at 3005 cm⁻¹ disappears completely [36]. The bands at 2956 cm⁻¹, 2923 cm⁻¹ and 2853 cm⁻¹ can be attributed to asymmetric CH₃ stretching, asymmetric CH₂ stretching and symmetric CH₂ stretching, respectively [36]. Their intensity relative to the carbonyl band at 1745 cm⁻¹ is lower for the thermally aged sample, indicating an increased oxygen content relative to the aliphatic chain content. Further, the peak indicating the carbonyl bond shows a slight shift to lower wavenumbers for the coating aged at 70 °C and also features a supplementary shoulder at 1709 cm⁻¹. While the main C=O peak is attributed to the stretching mode of the ester bond present in vegetable oils, the shoulder belongs to the C=O stretching mode of free fatty acids [36], indicating their formation at elevated temperatures as described in the literature (Figure 4c, full spectrum shown in Figure S3) [24,29].

The DSC cooling curve of fresh olive oil shows two exothermic transitions, the first one at ~-14 °C associated with the crystallization of mostly saturated triacylglycerols and the second one at ~-40 °C with the crystallization of unsaturated triacylglycerols [38–40]. Storage under argon atmosphere does not result in significant changes. After storage at norm climate, the crystallization peak of the unsaturated triacylglycerols is not visible anymore, but the crystallization offset is delayed to ~-61 °C. Both hydrolytic degradation and oxidative processes have been described for the auto-oxidation of olive oil at extended storage times, and especially, auto-oxidation can be attributed to the observed extended crystallization range [41,42]. The presence of thus-formed different smaller and larger molecules hinders crystallization, which is reflected in a decreased crystallization enthalpy, which is approximately 48 J/g for the freshly coated oil and decreases to 31 J/g after norm climate and 18 J/g after thermal aging [43]. As for the paper aged at 70 °C, the crystallization enthalpy is still further reduced compared with the other samples, while the crystallization onset shifts to slightly higher temperatures of -10 °C. This shift and the further increased crystallization range can be attributed to additionally enhanced oxidation and resulting coating heterogeneity (Figure 4d) [41].

The different analytical methods allow for drawing conclusions on chemical processes occurring during the storage of olive oil-coated paper. During aging in argon atmosphere, no significant chemical or morphological changes are observed. The slightly increased WCA can therefore be attributed exclusively to the penetration of the coating into the paper during storage. During aging at norm climate, additional small chemical changes happen, for which oxygen accessibility is a prerequisite. These include oxidation reactions discernible in ¹H-NMR spectroscopy by an increase in oxygen-adjacent hydrogen peak integral and a decrease in C=C-adjacent hydrogen peak integrals but not visible in less sensitive ATR-FTIR spectroscopy. SEC and DSC also indicate the formation of oxidation products of higher and lower molecular weight than the native olive oil triglyceride that inhibits crystallization. During thermal storage, these effects are strongly intensified and the C=C double bond is nearly fully consumed, as evidenced by both ¹H-NMR and ATR-FTIR spectroscopy. A significant amount of native olive oil triglycerides is transformed into lower and higher molecular weight fractions, as reflected in SEC. These factors indicate that in addition to oxidation, crosslinking or dimer-/oligomerization reactions consume the C=C double bond [16,44]. Oxidation products can be intermediate conjugated dienes, peroxides and finally, aldehydes and other low-molecular-weight compounds [18,20]. Furthermore, transesterification reactions are induced by the combination of heat and paper-intrinsic moisture [24,29] that lead to the liberation of free fatty acid evidenced through ATR-FTIR spectroscopy and the covalent attachment of fatty acids onto the hydroxyl groups of cellulose that ultimately results in paper hydrophobization.

To extend the scope of understanding, the coated papers aged at norm climate were examined at different storage times ranging from fresh samples to papers stored for 6 months. The analytical focus was placed on water contact angle measurements to show the effect on

water absorption and on DSC as the strongest indicator for chemical changes. While the initial water contact angle upon droplet deposition does not change significantly with aging time, water absorption speed decreases, initially taking place within less than 10 s and taking more than 3 min after storage for 6 months (Figure 5a). DSC cooling curves reflect the increase in the formation of oxidized species with storage time (Figure 5b). Similar effects were observed for aging at 70 °C for 1 day and 1 week. Water absorption time decreased with storage time and did so much faster than during norm climate aging (Figure 5c). Stable hydrophobization with water contact angles around 130° on the Soxhlet-extracted papers can already be achieved within 1 week of aging (inset Figure 5c), while 1 day proved insufficient for permanent hydrophobization, as droplet absorption was still immediate and water contact angles could not be measured. Similarly, the DSC curve measured after 1 day of storage does not indicate significant chemical modifications, while the DSC curve after 1 week looks very similar to that obtained after 4 weeks (Figure 5d), indicating that the hydrophobization process can be further tuned by time and temperature. Thus, not only storage conditions but also storage time can have a crucial influence on the physical and chemical properties of vegetable oil-based paper coatings.

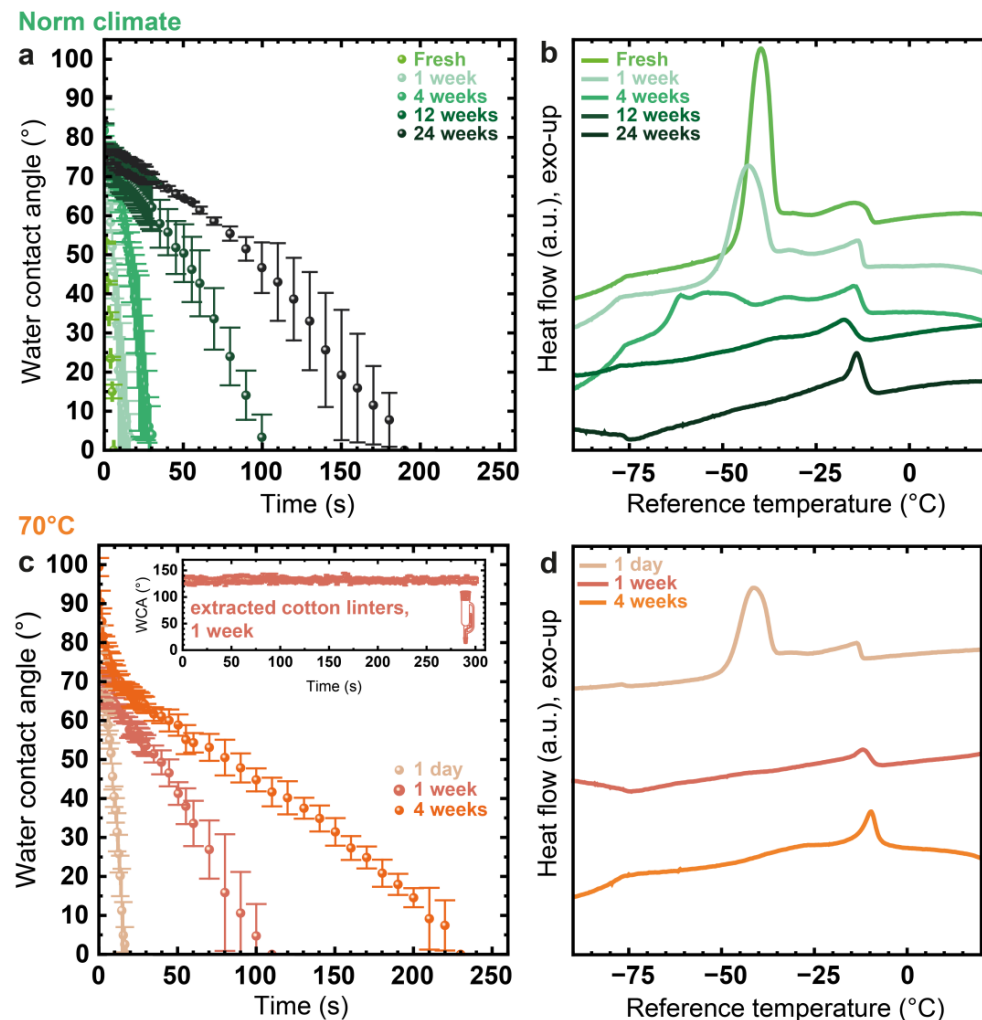


Figure 5. (a) Time-dependent WCA measurements show decreasing water absorbance speed with norm climate aging. (b) DSC cooling curves show the disappearance of the original triglyceride solidification peak and the occurrence of lower and higher molecular weight species with increasing aging time at norm climate. (c) Time-dependent WCA measurements showing absorption after varying aging times at 70 °C and (c-inset) on Soxhlet-extracted paper aged for 1 week. (d) DSC measurements indicate significant chemical modification even after 1 week of storage.

4. Conclusions and Outlook

In this work, we have shown that it is possible to produce olive oil-based paper coatings with water contact angles of more than 135° through a 4-week thermal treatment process followed by extraction of unbound vegetable oil, leaving behind an extremely low amount of coating attached covalently to the paper substrate. While this actual procedure is surely not immediately relevant for industrial application, it shows the potential to produce biobased hydrophobic coatings in an extraordinarily simple manner. Choosing a less material-consuming coating method, such as spray coating or gas-phase deposition, would be required to forego the extraction process, while careful tuning of treatment temperature and moisture exposition could greatly accelerate the covalent attachment process. Inquiries into both the recyclability of the coated papers as well as the reusability of the extracted oil are equally relevant for potential industrial applications. Analyzing the modifications occurring both during the thermal aging process and during the practically relevant storage at ambient conditions has proven the cruciality of storage time, temperature and oxygen accessibility for the properties of fatty acid-based coatings. Research in the field of fatty acid-based paper coatings must therefore consider these factors to allow for the reproducibility of results and to be able to account for the long-term stability of the coating.

Supplementary Materials: The following supporting information can be downloaded at: <https://www.mdpi.com/article/10.3390/coatings14030364/s1>, Protocol for gas chromatography–mass spectrometry/flame ionization detector (GC-MS/FID); Figure S1: Full ATR-FTIR spectrum of extracted cotton linters after varying aging processes showing a small C=O band indicating esterification exclusively after thermal aging; Figure S2: Full NMR spectra of olive oil extracted from cotton linters (fresh and after aging); Figure S3: ATR-FTIR spectra normalized to C=O peak intensity of freshly olive oil coated cotton linter paper and aged under different conditions.

Author Contributions: Conceptualization, A.L.-Z. and A.G.; investigation, A.L.-Z. and T.M.; writing—original draft preparation, A.L.-Z.; writing—review and editing, all authors; visualization, A.L.-Z.; supervision, A.G. and M.B. All authors have read and agreed to the published version of the manuscript.

Funding: This research was funded as part of the BioPlas4Paper project by the Agency for Renewable Resources (Fachagentur Nachwachsende Rohstoffe e.V.—FNR), grant number 2220HV017A.

Institutional Review Board Statement: Not applicable.

Informed Consent Statement: Not applicable.

Data Availability Statement: The data presented in this study are available on request from the corresponding authors.

Acknowledgments: The authors thank Marion Trautmann for SEC measurements and the NMR service group (all Department of Chemistry, Technical University Darmstadt) for service NMR measurements as well as Silke Radtke (Thünen Institute for Wood Research, Hamburg) for GC-MS/FID measurements.

Conflicts of Interest: The authors declare no conflicts of interest.

References

1. Samyn, P. Active Barrier Coating for Packaging Paper with Controlled Release of Sunflower Oils. *Molecules* **2021**, *26*, 3561. [[CrossRef](#)] [[PubMed](#)]
2. Crépy, L.; Chaveriat, L.; Banoub, J.; Martin, P.; Joly, N. Synthesis of cellulose fatty esters as plastics—Influence of the degree of substitution and the fatty chain length on mechanical properties. *ChemSusChem* **2009**, *2*, 165–170. [[CrossRef](#)] [[PubMed](#)]
3. David, G.; Gontard, N.; Guerin, D.; Heux, L.; Lecomte, J.; Molina-Boisseau, S.; Angellier-Coussy, H. Exploring the potential of gas-phase esterification to hydrophobize the surface of micrometric cellulose particles. *Eur. Pol. J.* **2019**, *115*, 138–146. [[CrossRef](#)]
4. Peydecastaing, J.; Girardeau, S.; Vaca-Garcia, C.; Borredon, M.E. Long chain cellulose esters with very low DS obtained with non-acidic catalysts. *Cellulose* **2006**, *13*, 95–103. [[CrossRef](#)]
5. Geissler, A.; Loyal, F.; Biesalski, M.; Zhang, K. Thermo-responsive superhydrophobic paper using nanostructured cellulose stearoyl ester. *Cellulose* **2014**, *21*, 357–366. [[CrossRef](#)]
6. Nau, M.; Seelinger, D.; Biesalski, M. Functional surface coatings from tailor-made long-chain hydroxypropyl cellulose ester nanoparticles. *Cellulose* **2018**, *25*, 5769–5780. [[CrossRef](#)]

7. Cordt, C.; Geissler, A.; Biesalski, M. Regenerative Superhydrophobic Paper Coatings by In Situ Formation of Waxy Nanostructures. *Adv. Mater. Interfaces* **2021**, *8*, 2001265. [[CrossRef](#)]
8. Onwukamike, K.N.; Grelier, S.; Grau, E.; Cramail, H.; Meier, M.A.R. Sustainable transesterification of cellulose with high oleic sunflower oil in a DBU-CO₂ switchable solvent. *ACS Sustain. Chem. Eng.* **2018**, *6*, 8826–8835. [[CrossRef](#)]
9. Huang, X.; Wang, A.; Xu, X.; Liu, H.; Shang, S. Enhancement of hydrophobic properties of cellulose fibers via grafting with polymeric epoxidized soybean oil. *ACS Sustain. Chem. Eng.* **2017**, *5*, 1619–1627. [[CrossRef](#)]
10. Saha, P.; Manna, S.; Sen, R.; Roy, D.; Adhikari, B. Durability of lignocellulosic fibers treated with vegetable oil–phenolic resin. *Carbohydr. Polym.* **2012**, *87*, 1628–1636. [[CrossRef](#)]
11. Shang, Q.; Liu, C.; Chen, J.; Yang, X.; Hu, Y.; Hu, L.; Zhou, Y.; Ren, X. Sustainable and robust superhydrophobic cotton fabrics coated with castor oil-based nanocomposites for effective oil–water separation. *ACS Sustain. Chem. Eng.* **2020**, *8*, 7423–7435. [[CrossRef](#)]
12. Loesch-Zhang, A.; Cordt, C.; Geissler, A.; Biesalski, M. A Solvent-Free Approach to Crosslinked Hydrophobic Polymeric Coatings on Paper Using Vegetable Oil. *Polymers* **2022**, *14*, 1773. [[CrossRef](#)] [[PubMed](#)]
13. Bellmann, M.; Loesch-Zhang, A.; Möck, D.M.J.; Appelt, J.; Geissler, A.; Viöl, W. Hydrophobic glass and paper coatings based on plasma polymerized vegetable oils using a novel atmospheric pressure plasma concept. *Plasma Process. Polym.* **2024**, e202300224. [[CrossRef](#)]
14. Samyn, P. Wetting and hydrophobic modification of cellulose surfaces for paper applications. *J. Mater. Sci.* **2013**, *48*, 6455–6498. [[CrossRef](#)]
15. Dankovich, T.A.; Hsieh, Y.-L. Surface modification of cellulose with plant triglycerides for hydrophobicity. *Cellulose* **2007**, *14*, 469–480. [[CrossRef](#)]
16. Bilancia, M.T.; Caponio, F.; Sikorska, E.; Pasqualone, A.; Summo, C. Correlation of triacylglycerol oligopolymers and oxidised triacylglycerols to quality parameters in extra virgin olive oil during storage. *Food Res. Int.* **2007**, *40*, 855–861. [[CrossRef](#)]
17. Kanavouras, A.; Cert, A.; Hernandez, R.J. Oxidation of Olive Oil under Still Air. *Food Sci. Technol. Int.* **2005**, *11*, 183–189. [[CrossRef](#)]
18. Gómez-Alonso, S.; Salvador, M.D.; Fregapane, G. Evolution of the oxidation process in olive oil triacylglycerol under accelerated storage conditions (40–60 °C). *J. Am. Oil Chem. Soc.* **2004**, *81*, 177–184. [[CrossRef](#)]
19. Ixtaina, V.Y.; Nolasco, S.M.; Tomás, M.C. Oxidative Stability of Chia (*Salvia hispanica* L.) Seed Oil: Effect of Antioxidants and Storage Conditions. *J. Am. Oil Chem. Soc.* **2012**, *89*, 1077–1090. [[CrossRef](#)]
20. Guiotto, E.N.; Ixtaina, V.Y.; Nolasco, S.M.; Tomás, M.C. Effect of Storage Conditions and Antioxidants on the Oxidative Stability of Sunflower–Chia Oil Blends. *J. Am. Oil Chem. Soc.* **2014**, *91*, 767–776. [[CrossRef](#)]
21. Malvis, A.; Šimon, P.; Dubaj, T.; Sládková, A.; Ház, A.; Jablonský, M.; Sekretár, S.; Schmidt, Š.; Kreps, F.; Burčová, Z.; et al. Determination of the Thermal Oxidation Stability and the Kinetic Parameters of Commercial Extra Virgin Olive Oils from Different Varieties. *J. Chem.* **2019**, *2019*, 4567973. [[CrossRef](#)]
22. van Durme, J.; Nikiforov, A.; Vandamme, J.; Leys, C.; de Winne, A. Accelerated lipid oxidation using non-thermal plasma technology: Evaluation of volatile compounds. *Food Res. Int.* **2014**, *62*, 868–876. [[CrossRef](#)]
23. Tenbohlen, S.; Koch, M. Aging Performance and Moisture Solubility of Vegetable Oils for Power Transformers. *IEEE Trans. Power Deliv.* **2010**, *25*, 825–830. [[CrossRef](#)]
24. Bandara, K.; Ekanayake, C.; Saha, T.K.; Annamalai, P.K. Understanding the ageing aspects of natural ester based insulation liquid in power transformer. *IEEE Trans. Dielect. Electr. Insul.* **2016**, *23*, 246–257. [[CrossRef](#)]
25. Rooney, D.; Weatherley, L.R. The effect of reaction conditions upon lipase catalysed hydrolysis of high oleate sunflower oil in a stirred liquid–liquid reactor. *Process Biochem.* **2001**, *36*, 947–953. [[CrossRef](#)]
26. Zervos, S. Natural and accelerated ageing of cellulose and paper: A literature review. In *Cellulose: Structure and Properties, Derivatives and Industrial Uses*; Lejeune, A., Deprez, T., Eds.; Nova Science Publishers: Hauppauge, NY, USA, 2010; ISBN 9781608763887.
27. Contreras, J.E.; Rodriguez, J.; Gaytan, C.; Greaves, B.; Prevost, T. Thermal Aging Performance of Cellulose Insulation in Natural Ester Liquid. *IEEE Trans. Dielect. Electr. Insul.* **2021**, *28*, 1357–1362. [[CrossRef](#)]
28. Franquet, J.; Fernandez, I.; Ortiz, A. Dielectric and Mechanical Assessment of Kraft and Diamond Dotted Paper Aged with Commercial Vegetable Oil. In Proceedings of the 2020 IEEE International Conference on Dielectrics. 2020 IEEE 3rd International Conference on Dielectrics (ICD), Valencia, Spain, 5–31 July 2020; pp. 696–699, ISBN 978-1-7281-8983-3.
29. Rapp, K.J.; McShane, C.P.; Luksich, J. Interaction mechanisms of natural ester dielectric fluid and kraft paper. In Proceedings of the 2005 IEEE International Conference on Dielectric Liquids. ICDL 2005, Coimbra, Portugal, 26 June–1 July 2005; pp. 387–390, ISBN 0-7803-8954-9.
30. Nguyen, D.V.; Nguyen, L.P.; Quach, T.N. Investigation of AC breakdown properties of paper insulators and enamel insulation impregnated with rice oil, corn oil and peanut oil for transformers. *IET Sci. Meas.* **2019**, *13*, 1352–1361. [[CrossRef](#)]
31. McShane, C.P.; Gauger, G.A.; Luksich, J. Fire resistant natural ester dielectric fluid and novel insulation system for its use. In Proceedings of the IEEE Transmission and Distributions Conference (Cat. No. 99CH36333), New Orleans, LA, USA, 11–16 April 1999; pp. 890–894.
32. Yang, L.; Liao, R.; Caixin, S.; Zhu, M. Influence of vegetable oil on the thermal aging of transformer paper and its mechanism. *IEEE Trans. Dielect. Electr. Insul.* **2011**, *18*, 692–700. [[CrossRef](#)]
33. ISO 5269-2:2004(E); Pulps—Preparation of Laboratory Sheets for Physical Testing—Part 2: Rapid-Köthen Method. International Organization for Standardization: Geneva, Switzerland, 2004.

34. Rueden, C.T.; Schindelin, J.; Hiner, M.C.; DeZonia, B.E.; Walter, A.E.; Arena, E.T.; Eliceiri, K.W. ImageJ2: ImageJ for the next generation of scientific image data. *BMC Bioinform.* **2017**, *18*, 529. [[CrossRef](#)]
35. ISO 25178-2:2021(E); Geometrical Product Specifications (GPS)—Surface Texture: Areal—Part 2: Terms, Definitions and Surface Texture Parameters. International Organization for Standardization: Geneva, Switzerland, 2021.
36. Zhang, Q.; Liu, C.; Sun, Z.; Hu, X.; Shen, Q.; Wu, J. Authentication of edible vegetable oils adulterated with used frying oil by fourier transform infrared spectroscopy. *Food Chem.* **2012**, *132*, 1607–1613. [[CrossRef](#)]
37. Sacchi, R.; Addeo, F.; Paolillo, L. ¹H and ¹³C NMR of virgin olive oil. An overview. *Magn. Reson. Chem.* **1997**, *35*, 133–145. [[CrossRef](#)]
38. Chiavaro, E.; Vittadini, E.; Rodriguez-Estrada, M.T.; Cerretani, L.; Bonoli, M.; Bendini, A.; Lercker, G. Monovarietal extra virgin olive oils: Correlation between thermal properties and chemical composition. *J. Agric. Food Chem.* **2007**, *55*, 10779–10786. [[CrossRef](#)] [[PubMed](#)]
39. Barba, L.; Arrighetti, G.; Calligaris, S. Crystallization and melting properties of extra virgin olive oil studied by synchrotron XRD and DSC. *Eur. J. Lipid Sci. Technol.* **2013**, *115*, 322–329. [[CrossRef](#)]
40. Che Man, Y.B.; Tan, C.P. Comparative differential scanning calorimetric analysis of vegetable oils: II. Effects of cooling rate variation. *Phytochem. Anal.* **2002**, *13*, 142–151. [[CrossRef](#)] [[PubMed](#)]
41. Chiavaro, E.; Mahesar, S.A.; Bendini, A.; Foroni, E.; Valli, E.; Cerretani, L. DSC Evaluation of Olive Oil during Accelerated Oxidation. *Ital. J. Food Sci.* **2011**, *23*, 164–172.
42. Chiavaro, E.; Cerretani, L.; Paradiso, V.M.; Summo, C.; Paciulli, M.; Gallina Toschi, T.; Caponio, F. Thermal and chemical evaluation of naturally auto-oxidised virgin olive oils: A correlation study. *J. Sci. Food Agric.* **2013**, *93*, 2909–2916. [[CrossRef](#)] [[PubMed](#)]
43. Vittadini, E.; Lee, J.H.; Frega, N.G.; Min, D.B.; Vodovotz, Y. DSC determination of thermally oxidized olive oil. *J. Am. Oil Chem. Soc.* **2003**, *80*, 533–537. [[CrossRef](#)]
44. Dobarganes, M.C.; Pérez-Camino, M.C.; Márquez-Ruíz, G. High Performance Size Exclusion Chromatography of Polar Compounds in Heated and Non-Heated Fats. *Fat. Sci. Technol.* **1988**, *90*, 308–311. [[CrossRef](#)]

Disclaimer/Publisher’s Note: The statements, opinions and data contained in all publications are solely those of the individual author(s) and contributor(s) and not of MDPI and/or the editor(s). MDPI and/or the editor(s) disclaim responsibility for any injury to people or property resulting from any ideas, methods, instructions or products referred to in the content.

5.3. Hydrophobic vegetable oil-based coatings deposited through plasma polymerization

Plasma-enhanced chemical vapor deposition (PECVD), also known as plasma polymerization, is a promising method to deposit highly crosslinked, covalently attached polymeric coatings through radical reactions. Plasma polymers can be obtained from a wide range of precursors without the use of solvents or supplementary derivatization steps. Vegetable oils are considered to be promising precursors for hydrophobization, as their use is well-established in hydrophobic finishing of wood surfaces.^[174] Furthermore, their high degree of unsaturation promises good structural retention and suitability for crosslinking in plasma polymerization.^[175] Thus, two oils containing a high amount of triple unsaturated fatty acids were used in this study, namely chia oil and tung oil. Chia oil mainly consists of α -linolenic acid, which comprises three isolated carbon-carbon double bonds, while tung oil mainly consists of α -elaeostearic acid, which features three conjugated carbon-carbon double bonds.^[151] The plasma polymerization device used within this work was the DiscJet, which combines the concepts of plasma jet and sliding discharge in one versatile device that is able to treat and coat nonconductive substrates independent of their thickness, roughness or material sensitivity. The precursor was applied as an aerosol transported by N₂ as carrier gas, while argon was used as plasma process gas. As vegetable oils have previously not been deposited with PECVD, first enquiries into their suitability for plasma polymerization in general were performed using glass slides as model substrates, while in a second step their ability to hydrophobize paper was evaluated.

Plasma polymer coatings were first deposited on glass slides to examine the influence of plasma power, which was varied from 50 W to 300 W. A coating deposited without plasma ignition served as reference sample. Furthermore, plasma polymer deposition was conducted at different N₂ flow rates because the amount of generated aerosol was much higher for chia oil than for tung oil due to its lower viscosity.

The coatings' surface morphology was visualized through reflected light microscopy, optical profilometry and atomic force microscopy (AFM). For chia oil coatings deposited without plasma ignition, thus-obtained images showed individual droplets. Upon plasma ignition a closed layer was observed whose topology varied depending on the applied plasma power. The surface roughness was determined on two scales by optical profilometry and AFM. Plasma polymerized (pp) chia oil coatings' large scale roughness, determined by profilometry, showed a decreasing trend with deposition power and improved layer closure. The small scale roughness, measured by AFM, increased with power and was accompanied by formation of dust particles. WCAs for pp(chia oil) were highest at 50 W and 3 L·min⁻¹ N₂ flow rate, as well as 100 W and 5 L·min⁻¹ N₂ flow rate, reaching $(72.1 \pm 11.6)^\circ$ and $(86.0 \pm 7.9)^\circ$, respectively.

TUKEY's test showed a significant influence of the plasma power especially at 5 L·min⁻¹ N₂ flow rate. Additionally, a significant increase in WCA was observed for all plasma-polymerized coatings compared to the non-polymerized ones. Moreover, coating thickness and WCA correlated well with each other. All thicknesses for coatings deposited at 5 L·min⁻¹ were above 100 nm, with the coating deposited at 100 W showing the highest thickness at (467 ± 34) nm. ATR-FTIR spectroscopy showed changes in chemical bonding after plasma polymerization of pp(chia oil) compared to untreated oil. The intensity of the =C_{cis}-H stretching mode at 3011 cm⁻¹ decreased with increasing plasma power, indicating double bond consumption as expected from literature.^[175] However, no correlation between ATR-FTIR spectra and water contact angles was observed.

In contrast, the WCAs measured for pp(tung oil) showed either no dependence on whether the coating was deposited with or without plasma ignition, or even decreased upon plasma application. Surface imaging showed incomplete layer closure even despite the higher flow rate of 10 L·min⁻¹. The coating thickness of pp(tung oil) was below one tenth of that of pp(chia oil), only ranging between 4 nm and 25 nm, and surface roughness values were in the same order of magnitude. These observations indicated that, presumably due to the comparatively low coating amount, the coating layer is not sufficiently closed to show an advantageous influence on WCAs. Hence, the precursor viscosity and the resulting coating amount have a decisive effect on the plasma polymer coating properties. Tung oil was therefore not deemed suitable for achieving hydrophobization through plasma polymerization under the selected conditions.

Finally, the suitability of pp(chia oil) for paper hydrophobization was examined, using the parameters that previously yielded best results, notably 100 W and 5 L·min⁻¹ N₂ flow rate. Glassine paper was used as model paper substrate because of its high smoothness generated by extensive pulp refining. It is thus still relatively well comparable to glass, in contrast to common laboratory handsheets. Moreover, it is extremely pure, so the risk of contamination through impurities affecting the plasma process is reduced.

Uncoated glassine paper and glassine paper coated with chia oil aerosol showed similar WCAs of around 40°. However, coating with pp(chia oil) enabled achieving a WCA of (75.2 ± 10.6)°. Whilst the high error indicated a certain coating inhomogeneity across the width of the discharge area, WCAs measured in the central discharge area reached 90° and showed good stability over time, thus proving the basic suitability of pp(chia oil) for paper hydrophobization.

Soxhlet extraction not only removed superfluous unbound oil, but also proved the covalent coating attachment to the paper substrate with a WCA of $(90.2 \pm 4.4)^\circ$.

Ultimately, this chapter shows the suitability of pp(chia oil) for application in plasma polymerization for improving hydrophobicity of glass and smooth paper substrates.

In the frame of this work, I was involved in conceptualization, writing and creating artwork depicting results, as well as investigation (optical profilometry for surface roughness and coating thickness, ATR-FTIR-spectroscopy and Soxhlet extraction) and data evaluation. Martin Bellmann was involved in conceptualization, investigation (aerosol flow, coating deposition, WCA and AFM measurements), writing and creating the artwork depicting the device. Dennis M. J. Möck was involved in conceptualization, investigation (viscosity, GC-MS/FID and optical microscopy measurements), and writing. All authors were involved in proof-reading. Further, Jörn Appelt, Andreas Geissler and Wolfgang Viöl were involved in supervision. Martin Bellmann, Andreas Geissler and Jörn Appelt were responsible for funding acquisition.

The following article has been published in *Plasma Processes and Polymers*.

M. Bellmann*, [A. Loesch-Zhang*](#), D. M. J. Möck, J. Appelt, A. Geissler, W. Viöl, **Hydrophobic glass and paper coatings based on plasma-polymerized vegetable oils using a novel atmospheric pressure plasma concept**, *Plasma Process. Polym.* **2024**, *21*, e2300224.

*M.B. and A.L. contributed equally to this work

Published by Wiley-VCH GmbH under Creative Commons Attribution 4.0 International (CC BY 4.0) License.

The supporting information has not been reprinted here, but can be accessed via the online version of this article: <https://onlinelibrary.wiley.com/doi/10.1002/ppap.202300224>.

RESEARCH ARTICLE

PLASMA PROCESSES
AND POLYMERS

Hydrophobic glass and paper coatings based on plasma polymerized vegetable oils using a novel atmospheric pressure plasma concept

Martin Bellmann^{1,2}  | Amelia Loesch-Zhang³ | Dennis M. J. Möck⁴ |
Jörn Appelt⁴ | Andreas Geissler^{3,5}  | Wolfgang Viöl^{1,2}

¹Fraunhofer Institute for Surface Engineering and Thin Films IST, Göttingen, Germany

²Faculty Engineering and Health, HAWK University of Applied Sciences and Arts, Göttingen, Germany

³Technical University Darmstadt, Macromolecular Chemistry and Paper Chemistry, Darmstadt, Germany

⁴Johann Heinrich von Thünen Institute, Federal Research Institute of Rural Areas, Forestry and Fisheries, Institute of Wood Research, Barsbüttel, Germany

⁵Papiertechnische Stiftung (PTS), Heidenau, Germany

Correspondence

Martin Bellmann, Fraunhofer Institute for Surface Engineering and Thin Films IST, Von-Ossietzky-Str. 99, Göttingen 37085, Germany.

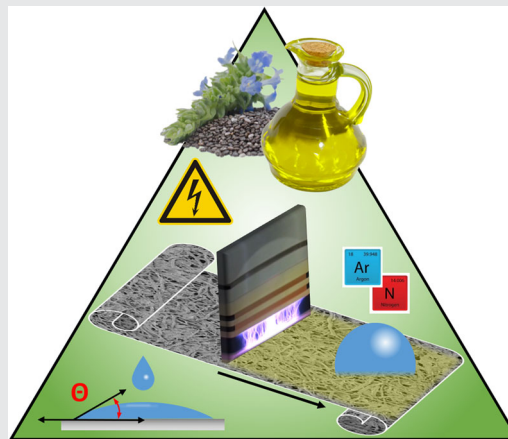
Email: martin.bellmann@ist.fraunhofer.de

Funding information

Fachagentur Nachwachsende Rohstoffe

Abstract

Atmospheric pressure plasma polymerization represents a promising coating technology, addressing drawbacks of traditional processes (solvent use, multistep procedures, etc.) while enabling deposition of thin cross-linked polymer layers with high contour fidelity. We address technological challenges with a novel plasma device that integrates multiple plasma source benefits and investigate the suitability of two plant-based precursors, chia and tung oil, for plasma polymerization to hydrophobize glass and paper. Chia oil enables the deposition of thin, covalently bonded hydrophobic polymer layers. Such coatings have diverse applications especially inside the paper industry, where water repellents in the form of internal and surface sizing have always been an essential functionalization step. Using bio-based precursors and reducing extra chemicals contributes to substituting fossil-based or harmful substances.



KEYWORDS

coating, jet-induced sliding discharge, paper, plasma-enhanced chemical vapor deposition (PECVD), vegetable oil

Abbreviations: AFM, atomic force microscopy; ATR-FTIR, attenuated total reflectance-Fourier transform infrared; CSBD, coplanar surface barrier discharge; GC-MS/FID, gas chromatography-mass spectrometry with flame ionization detector; HMDSN, hexamethyldisilazane; HMDSO, hexamethyldisiloxane; PECVD, plasma-enhanced chemical vapor deposition; pp(chia oil), plasma-polymerized chia oil; pp(tung oil), plasma-polymerized tung oil.

Martin Bellmann and Amelia Loesch-Zhang contributed equally to this study.

This is an open access article under the terms of the [Creative Commons Attribution](https://creativecommons.org/licenses/by/4.0/) License, which permits use, distribution and reproduction in any medium, provided the original work is properly cited.

© 2024 The Authors. *Plasma Processes and Polymers* published by Wiley-VCH GmbH.

1 | INTRODUCTION

Coatings are a significant area of application of synthetic polymers present in all sectors of industry. Their main asset is their versatility and tunability with respect to complex requirements in terms of appearance, haptics, barrier effect, and durability as well as flawlessness, homogeneity in thickness, and surface adhesion of the thin layers. Compared to the substrate itself, the individual mass fraction of a coating is certainly small, but in view of the wide variety of coated surfaces, the overall mass of coating materials used globally is enormous. As the general awareness of limited fossil-based resources and limited recyclability of synthetic polymer coatings has increased, the use of biobased raw materials and the adaption to more efficient coating processes has shifted into focus. A particularly promising single-step coating method that does not require additional drying energy and critical solvents and does not generate any superfluous waste, while being accessible to an extraordinarily wide range of coating raw materials, is plasma-enhanced chemical vapor deposition (PECVD).

The use of atmospheric pressure plasma for industrial pretreatment of all kinds of surfaces to improve adhesion has been an integral part of high quality joining and bonding for several decades. Plasma source concepts range from plasma jets based on thermal arc discharges to direct and indirect dielectrically impeded discharges and corona discharges.^[1-3] All these discharge concepts can be adapted relatively well to industrial processes for plasma-assisted surface activation, which for example allows surface hydrophilization. In the course of plasma-assisted surface activation, an additional process gas can often be emitted at high process speeds, since the entrained air constantly supplies new charge carriers, which, in interaction with the surface, can result in the desired hydrophilization.

Compared to plasma activation, PECVD or plasma polymerization is a significantly more complex system wherein many parameters interact.^[4] While the range of accessible properties is vast and ranges for instance from hydrophilic to hydrophobic surfaces, processing parameters need to be closely controlled to obtain reproducible coatings.^[5] During industrial coating processes, drag air represents a decisive interference factor. While for plasma surface activation only compressed air is required, the composition of which largely corresponds to that of the drag air, PECVD processes usually require inert gas mixtures of argon and nitrogen, which are additionally enriched with a precursor such as hexamethyldisiloxane or hexamethyldisilazane.^[3,6-8] Contamination with drag air may then impede reproducibility and must therefore be avoided. To realize a stable and reproducible discharge volume and to counteract the adversities of industrial

inline processes, we apply a novel discharge concept in the context of the studies discussed here. This concept combines the principles of a jet plasma with those of a sliding discharge, which results in an efficient symbiosis.^[2,9,10] A detailed description of the plasma source concept can be found in the materials and methods section in Section 2.2.

Using conventional paper coating processes, hydrophobic barrier properties are achieved either by extrusion coating, by lamination with petroleum-based plastic foils or by coating with aqueous polymer dispersions.^[11-13] The application of petroleum-based foils hinders recycling and worsens the sustainability of the paper.^[11] When using dispersion paints, additionally energy-intensive subsequent drying is necessary.^[13] In contrast, the use of plasma coatings eliminates wet chemistry processing, especially the drying step, and allows the application of very thin layers.

Plant-based drying oils have been used since ancient times in the protection and hydrophobic finishing of wood surfaces. Their key feature is a high content of unsaturated fatty acids, whose C=C double bonds are crosslinked in an autooxidation process on contact with oxygen, forming a solid solvent-resistant film. Typical drying oils are linseed oil, tung oil, and safflower oil.^[14,15] The number and position of double bonds have a decisive effect on drying. The triple unsaturated fatty acids linolenic acid (isolated double bonds) and α -elaeostearic acid (conjugated double bonds) are considered to dry particularly well. Conjugated double bonds in particular have a positive effect on the drying behavior of the fatty acids. With its high content of conjugated double bonds, tung oil is therefore considered to be one of the best drying oils available.^[14,15]

Although the successful application of drying oils appears highly interesting with respect to application for plasma polymer-based hydrophobic coatings, literature shows only few examples of plasma used to apply vegetable oil- or fatty acid-based hydrophobic coatings, all of them referring to plasma treatment. Coatings are usually applied by substrate immersion into the fatty acid or vegetable oil solution and combined with plasma treatment, frequently followed by Soxhlet extraction to remove unbound material. Oleic acid, butyric acid, sunflower oil, and olive oil have been applied this way,^[16-18] while butyric acid was also directly distilled into the reactor.^[16] Spray coating combined by plasma treatment has also been reported.^[19] However, these processes all have in common that they require either pretreatment or consecutive workup, thereby not only increasing the consumption of chemicals but also foregoing the advantage of a one-step process. Whilst manifold research has been conducted into plasma

polymers based on extractives, essential oils, and other biobased precursors,^[20] vegetable oils have to the best of our knowledge not yet been used as PECVD precursors for hydrophobic coatings.

Considering the urgent need for more sustainable coating processes and coating materials especially in the paper industry, we herein propose a solvent-free coating method based on a novel atmospheric pressure plasma source concept. This technical approach takes advantage of the geometric nature of the source and enables defined and reproducible coatings on almost all nonconductive materials. For the first time, vegetable oils are used as precursors and deposited directly onto the substrate in a PECVD process with a focus on varying deposition powers. Surface properties are examined using reflected light microscopy, optical profilometry, atomic force microscopy, and water contact angle measurements, while structural retention is analyzed by FTIR spectroscopy. The resulting coatings are covalently attached to the substrate and endow glass and paper surfaces with improved hydrophobic properties.

2 | MATERIALS AND METHODS

2.1 | Materials

Tung oil was obtained from Ligna (DICTUM GmbH; lot number 705286) and chia oil from Wallitzer Mühlen Öl (Wallitzer Tiernahrungs GmbH; lot number 100323). Microscope glass slides (grounded edges, frosted border, manufactured according to ISO 8037/I.) were purchased from Gerhard Menzel GmbH and cleaned directly before use with lint-free disposable wipes and isopropanol. Glassine paper (Pergamyn WIN HT 60 g/m²) was obtained from Glatfelter Oberschmitt GmbH. Argon ($\geq 99.996\%$) and nitrogen ($\geq 99.8\%$) were purchased from Linde GmbH.

2.2 | Plasma device setup and parameters

Commercially available coating concepts act either as punctual jet discharges or as so-called Diffuse Coplanar Surface Barrier Discharges (CSBD). Their discharge regions are punctual or linearly shaped, which makes homogeneous coating application on flat substrates challenging. Due to their punctual plasma flame, the jet systems generate a treatment profile (e.g., water contact angle, layer thickness, layer characteristics, etc.) that is very close to a Gaussian distribution. The greatest challenge in a two-dimensional application is to transfer the punctual

Gaussian character into an almost two-dimensional layer system by intelligently arranging an array of several plasma flames. The linear CSBD system, on the other hand, allows discharge widths of up to several meters, but requires extremely precise manufacturing of dielectrics for perfect surface flatness and perfect plane-parallel arrangement to the counter-electrode over the entire electrode width. Tiny deviations can lead to turbulence of the process gas or variations in the electric field and consequently to inhomogeneities in the layer. However, both concepts are very susceptible to drag air, which in the worst case can have a negative effect on the homogeneity of the deposited layer system. The plasma source concept presented in this work (Figure 1a), called DiscJet, addresses these challenges based on a combination of CSBD and a plasma-jet, which has been introduced by Bellmann et al. elsewhere^[9,10] and uses a rotationally symmetrical electrode arrangement. The resulting plasma can be described as a jet-induced sliding discharge, which is dielectrically hindered on one side via an aluminum oxide ceramic (1). Internally, it generates a dielectric plasma jet between the titanium high-voltage electrode (2) and the dielectrically hindered copper heat sink (3), which acts as the ground electrode. The argon process gas (supplied via inlet (4)) is expelled from the discharge channel and thus enables a “cold” plasma jet with a gas temperature of approx. 360 K and an electron energy of ~ 1 eV, which were determined using optical emission spectroscopy. This plasma jet hits the substrate surface (5) and glides over it—hence referred to as “floating potential” (7)—before being picked up by the ground electrode. This closed discharge circuit enables a homogeneous discharge on any nonconductive substrate independent of the surface geometry. An essential property of this rotationally symmetrical source is that, depending on the discharge distance between the bottom of the source and the substrate surface, a kind of dynamic pressure or gas cushion is formed. This gas cushion ensures a process area that is almost free of ambient air at blow-out distances of up to a maximum of 4 mm and is thus a good preventive tool against the influence of drag air. The high-voltage electrode made of titanium via 3D printing functions accordingly both as high-voltage electrode and gas mixing device.

The electrode features a vertical bore in the center through which the nitrogen carrier gas, supplied via inlet (6), is transported into the discharge zone (7) without encountering the plasma. This prevents premature polymerization and reduces agglomeration of the precursor inside the source. The process gas argon is fed in laterally and flows into the discharge gap (8) between the high-voltage and ground electrode via tangential holes in the outer shell of the electrode. The resulting gas spin ensures a particularly flat exit angle at the nozzle outlet. The carrier gas flow emerging simultaneously in the center is captured by the

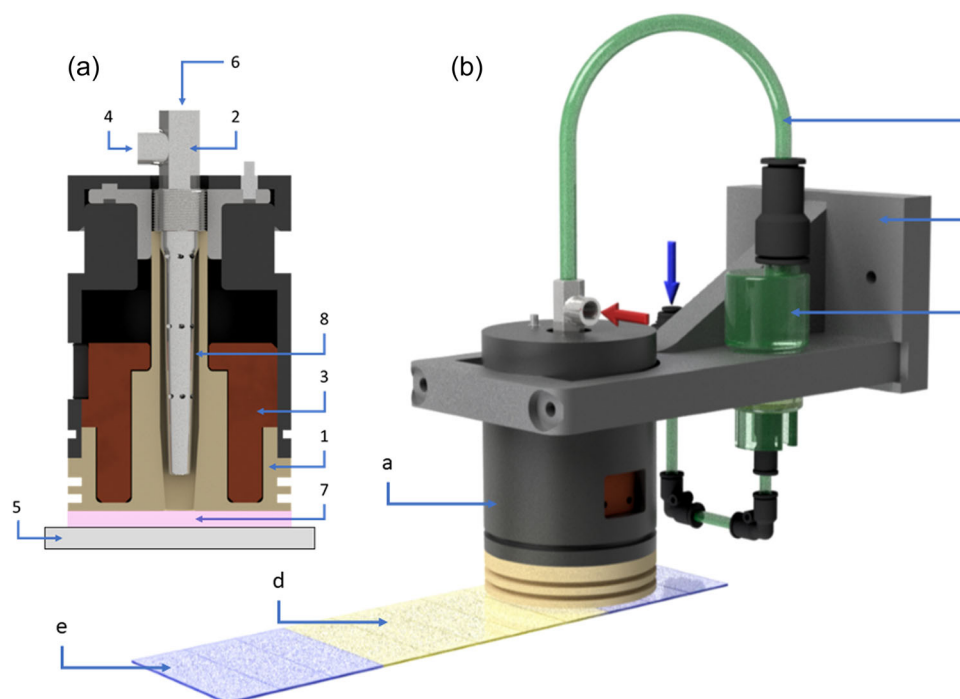


FIGURE 1 Experimental setup showing (a) a cross-section of the plasma source and its components and (b) the device setup during the plasma-enhanced chemical vapor deposition process.

process gas flow and transported uniformly and rotationally symmetrically to the outer bottom edge of the plasma source. This mechanism ensures the gas cushion characteristic, which is responsible for the almost complete displacement of ambient air from the process area and constitutes the unique feature compared to commercially available plasma coating concepts under atmospheric pressure.

The experimental setup for coating deposition is shown in Figure 1b. The coating module consists of the discharge concept (I), the nebulizer unit “IN 500” (Medisana GmbH) (II) and a holding module (III), which combines all components compactly. The carrier gas nitrogen flows into the bottom of the nebulizer unit containing the precursor oil, which is entrained through hoses of decreasing diameter (length \times diameter: subsequently 50×12 mm, $600 \times$ mm, $50 \times$ mm) (VI) before entering the high-voltage electrode and encountering the argon plasma flow.

For coating deposition on glass, five microscope slides (IV) were positioned seamlessly on the treatment base of the plasma system transverse to the coating direction. Three supplementary buffer slides (V) on each side were intended to prevent flow turbulence when passing over the substrate edges. Reversal of the movement direction took place after passing the outer edge of the last buffer slide. Transportation of the source across the substrates was ensured by the traversing table of the portal system “ISEL Gantry OverHead M20” (Isel Germany AG). The high

voltage components (generator “HV-X20” and transformer “HT-X1-34oil,” Tantec A/S) supply the plasma power. All power settings made on the Tantec generator were compared to the actual output power using the UI method. The obtained power levels generally correspond to the specified power levels of the generator (Supporting Information S1: Figure S1). Samples were coated at an input power of 0, 50, 100, 200, and 300 W (this corresponds to an average power density of 0, 2.1, 4.2, 8.3, and 12.5 kW/L), a plasma gap of 3 mm, an Ar flow rate of 15 L/min, an N₂ flow rate of 3, 5, or 10 L/min and five subsequent coating runs at 1 m/min coating speed. For a stable and homogeneous discharge, a ratio of process gas (Ar) to carrier gas (N₂) of 3:1 has proven to be effective. By varying this ratio, the different viscosities of chia and tung oil are taken into account. In case of the test parameters “0 W,” the tests were carried out without switching on the plasma generator. The samples were stored for 1 day at 23°C and 50% relative humidity before characterization.

2.3 | Characterization methods

2.3.1 | Viscosity

The kinematic viscosity of tung and chia oil was measured with a Ubbelohde viscometer according to DIN 51 562 at different temperatures (chia oil: 293.15,

296.15, 298.15, 313.15 K; tung oil: 293.15, 296.15, 298.15, 323.15, 343.15 K). Depending on the temperature and the viscosity the viscosimeter III/907715 (tung oil: 293.15, 296.15, 298.15 K) or II/48629 (chia oil: all temperatures; tung oil: 323.15, 343.15 K) was used with a heating bath and automatic lead time measuring system from Schott-Geräte GmbH (CT62, AVS 350, and AVS/S). The viscosity-temperature dependence was calculated with the measured values according to DIN 51 563. The dynamic viscosity was calculated by dividing the kinematic viscosity by the oil density, which was measured with a pycnometer (Isolab boro 3.3, 10 mL) from ISOLAB Laborgeräte GmbH.

2.3.2 | Plasma power measurement according to voltage-current (UI) method

For the plasma power measurements according to the UI method, a 1000:1 voltage probe “PA6015A” from Tektronix GmbH, a wide band current monitor with an amplification of 1 V/A from Pearson Electronics, Inc. and an Oscilloscope “RTB2004” from Rohde & Schwarz GmbH & Co. KG were used. The current monitor served as a current probe. Each power measurement consisted of at least 100 measurement runs. After determining voltage and current, the apparent power was calculated by multiplying both signals. The apparent power is the sum of reactive power and active power. As the reactive power equals zero on average, the active power, which corresponds to the plasma power, remains as the result.

2.3.3 | Gas chromatography-mass spectrometry with flame ionization detector (GC-MS/FID)

The fatty acid composition of tung and chia oil was determined by GC-MS/FID using an Agilent “HP 6890” gas chromatograph, “HP 5975C” mass spectrometer and flame ion detector (Agilent Technologies Deutschland GmbH) equipped with a “VF 5MS-60M” column (Agilent Technologies Deutschland GmbH) with an inner diameter of 0.25 mm and a film thickness of 0.25 μm . The “HP PTV” injector temperature was 573.15 K and the split ratio was 15:1 with an injection volume of 1 μL . Helium was used as carrier gas (2 mL/min flow rate).

The oils were mixed with dichloromethane (5.59 mg oil per mL dichloromethane), 100 μL dichloromethane containing fluoranthene as internal standard (2008 mg/mL) and 400 μL trimethylsulfonium hydroxide for the online methylation of the fatty acids, which was required to

enable transfer of the fatty acids into the gas phase and thus their measurement.

The measurement program was performed as follows: Holding at 318.15 K for 4 min; heating at 3 K/min up to 478.15 K; holding at 478.15 K for 13 min to separate the fatty acids and the internal standard, further heating at 3 K/min to 598.15 K; holding at 598.15 K for 20 min.

The FID signals for methylated palmitic acid, linoleic acid, oleic acid, linolenic acid, and stearic acid were calibrated against methylated standards. For methylated α -elaeostearic acid the same response factor as for methylated linolenic acid was used, as no standard was available. The mass fractions of the methylated fatty acids were calculated relative to unmethylated fatty acids based on the molecular weight.

2.3.4 | Amount of generated aerosol

The amount of aerosol generated at 293.15 K was measured by weighing the aerosol generator before and after 20 min perfusion by N_2 using a precision scale of the designation “MSE324S-100-DU” from Sartorius Lab Instruments GmbH & Co. KG with an accuracy of 0.1 mg. The material loss was determined at different N_2 flow rates (1, 3, 5, and 10 L/min) and the aerosol amount calculated to mg/min.

2.3.5 | Water contact angle measurements

The wetting properties of the deposited layers were determined by sessile drop method using the Drop Shape Analyzer “DSA100E” from Krüss GmbH and the associated “Advance” software. This enables the automated application of any number of water drops of a defined quantity. At least 10 water drops each with a volume of 2 μL were applied to the substrates in two offset rows with five drops each. Significance levels (p -values) between individual parameter sets were calculated by Tukey test using R software.

2.3.6 | Attenuated total reflectance-FTIR (ATR-FTIR) spectroscopy

ATR-FTIR spectra were measured on a PerkinElmer “Spectrum Three” FTIR spectrometer at a wavenumber range of 4000 to 650 cm^{-1} with a resolution of 4 cm^{-1} averaging across 10 scans. Spectra were recorded directly on the substrate. A background correction was performed using PerkinElmer “Spectrum” software. To allow for easier comparison, spectra were then

normalized to the maximum of the C=O band between 1800 and 1600 cm^{-1} for coatings deposited on glass, and to minima and maxima for coated paper samples.

2.3.7 | Atomic force microscopy (AFM)

The topography of the substrate surfaces was examined applying an atomic force microscope “Nanosurf Easyscan 2.0” and the associated software “Easyscan 2.0” from the company Nanosurf GmbH. For this purpose, cantilevers “ACLA-10” from “Applied NanoStructures, Inc.” were used in tapping mode.

2.3.8 | Optical profilometry

Optical profilometry was performed on a “PLu neox” optical profilometer from Sensofar Metrology using a Nikon EPI 20 \times objective across a 850.08 \times 709.35 μm^2 scan area, a Z-scan range of 60 μm and with a resolution of 0.69 $\mu\text{m}/\text{pixel}$. Surface roughness parameters according to ISO 25178 standard as well as the coating thickness were determined by “SensoScan 6.7” software after plane correction and averaged over three measurements. To determine the coating thickness, a scratch was manually made into the coating using a cutter blade and the surface profile measured as above. The thickness was determined in triplicate by the difference between the averaged heights of the bottom of the scratch and the unscratched coating.

2.3.9 | Reflected light microscopy

Reflected light microscopy images were taken with a “VHX-7000” digital microscope, a “VH- S30K” universal

stative and a “VH-Z100UR RZx100-x1000” universal zoom lens from Keyence Germany GmbH (Neu-Isenburg) at 1000 \times magnification.

3 | RESULTS AND DISCUSSION

Chia oil and tung oil were selected as precursors due to their high degree of unsaturation in the fatty acid acyl chain, as C=C double bonds have shown good structural retention during plasma polymerization.^[21]

Chia oil and tung oil samples were analyzed by GC-MS (Table 1) to examine the exact fatty acid compositions, which were in good accordance with literature data.^[22,23] The main difference between the two oils is the different content of the triple unsaturated fatty acids linolenic acid (70.1 wt. % in chia oil, not present in tung oil) and α -elaeostearic acid (63.7 wt. % plus 11.8 wt. % isomers in tung oil, none in chia oil) (Figure 2a,b).

From the kinematic viscosity and density respectively of chia oil (46.7 mm^2/s , 0.930 g/cm^3) and tung oil (328.4 mm^2/s , 0.938 g/cm^3) at 293.15 K, the dynamic viscosity at this temperature was calculated to be 43.4 mPa s for chia and 308.04 mPa s for tung oil. The measurements at other temperatures enabled calculating the temperature viscosity dependence according to DIN 51 563 (Figure 2c), with measured values being in accordance to literature.^[24] Overall, tung oil has a much higher viscosity compared to chia oil and the viscosity of both oils decreases with increasing temperature. The difference in fatty acid composition, with chia oil containing a high amount of isolated triple unsaturated linolenic acid chains and tung oil containing conjugated triple unsaturated chains of α -elaeostearic acid, explains the much higher viscosity of tung oil as conjugated double bonds strongly increase the viscosity compared to isolated ones.^[25]

TABLE 1 Content of fatty acids present in chia oil and tung oil as determined by gas chromatography-mass spectrometry.

	Fatty acid	Chemical formula	Content in chia oil (wt. %)	Content in tung oil (wt. %)
Saturated fatty acids	Palmitic acid	$\text{C}_{16}\text{H}_{32}\text{O}_2$	8.1	3.0
	Stearic acid	$\text{C}_{18}\text{H}_{36}\text{O}_2$	3.2	2.2
Monounsaturated fatty acids	Oleic acid	$\text{C}_{18}\text{H}_{34}\text{O}_2$	1.8	7.9
Polyunsaturated fatty acids	Linoleic acid	$\text{C}_{18}\text{H}_{32}\text{O}_2$	16.5	6.7
	Linolenic acid	$\text{C}_{18}\text{H}_{30}\text{O}_2$	70.1	-
	α -Elaeostearic acid	$\text{C}_{18}\text{H}_{30}\text{O}_2$	-	63.7
	Isomers of α -Elaeostearic acid	$\text{C}_{18}\text{H}_{30}\text{O}_2$	-	11.8
Identified total fatty acids			99.7	95.3

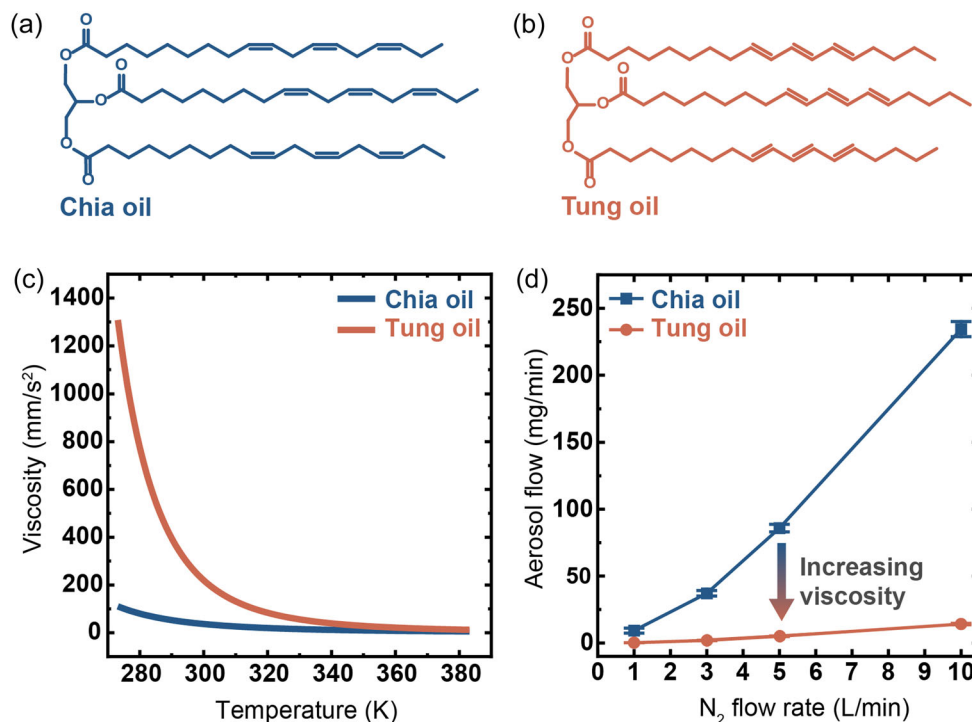


FIGURE 2 (a, b) Chemical structures of the main components of chia and tung oil showing isolated (Z) and conjugated (E) triple unsaturations respectively. (c) Comparison of the kinematic viscosities of chia oil and tung oil. (d) Amount of produced aerosol depending on applied N_2 flow rate at 293.15 K.

Gravimetric measurements show a strong correlation of viscosity and aerosol production. At equal N_2 flow rates, the amount of tung oil aerosol generated per minute is significantly lower than that of chia oil (Figure 2d). Due to its much higher viscosity, tung oil was deposited at 10 and 5 L/min flow rates, while chia oil was processed at 5 and 3 L/min to roughly approximate the aerosol production rates of both precursors and to avoid excessive coating amounts. The fact that the amounts of plasma polymer deposited on glass slides are too low to be determined gravimetrically, is an important indication of the economic nature of this coating approach.

Surface imaging shows the morphology of both plasma-polymerized chia oil (pp(chia oil)) (Figure 3a) and plasma-polymerized tung oil (pp(tung oil)) (Figure 3b) coatings deposited at 5 and 10 L/min N_2 flow rate, respectively. Reflected light microscopy, optical profilometry, and atomic force microscopy show the surfaces' optical appearance and roughness both at large and small scale.

Depending on the applied plasma power, different surface morphology phenomena can be observed. In the case of pp(chia oil) (Figure 3a), the reference coating deposited without plasma ignition (0 W) shows single individual droplets well separated with inter-droplet

distances of 10–20 μm and diameters ranging mainly from 2 to 9 μm , while diameters of 1 μm and below are an exception. At lower plasma powers (50 and 100 W) a closed layer starts to form as these large droplets merge and fully disappear at higher plasma powers (200 and 300 W). Additionally, starting from 100 W deposition power, smaller particles appear within the layer, which have diameters at submicron scale and occasionally up to 3 μm . While at 100 W, they still appear to be part of the coating layer, they seem to rest on the surface at higher powers. Interparticle distances are around 4–6 μm and decrease to submicron scale at higher powers. These particles might indicate that dust formation is a more prominent side effect at higher plasma powers. Other researchers have also found different surface morphologies depending on plasma power, ranging from broader, round peaks at lower power to narrow pointed peaks at higher power.^[26] Both profilometry and AFM images also show the occasional accumulation of droplets into large splashes of 10 μm diameter at higher plasma powers that might indicate oil aggregation during the deposition process.

Compared to pp(chia oil), the pp(tung oil) layers (Figure 3b) on glass slides show fewer individual droplets but appear more uniform and flat even without plasma application. During plasma polymerization, the

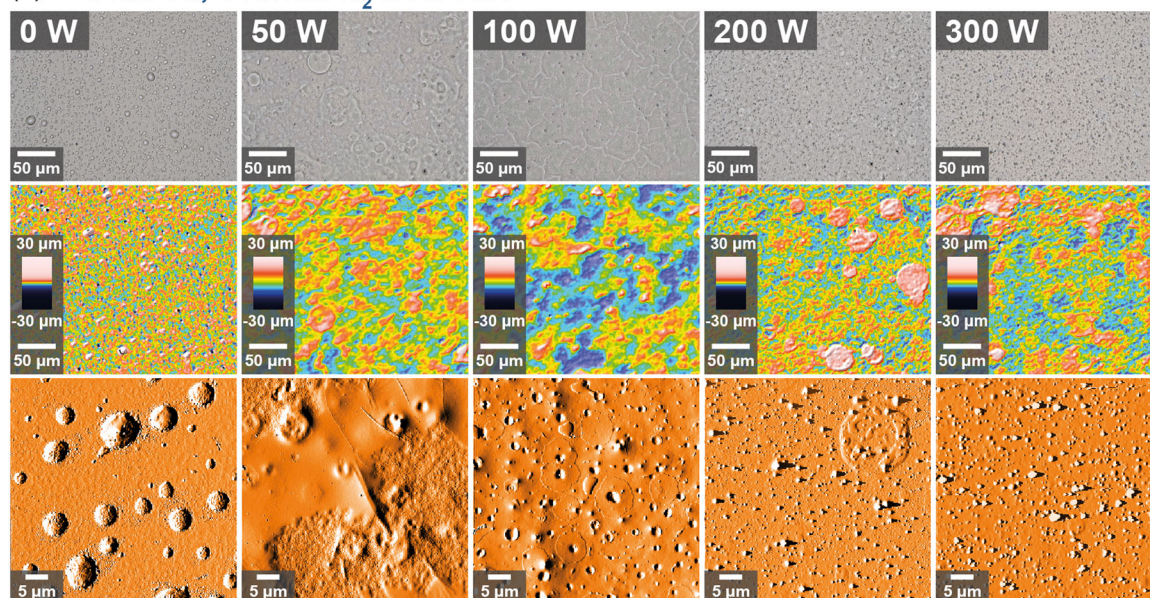
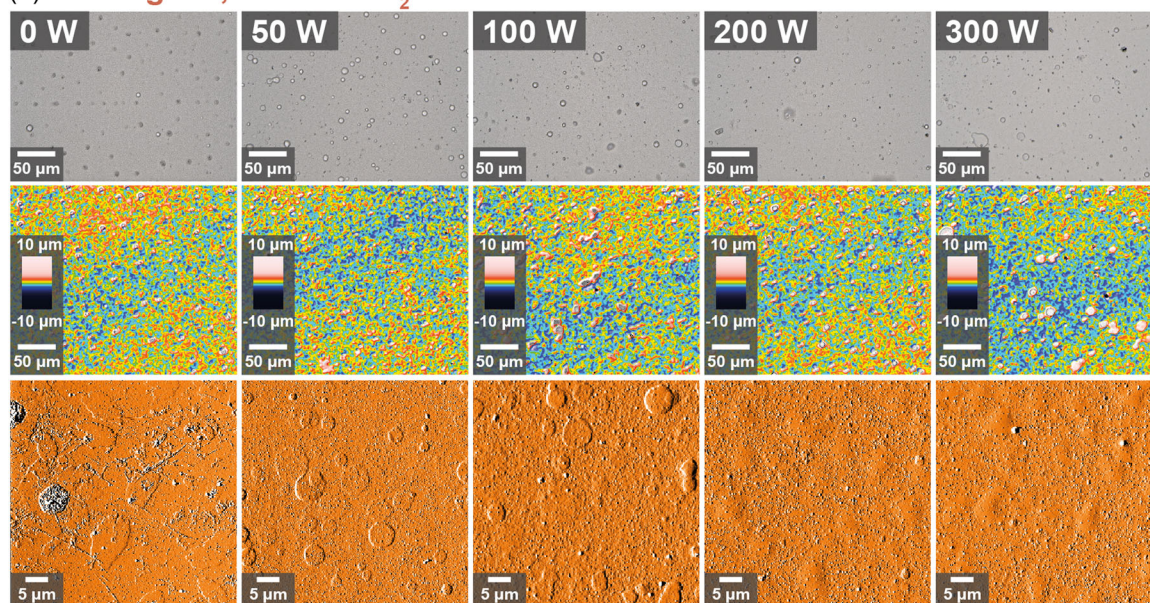
(a) Chia oil, 5 L/min N₂ flow rate(b) Tung oil, 10 L/min N₂ flow rate

FIGURE 3 Surface characterization of (a) plasma-polymerized chia oil and (b) plasma-polymerized tung oil at different deposition powers featuring microscopic imaging, optical profilometry, and atomic force microscopy (from top to bottom respectively). Optical profilometry images were cropped to enable displaying with same scale as microscopy images.

individual deposited droplets fuse and appear only as slight buckles, while increasing plasma power leads to formation of a closed polymer layer.

Apart from the selected input power, another important influence on the surface morphology is most likely the continuous sinusoidal voltage characteristic of the plasma discharge. A continuous plasma seems to result in a larger proportion of the monomer dissociating into volatile fragments which are not being incorporated into the layer but instead settle on the layer surface and

have a significant influence on the surface topography and layer thickness growth,^[8,27] which is in accordance with the observed morphology especially at increased plasma power (200, 300 W).

In agreement with other studies,^[28] the roughness measurements yielded significantly different roughness parameters depending on the methodology used and the examined area, with AFM roughness values being approximately one-tenth of those obtained by surface profilometry. Apart from the variation associated with

different measurement methods, it is likely that these differences are caused by two different types of roughness. For pp(chia oil) (Figure 4a), the merging of droplets with increasing deposition power is accompanied by lower large-scale surface roughness parameters measured by profilometry. Furthermore, small-scale roughness increases at high plasma power (200 and 300 W) and is characterized by the formation of small particles whose roughness is well resolved by AFM measurements. As previously observed,^[29] the small-scale AFM roughness increases with the N₂ flow rate due to enhanced particle aggregation at higher deposition rates. This extraordinary combination of large-scale and small-scale roughness and the order of magnitude thereof are in the case of pp(chia oil) in accordance with the idea of producing biomimetic surfaces for improved hydrophobicity.^[30]

The pp(tung oil) profilometry (Figure 4b) based surface roughness is in the same order of magnitude as the film thickness, so it should be considered with caution. In particular, for non-closed layers, the roughness only reflects the height of the individual droplets and cannot be directly compared to the surface roughness of the rather thick chia oil layers. AFM roughness values are in the same order of magnitude as those measured for pp(chia oil) and can equally be attributed to the formation of small particles.

Water contact angles of pp(chia oil) produced at both 3 and 5 L/min N₂ flow rates reach their maximum at low plasma powers of 50 and 100 W, respectively (Figure 5a,b), for which a combination of effects is likely responsible. One factor is better structural retention at lower plasma powers, while at higher powers precursor fragmentation and occurrence of post-deposition oxidation processes increase.^[31] Further, the decrease in water contact angles and simultaneous increase in particle agglomerations with

rising plasma power indicates overtreatment and decreasing conversion of the monomer into layer components as well as increased generation of volatile fragments.^[32] The comparatively good results at 50 and 100 W imply that the reduction of plasma power in the present setup counteracts these undesirable phenomena of continuous wave technology. For plasma polymerizations conducted in pulsed mode instead of continuous wave mode, it is known from the literature that varying the pulse-pause ratio has a decisive influence on structural retention of the precursors, on the layer formation (layer thickness, layer topography, etc.) and thus on the efficiency of the coating^[7,33] as well as polar group formation.^[7,8] Therefore presumably with appropriate pulsing, good hydrophobicity can be achieved even if a significant increase in plasma power is performed.

The Tukey test confirms that the applied plasma power indeed has a highly significant influence on the water contact angle especially at low plasma powers (*p*-values given in Supporting Information S1: Table S1). Its significance decreases with power until, especially at low N₂ flow rates, it is not significant anymore.

For coatings applied without plasma ignition (0 W), the water contact angles are very low, since the coating is still fluid and the surface coating is not closed, as observed in microscopy images. After Soxhlet extractions, glass slides coated with pp(chia oil) at 100 W and 5 L/min N₂ flow still show contact angles of $(89.5 \pm 1.6)^\circ$, indicating covalent coating attachment. The durability thereof was also rather good, as the static water contact angle decreases only to $(78.8 \pm 1.3)^\circ$ during the first 3 min after droplet deposition (Supporting Information S1: Figure S2).

Pp(tung oil) (Figure 5c,d), on the other hand, shows much lower contact angles than pp(chia oil), ranging between 30° and 50°. A decrease in the water contact

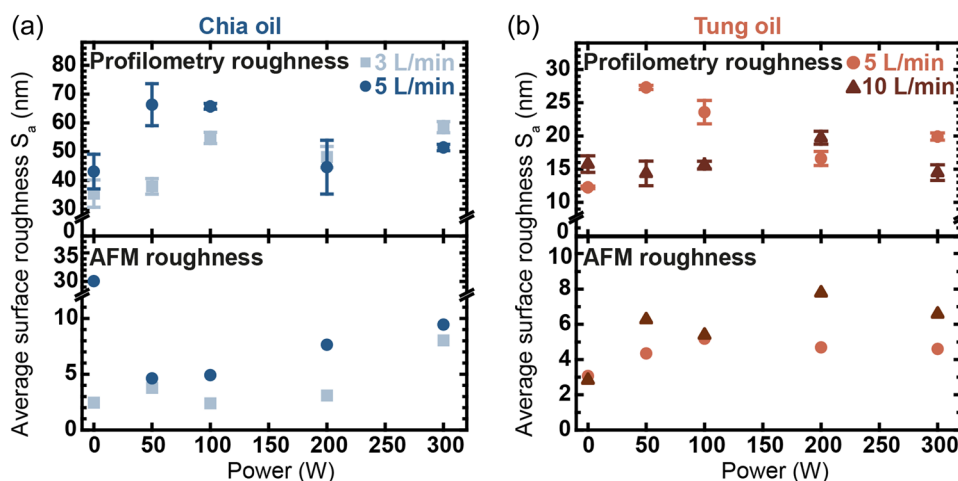


FIGURE 4 Average surface roughness values determined for (a) chia oil and (b) tung oil using optical profilometry and atomic force microscopy for roughness determination.

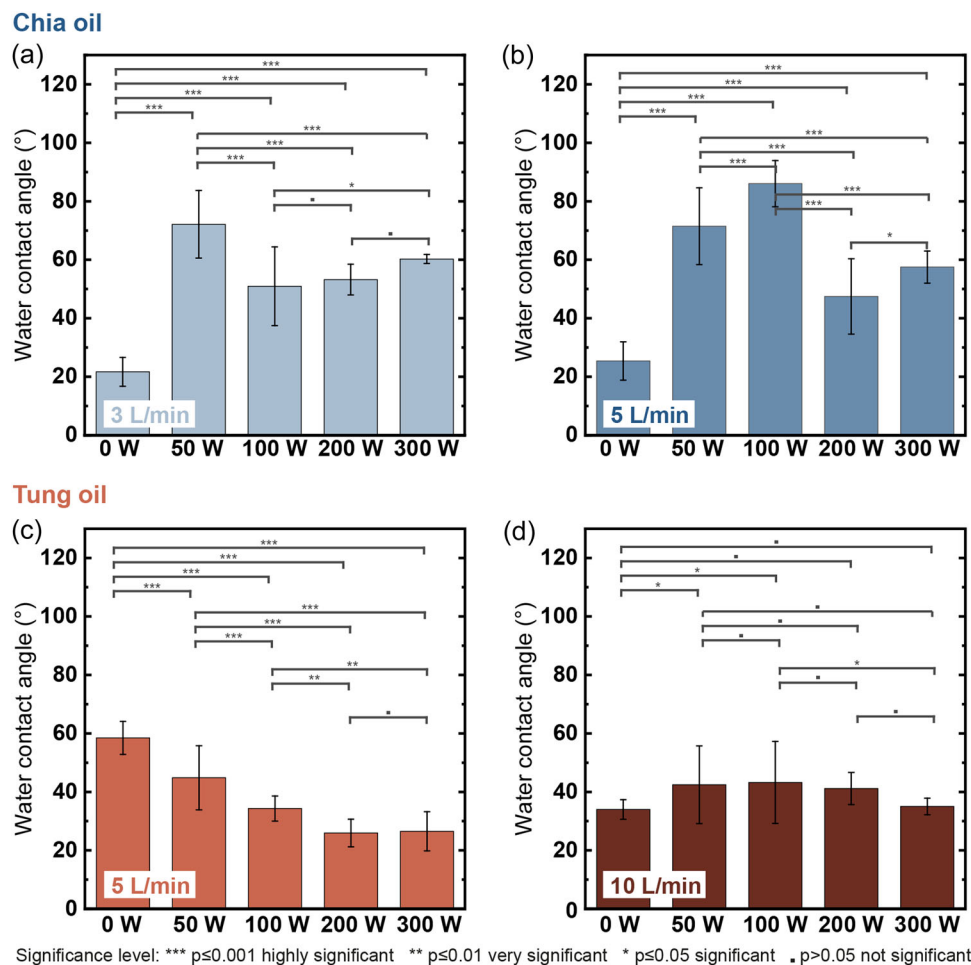


FIGURE 5 Water contact angle measurements of plasma-polymerized chia oil coatings deposited at (a) 3 L/min and (b) 5 L/min N₂ flow and plasma-polymerized tung oil coatings deposited at (c) 5 L/min and (d) 10 L/min N₂ flow including p -values determined through Tukey testing.

angle at 5 L/min N₂ flow rate compared to the reference is observed at all powers and found highly significant through Tukey testing, while the significance of the parameter power is lower for coatings deposited at 10 L/min N₂ flow rate. This decrease can most likely be attributed to the fact that due to the high viscosity of tung oil, a much lower amount of oil is vaporized and transported onto the glass slide. Thus, no closed oil layer is formed on the substrate and the influence of the glass on the water contact angle as well as the amount of coating deposited is more significant.

Interestingly, in the case of pp(chia oil) the contact angles correlate with the coating thickness (Figure 6a) as well as the macroscopic surface roughness (Figure 4a). The thickest coating is observed for the pp(chia oil) coating deposited at 5 L/min N₂ flow and 100 W deposition power, which also shows an extraordinarily high water contact angle. This significant difference between the two carrier gas flows only occurs at 100 W.

As replicate experiments show similar results, it can be assumed that this is not due to artifacts, but rather shows an extraordinarily favorable interaction between plasma power and carrier gas flow. It is well known, that the influence of plasma parameters on coating properties is not necessarily linear.^[32] For instance, the decrease of thickness at higher deposition rates is presumably due to a competition between coating deposition and ablation, with the latter dominating at higher plasma powers.^[32]

Due to the high viscosity of tung oil, the coating thickness of pp(tung oil) (Figure 6b) is only one-tenth of that of the chia oil coating, ranging between 4 nm and 25 nm for depositions performed at 300 W and 50 W respectively with a N₂ flow of 5 L/min. The coating thickness decreases with N₂ flow (Supporting Information S1: Figure S3) and could not be measured at all for samples coated at 10 L/min N₂ flow. It can be assumed that the combination of low aerosol formation and additionally the fragmentation of already generated

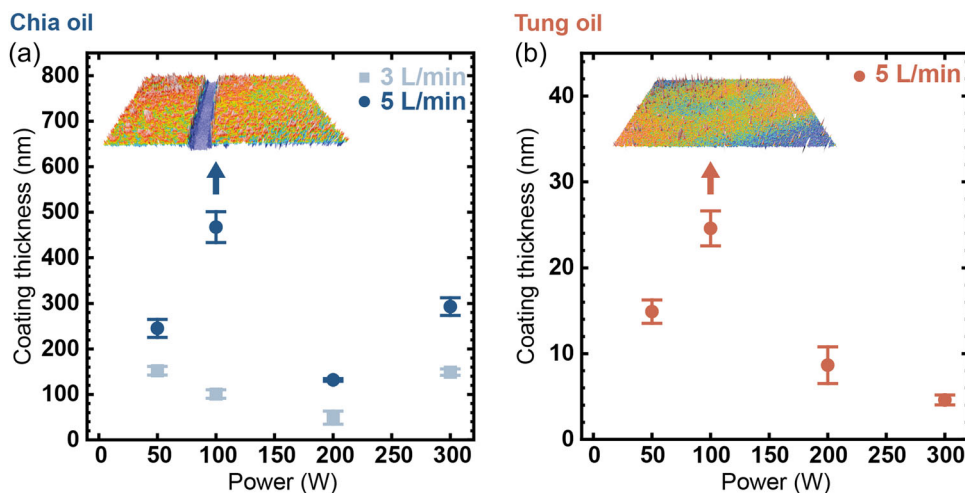


FIGURE 6 Comparison of (a) plasma-polymerized chia oil and (b) plasma-polymerized tung oil coatings formed by different plasma power and carrier gas flow in terms of coating thickness.

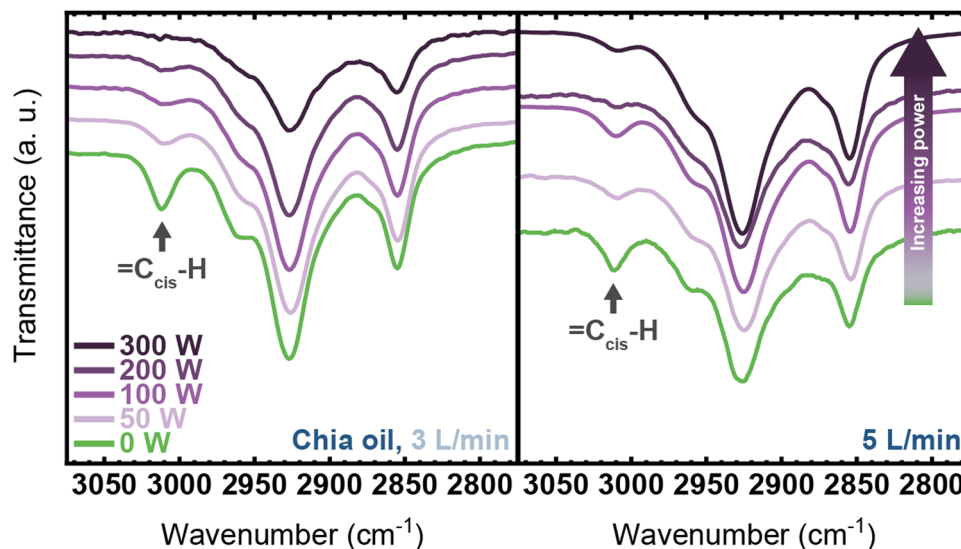


FIGURE 7 Sections of Fourier transform infrared spectra of plasma-polymerized chia oil deposited at 3 L/min and 5 L/min N₂ flow show a decreasing signal for the carbon–carbon double bond with increasing plasma power. Spectra are normalized to the intensity of the C=O band at 1746 cm⁻¹.

polymer chains lead to an inadequately closed layer from the coating process and the hydrophilic glass surface being exposed. The hydrophobic character of the layer is thus only inadequately reflected via the contact angles, which leads in particular to high standard deviations and to inhomogeneous surface properties.

ATR-FTIR spectroscopy enables chemical characterization of plasma polymer coatings. While the common penetration depth of ATR-FTIR spectroscopy is about 1 μm, coating thickness measurements on glass indicate a coating thickness of several tens to hundreds of nanometers for pp(tung oil) and pp(chia oil) respectively.

Therefore, signals of plasma-polymerized oils are only detected with extremely low intensity, especially in the case of pp(tung oil) coatings (Supporting Information S1: Figure S4). As a result, only spectra of pp(chia oil) coatings deposited both at 3 L/min and 5 L/min N₂ flow rate are shown here (Figure 7, full spectrum shown in Supporting Information S1: Figure S5).

Although the glass signal covers most coating ATR-FTIR signals in the fingerprint area, characteristic bands of chia oil are clearly visible despite their relatively low intensity: these are the =C_{cis}-H stretching mode at 3011 cm⁻¹, the antisymmetric CH₃ stretching mode at

2960 cm^{-1} , the antisymmetric CH_2 stretching mode at 2926 cm^{-1} , the symmetrical CH_2 stretching mode at 2854 cm^{-1} and the $\text{C}=\text{O}$ stretching mode at 1746 cm^{-1} .^[34] The spectra of pp(chia oil) coatings deposited at 3 L/min N_2 flow rate clearly show a decrease in the intensity of the $=\text{C}_{\text{cis}}-\text{H}$ vibration at 3011 cm^{-1} with increasing plasma power, indicating $\text{C}=\text{C}$ double bond consumption during plasma polymerization, as has been described in literature.^[20,34] Additionally, lower plasma powers correlate with lower substrate and plasma temperatures that facilitate the absorption and condensation of unfragmented species, resulting in IR spectra showing better structural retention. Furthermore, the relative intensity of the CH group signals also decreases slightly relative to the $\text{C}=\text{O}$ signals as the applied power increases, hinting at oxidation processes becoming more prominent at higher plasma powers.^[8] Although a similar trend can be observed for coatings deposited at 5 L/min, the effects are much less pronounced, most likely due to the higher flow rate not allowing for as much contact of individual molecules with the plasma. The smallest $\text{C}=\text{C}$ band occurs in this case for the coating deposited at 200 W. Yet, the consumption of $\text{C}=\text{C}$ double bonds or the oxygen incorporation do not directly correspond to the water contact angles, indicating that these factors do not correlate quantitatively. Rather, the effect on the water contact angle appears to be dominated by surface morphology.

Chia oil, being the more promising of the examined coating materials with respect to obtaining hydrophobic coatings, was additionally selected to perform first hydrophobicity tests on paper. Glassine paper was

chosen as a substrate due to its high purity compared to other papers and to its low surface roughness obtained by intensive pulp refining. Plasma polymerization was performed at the previously determined conditions of 100 W and 5 L/min N_2 flow rate. Contact angles did not increase significantly when no plasma power was applied but increased to $(75.2 \pm 10.6)^\circ$ on the deposited pp(chia oil) coating (Figure 8a). The large error herein is due to the measurement taken all across the 7 cm wide discharge area, while contact angles measured in the central discharge area reach up to 90° and good stability over time (Figure 8b). The static water contact angle is therefore slightly higher and the droplet absorption much slower than for coatings on glass, which is attributed to the inherent roughness of paper. After Soxhlet extraction, the water contact angle even increased to averaged $(90.2 \pm 4.4)^\circ$, indicating chia oil covalent attachment to the paper substrate just like on glass slides.

Topographic measurements show no significant change in the paper surface roughness after aerosol coating and plasma polymerization compared to untreated glassine paper, indicating that the roughness is dominated by the paper properties. As with the glass samples, ATR-FTIR spectroscopic detection of the coatings on paper is challenging because the deposited thin polymer layer provides only low signal intensities compared to the substrate. In the case of the paper, this is complicated by the fact that the cellulose signals overlap those of the oil (Supporting Information S1: Figure S5), so that no reliable evaluation of the spectra is possible. Nonetheless, the possibility to achieve

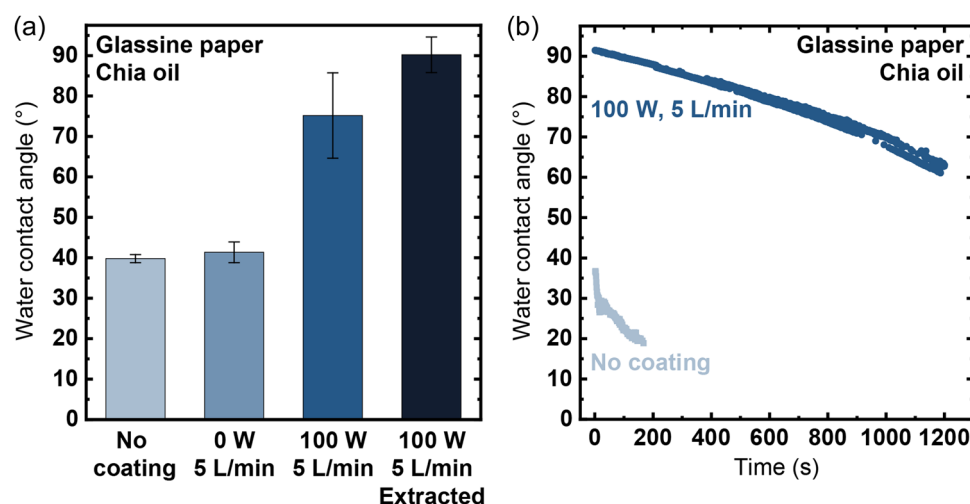


FIGURE 8 (a) Comparison of water contact angles on uncoated, chia oil coated, plasma-polymerized chia oil (pp[chia oil]) coated and pp(chia oil) coated extracted glassine paper, averaged across entire paper surface; (b) time-dependent water contact angle measurements in central discharge area show hydrophobic behavior and good durability after coating.

covalently attached hydrophobic paper coatings by plasma polymerization of chia oil has been proven.

4 | CONCLUSIONS AND OUTLOOK

In this work, the plant-based precursors tung and chia oil were deposited on glass and paper surfaces for the first time using a single-step PECVD process. The novel plasma source used for this purpose combines the technological advantages of jet plasma and sliding discharge and allows coating deposition at atmospheric pressure while displacing the ambient air in the plasma gap. The oils introduced as aerosols into this reactive zone were proven to be crosslinked and covalently attached to the respective substrates, with layer thicknesses of 4–470 nm being achieved, depending on the gas flow and the plasma power. Multiscale surface morphologies were observed. Specifically, the plasma polymerized chia oil coatings exhibited hydrophobic properties with static water contact angles of up to 90° at 100 W plasma deposition power. Even better hydrophobization is expected to be achievable by further investigating into the various plasma parameters and by introducing pulsed discharge modes. Nonetheless, the findings presented herein are already of great interest to all industries performing solvent-based coating processes, such as those required in paper finishing, for shifting their production toward biobased and green chemistry-based production principles.

AUTHOR CONTRIBUTIONS

Martin Bellmann, Amelia Loesch-Zhang, and Dennis M. J. Möck were involved in conceptualization, investigation, and writing—original draft. All authors were involved in writing—reviewing and editing. Jörn Appelt, Andreas Geissler, and Wolfgang Viöl were involved in supervision.

ACKNOWLEDGMENTS

The authors would like to thank Christiane Riegert for the viscosity measurements, Silke Radtke for the GC-MS measurements, Jannik Schulz for the plasma performance measurements, Julia Mrotzek for the optical emission spectroscopy measurements, Oliver Elle for assistance with statistical analysis and Nurul Aiman Binti Omar and Kim Julian Petersen for their support in the laboratory as well as Markus Biesalski and Kristina Lachmann for fruitful discussions. This work was generated in the research project “BioPlas4Paper” and is funded by the Fachagentur Nachwachsende Rohstoffe e. V. (funding number: 2220HV017A-C).

CONFLICT OF INTEREST STATEMENT

The authors declare no conflict of interest.

DATA AVAILABILITY STATEMENT

The data that support the findings of this study are available from the corresponding author upon reasonable request.

ORCID

Martin Bellmann  <http://orcid.org/0009-0000-8985-7470>

Andreas Geissler  <http://orcid.org/0000-0002-4284-7942>

REFERENCES

- [1] J. Vida, M. Shekargoftar, J. Sirviö, T. Homola (Eds.) *Large Area Roll-to-roll Atmospheric Plasma Treatment of Nanocellulose Transparent Paper*, Brno, **2019**; (b) F. Lisco, A. Shaw, A. Wright, J. M. Walls, F. Iza, *Solar Energy*. **2017**, *146*, 287; (c) B. Hünnekens, F. Peters, G. Avramidis, A. Krause, H. Militz, W. Viöl, *J. Appl. Polym. Sci.* **2016**, *133*, 43376; (d) M. Bellmann, C. Gerhard, C. Haese, S. Wieneke, W. Viöl, *Surface Eng.* **2012**, *28*, 754; (e) S. S. Palaskar, *Int. J. Adhes. Adhesives*. **2023**, *125*, 103428.
- [2] M. Bellmann, R. Wascher, G. Avramidis, W. Viöl, *Jahresmagazin Werkstofftechnik* **2021**, 66.
- [3] L. Kotte, *Dissertation*, Technische Universität Dresden, Dresden, **2015**.
- [4] N. Weidler, *Dissertation*, Technische Universität Darmstadt, Darmstadt, **2017**.
- [5] J. L. Hodgkinson, D. W. Sheel, *Surface Coat. Technol.* **2013**, *230*, 73.
- [6] (a) I. Dani, V. Hopfe, D. Rogler, E. Lopez, G. Mäder, *Vakuum Forschung Praxis*. **2006**, *18*, 30; (b) M. Resnik, E. Levičnik, Ž. Gosar, R. Zaplotnik, J. Kovač, J. Ekar, M. Mozetič, I. Junkar, *Polymers* **2021**, *13*, 2148.
- [7] V. Jalaber, D. Del Frari, J. de Winter, K. Mehennaoui, S. Planchon, P. Choquet, C. Detrembleur, M. Moreno-Couranjou, *Front. Chem.* **2019**, *7*, 183.
- [8] E. Kedroňová, L. Zajičková, D. Hegemann, M. Klíma, M. Michlíček, A. Manakhov, *Plasma Process. Polym.* **2015**, *12*, 1231.
- [9] M. Bellmann, C. Ochs, M. Harms, W. Viöl, WO 2017/157975, **2017**.
- [10] M. Bellmann, C. Ochs, M. Harms, W. Viöl, *Jahresmagazin Werkstofftechnik* **2019**, 60.
- [11] V. Rastogi, P. Samyn, *Coatings* **2015**, *5*, 887.
- [12] (a) M. Mujtaba, J. Lipponen, M. Ojanen, S. Puttonen, H. Vaittinen, *Sci. Total Environ.* **2022**, *851*, 158328; (b) K. Marsh, B. Bugusu, *J. Food Sci.* **2007**, *72*, R39.
- [13] T. Kimpimäki, A. V. Savolainen in *Surface Application of Paper Chemicals* (Eds.: J. Brander, I. Thorn), Springer Science+Business Media B.V, Dordrecht, **1997**, pp. 208.
- [14] F. Tanasă, C.-A. Teacă, M. Zănoagă in *Handbook of Modern Coating Technologies* (Eds.: M. Aliofkhaezrai, N. Ali, M. Chipara, N. Bensaada Laidani, J. T. de Hosson), Elsevier, Amsterdam, **2021**, pp. 175.
- [15] Z. W. Wicks, in *Kirk-Othmer encyclopedia of chemical technology*, **2000**. <https://doi.org/10.1002/0471238961.0418250923090311.a01>

- [16] M.-C. Popescu, M. Totolin, C. M. Tibirna, A. Sdrobis, T. Stevanovic, C. Vasile, *Int. J. Biol. Macromol.* **2011**, *48*, 326.
- [17] L. Cabrales, N. Abidi, *Appl. Surface Sci.* **2012**, *258*, 4636.
- [18] A. Loesch-Zhang, C. Cordt, A. Geissler, M. Biesalski, *Polymers* **2022**, *14*, 1773.
- [19] Y. Ferreira da Silva, V. d. M. Queiroz, I. C. S. Kling, B. S. Archanjo, R. N. Oliveira, R. A. Simao, *Plasma Process. Polym.* **2020**, *17*, 2000035.
- [20] A. Loesch-Zhang, A. Geissler, M. Biesalski, *Plasma Process. Polym.* **2023**, *20*, e2300016.
- [21] (a) H. Yasuda, C. E. Lamaze, *J. Appl. Polym. Sci.* **1973**, *17*, 1533; (b) J. Mertens, J. Baneton, A. Ozkan, E. Pospisilova, B. Nysten, A. Delcorte, F. Reniers, *Thin Solid Films* **2019**, *671*, 64.
- [22] I. Dominguez-Candela, A. Lerma-Canto, S. C. Cardona, J. Lora, V. Fombuena, *Materials* **2022**, *15*, 3250.
- [23] M. Li, J. L. Xia, S. H. Li, K. Huang, M. Wang, *Adv. Mater. Res.* **2012**, *554-556*, 2018.
- [24] G. Uzunova, K. Nikolova, M. Perifanova, G. Gentscheva, M. Marudova, G. Antova, *Bulg. Chem. Commun.* **2016**, *48*, 131.
- [25] G. Bier, *Die Makromolekulare Chemie* **1949**, *4*, 41.
- [26] K. Bazaka, M. V. Jacob, B. F. Bowden, *J. Mater. Res.* **2011**, *26*, 1018.
- [27] A. Perraudeau, C. Dublanche-Tixier, P. Tristant, C. Chazelas, *Appl. Surface Sci.* **2019**, *493*, 703.
- [28] M. Da Silva Bullmann, V. V. de Castro, D. A. K. Coutinho, F. C. Lopes, N. Maurmann, M. B. Pereira, M. Rodrigues, P. Pranke, M. P. Ferraz, M. A. Lopes, L. T. Arenas, C. de F. Malfatti, *Plasma Process. Polym.* **2023**, *20*, e2300075.
- [29] M. V. Jacob, C. D. Easton, L. J. Anderson, K. Bazaka, *Int. J. Modern Phys. Conf. Ser.* **2014**, *32*, 1460319.
- [30] B. Bhushan, K. Koch, Y. C. Jung, *Soft Matter* **2008**, *4*, 1799.
- [31] (a) J. Ahmad, K. Bazaka, J. D. Whittle, A. Michelmore, M. V. Jacob, *Plasma Process. Polym.* **2015**, *12*, 1085; (b) M. Drabik, D. Lohmann, J. Hanus, A. Shelemin, P. Rupper, H. Biederman, D. Hegemann, *Plasma* **2018**, *1*, 156.
- [32] H. K. Yasuda in *ACS Symposium Series/American Chemical Society, Vol. 108* (Eds.: M. Shen, A. T. Bell), American Chemical Society, Washington, DC., **1979**, pp. 37.
- [33] M. Jaritz, P. Alizadeh, S. Wilski, L. Kleines, R. Dahlmann, *Plasma Process. Polym.* **2021**, *18*, 2100018.
- [34] (a) Q. Zhang, C. Liu, Z. Sun, X. Hu, Q. Shen, J. Wu, *Food Chem.* **2012**, *132*, 1607; (b) P. Samyn, D. van Nieuwkerke, G. Schoukens, L. Vonck, D. Stanssens, H. Van Den Abbeele, *Appl. Spectros.* **2012**, *66*, 552.

SUPPORTING INFORMATION

Additional supporting information can be found online in the Supporting Information section at the end of this article.

How to cite this article: M. Bellmann, A. Loesch-Zhang, D. M. J. Möck, J. Appelt, A. Geissler, W. Viöl, *Plasma Process. Polym.* **2024**;21:e2300224.
<https://doi.org/10.1002/ppap.202300224>

5.4. Vegetable oil-based plasma polymer coatings on varying paper substrates

The feasibility of depositing hydrophobic vegetable oil-based coatings on smooth glassine paper through plasma polymerization using the DiscJet device has been successfully proven. In view of practical applications, its suitability for coating topographically more challenging paper substrates needs to be examined. With respect to wetting behavior, both surface chemistry and surface roughness are crucial factors. Thus, the influence of paper porosity in particular is of decisive importance for determining suitable plasma polymerization conditions to endow paper with hydrophobicity. The final section of this investigation therefore examines plasma polymerization of vegetable oils on various porous paper substrates.

Cotton linter laboratory handsheets were chosen as substrates due to their high cellulose content and high purity.^[130] They were calendered with three different line pressures (5 N·mm⁻¹, 50 N·mm⁻¹, 300 N·mm⁻¹) to obtain different porosity and surface roughness. Glassine paper was again selected as a smooth reference substrate.

Initially, the influence of mere plasma treatment on the surface properties of cotton linter papers calendered at 300 N·mm⁻¹ (CL-300) was examined varying the parameters plasma power (10 W to 400 W), substrate-source distance (1.5 mm to 6 mm) and number of plasma treatment runs (1 to 5). WCAs decreased from 28° for untreated paper to less than 20° after plasma treatment independent of the selected parameters. The only observable trend was a decrease in WCA with increasing plasma power. Neither surface roughness parameters nor surface morphology displayed by scanning electron microscopy (SEM) images showed significant changes upon plasma treatment. Only for the parameter set of 100 W, 3 mm substrate-source distance and five treatment runs, ATR-FTIR spectra showed a low intensity carbonyl band at 1720 cm⁻¹. Hence, it was assumed that oxidation reactions were caused by plasma treatment and led to paper surface hydrophilization. However, the extent of these modifications was in most cases too small compared to the unmodified bulk paper to manifest a significant change in surface topology, or to be detectable by the relatively large penetration depth of ATR-FTIR spectroscopy.

The parameters selected for PECVD of vegetable oil were based on previous results, namely 100 W, 3 mm substrate-source distance, 15 L·min⁻¹ argon flow rate and 5 L·min⁻¹ N₂ flow rate. Only the number of coating runs was varied between one and five, in order to account for the porosity of paper samples and the possible need for different coating amounts to achieve good pore coverage. Chia oil was used as hydrophobizing precursor material.

All cotton linter papers showed slower water droplet absorption after coating with pp(chia oil). Droplet absorption times increased with increasing coating amount and increasing paper

porosity. The most porous paper, calendered with a line pressure of $5 \text{ N}\cdot\text{mm}^{-1}$ (CL-5) displayed a median droplet absorption time of 45 s after five coating runs, with some values reaching almost 5 min, which correlated with the largest coating amount as visualized by ATR-FTIR spectra. However, large deviations between individual values indicated that the coating was not homogeneously distributed across the substrate. Surface roughness was determined by intrinsic paper roughness, as roughness measurements showed no significant change independent of the applied coating amount. CLSM allowed visualization of the coating on the paper substrate, which in top-view mode was observed filling the pores between the fibers both after coating with one and five coating runs. The cross-sectional view additionally displayed μm -thin paper surface coverage after five coating runs.

X-ray photoelectron spectroscopy (XPS) evidenced the coating presence through the C1s peak, where the integral indicating the content in C–C and C–H bound carbons increased dramatically after coating with pp(chia oil). No large differences were observed comparing coatings with one and five coating runs, due to the restricted penetration depth of XPS that was inferior to the coating thickness. After Soxhlet extraction, the C–C/C–H content decreased only slightly while the O–C=O content increased slightly, which was most likely due to minor surface chemistry modifications during extraction or storage. However, the largest part of the detectable coating remained covalently attached to the surface.

Additionally, covalent pp(chia oil) attachment was evidenced after Soxhlet extraction, both through ATR-FTIR spectra showing the carbonyl bond, as well as through SEM images depicting fiber coverage with an equalizing layer most likely originating from pp(chia oil). Moreover, droplet absorption times were further lowered compared to unextracted papers, with individual measurements showing droplets that were stable with WCAs above 100° for more than 5 min on all papers after five coating runs. Again, however, the coating inhomogeneity was visible.

On smooth glassine paper, improved hydrophobicity was also observed, with WCAs ranging between 80° and 90° independent of the number of coating runs. Like on cotton linter papers, the surface roughness was no decisive factor influencing hydrophobicity. CLSM imaging enabled visualization of the coating's presence but also of its shortcomings in homogeneity.

Finally, the suitability of pp(chia oil) for hydrophobizing glassine paper was compared to that of two other vegetable oils, safflower oil and olive oil. These feature a slightly higher viscosity and further differ from chia oil in their fatty acid composition, as safflower oil usually mainly contains diunsaturated linoleic acid, while olive oil mostly contains monounsaturated oleic acid. It was found that after two coating runs, which overall proved to be the best number of runs,

both pp(safflower oil) and pp(olive oil) coatings yielded significantly higher WCAs than pp(chia oil), featuring $(92.2 \pm 14.7)^\circ$ and $(101.0 \pm 7.3)^\circ$ respectively.

Thus, it has been shown that pp(chia oil) is suitable for improving water repellency on papers of different porosity, while additional vegetable oils have proven the potential to do the same. Despite a certain coating inhomogeneity requiring process optimization, this is a good proof of concept for the potential of plasma-polymerized vegetable oils to hydrophobize porous paper substrates.

In the frame of this work, I was involved in conceptualization, data acquisition and interpretation (paper production, coating deposition, staining, SEM imaging, optical profilometry for surface roughness, WCA and water absorption times measurements, ATR-FTIR spectroscopy, CLSM), writing and creating artwork. Martin Bellmann was involved in coating deposition and data evaluation. Kristina Lachmann was involved in data acquisition and interpretation (XPS). Andreas Geissler was involved in data acquisition and evaluation (viscosity measurement, mercury intrusion porosimetry), as well as conceptualization, interpretation, supervision and funding acquisition. Markus Biesalski was involved in supervision. All authors were involved in proof-reading.

The following article has been published in *Advanced Materials Interfaces*:

A. Loesch-Zhang, M. Bellmann, K. Lachmann, M. Biesalski, A. Geissler, **Plasma Polymerization of Vegetable Oils onto Paper Substrates of Varying Porosity for Improved Hydrophobicity**, *Adv. Mater. Interfaces* **2024**, 2400507.

Published by Wiley-VCH GmbH under Creative Commons Attribution 4.0 International (CC BY 4.0) License.

The supporting information has not been reprinted here, but can be accessed via the online version of this article: <https://onlinelibrary.wiley.com/doi/full/10.1002/admi.202400507>.

Plasma Polymerization of Vegetable Oils onto Paper Substrates of Varying Porosity for Improved Hydrophobicity

Amelia Loesch-Zhang, Martin Bellmann, Kristina Lachmann, Markus Biesalski, and Andreas Geissler*

Paper finishing, in particular, coating paper with desired barrier functions is well-developed as of today. However, due to large amounts of material and process energy as well as the use of non-renewable resources for such coatings, common technologies are not sustainable. Given the increasing importance of paper in manifold applications, more sustainable routes with low-energy processes as well as biogenic material alternatives are highly needed. To address this challenge, a solvent-free and material-efficient approach is proposed to bio-based paper coatings by depositing chia oil-based plasma polymers using a jet-induced sliding discharge concept at atmospheric pressure. Depending on the amount of coating and the paper porosity, this treatment retards water absorption. Coating visualization is enabled through confocal laser scanning microscopy (CLSM) and scanning electron microscopy (SEM). Like chia oil, safflower oil, and olive oil show the ability to hydrophobize paper and the great potential within plasma polymerized vegetable oils to make the paper coating more sustainable.

1. Introduction

For many applications in the packaging and lightweight construction sectors, paper offers notable advantages such as high specific strength, good availability, and well-established recyclability. However, the material has one shortcoming, namely its sensitivity to humidity. On water ingress, paper loses its stability and further falls victim to microbial colonization, leading to further deterioration in the long term.^[1] Accordingly, strategies are required to either make paper wet-strength or hydrophobic and thus protect it from moisture. In industry, water barriers are achieved through sizing or coating approaches, whose components are usually based on inorganic or fossil-based organic materials. Suitable thermoplastic polymers for water barrier production are increasingly being applied from dispersion in order to minimize coating quantities and meet

legal recycling requirements. This, of course, is accompanied by an increased demand for drying energy to remove superfluous water.^[2,3] Replacing fossil-based coatings with bio-based materials is crucial in the quest for a more sustainable economy and challenges many scientists.^[4] Therein, using long-chain aliphatics such as waxes is a promising approach for achieving hydrophobic paper surfaces.^[5] Fatty acids and vegetable oils have equally been utilized for paper hydrophobization, either as crosslinked coatings,^[6,7] as components in hybrid organic nanoparticles^[8] or covalently attached to the cellulosic substrate.^[9,10] However, these processes require either multiple reaction steps, large amounts of solvent, supplementary chemicals, or elevated temperatures.

Plasma-enhanced chemical vapor deposition (PECVD), also known as plasma polymerization, performed at atmospheric pressure offers the possibility to forego these disadvantages, as it does not require any solvents, supplementary chemicals, nor subsequent drying processes, but is nonetheless able to deposit highly crosslinked, covalently attached coatings, thus opening up a large variety of applications.^[11]

PECVD has been explored for paper hydrophobization with silicon- and fluorine-based precursors, achieving both hydrophobic and superhydrophobic properties.^[12,13] For instance, hexamethyldisilazane coated filter paper showed conformal coating and


A. Loesch-Zhang, M. Biesalski, A. Geissler
Macromolecular Chemistry and Paper Chemistry
Technical University Darmstadt
Peter-Grünberg-Str. 8, 64287 Darmstadt, Germany
E-mail: andreas.geissler@tu-darmstadt.de

M. Bellmann
Fraunhofer Institute for Surface Engineering and Thin Films IST
Von-Ossietzky-Str. 99, 37085 Göttingen, Germany

M. Bellmann
Faculty Engineering and Health
HAWK University of Applied Sciences and Arts
Von-Ossietzky-Str. 99, 37085 Göttingen, Germany

K. Lachmann
Fraunhofer Institute for Surface Engineering and Thin Films IST
Riedenkamp 2, 38108 Braunschweig, Germany

A. Geissler
Forschungsstiftung der Papierindustrie (PTS)
Pirnaer Str. 37, 01809 Heidenau, Germany

 The ORCID identification number(s) for the author(s) of this article can be found under <https://doi.org/10.1002/admi.202400507>

© 2024 The Author(s). Advanced Materials Interfaces published by Wiley-VCH GmbH. This is an open access article under the terms of the [Creative Commons Attribution](https://creativecommons.org/licenses/by/4.0/) License, which permits use, distribution and reproduction in any medium, provided the original work is properly cited.

DOI: 10.1002/admi.202400507

static water contact angles (WCAs) above 120°. [14] In an example focusing on fluorocarbon-plasma polymer coated papers, a coating thickness above 200 nm was required to achieve permanent hydrophobization, while scanning electron microscopy (SEM) images showed no distinct changes on the fiber surface even at 2.4 μm coating thickness. [15] However, bio-based hydrophobizing agents such as vegetable oils have not yet been utilized in PECVD. Indeed, the use of biogenic precursors in PECVD has so far been focused on essential oils, extractives such as terpenes and phenols, amino acids, proteins, and enzymes as well as derivatives of lactic acid, [16] with recent research including silk fibroin and chitosan. [17]

With respect to vegetable oils or fatty acids, the only use related to plasma has been the precursor application through spray coating or impregnation combined with plasma treatment. For instance, cotton fabric showed WCAs above 150° after oleic acid was grafted onto its surface. The process consisted of three steps, namely the fabric activation with argon microwave frequency plasma at reduced pressure, immersion into an ethanolic solution of oleic acid and a subsequent argon plasma treatment. [18] Similarly, oleic acid, sunflower oil, and olive oil were grafted onto softwood kraft pulp fibers and Spanish broom fibers through substrate immersion into precursor solutions in acetone and plasma treatment followed by extraction of unbound material. [19] A mixture of copaiba oil and silicone oil was intended to produce antibacterial and hydrophobic properties on vegetable ivory and applied through spray coating combined with atmospheric pressure plasma jet treatment using ambient air. The pure copaiba oil-based coating yielded WCAs of (83.6 ± 3.5)° and the mixture (94.6 ± 2.4)°, compared to (31.5 ± 8.7)° for the uncoated substrate. [20]

Recently, we reported the first study of the deposition of vegetable oils in PECVD. Therein, two oils with a high degree of unsaturation, namely chia oil and tung oil, were compared with respect to their suitability for generating hydrophobic plasma polymer coatings. While tung oil-based plasma polymers showed no hydrophobizing effect under the examined plasma parameters, chia oil-based plasma polymers improved the hydrophobicity of both glass slides and glassine paper with WCAs up to (86.0 ± 7.9)° and (75.2 ± 10.6)° respectively. [21] While these two substrates are characterized by their smoothness, roughness is known to significantly contribute to surface-wetting behavior. In this work, we explore the potential of plasma polymerized (pp) chia oil to improve hydrophobicity of paper substrates with varying porosities and improve understanding of the deposition of plasma polymer-based coatings on porous substrates. After the initial characterization of the various base papers and the influence of plasma treatment on one exemplary base paper, coatings on papers of varying porosity with plasma-polymerized vegetable oil will be analyzed. Finally, an outlook on plasma polymer coatings with different oil-based precursors will be given.

2. Results and Discussion

Two different kinds of base paper were used to examine the suitability of PECVD to coat porous substrates. Cotton linter laboratory handsheets were used as the coarser material. Their porosity and smoothness were adjusted by calendering with three line pressures (5 N mm⁻¹ (CL-5), 50 N mm⁻¹ (CL-50), and

300 N mm⁻¹ (CL-300)). Glassine paper (GP) was selected as smooth and dense substrate for comparison, with its smoothness and low porosity caused by a high refining degree as well as densification. All substrates were characterized with respect to their surface morphology, porosity and water absorption time (Figure 1). Scanning electron microscopy (SEM) showed the densification produced by calendering, with quite loose fiber arrangement and many loose fibrils observed for CL-5 to large flattened fibril-free areas for CL-300. Contrarily, GP is extremely smooth and barely shows any individual fibers and no fibrils at all (Figure 1a). A similar trend is observed for surface roughness. Average surface roughness S_a values decrease from (5.7 ± 0.2) μm for CL-5 through (3.2 ± 0.7) μm for CL-50 to (2.7 ± 0.2) μm for CL-300. Finally, GP only shows an average surface roughness of (1.33 ± 0.11) μm (Figure 1b). Similarly, the porosity decreases from (52.7 ± 1.6) % through (35.3 ± 0.9) % to (24.7 ± 0.5) % for cotton linter papers with increasing degree of calendering. Glassine paper has an even lower porosity of only (4.5 ± 1.1) % (Figure 1c). The available pore space in the paper influences the water absorption capacity, so that the water absorption times increase with the degree of calendering. Still, the water absorption time for all cotton linter papers is well below 1 s, whereas it is in the range of several minutes for glassine paper (Figure 1d). However, this cannot be determined with accuracy, as glassine paper shows strong swelling in the imbibed area which renders the substrate contours unclear. At the same time, water evaporation takes place, which makes a precise measurement impossible.

Plasma treatment without the use of any precursor was performed to examine the influence of plasma processing on paper surface properties. The modifications occurring on various plasma-treated cellulosic substrates under the influence of different treatment conditions have been well-examined by others [24,25–27] and measurements shown here are intended as reference compared to plasma polymer-coated samples. Thus, based on the subsequently used parameters of 100 W plasma power and 3 mm substrate-source distance, variations of 10 to 400 W and 1.5 to 6 mm were carried out.

Furthermore, the number of treatment runs was varied from 1 to 5 as in the subsequent coating process. CL-300 was chosen as substrate because it is smooth and dense enough to enable 0 s water contact angle measurements (contrary to CL-50 and CL-5, where water absorption is too fast) and its surface properties range in the middle of the four examined substrates.

Water contact angle measurements show an immediate decrease in water contact angles from (28.2 ± 1.2)° for untreated paper by at least 10° for treated paper. Whilst variation of substrate-source-distance and number of treatment runs show no clear trend with respect to hydrophilization, increasing the plasma power decreases the WCA, from (15.6 ± 3.8)° obtained after treatment at 10 W to (5.0 ± 1.1)° after treatment at 400 W (Figure 2a–c). Note that errors may be caused by the non-homogeneous compression of the paper, which influences density and resultingly water absorbance and roughness, as it is most likely the case for the diverging low WCA for 25 W treatment. Neither surface roughness (Figure 2d–f) nor SEM imaging (Figure 2g,h) show any significant morphological change, indicating that the change in WCA is of purely chemical nature. Increased fibrillation after plasma treatment as reported elsewhere was not observed under the selected parameters and shows

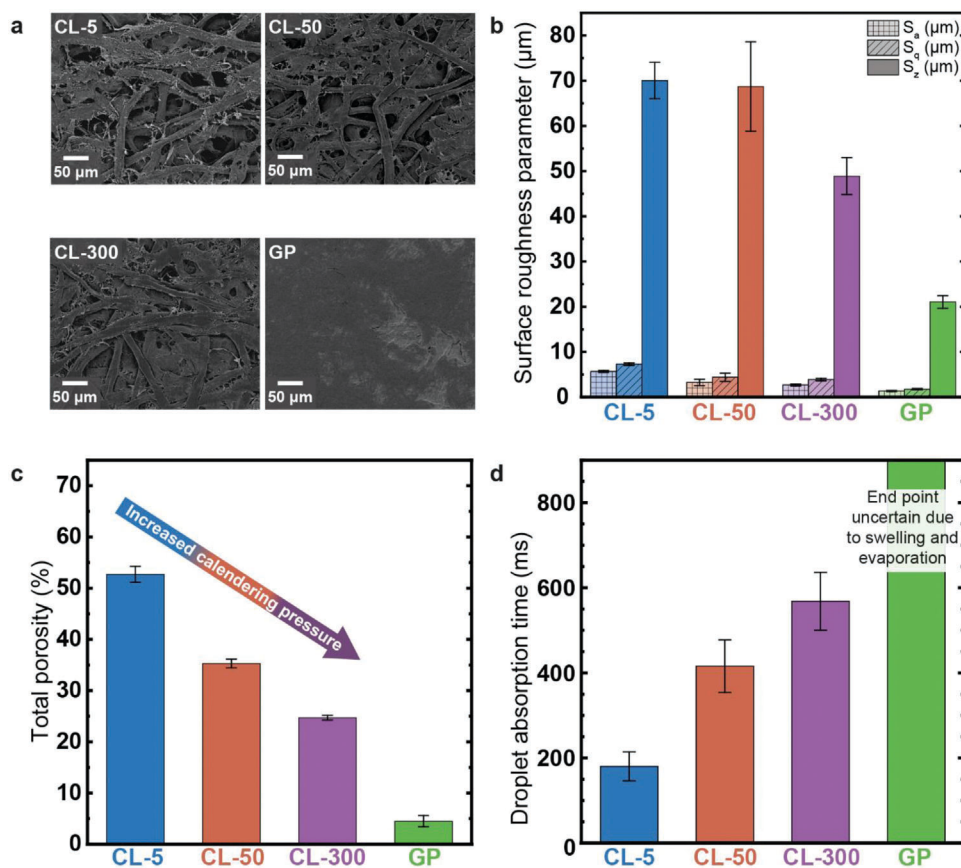


Figure 1. Characterization of the uncoated base papers using (a) scanning electron microscopy, (b) optical profilometry, (c) mercury intrusion porosimetry and (d) droplet absorption time measurement, showing that increased line pressure when calendering cotton linter paper shows increased fiber flattening, decreasing roughness and porosity and increased water absorption times, while glassine paper is still smoother, less porous and droplet absorption times cannot be determined precisely.

the non-aggressive nature of the plasma source used herein. Finally, Attenuated Total Reflectance - Fourier Transform Infrared (ATR-FTIR) spectroscopy shows the formation of a small, yet clearly observable carbonyl band at 1720 cm^{-1} after 5 treatment runs, while otherwise, no significant changes were observed (Figure 2i; Figure S1, Supporting Information). The formation of carbonyls is attributed to the generation of radicals during plasma treatment and the subsequent oxidation with oxygen from the ambient air. It is likely that such processes occur in all samples, as they show increased hydrophilicity which is usually attributed to the presence of an increased number of polar species. The penetration depth of ATR-FTIR spectroscopy does not allow for the detection of such minute differences in surface chemistry, but the phenomenon itself has been well described previously.^[26,27]

Plasma polymerization was performed using chia oil as coating material, which was considered a promising precursor to improve surface hydrophobicity in our recent investigations.^[21] In this study on papers with varying porosity, most PECVD parameters were kept constant. Only the number of coating runs was varied, as porous substrates were expected to require different coating amounts to achieve sufficient coverage for surface hydrophobization. In a first step, the three calendered cotton linter

papers were compared with respect to their surface properties after coating with pp(chia oil) with one, two or five coating runs.

Generally, an increased water absorption time was observed for all pp(chia oil) coated papers. Water absorption times increase with growing coating amount and paper roughness. Indeed, the highest water absorption time of up to 300 s was observed for sample CL-5, which was coated five times (Figure 3a). The initial paper roughness therefore has a fundamental influence on the hydrophobization effect. However, profilometric measurements indicate that the coating itself does not significantly change the paper roughness (Figure 3b). ATR-FTIR spectroscopy shows increasing bands characteristic for vegetable oils, notably the =C-H vibration at 3011 cm^{-1} , the CH_3 and CH_2 vibrations at 2924 and 2854 cm^{-1} as well as the $\text{C=O}_{\text{ester}}$ vibration at 1743 cm^{-1} .^[28] Although it is not a quantitative method, the increase in band maxima and integrals is a strong indicator of the increased coating deposited with an increased number of coating runs (Figure 3c, full spectra in Figure S2, Supporting Information).

With respect to the absorption kinetics, the large scattering of values, especially present on CL-5, is unfortunately indicative of an inhomogeneous coating distribution on the paper substrate. Hence, the extremely low water absorption time for the coating

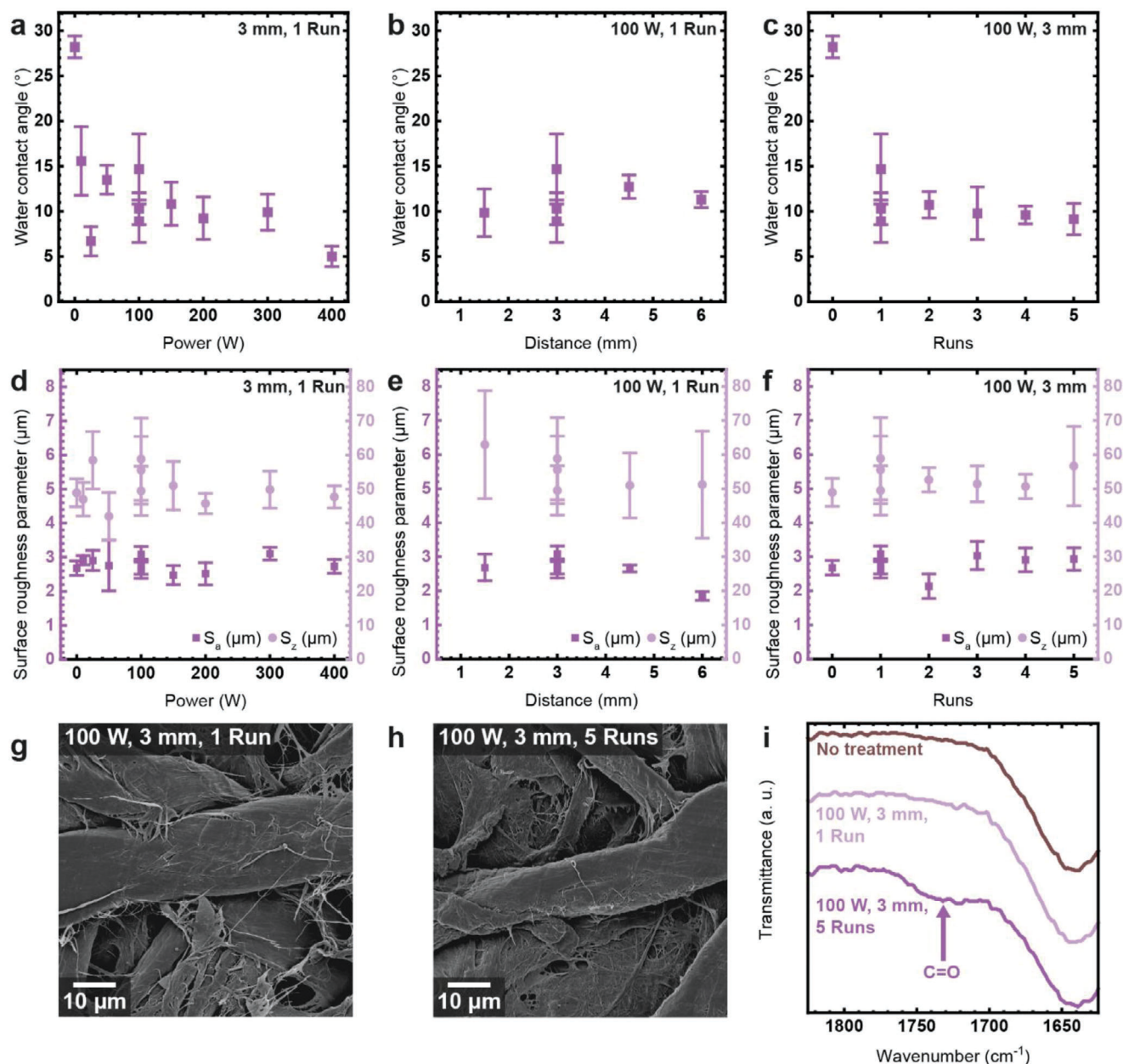


Figure 2. Plasma treatment of CL-300 paper varying either power, substrate-source distance, or number of treatment runs. (a–c) Plasma treatment decreases water contact angle, only power has a significant effect; (d–f) Surface roughness does not change significantly; (g,h) SEM images comparing surface morphology after one and five treatment runs show no significant changes; (i) ATR-FTIR spectroscopy shows the formation of a small carbonyl band after five treatment runs not present at other parameter settings.

applied with two runs is assumed to be an outlier. Nonetheless, we consider these results to give valid indications of the influence of paper porosity on water absorption.

Confocal laser scanning microscopy (CLSM) enables visualization of the coating covering the substrate surface. To this end, coated paper samples were stained in two steps, first with the cellulose-selective staining agent Calcofluor White (CFW, herein depicted in cyan), and second with the fat-selective staining agent Sudan III (S3, herein depicted in magenta).^[29] A difference in fluorescence intensity between coated and uncoated areas was

accordingly expected to indicate the presence of the pp(chia oil) coating on the papers. On CL-5 coated with five runs, this was indeed the case, as the cross-sections show a micrometer-thin purely magenta-stained layer indicating the presence of oil, which is not at all visible on the uncoated and once-coated sample. Similarly, the gray values of both CFW and S3 stains start increasing at exactly the same paper position for the uncoated and single-coated sample. For the five runs-coated sample, an offset between the gray values of the two staining agents is visible, with the S3 gray value increasing directly at the paper surface and

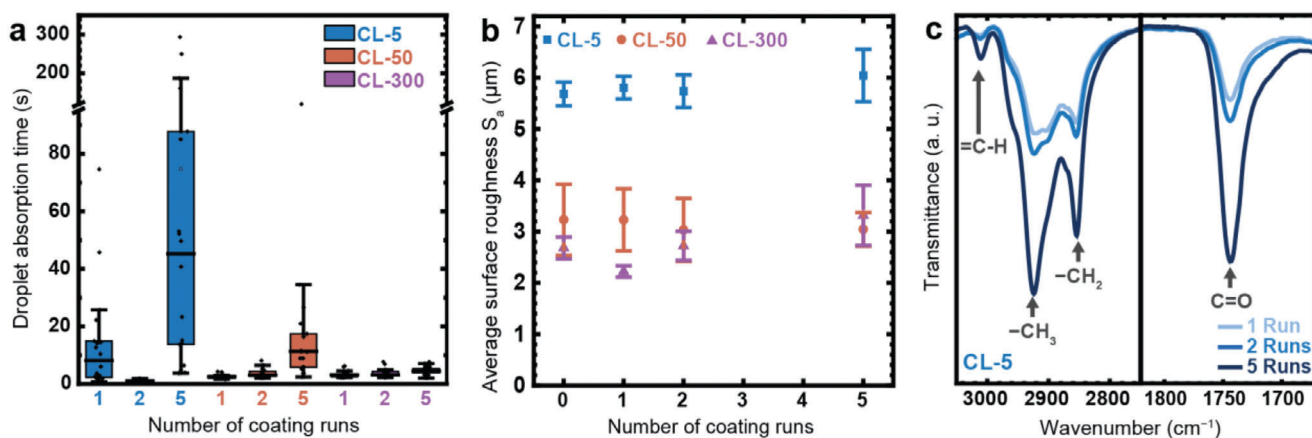


Figure 3. Examination of the modification of cotton linter papers calendered with different line pressure (increasing from CL-5 to CL-50 to CL-300) coated with pp(chia oil) at one, two, and five coating runs. (a) Absorption times of 2 μL water droplets increase with number of coatings runs and are highest for the most porous paper CL-5; (b) Surface roughness does not change significantly; (c) Characteristic ATR-FTIR bands increase with number of coating runs, measured on CL-5 but similar on all samples.

the CFW gray value just increasing slightly below (Figure 4a). Although it can be argued that the surface of the two other samples also appears to be slightly more rough, top-view images support the assumption that stain intensity change is indicative of the coating presence. Indeed, both the integrated intensity of CFW fluorescence and the CFW/S3 ratio decrease with increasing coating amount. Accordingly, the presence of an S3-stained oil-based coating leads to decreased detection of CFW fluorescence, as has been observed previously.^[10] Furthermore, stained individual fibers and empty pores are clearly visible for the uncoated sample in both CFW and S3 channels, whilst for both coated samples the inter-fiber space is also stained, proving the presence of oil after both one and five coating runs (Figure 4b).

The pp(chia oil) coated papers were Soxhlet-extracted to examine covalent coating attachment to the paper substrate and remove possible superfluous unbound molecules.

X-ray photoelectron spectroscopy (XPS) measurements and deconvolution of the C1s peak display changes in surface chemistry of coated/non-extracted and coated/extracted papers compared to uncoated cotton linter papers (Figure 5; Figure S3, Supporting Information). For an uncoated paper, the predominant peaks are the C2 peak at 286.4 eV and the C3 peak at 287.7 eV, which are attributed to C—O moieties, as present in the cellulosic hydroxyl group, and to O—C—O moieties, resulting from the cellulosic acetal group, respectively. Additional C1 and C4 peaks at 284.8 and 289.2 eV represent C—C/C—H and O=C—O-bound carbons respectively, and originate from impurities such as lignin, extractives or fatty acids frequently present in natural cellulose such as obtained from cotton linters.^[25,30–32] The untreated paper contains 60 at.-% C and 39 at.-% O, resulting in an O/C ratio of 0.66, which is lower than the theoretically expected value for pure cellulose of 0.83. Again, this is due to impurities in cotton linters.^[30,32,33] After coating, the carbon content increases to 86 at.-% C and 13 at.-% O (O/C ratio of 0.15) both for one and five coating runs. The intensity of the carbons in the paper, notably the C2 and C3 peaks, decreases relative to the C1 and C4 peaks indicating the presence of the oil's aliphatic fatty acid chain with

C—H and C—C bonds, and the ester group with O=C—O bond, respectively. The O/C ratio increases slightly to 0.21 after Soxhlet extraction, as does the C4 peak indicating carboxylic acid presence, while the integral of the C1 peak decreases slightly. This shows that the largest part of the coating is covalently attached to the substrate and therefore still present after extraction. Furthermore, the extraction process and storage can also slightly contribute to surface chemistry modification, for instance through oxidation reactions or molecular rearrangement.^[10,34] Interestingly, the C1 content does not increase with a higher number of coating runs. As XPS penetration depth is less than 10 nm, this might either be for the paper roughness being too high to detect possible differences, or because the layer thickness, especially on the topmost fiber surface, surpasses the penetration depth after one coating run and further modifications in coating thickness are accordingly not visible.

Besides clear indications obtained through XPS, covalent pp(chia oil) attachment is further well-proven through ATR-FTIR spectroscopy. Whilst for one and two coating runs, the characteristic CH_3 and CH_2 bands cannot be clearly distinguished from those present in cellulose, their presence at 2925 and 2854 cm^{-1} is evident after extracting the coating formed through five coating runs, and even a slight trace of the $=\text{C—H}$ vibration at 3006 cm^{-1} is still detectable. Additionally, the $\text{C=O}_{\text{ester}}$ band at 1742 cm^{-1} is well visible in all three samples and increases with number of coating runs (Figure 6a, full spectrum in Figure S5, Supporting Information).^[28] After extraction, water droplet absorption times increase significantly compared to unextracted samples. Again, trends are similar, with the slowest absorption for the most porous substrate, CL-5, and the highest number of coating runs (Figure 6b). As the large deviations in absorption times show again, the coating is not distributed perfectly homogeneously across the substrate surface. Time-dependent water contact angles were measured in the position with the highest absorption times and show good droplet stability over time as well as static water contact angles above 100° for CL-50 and CL-300 and above 120° for more porous CL-5 (Figure S4, Supporting Information). Although the coatings are not completely

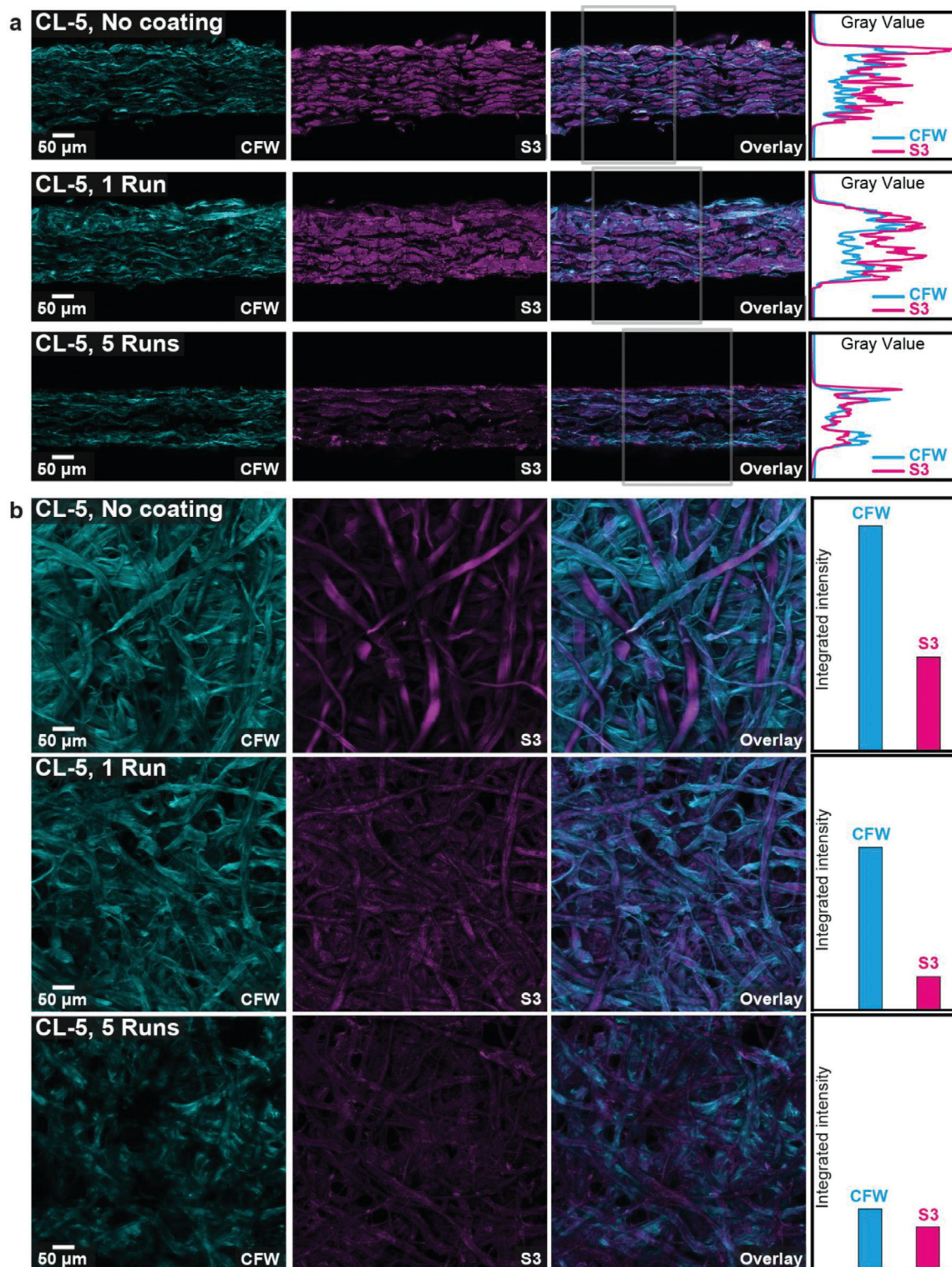


Figure 4. CLSM images of CL-5 showing CFW-based cellulose stain, S3-based oil stain, and overlay of the two channels. (a) Cross-sections displayed in maximum intensity z-stack projection comparing uncoated paper to papers coated with one and five coating runs; squares indicate the area from which gray values were calculated. The coating presence is clearly visible only for the sample coated with five runs both in cross-section view and through plotting gray values against image line for marked area. Images taken with the same settings and not further modified. (b) Top-view CLSM images displayed in sum slices z-stack projection and bar plots show the integrated intensity of the fluorescence of both staining agents. CFW intensity and CFW/S3 intensity ratio decrease with coating amount. Inter-pore filling stain in S3-channel indicates presence of pp(chia oil) in both coated samples. Images taken with the same settings and not further modified.

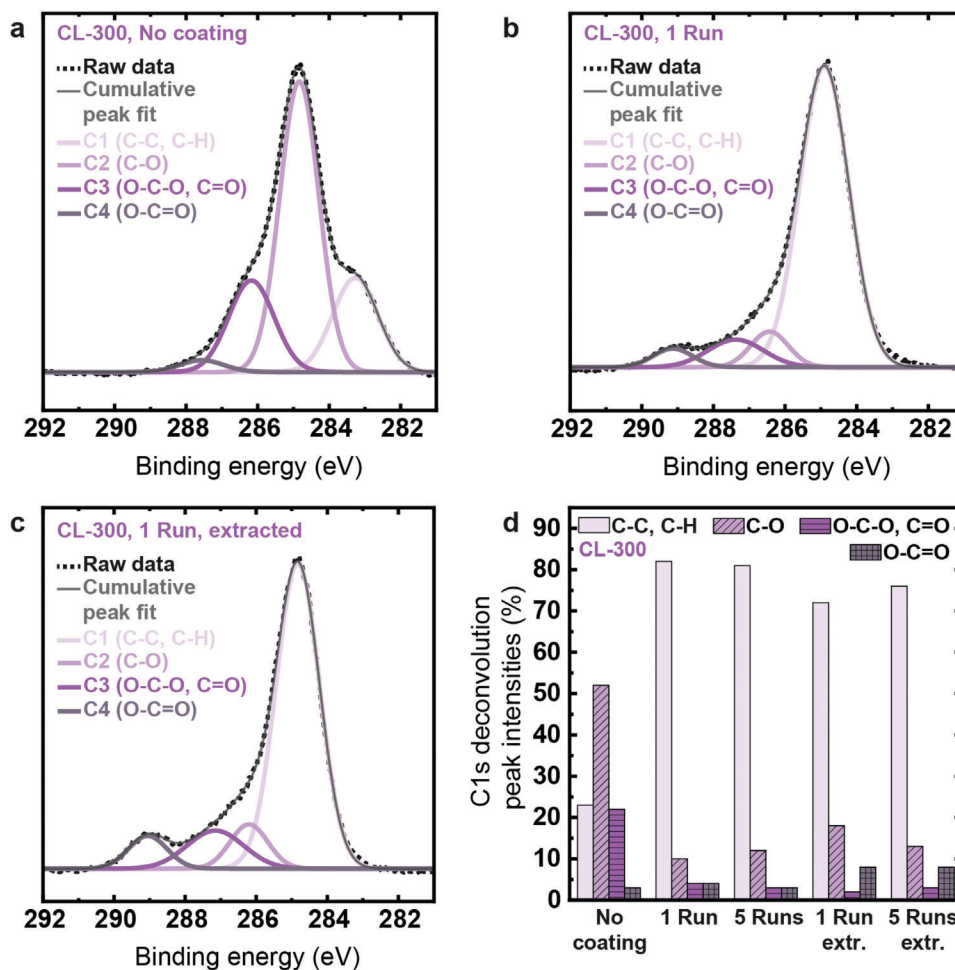


Figure 5. Deconvolution of C1s peak in XPS spectra of (a) uncoated CL-300; (b) CL-300 coated with one coating run and (c) CL-300 coated with one coating run and extracted; (d) comparison of content of differently bound carbon atoms shows the presence of vegetable oil functional groups after coating and after extraction.

homogeneous, their potential to hydrophobize surfaces of varying roughness is evident.

SEM images enable visualization of pp(chia oil) on cellulose fibers present after Soxhlet extraction. Independent of the applied calendaring pressure, uncoated papers show single fibers with microfibrils at their surface. No significant changes are visible on papers coated with one run. However, after five coating runs, the cellulose fibers and fibrils are covered with an equalizing layer that fills the interfibrillar spaces and can be interpreted as evidence for the presence of pp(chia oil) (Figure 6c). Similar coverage effects have been observed on deposition of fluorocarbon- and silicon-based plasma polymers.^[13,35] Considering these analytical methods altogether, it is clear that covalent pp(chia oil) attachment occurs already after one coating run. This already leads to improved resistance to water penetration and is evidenced through ATR-FTIR spectroscopy, but a larger coating amount is required for permanent hydrophobization.

To study the possible impact of the substrate's surface topology, pp(chia oil) was applied onto glassine paper, a rather smooth paper substrate, for comparison. Significant improvements in water contact angle were observed comparing uncoated paper (WCA

≈40°) to coated paper (80–90°). No significant modifications were observed between different numbers of coating runs, with the exception of four runs (Figure 7a). Whether this is a true significance or an outlier cannot yet be ascertained, as five runs do not lead to a significant modification anymore. Nonetheless, it seems possible that too many coating runs deteriorate the coating quality due to an excess amount of possibly unattached oil. The surface roughness does not change significantly comparing uncoated and coated papers, like observed for cotton linter papers (Figure 7b).

On coated glassine paper, CLSM images clearly demonstrate the presence of pp(chia oil), which is detectable even after one coating run. The non-visibility of CFW stain is evident after both one and five coating runs in cross-section images, respectively. The spatially resolved gray values show that the intensity of the CFW peak at the paper surface decreases greatly upon coating. However, individual stained spots are still visible. Interestingly, CFW cannot penetrate deeply into either coated or uncoated glassine paper (Figure 8a). Top-view images confirm these observations. The CFW stain, which is homogeneously distributed on the surface of the uncoated paper, is only visible in certain spots,

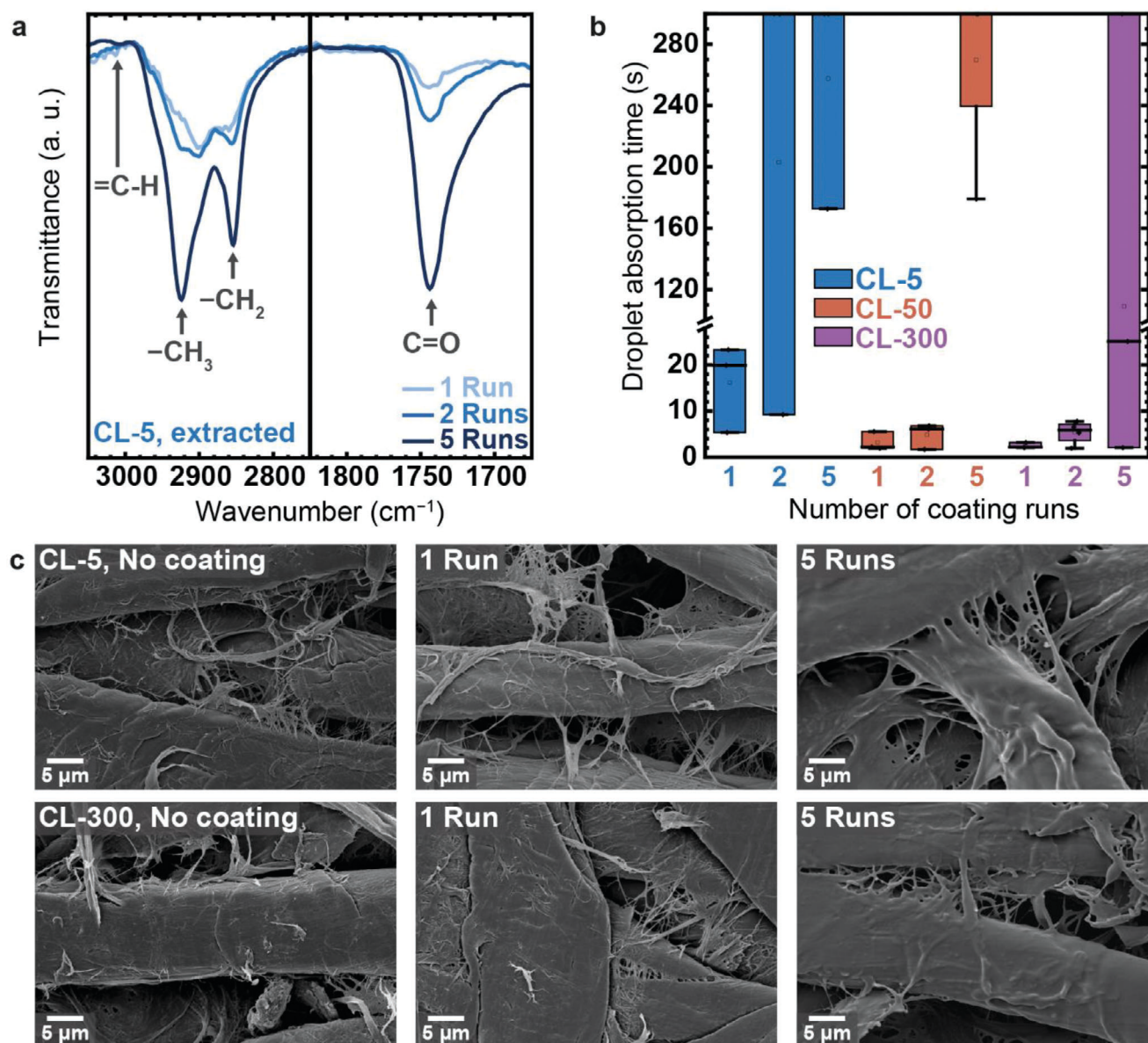


Figure 6. (a) FTIR spectroscopy indicates pp(chia oil) presence through characteristic bands, especially for five coating runs; (b) Water absorption times for 2 μL -sized droplets increase compared to unextracted paper and with increasing porosity and number of coating runs; (c) SEM images show the presence of a closed smooth layer on individual fibers and interfibrillar spaces after five runs as opposed to uncoated papers, but no distinct modification after one coating run.

while most of the surface does not fluoresce anymore. The S3 stain, on the other hand, is well-distributed across the entire paper surface independent of coating presence. The CFW/S3-ratio decreases with an increase in integrated S3 fluorescence intensity after coating (Figure 8b). Again, this is vivid proof of the presence of pp(chia oil) on paper.

Finally, the suitability of chia oil to hydrophobize glassine paper through plasma polymerization was compared to that of other vegetable oils, namely safflower oil and olive oil. These two differ from chia oil in the degree of unsaturation of the fatty acid chains, as safflower oil contains mainly double unsaturated linoleic acid chains, and olive oil's key fatty acid component

are mono-unsaturated oleic acid chains, while chia oil mainly contains triple unsaturated linolenic acid chains (Figure 9a).^[36] Moreover, the oils differ slightly in their viscosity (Figure 9b), but not so much as compared to the previously examined tung oil, which was deemed unsuitable for plasma polymerization with the setup and parameters used herein.^[21] Plasma polymers based on all three oils were deposited with the same parameters and different numbers of coating runs, whereof two coating runs show the best and most homogeneous results across all examined oils (Figure S6, Supporting Information). Indeed, water contact angle measurements of papers coated with two runs show the suitability of all oils to improve paper hydrophobicity. Interestingly,

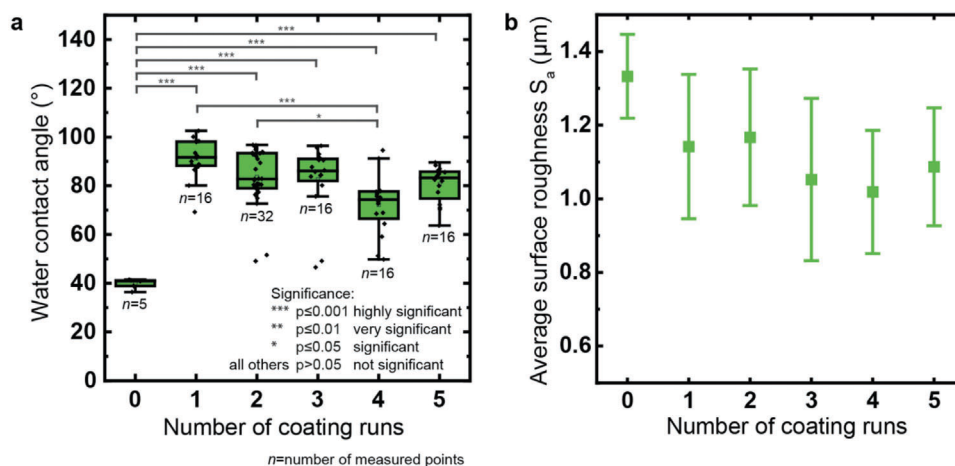


Figure 7. Comparison of uncoated glassine paper and pp(chia oil) coated paper with one to five coating runs; (a) water contact angles, p-values show significances according to Tukey's test, non-indicated values are not significant; (b) surface roughness does not change significantly.

water contact angles increase from pp(chia oil) to pp(safflower oil) and were highest for pp(olive oil) with $\approx 100^\circ$ (Figure 9c). Based on a previous study by MERTENS et al.,^[37] a higher double bond content had initially been expected to lead to an increased degree of crosslinking while enabling good structural retention. As the current results show opposing behavior, it is possible that instead of the supplementary double bonds supporting crosslinking, oxidation reactions preferentially occur at the sites of the double bonds and lead to incorporation of an increased number of hydrophilic groups. Alternatively, the precursor viscosity, which was previously found to play a decisive role in aerosol generation and formation of closed layers,^[21] might be relevant even though the difference between the three oils is not large. Furthermore, the presence of minor components in the oils is another potential influencing factor whose specific effect has not yet been investigated. These research questions need to be answered to, in the future, fully exploit the potential of hydrophobization with plasma-polymerized vegetable oils shown here.

The majority of paper products, with the exception of tissue and filters, have some form of water-repellent coating or are hydrophobized in order to meet the respective usage requirements. Depending on the area of application, this functionalization can be implemented to very different extent. This ranges from low sizing degrees, such as those required to control the absorption of liquid in printing or coating processes, through products that are in use for a few minutes, such as paper straws, to extremely modified papers that can be exposed to weathering for longer periods or even used as liquid packaging material. Compared to these permanent liquid barriers, which are often realized by means of plastic coatings, the approach presented here is of course not yet competitive in terms of long-term stability. However, it should be noted that the contact angles of $\approx 100^\circ$ achieved with pp(olive oil) are already in the same dimension as with the usual industrial alkyl ketene dimer sizing of packaging papers or with surface coatings using polymer latex-based formulations.^[3] However, industrial sizing agents like alkyl ketene dimer and alkenyl succinic anhydride as well as polymer latices are produced through multi-step reactions based on non-renewable materials and beyond that, sizing processes require large amounts of material

and drying energy. Thus the properties obtained can not simply be compared to the results presented herein without taking green chemistry principles into account. Material consumption is indeed an issue that can also be found in several works of recent research using fatty acids or vegetable oils for paper hydrophobization. For instance, grafting of oleic acid to cotton fabric resulted in WCAs of 150° , but demanded, besides two plasma treatment steps, immersion into an ethanolic solution of oleic acid as well as subsequent rinsing.^[18] Although the coatings presented herein are inferior in terms of hydrophobicity, their production requires only one step instead of multiple ones. Other examples of works aiming at solvent-free vegetable oil-based coatings through thermal curing or photocuring achieved WCAs of 97° and 121° respectively using olive oil.^[6,10] However, in these cases the paper was fully impregnated with the coating, contrary to this work where the coating was more economically deposited only on the substrate surface. Use of tung oil and a photoinitiator achieved WCAs of 127° and a Cobb₆₀ value of 17 g m^{-2} , but entailed more than 6 g m^{-2} coating pick-up on papers of 79 g m^{-2} grammage.^[38] Therefore, although process optimization is needed for coatings based on plasma polymerized vegetable oils to achieve the same water repellency as conventional ones, and cost and complexity of the plasma technology need to be assessed, many aspects of the method presented herein are well in accordance with green chemistry principles^[39] and in this respect a promising alternative to well-established but less sustainable technological processes.

3. Conclusion

This work examines bio-based plasma polymer coatings for hydrophobization of paper with varying porosity using chia oil, safflower oil, and olive oil. The pp(chia oil) coatings improve water repellency on all examined substrates, favored by higher paper porosity and larger coating amounts. The coating presence was evidenced through CLSM and SEM images and its covalent bonding to the cellulose was confirmed by ATR-FTIR and XPS spectroscopy. While the coatings are not perfectly homogeneous, the possibility to significantly improve water barrier properties

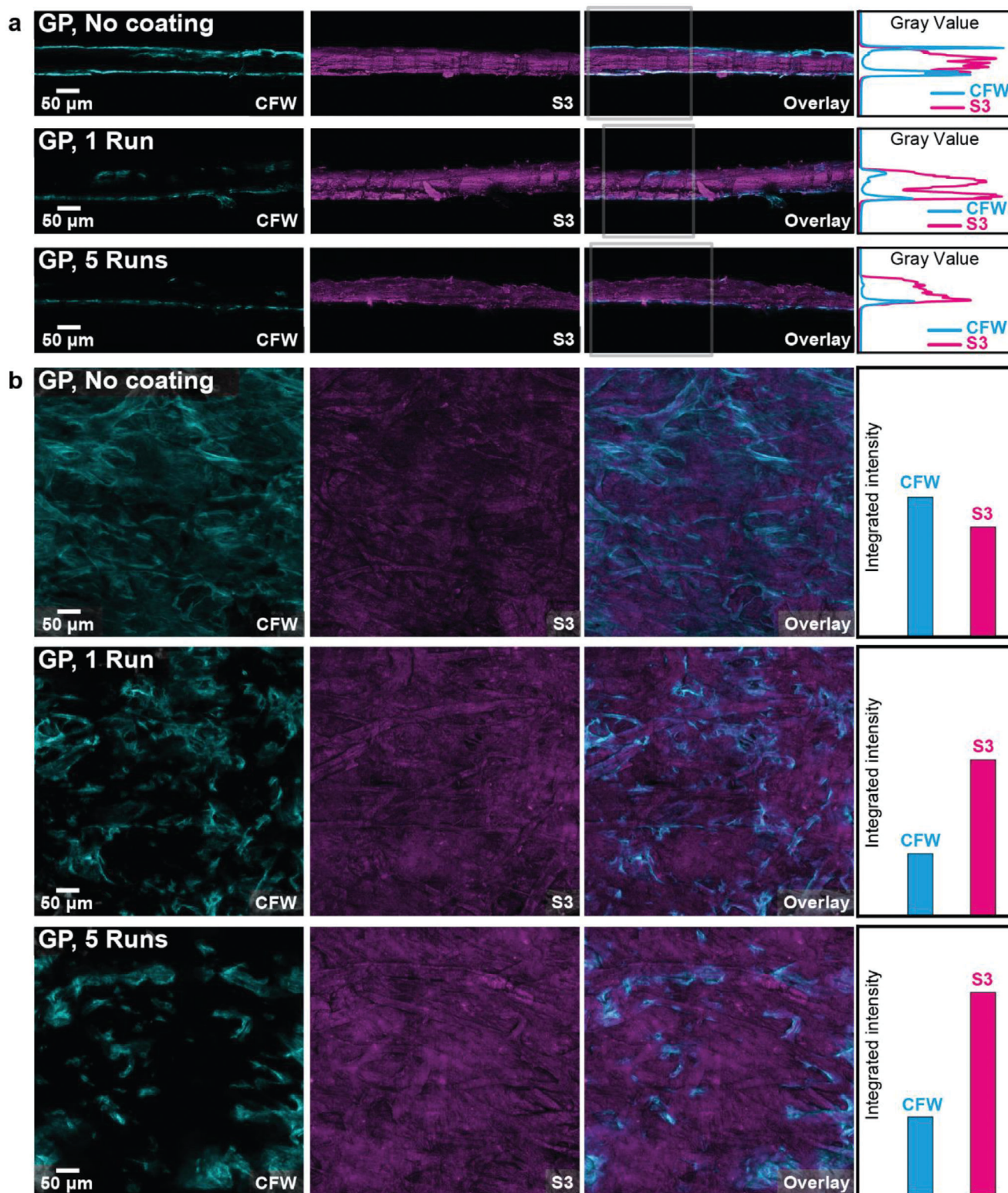


Figure 8. CLSM images of glassine paper showing CFW-based cellulose stain, S3-based oil stain, and overlay of the two channels. (a) Cross-sections displayed in maximum intensity z-stack projection comparing uncoated paper to paper coated with one and five coating runs; squares indicate the area from which gray values were calculated. The coating presence is clearly visible both in the cross-section view and through plotting gray values against image line for marked area, the latter showing a decrease in CFW gray value with increased number of coating runs. Images taken with the same settings and not further modified. (b) Top-view CLSM images displaced in sum slices z-stack projection and bar plots showing the integrated intensity of the fluorescence of both staining agents. CFW intensity and CFW/S3 intensity ratio decrease with coating amount. Inter-pore filling stain in S3-channel indicates the presence of pp(chia oil) in both coated samples. Images taken with the same settings and not further modified.

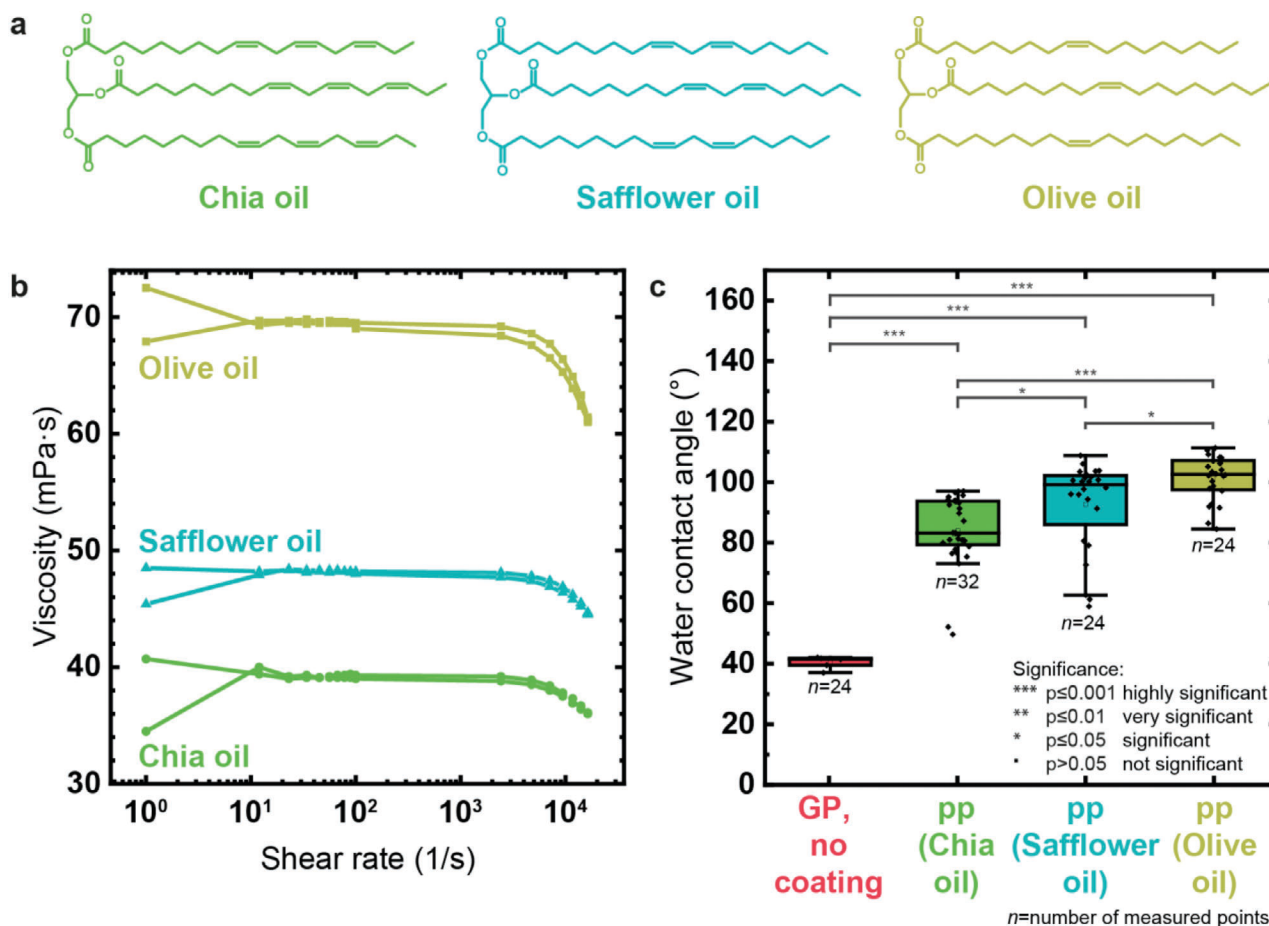


Figure 9. (a) Chemical structures of the main components of chia oil, safflower oil and olive oil, differing in their C=C double bond content; (b) Shear-rate dependent viscosity of the three examined oils increases from chia oil through safflower oil to olive oil; (c) Water contact angles on glassine paper increase significantly from pp(chia oil) through pp(safflower oil) to pp(olive oil), with all coatings deposited at the same parameters and with two coating runs.

is clearly evidenced. Subsequent improvement of coating homogeneity and optimization of plasma parameters are however required. For industrial scale-up, it is necessary either to increase the dimensions of the DiscJet or to operate it in arrays, which would additionally enable the option for multi-layer coatings. Alternatively, a change of the plasma source concept would be required, whereby investigations into the influence of drag air as a function of process speed would be essential. Despite the need for further development, this work shows the potential of vegetable oil-based plasma polymers as a solvent-free and material-efficient coating strategy to improve current paper coating technology, for instance with respect to packaging or lightweight construction applications.

4. Experimental Section

Materials: Glassine paper (Pergamyn WIN HT 60 g m⁻²) was provided by Spezialpapierfabrik Ober-Schmitten GmbH (Nidda, Germany). Glass slides were obtained from EpreDia (Breda, Netherlands). Chia oil was purchased from Wallitzer-Tiernahrungs GmbH (Rheinsberg, Germany), safflower oil and olive oil from Oelmuehle Solling (Boffzen, Germany), acetone and ethanol (analytical grade) from Merck (Darmstadt,

Germany), staining agent Fluorescent Brightener 28 (Calcofluor White) from Sigma Aldrich (St. Louis, MO, USA) and Sudan III staining solution (2.5 g L⁻¹ in ethanol) from Morphisto (Offenbach, Germany). Nitrogen (≥99.8%) and argon (≥99.996%) gases were obtained from Linde GmbH (Pullach, Germany).

Plasma-Enhanced Chemical Vapor Deposition (PECVD): PECVD was performed on a jet-induced sliding discharge device ("DiscJet") at atmospheric pressure as described elsewhere.^[21,22] In brief, the precursor was introduced into the plasma source as an aerosol carried by N₂-gas. Argon was used as process gas and introduced into the plasma source through a separate inlet. Plasma was generated using generator HV-X20 and transformer HT-X1-34oil (Tantec A/S, Lunderskov, Denmark). Ar process gas and N₂ gas carrying the precursor were mixed at the high voltage electrode outlet, where the discharge generated a floating potential between the plasma source and the substrates placed below and caused plasma polymerization to occur directly on the substrate surface. Substrates were placed seamlessly next to each other and transversal to the coating direction with three buffer substrates on each side to prevent turbulences. The plasma source was moved across the substrates at 1 m min⁻¹ using an ISEL Gantry OverHead M20 portal system (Isel Germany AG, Eichenzell, Germany) with a varying number of coating runs.

Plasma polymerization of vegetable oils was performed with parameters that were previously found to be promising for surface hydrophobization.^[21] The plasma power was kept at 100 W, the substrate-source-distance at 3 mm and the argon process and nitrogen carrier gas

flow rates at 15 and 5 L min⁻¹ respectively. Only the number of coating runs was modified in order to identify the interactions of varying amounts of coating with different porous paper substrates. For reference measurements of mere plasma treatment on paper, the base parameters were kept at 100 W, 3 mm, and 1 run, while one parameter out of these was modified. The power was varied between 10 and 400 W, the distance between 1.5 and 6 mm and the number of treatment runs from 1 to 5.

Paper Making and Sample Preparation: To produce cotton linter laboratory handsheets, aqueous cotton linter dispersion (2.2 wt.%) was diluted to 0.16 wt.% and stirred for 30 min. Handsheets were formed from this dispersion in accordance with ISO 5269-2 on a Haage sheet-former BBS (Haage Anagramm Technologien GmbH, Preissenberg, Germany), followed by drying under reduced pressure (93 °C, 10 min) and determination of sheet grammage (100 g m⁻²) by bone-dried paper weight. Calendering was performed using a CA5/300 laboratory calender (Sumet Systems GmbH, Denklingen, Germany) equipped with two steel rolls at 0.5 m min⁻¹, at room temperature and under line pressures of 5, 50, and 300 N mm⁻¹. Glassine paper was used without further modification. Paper strips (70 × 20 mm) were glued onto microscope slides (75 × 25 mm) along the edges, leaving the central part of the samples untouched to enable measurements.

Absorption Time and Water Contact Angle (WCA) Measurement: Paper samples were stored under controlled climate conditions (23 °C, 50% RH) for at least 24 h before measurement. Both absorption time and water contact angles were measured by placing 2 µL droplets of ultrapure water on the substrate surface, using the sessile drop method on a Dataphysics OCA 35 device (Dataphysics, Filderstadt, Germany) and processed with Dataphysics SCA20 software. Static water contact angles were measured immediately after droplet deposition. Absorption time measurements and time-dependent WCA measurements were based on the recorded videos, wherein the frame rate was adapted to the absorption times (14 frames s⁻¹ for uncoated paper, 3.58 frames s⁻¹ for coated papers and 1 frame s⁻¹ for extracted papers). A total of at least 5, 18, or 3 absorption time measurements was performed on uncoated, coated, and extracted cotton linter papers, respectively. The number of WCA measurements on glassine paper is shown in the respective graphs. Significance levels (p-values) were determined through Tukey's test using R software.

Optical Profilometry: Surface roughness parameters were determined according to ISO 25 178 standard through optical profilometry using a PLu neox optical profilometer (Sensofar Metrology, Barcelona, Spain) equipped with a Nikon EPI 20x objective measuring across 850.08 × 709.35 µm² scan area in a 100 µm z-stack and at a resolution of 0.69 µm pixel⁻¹. Surface roughness parameters were determined after plane correction through SensoScan 6.7 software and averaged across five measurements (three for uncoated glassine paper).

Mercury Intrusion Porosimetry: Mercury intrusion porosimetry was performed on a Poremaster 60 GT (Quantachrome Instruments Inc., now Anton Paar, Graz, Austria) and evaluated using Poremaster for Windows 8.11 software. Measurements were performed based on ISO 15901-1:2026-04 standard.

Scanning Electron Microscopy (SEM): SEM samples were fixed onto conducting carbon tape and sputtercoated using a Cressington Turbo 208HR sputter coater (Cressington Scientific Instruments, Watford, UK) with a 10 nm layer of Pd/Pt (20/80). SEM images were recorded on a Philips XL 30 FEG high-resolution scanning electron microscope (SEMTECH Solutions, Inc., North Billerica, MA, USA) at beam voltage 5 kV, spot size 5, and 500x or 5000x magnification.

Confocal Laser Scanning Microscopy (CLSM): Paper samples intended for CLSM measurements were Soxhlet-extracted (acetone, 300 mL, 6 h) prior to use to remove any trace materials that might influence the staining behavior. Staining was performed in two steps after plasma polymer deposition. First, samples were stained with Calcofluor White (CFW) by immersion into aqueous CFW solution (100 µM, 15 min), removal of excessive staining agent through shaking in distilled water (15 min) and drying under reduced pressure (40 °C, 1.5 h). Second, samples were stained with Sudan III (S3) solution by immersion into ethanol (10 s) followed by immersion in ethanolic S3 solution (10 vol.% in ethanol, 5 min), removal of excess dye through shaking in ethanol (3 × 15 min) and drying under

reduced pressure (40 °C, 1.5 h). Uncoated reference paper was subjected to the same procedure.

To obtain cross sections, paper samples were cut using a razor blade from bottom to top and placed on a microscope slide with the cut side pointing toward the bottom and held by adhesive putty. Top view images were recorded by placing the samples between two coverslips. All measurements were performed in air.

CLSM images were recorded on a Leica TCS SP8 microscope (Leica Microsystems, Mannheim, Germany) using an HC PL APO CS2 20x / 0.75 DRY objective. The plane-to-plane distance in image stacks was 2 µm. CFW and S3 excitation and emission detection were performed in two separate channels, with excitation at 405 and 552 nm and emission detection at (424–496) and (561–681) nm, respectively. Measurements from the same dataset (cross-sections or top-view images) were taken with the same settings. ImageJ^{2[23]} software (Version 1.54b) was used for image processing and calculations. For cross-sections, maximum intensity images were generated from the 3D stacks and gray values were calculated therefrom in the indicated region of interest. For top view images, images and integrated intensities are based on sum slices of the entire stack.

Attenuated Total Reflectance-Fourier Transform Infrared (ATR-FTIR) Spectroscopy: ATR-FTIR measurements were performed on a Perkin Elmer Spectrum 3 FTIR spectrometer (Perkin Elmer, Waltham, MA, USA) directly on the paper substrate between 4000 and 650 cm⁻¹ using a resolution of 4 cm⁻¹ and 10 scans. Baseline correction was done using Spectrum software (Version 10.7.2). For easier comparison, spectra were normalized to minimum and maximum intensity.

Rheology: Viscosity measurements were performed on a MCR 302 rheometer (Anton Paar, Graz, Austria) between parallel plates of 50 mm diameter and at a measuring gap of 0.5 mm. The shear rate was increased linearly with 10 measuring points each being placed in the range between 1 and 100 s⁻¹ and from 100 to 21 000 s⁻¹. Directly afterward, the shear rate was reduced in identical gradual steps, so that finally 40 individual measurements per sample were recorded.

X-Ray Photoelectron Spectroscopy (XPS): XPS measurements were performed on a PHI 5500 Multi-Technique System (Perkin Elmer, Waltham MA, USA) with MgK α radiation at 1253 eV and a photoemission angle of 45° with a measured area of 1–2 mm. Spectra were analyzed using MultiPak V5.0A software. Origin 2022b software was used for deconvolution based on the data received by spectra analyses.

Supporting Information

Supporting Information is available from the Wiley Online Library or from the author.

Acknowledgements

The authors would like to thank Stefan Lupatsch (PTS, Heidenau) for mercury intrusion porosimetry and Jan Petersen (Fraunhofer IST, Braunschweig) for XPS measurements as well as Dennis Möck and Jörn Appelt (Thünen Institute for Wood Research, Hamburg) and Tobias Meckel (Technical University, Darmstadt) for fruitful discussions. Funding Statement This work was generated in the research project “BioPlas4Paper” and is funded by the Fachagentur Nachwachsende Rohstoffe e. V. (funding number: 2220HV017A-C).

Open access funding enabled and organized by Projekt DEAL.

Conflict of Interest

The authors declare no conflict of interest.

Author Contributions

A.L., M.Be., K.L., and A.G. were involved in investigation. A.L. was involved in conceptualization and writing—original draft. All authors were involved in writing—reviewing and editing. A.G. and M.Bi. were involved in supervision.

Data Availability Statement

The data that support the findings of this study are available from the corresponding author upon reasonable request.

Keywords

cellulose, CLSM, coating, paper, plasma-enhanced chemical vapor deposition (PECVD), vegetable oil

Received: June 6, 2024

Revised: August 16, 2024

Published online:

- [1] a) D. Klemm, B. Heublein, H.-P. Fink, A. Bohn, *Angew. Chem., Int. Ed.* **2005**, *44*, 3358; b) J. F. Łątka, A. Jasiołek, A. Karolak, P. Niewiadomski, P. Noszczyk, A. Klimek, S. Zielińska, S. Misiurka, D. Jezierska, J. *Build. Eng.* **2022**, *50*, 104135; c) B. Zaffora, L. Coisne, C. Gérard, *LWT* **2024**, *193*, 115767; d) D. Klemm, B. Philipp, T. Heinze, U. Heinze, W. Wagenknecht, *Comprehensive Cellulose Chemistry*, Wiley-VCH, Weinheim, Chichester **1998**.
- [2] a) M. A. Hubbe, *BioResources* **2007**, *2*, 106; b) (Ed.: H. Holik), *Handbook of Paper and Board*, Wiley-VCH, Weinheim **2013**; c) A. Kathuria, S. Zhang, *Front. Mater.* **2022**, *9*, 929501; d) M. Suhr, G. Klein, I. Kourti, M. R. Gonzalo, G. G. Santonja, S. Roudier, L. D. Sancho, *paper and board. Industrial emissions directive 2010/75/EU (integrated pollution prevention and control)*, Publications Office of the European Union, Luxembourg **2015**; e) S. Harrod, *The Future of Functional and Barrier Coatings for Paper and Board to 2026*, Smithers Information Ltd, Leatherhead, UK, **2021**.
- [3] P. Samyn, *J. Mater. Sci.* **2013**, *48*, 6455.
- [4] a) V. Rastogi, P. Samyn, *Coatings* **2015**, *5*, 887; b) A. Adibi, B. M. Trinh, T. H. Mekonnen, *Prog. Org. Coat.* **2023**, *181*, 107566; c) I. S. Bayer, *Adv. Mater. Interfaces* **2020**, *7*, 2000095.
- [5] a) B.-Y. Liu, C.-H. Xue, Q.-F. An, S.-T. Jia, M.-M. Xu, *Chem. Eng. J.* **2019**, *371*, 833; b) W. Zhang, P. Lu, L. Qian, H. Xiao, *Chem. Eng. J.* **2014**, *250*, 431; c) A. Geissler, F. Loyat, M. Biesalski, K. Zhang, *Cellulose* **2014**, *21*, 357; d) C. Cordt, A. Geissler, M. Biesalski, *Adv. Mater. Interfaces* **2021**, *8*, 2001265; e) C. Breuer, C. Cordt, B. Hiller, A. Geissler, M. Biesalski, *Adv. Mater. Interfaces* **2024**, *11*, 2301048.
- [6] A. Loesch-Zhang, C. Cordt, A. Geissler, M. Biesalski, *Polymers* **2022**, *14*, 1773.
- [7] Q. Shang, J. Chen, C. Liu, Y. Hu, L. Hu, X. Yang, Y. Zhou, *Prog. Org. Coat.* **2019**, *137*, 105346.
- [8] P. Samyn, G. Schoukens, D. Stanssens, L. Vonck, H. van den Abbeele, *Cellulose* **2013**, *20*, 2625.
- [9] X. Huang, A. Wang, X. Xu, H. Liu, S. Shang, *ACS Sustainable Chem. Eng.* **2017**, *5*, 1619.
- [10] A. Loesch-Zhang, T. Meckel, M. Biesalski, A. Geissler, *Coatings* **2024**, *14*, 364.
- [11] a) S. E. Alexandrov, M. L. Hitchman, *Chem. Vap. Depos.* **2005**, *11*, 457; b) J. Ibrahim, S. A. Al-Bataineh, A. Michelmor, J. D. Whittle, *Plasma Chem. Plasma Process.* **2021**, *41*, 47; c) D. Merche, N. Vandencastele, F. Reniers, *Thin Solid Films* **2012**, *520*, 4219; d) F. Massines, C. Sarra-Bournet, F. Fanelli, N. Naudé, N. Gherardi, *Plasma Process Polym.* **2012**, *9*, 1041.
- [12] a) A. Grüniger, P. Rudolf von Rohr, *Surf. Coat. Technol.* **2003**, *174*, 1043; b) T. Jinkarn, S. Thawornwiriyanan, D. Boonyawan, P. Rachtanapun, S. Sane, *Packag. Technol. Sci.* **2012**, *25*, 19; c) S. Vaswani, J. Koskinen, D. W. Hess, *Surf. Coat. Technol.* **2005**, *195*, 121; d) J. Profili, S. Asadollahi, P. Vinchon, A. Dorris, S. Beck, A. Sarkassian, L. Stafford, *Prog. Org. Coat.* **2020**, *147*, 105865.
- [13] V. Kumar, J. Pulpytel, H. Rauscher, I. Mannelli, F. Rossi, F. Arefi-Khonsari, *Plasma Process Polym.* **2010**, *7*, 926.
- [14] I. H. Tan, M. L. P. Da Silva, N. R. Demarquette, *J. Mater. Chem.* **2001**, *11*, 1019.
- [15] D. Liu, Y. Yin, D. Li, J. Niu, Z. Feng, *Thin Solid Films* **2009**, *517*, 3656.
- [16] A. Loesch-Zhang, A. Geissler, M. Biesalski, *Plasma Process Polym.* **2023**, *20*, 2300016.
- [17] a) A. Arkhangelskiy, A. Quaranta, A. Motta, Y. Yang, V. K. Yadavalli, D. Maniglio, *Adv. Mater. Interfaces* **2022**, *9*, 2200454; b) A. Arkhangelskiy, D. Maniglio, A. Bucciarelli, V. K. Yadavalli, A. Quaranta, *Adv. Mater. Interfaces* **2021**, *8*, 2100324.
- [18] L. Cabrales, N. Abidi, *Appl. Surf. Sci.* **2012**, *258*, 4636.
- [19] a) M.-C. Popescu, M. Totolin, C. M. Tibirna, A. Sdrobis, T. Stevanovic, C. Vasile, *Int. J. Biol. Macromol.* **2011**, *48*, 326; b) M. Totolin, C. Vasile, C. M. Tibirna, M.-C. Popescu, *Cell. Chem. Technol.* **2008**, *42*, 317.
- [20] Y. Ferreira da Silva, V. d. M. Queiroz, I. C. S. Kling, B. S. Archanjo, R. N. Oliveira, R. A. Simao, *Plasma Process Polym.* **2020**, *17*, 2000035.
- [21] M. Bellmann, A. Loesch-Zhang, D. M. J. Möck, J. Appelt, A. Geissler, W. Viöl, *Plasma Process Polym.* **2024**, *21*, 202300224.
- [22] W. Viöl, M. Bellmann, C. Ochs, M. Harms, WO 2017/157975 A1, **2017**.
- [23] C. T. Rueden, J. Schindelin, M. C. Hiner, B. E. DeZonia, A. E. Walter, E. T. Arena, K. W. Eliceiri, *BMC Bioinform.* **2017**, *18*, 529.
- [24] a) N. Abidi, E. Hequet, *J. Appl. Polym. Sci.* **2004**, *93*, 145; b) Y. Kusano, B. Madsen, L. Berglund, Y. Aitomäki, K. Oksman, *Surf. Eng.* **2018**, *34*, 825; c) G. Carlsson, G. Strom, G. Annergren, *Nord. Pulp Pap. Res. J.* **1995**, *10*, 17; d) H. Xiao, B. He, J. Li, *Holzforchung* **2015**, *69*, 1001.
- [25] C. M. G. Carlsson, G. Stroem, *Langmuir* **1991**, *7*, 2492.
- [26] L. C. Vander Wielen, M. Östenson, P. Gatenholm, A. J. Ragauskas, *Carbohydr. Polym.* **2006**, *65*, 179.
- [27] J. Vida, M. Shekargoftar, J. Sirviö, T. Homola Proceedings 11th International Conference on Nanomaterials - Research & Application (NANOCON 2019), Brno, Czech Republic **2020**, p. 257.
- [28] Q. Zhang, C. Liu, Z. Sun, X. Hu, Q. Shen, J. Wu, *Food Chem.* **2012**, *132*, 1607.
- [29] a) R. H. Whitehead, *Am. J. Physiol.* **1909**, *24*, 294; b) S. Bump, A. Böhm, L. Babel, S. Wendenburg, F. Carstens, S. Schabel, M. Biesalski, T. Meckel, *Cellulose* **2015**, *22*, 73.
- [30] S. Sapiuha, M. Verreault, J. E. Klemberg-Sapiuha, E. Sacher, M. R. Wertheimer, *Appl. Surf. Sci.* **1990**, *44*, 165.
- [31] M. N. Belgacem, G. Czeremuszkin, S. Sapiuha, A. Gandini, *Cellulose* **1995**, *2*, 145.
- [32] A. Sczostak, *Macromol. Symp.* **2009**, *280*, 45.
- [33] C. Gaiolas, A. P. Costa, M. S. Silva, W. Thielemans, M. E. Amaral, *Ind. Crops Prod.* **2013**, *43*, 114.
- [34] N. V. Bhat, D. J. Upadhyay, *J. Appl. Polym. Sci.* **2002**, *86*, 925.
- [35] a) S. Sapiuha, C. A. Ferguson, R. P. Beatson, M. R. Wertheimer, *Plasma Chem. Plasma Process.* **1989**, *9*, 225; b) H. T. Sahin, *Appl. Surf. Sci.* **2013**, *265*, 558.
- [36] a) R. Ayerza, *J. Am. Oil Chem. Soc.* **1995**, *72*, 1079; b) L. Velasco, J. M. Fernandez-Martinez, *Proceedings of the Vth International Safflower Conference*, Williston, North Dakota and Sidney, Montana, USA **2001**, pp. 133; c) (Eds.: R. Aparicio, J. Harwood), *Handbook of Olive Oil. Analysis and Properties*, Springer US, Boston, MA **2013**.
- [37] J. Mertens, J. Baneton, A. Ozkan, E. Pospisilova, B. Nysten, A. Delcorte, F. Reniers, *Thin Solid Films* **2019**, *671*, 64.
- [38] F. M. Silva, R. J. Pinto, A. M. Barros-Timmons, C. S. Freire, *Prog. Org. Coat.* **2023**, *178*, 107476.
- [39] P. T. Anastas, J. C. Warner, *Green chemistry: Theory and Practice*, Oxford University Press, New York **1998**.

6. Summary and outlook

In the strife for a more sustainable world, replacing fossil-based plastics with biobased materials is of utmost importance. In this context, paper shows a high potential to serve as substitute, since it is not only easily available and biocompatible, but additionally its recycling process is well established. However, the need to finish paper to make it durable against moisture leads to incorporation of non-sustainable components into this sustainable material. Therefore, innovative finishing strategies are required that are in line with the principles of green chemistry. Renewable materials should be selected as raw materials and the use of sometimes hazardous chemicals and complex derivatization reactions must be minimized. At the same time, it is essential that new processing methods become more energy and material efficient in order to reduce the amount of generated waste.

Penetration of moisture into paper can be prevented through durable, non-water-soluble coatings. Conventional hydrophobization strategies usually rely on sizing agents that adsorb or covalently attach to the fibers or form a crosslinked network, or on polymeric or inorganic coatings. Generally, the material is first applied to the paper and then crosslinked or attached to the fibers through an external stimulus such as light or heat. However, such approaches usually require multi-step reactions, derivatization or hazardous chemicals and mostly rely on non-renewable resources.

Thus, the aim of this work was to find simple, solvent- and derivatization-free processes for producing biobased paper coatings that are either crosslinked, covalently attached or both. Unsaturated vegetable oils were selected as raw materials due to their good availability from widespread resources, their intrinsically hydrophobic character and the presence of carbon-carbon double bonds that can take part in simple chemical reactions.

In a first step, a conventional approach for obtaining crosslinked coatings on paper was examined. Herein, a mixture of olive oil, or its main component oleic acid, and 1,8-octanedithiol was applied onto cotton linter laboratory handsheets through dip coating and crosslinked using UV light, making use of the thiol-ene click reaction. Oleic acid was used as simple model material to monitor crosslinking and optimize reaction conditions on glass slides. An irradiation dose of $20 \text{ J}\cdot\text{cm}^{-2}$ at 254 nm wavelength showed best double bond conversion. Using these parameters for crosslinking olive oil-dithiol coatings on paper, water contact angles up to 121° were obtained.

Secondly, an approach for covalently attaching vegetable oils to cotton linter paper substrates through thermal treatment at 70°C was evaluated. After four weeks, papers showed a water contact angle of 97° , which was further increased to 138° through Soxhlet extraction. The aging

process was extensively examined by comparison to storage at norm climate conditions and under argon atmosphere. Aging effects were attributed to a combination of oxidation and transesterification reactions, whereby the fatty acid chains were covalently attached to the paper substrate. The decisive influence of time and temperature was shown. A storage time of one week already proved to be sufficient for good hydrophobization and thus shows the potential for further acceleration of the aging process.

Plasma polymerization, or more precisely plasma-enhanced chemical vapor deposition, was selected as third approach for depositing covalently attached, highly crosslinked coatings. First, chia oil and tung oil, which have a similar degree of unsaturation but differ greatly in viscosity, were examined with respect to their ability to hydrophobize glass model substrates and in terms of their coating characteristics. Surface morphology and chemistry were shown to depend on the applied plasma power. Tung oil was found to be not at all suitable for hydrophobizing glass, but plasma polymerized chia oil increased the water contact angle of the initially highly hydrophilic glass substrate to $(86.0 \pm 7.9)^\circ$. Therefore, chia oil was used for further studies on the hydrophobization of paper, using cotton linter papers of different porosity as well as smooth glassine paper for reference. Here, water absorption was slowed down significantly, especially on the most porous paper and using a higher coating amount, but overall the coatings were rather inhomogeneous. After Soxhlet extraction, the best measurements showed that water absorption was retarded for more than five minutes with stable water contact angles of over 100° on all cotton linters substrates. Coating presence and covalent attachment were evidenced through various analytical and imaging methods. Finally, water contact angles of coatings from plasma polymerized chia oil were compared to those from safflower oil and olive oil deposited on glassine paper, ranging from $(83.6 \pm 11.3)^\circ$ through $(92.2 \pm 14.7)^\circ$ to $(101.0 \pm 7.3)^\circ$ respectively. Thus, although the plasma polymer coatings are not satisfactory in terms of homogeneity, their potential for paper hydrophobization is clearly evident.

While each of these methods is an interesting approach for producing water repellent coatings from vegetable oil, several shortcomings need to be considered. The first issue to be addressed concerning sustainable development is most certainly the use of food-grade oils within the frame of this work. With regard to olive oil, a replacement with qualities not intended for the food sector is conceivable, although the use of completely different vegetable oils that do not compete with human nutrition at all would be preferable. This is especially valid for the plasma polymerization approach, where the fundamental usability of different unsaturated oils has been proven, taking into account the limitation through viscosity. Additionally, hydrophobization through thermal curing promises versatility in the choice of vegetable oil or fatty acid, as it proceeds in large parts via an esterification reaction.

The thiol-ene reaction-induced photocuring of vegetable oils and thiols is an interesting strategy to forego the use of solvents and derivatives. However, the current approach certainly has shortcomings with respect to many other green chemistry principles, such as atom economy, where a more material-economic coating approach than dip coating or size press coating is imperative, or safer chemicals, amongst which the dithiol used herein cannot be counted. Although the use of natural thiols is thinkable, their odor remains an issue. Hence, investigation into other photocrosslinkable agents with good sensitivity towards alkene groups would be required. Nonetheless, this approach shows that in principle, hydrophobic crosslinked vegetable oil-based paper coatings can be achieved without solvents, photoinitiators or supplementary derivatization steps.

With respect to the approach based on thermal attachment, the dip coating method requiring rather large amounts of material, the subsequent Soxhlet extraction step, the energy needed for maintaining elevated temperatures and the long storage time are issues that need to be addressed. Dip-coating can relatively easily be replaced by more material-economic methods such as spray coating. Reducing the amount of coating material to a minimum might further render the extraction step obsolete. However, more extensive research is required to find optimal conditions under which the transesterification takes place faster and at lower temperatures. Here, transesterification might be accelerated for instance either by adapting the ambient humidity or by choosing an oil with higher acid number.

Finally, plasma polymerization also bears some hazards that are not yet fully understood and must be addressed in near future, such as the formation of radicals and ozone during plasma ignition. Additionally, oil particles are liberated during aerosol generation and the gas consumption of the current setup is rather high. Nonetheless, this is certainly the most material-economic approach, it generates only gas phase waste and the coating does not demand any chemical workup. A quantitative assessment of the overall energy consumption, comparing plasma polymerization to a conventional paper coating process, would additionally enable evaluation of the potential to improve energy efficiency. With respect to current results, issues with heterogeneity can be addressed through continuous optimization of the plasma source. The range of applicable plasma parameters should be explored to enhance coating properties, using Design of Experiments as a valuable addition for a better understanding the effects and interactions of individual parameters. Moreover, the use of pulsing in plasma polymer deposition is very promising for better structural retention of the precursor and maintaining discharge homogeneity and stability.

So far, none of the hydrophobization strategies suggested herein has been evaluated at industrial scale. While dip coating can likely be replaced by other coating techniques, scale-up

of the plasma polymerization process is more difficult. On the one hand, drag air is a challenge with respect to the high processing speeds of paper machines, and on the other hand, the dimensions of the plasma source used herein are far below the width of a paper roll. Thus, further development steps towards technology optimization are required.

Not only the production and usage, but also the end of life of a material needs to be considered when evaluating its sustainability. The biodegradability and recyclability of the obtained coatings have not yet been analyzed for any of the proposed solutions and thus remain open to investigation.

In summary, each of the coating approaches discussed above, the thiol-ene crosslinking method, the thermally induced covalent attachment and finally plasma polymerization, addresses some green chemistry principles while at the same time displaying some shortcomings in other respects, with the plasma polymerization approach likely being the most environmentally benign one. Only life cycle assessment, however, will allow to quantify these effects. Nonetheless, the potential of vegetable oils to hydrophobize paper with either crosslinked, covalently attached or crosslinked and attached coatings in a solvent-free manner is undisputable.

7. Zusammenfassung

Für die Schaffung einer nachhaltigeren Welt ist der Austausch aus fossilen Rohstoffen erzeugten Kunststoffes durch biobasierte Materialien von höchster Bedeutung. Papier besitzt in diesem Kontext aufgrund seiner guten Verfügbarkeit, Biokompatibilität und Rezyklierbarkeit erhebliches Potential als Substitut. Für einige Anwendungen muss jedoch die Beständigkeit des Papiers gegenüber Feuchtigkeit erhöht werden, was häufig zur Verwendung nicht nachhaltiger Additive oder Kompositmaterialien führt. Neuartige Strategien zur Veredelung von Papier, welche auf erneuerbaren Rohstoffen basieren und im Einklang mit den Prinzipien der Grünen Chemie stehen, stellen einen vielversprechenden und notwendigen Lösungsansatz für dieses Problem dar. Dazu gehören insbesondere Prozesse, die energieeffizient sind, unnötigen Abfall vermeiden und den Verbrauch von zusätzlichen sowie umwelt- oder gesundheitsschädlichen Chemikalien und Derivaten reduzieren.

Dauerhafte, wasserunlösliche Beschichtungen dienen dazu, das Eindringen von Feuchtigkeit in Papier zu verhindern. Konventionelle Hydrophobierungsstrategien basieren dabei üblicherweise entweder auf Leimungsmitteln, welche adsorbiert oder kovalent an die Fasern angebunden werden oder ein Netzwerk um die Fasern bilden, oder auf anorganischen beziehungsweise polymerbasierten Beschichtungsmaterialien. Häufig wird die Beschichtung erst auf das Papier aufgebracht und anschließend durch einen externen Stimulus, wie beispielsweise Licht oder Hitze, vernetzt oder an die Fasern angebunden. Diese Ansätze erfordern jedoch meist mehrstufige Reaktionen, Derivatisierungen oder schädliche Chemikalien und beruhen üblicherweise auf fossilen Rohstoffen.

Daher ist das Ziel dieser Arbeit, auf den Prinzipien der Grünen Chemie basierende Ansätze zur Herstellung vernetzter, kovalent angebundener oder kovalent angebundener vernetzter biobasierter Papierbeschichtungen zu finden. Die hierzu herangezogenen Prozesse sollen möglichst einfach sein, ohne Lösungsmittel auskommen und keine zusätzliche Derivatisierung der Naturstoffe erfordern. Als Ausgangsstoffe wurden aufgrund ihrer guten Verfügbarkeit und intrinsischen Hydrophobie ungesättigte Pflanzenöle gewählt. Weiterhin kann die darin vorhandene Kohlenstoff-Kohlenstoff-Doppelbindung leicht für chemische Reaktionen genutzt werden.

Zu Beginn wurde ein konventioneller Ansatz zum Erhalt vernetzter Papierbeschichtungen untersucht. Dazu wurde eine Mischung aus Olivenöl, oder seinem Hauptbestandteil Ölsäure, und 1,8-Oktandithiol auf Baumwollinterpapier mittels Tauchbeschichtung aufgebracht. Anschließend erfolgte die Vernetzung über eine durch UV-Belichtung induzierte Thiol-En Click-Reaktion. Ölsäure diente dabei als einfaches Modellmaterial, um den Vernetzungsprozess auf

Glassubstraten zu untersuchen und die Reaktionsbedingungen zu optimieren. Eine Belichtungs-dosis von $20 \text{ J}\cdot\text{cm}^{-2}$ bei einer Wellenlänge von 254 nm führte zum höchsten Umsatz an Doppelbindungen. Die so ermittelten Parameter wurden für die Vernetzung einer Olivenöl-Thiol-Beschichtung auf Papier genutzt, wodurch Wasserkontaktwinkel von bis zu 121° erreicht werden konnten.

Im zweiten Schritt wurde die kovalente Anbindung von Pflanzenölen an Baumwollinterpapiere durch thermische Behandlung bei 70°C untersucht. Nach vierwöchiger Inkubation wiesen die Papiere einen Wasserkontaktwinkel von 97° auf, welcher durch Soxhlet-Extraktion auf 138° gesteigert werden konnte. Der Alterungsprozess wurde genauer untersucht, indem die Lagerung bei 70°C mit der bei Normklima und unter Argon verglichen wurde. So konnte die Alterung auf ein Zusammenspiel aus Oxidations- und Umesterungsreaktionen zurückgeführt werden, auf welche Zeit und Temperatur einen entscheidenden Einfluss ausüben. Erste Versuche zeigten, dass bereits eine Lagerungszeit von einer Woche zur Hydrophobierung ausreichend ist und diese gegebenenfalls sogar weiter reduziert werden kann.

Schließlich wurde die Papierhydrophobierung mit Pflanzenölen durch plasmaunterstützte chemische Gasphasenabscheidung, auch bekannt als Plasmapolymersation, untersucht. Diese ermöglicht die Abscheidung hochvernetzter, kovalent an die Substratoberfläche angebundener Schichten. Chiaöl und Tungöl wurden als erste Ausgangsstoffe verwendet, da sie einen ähnlichen Sättigungsgrad besitzen, sich jedoch stark in ihrer Viskosität unterscheiden. Mithilfe von Glas als Modellsubstrat wurden sowohl die Eignung beider Öle zur Oberflächenhydrophobierung als auch die Eigenschaften der entstehenden Beschichtungen untersucht. Die Oberflächenmorphologie und -chemie der Schichten zeigten sich dabei abhängig von der eingestellten Plasmaleistung. Tungöl erwies sich als völlig ungeeignet zur Glashydrophobierung. Die Beschichtung mit plasmapolymersiertem Chiaöl hingegen erhöhte den Wasserkontaktwinkel der Glassubstrate auf bis zu $(86.0 \pm 7.9)^\circ$. Daher wurde zunächst nur Chiaöl für weitergehende Untersuchungen zur Papierhydrophobierung eingesetzt. Als Substrate wurden Baumwollinterpapiere verschiedener Porosität sowie Glassinepapier als vergleichsweise glattes Referenzsubstrat verwendet. Die Wasseraufnahmegeschwindigkeit dieser Papiere konnte durch die Plasmabeschichtung bedeutend verringert werden, vor allem auf dem Papier höchster Porosität und bei Abscheidung gesteigerter Beschichtungsmengen. Insgesamt wiesen die Beschichtungen jedoch eine starke Inhomogenität auf. Nach Soxhlet-Extraktion zeigten die besten Messwerte auf allen Baumwollintersubstraten eine Verzögerung der Wassertropfenaufnahme für mehr als fünf Minuten bei stabilen Wasserkontaktwinkeln über 100° . Das Vorhandensein der Beschichtung und ihre kovalente Anbindung wurden durch verschiedene chemisch-analytische und bildgebende Verfahren nachgewiesen. Schließlich

wurden Beschichtungen aus plasmapolymersiertem Chiaöl auf Glassinepapier mit solchen aus plasmapolymersiertem Distelöl und Olivenöl verglichen, wobei die Wasserkontaktwinkel von $(83.6 \pm 11.3)^\circ$ bei Verwendung von Chiaöl über $(92.2 \pm 14.7)^\circ$ für Distelöl bis hin zu $(101.0 \pm 7.3)^\circ$ bei Einsatz von Olivenöl reichten. Auch wenn die Homogenität der Plasmapolymerschichtungen noch nicht zufriedenstellend war, konnte die grundsätzliche Machbarkeit der Papierhydrophobierung durch plasmapolymersierte Pflanzenöle so zweifelsfrei nachgewiesen werden.

Obwohl jede dieser Methoden einen interessanten Ansatz zur Herstellung wasserabweisender Beschichtungen auf Basis von Pflanzenölen darstellt, sind einige Nachteile nicht von der Hand zu weisen. Das erste Problem im Hinblick auf Nachhaltigkeit ist zweifelsohne die Verwendung von Pflanzenölen in Lebensmittelqualität. Im Fall von Olivenöl ist hier der Einsatz einer nicht zum menschlichen Verzehr geeigneten Qualitätsstufe denkbar. Die Nutzung anderer Pflanzenöle, welche nicht in Konkurrenz zur menschlichen Nahrungsmittelproduktion stehen, wäre jedoch vorzuziehen. Das gilt insbesondere für den Einsatz dieser in der Plasmapolymersation, für welche die grundsätzliche Nutzbarkeit verschiedener ungesättigter Öle unter Berücksichtigung der Viskosität nachgewiesen wurde. Auch die Hydrophobierung mittels thermischer Anbindung ist unter Verwendung verschiedener Pflanzenöle oder Fettsäuren denkbar, da sie in großen Teilen auf einer Veresterungsreaktion basiert.

Auch wenn die Photovernetzung von Pflanzenölen und Thiolen unter Nutzung der Thiol-En-Reaktion eine interessante Strategie zum Verzicht auf Lösungsmittel und Derivatisierungsreaktionen darstellt, ist der Prozess in Bezug auf viele andere Prinzipien der Grünen Chemie problematisch. Dazu gehört beispielweise die Atomökonomie, welche eine weniger materialintensive Beschichtungsmethode als die Tauchbeschichtung oder die Leimpresse zwingend erforderlich macht, oder die Verwendung unbedenklicher Chemikalien, zu denen das hier verwendete Thiol nicht gezählt werden kann. Obwohl die Verwendung natürlicher Thiole denkbar wäre, bleibt das Problem des charakteristischen Thiol-Geruchs bestehen. Alternativ ist daher die Untersuchung anderer Photovernetzer in Erwägung zu ziehen. Nichtsdestotrotz zeigt dieser Ansatz, dass die Herstellung hydrophober vernetzter Papierbeschichtungen auf Pflanzenölbasis ohne die Verwendung von zusätzlichen Lösungsmitteln, Photoinitiatoren oder Derivatisierungsschritten möglich ist.

Im Hinblick auf die thermische Anbindungsmethode stellen der hohe Materialverbrauch der Tauchbeschichtung, die anschließende Soxhlet-Extraktion, die Energie, die für hohe Lagerungstemperaturen notwendig ist, sowie die langen Reaktionszeiten Probleme dar, die der Nachhaltigkeit des Prozesses entgegenstehen. Die Tauchbeschichtung könnte leicht durch materialsparende Methoden wie die Sprühbeschichtung ersetzt werden. Die Verringerung der

Beschichtungsmenge auf ein Minimum könnte gleichzeitig die abschließende Soxhlet-Extraktion überflüssig machen. Um effizientere Umesterungsbedingungen, beispielsweise hinsichtlich der Temperatur, zu identifizieren, sind weiterführende Untersuchungen erforderlich. In diesem Kontext könnten beispielsweise auch Änderungen der Umgebungsfeuchte sowie die Verwendung eines Öls mit höherer Säurezahl die Umesterung beschleunigen.

Schließlich beinhaltet auch die Plasmapolymersation einige noch nicht vollständig erforschte Risiken, wie die Bildung von Radikalen und Ozon während der Plasmaentladung. Weiterhin werden durch die Aerosolbildung Ölpartikel freigesetzt und der Gasverbrauch ist beim aktuellen Verfahren sehr hoch. Nichtsdestotrotz ist die Plasmapolymersation der Ansatz mit dem geringsten Materialverbrauch, es entstehen nur gasförmige Restprodukte und eine chemische Aufarbeitung der Beschichtung ist nicht nötig. Ein quantitativer Vergleich des Energiebedarfs der Plasmapolymersation im Vergleich zu einer konventionellen Papierbeschichtung könnte zusätzlich der Evaluierung von Möglichkeiten zur Energieeinsparung dienen. Die aktuell problematische Inhomogenität der Beschichtung kann durch kontinuierliche Verbesserung der Plasmaquelle beseitigt werden. Weiterhin ist die Vielfalt der möglichen Plasmaparameter zu variieren, um optimale Beschichtungseigenschaften zu erzielen. Hierbei wäre der Einsatz von statistischer Versuchsplanung vorteilhaft, da sie ein besseres Verständnis der Effekte und Wechselwirkungen der einzelnen Parameter ermöglichen würde. Zusätzlich ist die Plasmapulung ein weiterer vielversprechender Ansatz, um die Strukturretention des Präkursors sowie die Entladungshomogenität und -stabilität zu verbessern.

Für keinen der untersuchten Hydrophobierungsansätze wurden bisher Versuche im industriellen Maßstab durchgeführt. Während die Tauchbeschichtung voraussichtlich gut durch andere Beschichtungsmethoden ersetzt werden könnte, gestaltet sich das Hochskalieren der Plasmapolymersation schwieriger. Nicht nur sind die hohen Prozessgeschwindigkeiten der industriellen Papiermaschinen aufgrund des möglichen Einflusses von Schleppluft herausfordernd, auch die Dimension der bisher genutzten Plasmaquelle ist deutlich geringer als die übliche Breite einer Papierbahn, sodass weitere Entwicklungsschritte zur Technologieoptimierung erforderlich sind.

Neben seiner Herstellung darf in der Nachhaltigkeitsbetrachtung eines Materials natürlich auch das Ende seines Lebenszyklus nicht außer Acht gelassen werden. Die Bioabbaubarkeit und Recyklierbarkeit sind leider bisher für keine der hier vorgeschlagenen Beschichtungen untersucht worden. Ihre Ermittlung stellt einen weiteren unerlässlichen Baustein auf der Suche nach nachhaltigeren Papierbeschichtungen dar.

Zusammenfassend adressieren die drei in dieser Arbeit vorgestellten Ansätze zur Papierhydrophobierung (die Photovernetzung mittels Thiol-En-Chemie, die kovalente Anbindung durch thermische Behandlung und die Plasmapolymerisation) jeweils einige Prinzipien der Grünen Chemie, weisen aber auch Schwächen in anderen Bereichen auf. Die Plasmapolymerisation ist insgesamt als am vorteilhaftesten einzuschätzen. Schlussendlich kann hier jedoch nur eine umfassende Lebenszyklenanalyse eine verlässliche und quantitative Aussage treffen. Nichtsdestotrotz konnte das große Potential der Verwendung von Pflanzenölen zur lösungsmittelfreien Papierhydrophobierung durch Netzwerkbildung beziehungsweise kovalente Anbindung unbestreitbar belegt werden.

8. References

- [1] P. T. Anastas, J. C. Warner, *Green chemistry: Theory and Practice*, Oxford University Press, New York, **1998**.
- [2] H. Holik (Ed.) *Handbook of paper and board*, Wiley-VCH, Weinheim, **2013**.
- [3] D. Klemm, B. Philipp, T. Heinze, U. Heinze, W. Wagenknecht, *Comprehensive cellulose chemistry*, Wiley-VCH, Weinheim, Chichester, **1998**.
- [4] M. N. Belgacem, A. Gandini, *Compos. Interfaces* **2005**, *12*, 41.
- [5] DIE PAPIERINDUSTRIE, *Leistungsbericht PAPIER 2024*, Berlin, **2024**.
- [6] *Plastics - the fast Facts 2023*, Frankfurt am Main, **2023**.
- [7] S. Basak, M. S. Dangate, S. Samy, *Prog. Org. Coat.* **2024**, *186*, 107938.
- [8] B. Zaffora, L. Coisne, C. Gérard, *LWT* **2024**, *193*, 115767.
- [9] J. F. Łątka, A. Jasiołek, A. Karolak, P. Niewiadomski, P. Noszczyk, A. Klimek, S. Zielińska, S. Misiurka, D. Jezierska, *J. Build. Eng.* **2022**, *50*, 104135.
- [10] J. H. Bos, *Das Papierbuch. Handbuch der Papierherstellung*, ECA Pulp & Paper b.v, Houten, **2006**.
- [11] Papier.Aktuell. Pressedienst der deutschen Zellstoff- und Papierindustrie, *Energiepreise in Deutschland viel zu hoch, Verband warnt vor den einschneidenden Folgen*, Berlin, **2023**.
- [12] United Nations General Assembly, *Transforming our world: the 2030 Agenda for Sustainable Development. A/RES/70/1*, **2015**.
- [13] I. Francolini, L. Galantini, F. Rea, C. Di Cosimo, P. Di Cosimo, *Int. J. Mol. Sci.* **2023**, *24*, 9268.
- [14] a) L. M. Hillscher, V. J. Liebich, O. Avrutina, M. Biesalski, H. Kolmar, *Chemtexts* **2021**, *7*, 14; b) S. Das, Gagandeep, R. Bhatia, *Rev. Anal. Chem.* **2022**, *41*, 112.
- [15] a) E. Rezvani Ghomi, S. Khalili, S. Nouri Khorasani, R. Esmaeely Neisiany, S. Ramakrishna, *J. Appl. Polym. Sci.* **2019**, *136*, 47738; b) A. Haider, S. Haider, I.-K. Kang, A. Kumar, M. R. Kummara, T. Kamal, S. S. Han, *Int. J. Biol. Macromol.* **2018**, *108*, 455.
- [16] R. Sangl in *Taschenbuch der Papiertechnik* (Ed.: J. Blechschmidt), Hanser, München, **2013**.
- [17] a) Y. He, H. Li, X. Fei, L. Peng, *Carbohydr. Polym.* **2021**, *252*, 117156; b) N. Asim, M. Badiei, M. Mohammad, *Emergent Mater.* **2022**, *5*, 703.
- [18] G. Engelhardt, K. Granich, K. Ritter, *Das Leimen von Papier*, VEB Fachbuchverlag, Leipzig, **1972**.
- [19] J. Anderson in *Surface application of paper chemicals* (Eds.: J. Brander, I. Thorn), Blackie Academic & Professional, London, **1997**.

-
- [20] J. Laine, P. Stenius in *Papermaking science and technology* (Ed.: R. Alén), Finnish Paper Engineers' Association; Paperi ja puu, Helsinki, **2007**.
- [21] T. Lindström, P. T. Larsson, *Nord. Pulp Pap. Res. J.* **2008**, *23*, 202.
- [22] M. A. Hubbe, *BioResources* **2007**, *2*, 106.
- [23] E. Martorana, *Dissertation*, Technische Universität Dresden, Dresden, **2010**.
- [24] J. M. Gess, J. M. Rodríguez (Eds.) *The sizing of paper*, TAPPI Press, Atlanta, **2005**.
- [25] H. Zhang, D. Kannangara, M. Hilder, R. Ettl, W. Shen, *Colloids Surf. A: Physicochem. Eng. Asp.* **2007**, *297*, 203.
- [26] C. Quan, O. Werner, L. Wågberg, C. Turner, *J. Supercrit. Fluids* **2009**, *49*, 117.
- [27] R. Bourbonnais, R. H. Marchessault, *Biomacromolecules* **2010**, *11*, 989.
- [28] a) L. Candy, C. Vaca - Garcia, E. Borredon, *Eur. J. Lipid Sci. Technol.* **2005**, *107*, 3; b) J. Quesada, *Eur. J. Lipid Sci. Technol.* **2003**, *105*, 281; c) E. Lackinger, L. Schmid, J. Sartori, A. Isogai, A. Potthast, T. Rosenau, *Holzforschung* **2011**, *65*, 3.
- [29] A. Adibi, B. M. Trinh, T. H. Mekonnen, *Prog. Org. Coat.* **2023**, *181*, 107566.
- [30] R. Sangl, W. Auhorn, W. Kogler, M. Tietz in *Handbook of paper and board* (Ed.: H. Holik), Wiley-VCH, Weinheim, **2013**, pp. 745–784.
- [31] V. Rastogi, P. Samyn, *Coatings* **2015**, *5*, 887.
- [32] A. B. Lindstrom, M. J. Strynar, E. L. Libelo, *Environ. Sci. Technol.* **2011**, *45*, 7954.
- [33] M. Nau, N. Herzog, J. Schmidt, T. Meckel, A. Andrieu - Brunsen, M. Biesalski, *Adv. Mater. Interfaces* **2019**, *6*, 1900892.
- [34] Ç. Koşak Söz, S. Trosien, M. Biesalski, *ACS Appl. Mater. Interfaces* **2018**, *10*, 37478.
- [35] P. Samyn, *J. Mater. Sci.* **2013**, *48*, 6455.
- [36] N. Kaushal, A. K. Singh, *Int. J. Biol. Macromol.* **2023**, *246*, 125709.
- [37] a) A. G. Cunha, A. Gandini, *Cellulose* **2010**, *17*, 875; b) M. A. Hubbe, O. J. Rojas, L. A. Lucia, *BioResources* **2015**, *10*, 6095; c) M. Z. Islam, M. E. Sarker, M. M. Rahman, M. R. Islam, A. T. M. F. Ahmed, M. S. Mahmud, M. Syduzzaman, *J. Reinf. Plast. Compos.* **2022**, *41*, 526; d) Z. Jiang, T. Ngai, *Polymers* **2022**, *14*, 1533; e) S. Rodríguez-Fabià, J. Torstensen, L. Johansson, K. Syverud, *Cellulose* **2022**, *29*, 5375; f) Y. Habibi, *Chem. Soc. Rev.* **2014**, *43*, 1519; g) K. Missoum, M. N. Belgacem, J. Bras, *Materials* **2013**, *6*, 1745.
- [38] D. Roy, M. Semsarilar, J. T. Guthrie, S. Perrier, *Chem. Soc. Rev.* **2009**, *38*, 2046.
- [39] W. Shang, J. Huang, H. Luo, P. R. Chang, J. Feng, G. Xie, *Cellulose* **2013**, *20*, 179.
- [40] a) J. Peydecastaing, S. Girardeau, C. Vaca-Garcia, M. E. Borredon, *Cellulose* **2006**, *13*, 95; b) C. S. R. Freire, A. J. D. Silvestre, C. P. Neto, M. N. Belgacem, A. Gandini, *J. Appl. Polym. Sci.* **2006**, *100*, 1093; c) S. Boufi, M. N. Belgacem, *Cellulose* **2006**, *13*, 81; d) J. Bras, C. Vaca-Garcia, M.-E. Borredon, W. Glasser, *Cellulose* **2007**, *14*, 367.

-
- [41] a) T. H. Mekonnen, M. Misra, A. K. Mohanty in *Biocomposites : Woodhead Publishing Series in Composites Science and Engineering* (Eds.: M. Misra, J. K. Pandey, A. K. Mohanty), Woodhead Publishing, **2015**, pp. 201–235; b) K. Khwaldia, E. Arab - Tehrani, S. Desobry, *Comp. Rev. Food Sci. Food Saf.* **2010**, *9*, 82.
- [42] J.-W. Rhim, J.-H. Lee, S.-I. Hong, *Packag. Technol. Sci.* **2007**, *20*, 393.
- [43] S. Antonsson, G. Henriksson, M. Johansson, M. E. Lindström, *Ind. Crops Prod.* **2008**, *27*, 98.
- [44] Q. Hua, L.-Y. Liu, M. A. Karaaslan, S. Renneckar, *Front. Chem.* **2019**, *7*, 515.
- [45] E.-L. Hult, J. Ropponen, K. Poppius-Levlin, T. Ohra-Aho, T. Tamminen, *Ind. Crops Prod.* **2013**, *50*, 694.
- [46] N. Maximova, M. Österberg, J. Laine, P. Stenius, *Colloids Surf. A: Physicochem. Eng. Asp.* **2004**, *239*, 65.
- [47] R. Shorey, T. H. Mekonnen, *Int. J. Biol. Macromol.* **2022**, *209*, 472.
- [48] K. Khwaldia, A. H. Basta, H. Aloui, H. El-Saied, *Carbohydr. Polym.* **2014**, *99*, 508.
- [49] S.-Y. Lin, J. M. Krochta, *J. Food Sci.* **2003**, *68*, 229.
- [50] J. Han, S. Salmieri, C. Le Tien, M. Lacroix, *J. Agric. Food Chem.* **2010**, *58*, 3125.
- [51] C. Guillaume, J. Pinte, N. Gontard, E. Gastaldi, *Food Res. Int.* **2010**, *43*, 1395.
- [52] M. Gällstedt, A. Brottman, M. S. Hedenqvist, *Packag. Technol. Sci.* **2005**, *18*, 161.
- [53] a) H. J. Park, S. H. Kim, S. T. Lim, D. H. Shin, S. Y. Choi, K. T. Hwang, *J. Am. Oil Chem. Soc.* **2000**, *77*, 269; b) T. A. Trezza, P. J. Vergano, *J. Food Sci.* **1994**, *59*, 912.
- [54] F. Ham-Pichavant, G. Sèbe, P. Pardon, V. Coma, *Carbohydr. Polym.* **2005**, *61*, 259.
- [55] N. Bordenave, S. Grelier, V. Coma, *Biomacromolecules* **2010**, *11*, 88.
- [56] A. Geissler, F. Loyal, M. Biesalski, K. Zhang, *Cellulose* **2014**, *21*, 357.
- [57] C. Cordt, A. Geissler, M. Biesalski, *Adv. Mater. Interfaces* **2021**, *8*, 2001265.
- [58] C. Breuer, C. Cordt, B. Hiller, A. Geissler, M. Biesalski, *Adv. Mater. Interfaces* **2024**, *11*, 2301048.
- [59] D. Li, T. Iversen, M. Ek, *Holzforschung* **2015**, *69*, 721.
- [60] Q. Shang, J. Chen, C. Liu, Y. Hu, L. Hu, X. Yang, Y. Zhou, *Prog. Org. Coat.* **2019**, *137*, 105346.
- [61] W. Zhang, P. Lu, L. Qian, H. Xiao, *Chem. Eng. J.* **2014**, *250*, 431.
- [62] B.-Y. Liu, C.-H. Xue, Q.-F. An, S.-T. Jia, M.-M. Xu, *Chem. Eng. J.* **2019**, *371*, 833.
- [63] W. Zhang, H. Xiao, L. Qian, *Appl. Surf. Sci.* **2014**, *300*, 80.
- [64] R. d'Agostino, P. Favia, C. Oehr, M. R. Wertheimer, *Plasma Process. Polym.* **2005**, *2*, 7.
- [65] H. Biederman, *Plasma Polymer Films*, Imperial College Press, London, **2004**.
- [66] S. E. Alexandrov, M. L. Hitchman, *Chem. Vap. Depos.* **2005**, *11*, 457.

-
- [67] a) K. Jesch, J. E. Bloor, P. L. Kronick, *J. Polym. Sci. A Polym. Chem.* **1966**, *4*, 1487; b) J. Friedrich, *Plasma Process. Polym.* **2011**, *8*, 783.
- [68] a) D. Merche, N. Vandencastele, F. Reniers, *Thin Solid Films* **2012**, *520*, 4219; b) F. Fanelli, *Surf. Coat. Technol.* **2010**, *205*, 1536.
- [69] a) A. Arkhangelskiy, D. Maniglio, A. Bucciarelli, V. K. Yadavalli, A. Quaranta, *Adv. Mater. Interfaces* **2021**, *8*, 2100324; b) A. Arkhangelskiy, A. Quaranta, A. Motta, Y. Yang, V. K. Yadavalli, D. Maniglio, *Adv. Mater. Interfaces* **2022**, *9*, 2200454.
- [70] K. Johansson in *Woodhead Publishing series in textiles*, Vol. 62 (Ed.: R. Shishoo), CRC Press, Boca Raton, Fla., **2007**, pp. 247–281.
- [71] a) R. Barni, S. Zanini, D. Beretta, C. Riccardi, *Eur. Phys. J. Appl. Phys.* **2007**, *38*, 263; b) T. Desmet, R. Morent, N. de Geyter, C. Leys, E. Schacht, P. Dubruel, *Biomacromolecules* **2009**, *10*, 2351; c) H. T. Sahin, S. Manolache, R. A. Young, F. Denes, *Cellulose* **2002**, *9*, 171; d) K. Schröder, A. Meyer-Plath, D. Keller, W. Besch, G. Babucke, A. Ohl, *Contrib. Plasma Phys.* **2001**, *41*, 562.
- [72] F. S. Denes, Z. Q. Hua, E. Barrios, R. A. Young, J. Evans, *J. Macromol. Sci. A* **1995**, *32*, 1405.
- [73] U. Vohrer, I. Trick, J. Bernhardt, C. Oehr, H. Brunner, *Surf. Coat. Technol.* **2001**, *142-144*, 1069.
- [74] P.-Y. Cheng, J.-H. Tsai, J.-Z. Chen, *Cellulose* **2020**, *27*, 10293.
- [75] N. Raj, V. Breedveld, D. W. Hess, *Lab Chip* **2019**, *19*, 3337.
- [76] J. Vanneste, T. Ennaert, A. Vanhulsel, B. Sels, *ChemSusChem* **2017**, *10*, 14.
- [77] N. Abidi, E. Hequet, *J. Appl. Polym. Sci.* **2004**, *93*, 145.
- [78] a) H. Z. Jung, T. L. Ward, R. R. Benerito, *Text. Res. J.* **1977**, *47*, 217; b) T. L. Ward, H. Z. Jung, O. Hinojosa, R. R. Benerito, *Surf. Sci.* **1978**, *76*, 257.
- [79] K. Kolářová, V. Vosmanská, S. Rimpelová, V. Švorčík, *Cellulose* **2013**, *20*, 953.
- [80] S. Prabhu, K. Vaideki, S. Anitha, *Carbohydr. Polym.* **2017**, *156*, 34.
- [81] S. Inbakumar, R. Morent, N. de Geyter, T. Desmet, A. Anukaliani, P. Dubruel, C. Leys, *Cellulose* **2010**, *17*, 417.
- [82] A. D. Kramar, B. M. Obradović, A. Vesel, M. M. Kuraica, M. M. Kostić, *Cellulose* **2018**, *25*, 4199.
- [83] K. K. Wong, X. M. Tao, C. Yuen, K. W. Yeung, *Text. Res. J.* **1999**, *69*, 846.
- [84] E. Sinha, *J. Ind. Text.* **2009**, *38*, 317.
- [85] G. Carlsson, G. Strom, G. Annergren, *Nord. Pulp Pap. Res. J.* **1995**, *10*, 17.
- [86] L. C. Vander Wielen, M. Östenson, P. Gatenholm, A. J. Ragauskas, *Carbohydr. Polym.* **2006**, *65*, 179.

-
- [87] L. C. Vander Wielen, D. H. Page, A. J. Ragauskas, *Holzforschung* **2005**, *59*, 65.
- [88] C. M. Jardim, R. C. Oliveira, J. S. Hsieh, A. J. Ragauskas, T. Elder, *Tappi J.* **2015**, *14*, 585.
- [89] H. Xiao, B. He, J. Li, *Holzforschung* **2015**, *69*, 1001.
- [90] U. Henniges, S. Okubayashi, T. Rosenau, A. Potthast, *Biomacromolecules* **2012**, *13*, 4171.
- [91] M. Benoit, A. Rodrigues, Q. Zhang, E. Fourré, K. D. O. Vigier, J.-M. Tatibouët, F. Jérôme, *Angew. Chem. Int. Ed.* **2011**, *50*, 8964.
- [92] J. Delaux, C. Ortiz Mellet, C. Canaff, E. Fourré, C. Gaillard, A. Barakat, J. M. García Fernández, J.-M. Tatibouët, F. Jérôme, *Chem. Eur. J.* **2016**, *22*, 16522.
- [93] M. Benoit, A. Rodrigues, K. de Oliveira Vigier, E. Fourré, J. Barrault, J.-M. Tatibouët, F. Jérôme, *Green Chem.* **2012**, *14*, 2212.
- [94] J. Wu, F. Zeng, B. Chen, *Plasma Sci. Technol.* **2008**, *10*, 743.
- [95] a) J. Vida, M. Shekargoftar, J. Sirviö, T. Homola in *NANOCON Conference Proceedings*, **2020**, pp. 257–261; b) Y. Kusano, B. Madsen, L. Berglund, Y. Aitomäki, K. Oksman, *Surf. Eng.* **2018**, *34*, 825.
- [96] R. A. Pertile, F. K. Andrade, C. Alves, M. Gama, *Carbohydr. Polym.* **2010**, *82*, 692.
- [97] C. M. G. Carlsson, G. Stroem, *Langmuir* **1991**, *7*, 2492.
- [98] A. Vesel, M. Mozetic, A. Hladnik, J. Dolenc, J. Zule, S. Milosevic, N. Krstulovic, M. Klanjšek-Gunde, N. Hauptmann, *J. Phys. D: Appl. Phys.* **2007**, *40*, 3689.
- [99] L. Hecht, J. Philipp, K. Mattern, A. Dietzel, C.-P. Klages, *Microfluid. Nanofluidics* **2016**, *20*, 25.
- [100] M. Pykönen, H. Sundqvist, O.-V. Kaukonen, M. Tuominen, J. Lahti, P. Fardim, M. Toivakka, *Surf. Coat. Technol.* **2008**, *202*, 3777.
- [101] a) L. C. Vander Wielen, A. J. Ragauskas, *Eur. Pol. J.* **2004**, *40*, 477; b) P. Bataille, M. Dufourd, S. Sapiéha, *Polym. Int.* **1994**, *34*, 387; c) I. Sakata, D. A. I. Goring, *J. Appl. Polym. Sci.* **1976**, *20*, 573; d) Z. Song, J. Tang, J. Li, H. Xiao, *Carbohydr. Polym.* **2013**, *92*, 928; e) P. K. Panda, M. Jassal, A. K. Agrawal, *Plasma Chem. Plasma Process.* **2015**, *35*, 677.
- [102] C. Gaiolas, A. P. Costa, M. Nunes, M. J. S. Silva, M. N. Belgacem, *Plasma Process. Polym.* **2008**, *5*, 444.
- [103] a) S. Sousa, C. Gaiolas, A. P. Costa, C. Baptista, M. E. Amaral, *Cell. Chem. Technol.* **2016**, *50*, 711; b) M. Totolin, C. Vasile, C. M. Tibirna, M.-C. Popescu, *Cell. Chem. Technol.* **2008**, *42*, 317.
- [104] M.-C. Popescu, M. Totolin, C. M. Tibirna, A. Sdrobis, T. Stevanovic, C. Vasile, *Int. J. Biol. Macromol.* **2011**, *48*, 326.

-
- [105] C. Gaiolas, M. N. Belgacem, L. Silva, W. Thielemans, A. P. Costa, M. Nunes, M. J. S. Silva, *J. Colloid Interface Sci.* **2009**, *330*, 298.
- [106] L. Cabrales, N. Abidi, *Appl. Surf. Sci.* **2012**, *258*, 4636.
- [107] R. Liepins, J. Kearney, *J. Appl. Polym. Sci.* **1971**, *15*, 1307.
- [108] R. Liepins, H. Yasuda, *J. Appl. Polym. Sci.* **1971**, *15*, 2957.
- [109] D. Liu, Y. Yin, D. Li, J. Niu, Z. Feng, *Thin Solid Films* **2009**, *517*, 3656.
- [110] V. Kumar, J. Pulpytel, H. Rauscher, I. Mannelli, F. Rossi, F. Arefi-Khonsari, *Plasma Process. Polym.* **2010**, *7*, 926.
- [111] B. Balu, V. Breedveld, D. W. Hess, *Langmuir* **2008**, *24*, 4785.
- [112] P. Dimitrakellis, A. Travlos, V. P. Psycharis, E. Gogolides, *Plasma Process. Polym.* **2017**, *14*, 1600069.
- [113] S. M. Mukhopadhyay, P. Joshi, S. Datta, J. G. Zhao, P. France, *J. Phys. D: Appl. Phys.* **2002**, *35*, 1927.
- [114] a) R. Mahlberg, H.-M. Niemi, F. Denes, R. M. Rowell, *Int. J. Adhes. Adhes.* **1998**, *18*, 283; b) M. M. Hossain, S. Wu, A. Nasir, D. Mohotti, N. A. Robinson, Y. Yuan, E. Agyekum-Oduro, A. Akter, K. A. Bhuiyan, R. Ahmed et al., *Surf. Interfaces* **2022**, *35*, 102462; c) A. Grüniger, P. Rudolf von Rohr, *Surf. Coat. Technol.* **2003**, *174-175*, 1043.
- [115] a) G. Avramidis, E. Hauswald, A. Lyapin, H. Militz, W. Viöl, A. Wolkenhauer, *Wood Mater. Sci. Eng.* **2009**, *4*, 52; b) M. Odrášková, Z. Szalay, J. Ráhel', A. Zahoranová, M. Černák, H.-J. Hartfuss, M. Dudeck, J. Musielok, M. J. Sadowski, *AIP Conf. Proc.* **2008**, *993*, 391.
- [116] S. Sapiaha, C. A. Ferguson, R. P. Beatson, M. R. Wertheimer, *Plasma Chem. Plasma Process.* **1989**, *9*, 225.
- [117] S. Babaei, J. Profili, S. Asadollahi, A. Sarkassian, A. Dorris, S. Beck, L. Stafford, *Plasma Process. Polym.* **2020**, *17*, 2000091.
- [118] J. Profili, S. Babaei, M. Al Rashidi, A. Dorris, S. Asadollahi, A. Sarkissian, L. Stafford, *Coatings* **2023**, *13*, 924.
- [119] S. Babaei, J. Profili, M. Al Rashidi, A. Dorris, S. Beck, S. Asadollahi, A. Sarkissian, L. Stafford, *Cellulose* **2023**, *30*, 7889.
- [120] J. Profili, S. Asadollahi, P. Vinchon, A. Dorris, S. Beck, A. Sarkassian, L. Stafford, *Prog. Org. Coat.* **2020**, *147*, 105865.
- [121] I. H. Tan, M. L. P. Da Silva, N. R. Demarquette, *J. Mater. Chem.* **2001**, *11*, 1019.
- [122] H. T. Sahin, *Appl. Surf. Sci.* **2013**, *265*, 558.
- [123] A. Loesch-Zhang, M. Bellmann, K. Lachmann, M. Biesalski, A. Geissler, *Adv. Mater. Interfaces* **2024**, 2400507.

-
- [124] D. Fengel, G. Wegener, *Wood. Chemistry, ultrastructure, reactions*, Walter de Gruyter, Berlin, New York, **1989**.
- [125] D. Klemm, B. Heublein, H.-P. Fink, A. Bohn, *Angew. Chem. Int. Ed.* **2005**, *44*, 3358.
- [126] H. Staudinger, *Ber. Dtsch. Chem. Ges. A/B* **1920**, *53*, 1073.
- [127] D. P. Delmer, Y. Amor, *Plant Cell* **1995**, *7*, 987.
- [128] a) A. N. Heyn, *J. Ultrastruct. Res.* **1969**, *26*, 52; b) I. Ohad, I. O. Danon, S. Hestrin, *J. Cell Biol.* **1962**, *12*, 31; c) E. Schnepf, *Planta* **1965**, *67*, 213.
- [129] H. A. Krässig, *Cellulose. Structure, accessibility and reactivity*, Gordon and Breach, Amsterdam, **1993**.
- [130] H. Temming, *Temming-Linters: technische Informationen über Baumwollcellulose*, Peter Temming Aktiengesellschaft, Glückstadt, **1965**.
- [131] J. W. S. Hearle, *J. Polym. Sci.* **1958**, *28*, 432.
- [132] R. H. Atalla, D. L. Vanderhart, *Science* **1984**, *223*, 283.
- [133] a) J. Credou, T. Berthelot, *J. Mater. Chem. B* **2014**, *2*, 4767; b) A. Kulachenko in *Mechanics of paper products* (Eds.: S. Östlund, K. Niskanen), De Gruyter, Berlin, **2021**.
- [134] M. A. Hubbe, *BioResources* **2006**, *1*, 281.
- [135] U. Hirn, R. Schennach, *Sci. Rep.* **2015**, *5*, 10503.
- [136] A. Sczostak, *Macromol. Symp.* **2009**, *280*, 45.
- [137] a) K. Götze (Ed.) *Chemiefasern nach dem Viskoseverfahren*, Springer, Berlin, **1967**; b) M. L. Rollins, V. W. Tripp, *Text. Res. J.* **1954**, *24*, 345.
- [138] J. Blechschmidt in *Taschenbuch der Papiertechnik* (Ed.: J. Blechschmidt), Hanser, München, **2013**.
- [139] R. Alén in *Papermaking science and technology* (Ed.: R. Alén), Finnish Paper Engineers' Association; Paperi ja puu, Helsinki, **2007**.
- [140] H. Holik in *Taschenbuch der Papiertechnik* (Ed.: J. Blechschmidt), Hanser, München, **2013**.
- [141] International Organization for Standardization, *Pulps - Preparation of laboratory sheets for physical testing - Part 2: Rapid-Köthen method (ISO 5269-2:2004(E))*, **2004**, Geneva, Switzerland.
- [142] J. Grön, R. Rantanen in *Papermaking science and technology* (Ed.: E. Lehtinen), Fapet, Helsinki, **2000**.
- [143] S. Harrod, *The Future of Functional and Barrier Coatings for Paper and Board to 2026*, Smithers Information Ltd, Leatherhead, UK, **2021**.
- [144] X. Tang, X. Yan, *J. Sol-Gel Sci. Technol.* **2017**, *81*, 378.

-
- [145] J. J. Mikolei, L. Neuenfeld, S. Paech, M. Langhans, M. Biesalski, T. Meckel, A. Andrieu - Brunsen, *Adv. Mater. Interfaces* **2022**, 9, 2200064.
- [146] P. Svenka, E. Davydenko in *Taschenbuch der Papiertechnik* (Ed.: J. Blechschmidt), Hanser, München, **2013**.
- [147] F. Pudel, S. Wiesen, *Adv. Biochem. Eng./Biotechnol.* **2019**, 166, 69.
- [148] L. Roth, K. Kormann, *Ölpflanzen, Pflanzenöle. Fette, Wachse, Fettsäuren, Botanik, Inhaltsstoffe, Analytik*, ecomed, Landsberg, **2000**.
- [149] Z. W. Wicks in *Encyclopedia of chemical technology* (Eds.: R. E. Kirk, D. F. Othmer), Wiley, New York, Chichester, **2004**.
- [150] Foreign Agricultural Service/USDA, *Oilseeds: World Markets and Trade*, **2024**, can be found under <https://apps.fas.usda.gov/psdonline/circulars/oilseeds.pdf>.
- [151] S. Krist, *Lexikon der pflanzlichen Fette und Öle*, Springer, Vienna, **2013**.
- [152] R. Ayerza, *J. Am. Oil Chem. Soc.* **1995**, 72, 1079.
- [153] L. M. Khan, M. A. Hanna, *J. Agric. Eng. Res.* **1983**, 28, 495.
- [154] C. Lux, Z. Szalay, W. Beikircher, D. Kováčik, H. K. Pulker, *Holz Roh. Werkst.* **2013**, 71, 539.
- [155] a) J. Salge, *Surf. Coat. Technol.* **1996**, 80, 1; b) S. Meiners, J. Salge, E. Prinz, F. Förster, *Surf. Coat. Technol.* **1998**, 98, 1121.
- [156] a) S. Masuda, K. Akutsu, M. Kuroda, Y. Awatsu, Y. Shibuya, *IEEE Trans. on Ind. Applicat.* **1988**, 24, 223; b) V. I. Gibalov, G. J. Pietsch, *J. Phys. D: Appl. Phys.* **2000**, 33, 2618; c) J. Engemann, D. Korzec, *Thin Solid Films* **2003**, 442, 36.
- [157] M. Šimor, J. Ráhel', P. Vojtek, M. Černák, A. Brablec, *Appl. Phys. Lett.* **2002**, 81, 2716.
- [158] M. Odrášková, J. Ráhel', A. Zahoranová, R. Tiňo, M. Černák, *Plasma Chem. Plasma Process.* **2008**, 28, 203.
- [159] a) A.-M. Zhu, L.-H. Nie, Q.-H. Wu, X.-L. Zhang, X.-F. Yang, Y. Xu, C. Shi, *Chem. Vap. Depos.* **2007**, 13, 141; b) V. Stepanova, J. Kelar, O. Galmiz, M. Zemanek, P. Slavicek, A. Bucek, M. Cernak, *Contrib. Plasma Phys.* **2017**, 57, 182.
- [160] a) S. Förster, C. Mohr, W. Viöl, *Surf. Coat. Technol.* **2005**, 200, 827; b) H. Koinuma, H. Ohkubo, T. Hashimoto, K. Inomata, T. Shiraishi, A. Miyanaga, S. Hayashi, *Appl. Phys. Lett.* **1992**, 60, 816; c) M. Laroussi, X. Lu, *Appl. Phys. Lett.* **2005**, 87, 113902; d) M. Laroussi, T. Akan, *Plasma Process. Polym.* **2007**, 4, 777; e) C. Cheng, Z. Liye, R.-J. Zhan, *Surf. Coat. Technol.* **2006**, 200, 6659; f) O. V. Penkov, M. Khadem, W.-S. Lim, D.-E. Kim, *J. Coat. Technol. Res.* **2015**, 12, 225.
- [161] J. Winter, R. Brandenburg, K.-D. Weltmann, *Plasma Sources Sci. Technol.* **2015**, 24, 64001.

-
- [162] a) Q. Y. Nie, Z. Cao, C. S. Ren, D. Z. Wang, M. G. Kong, *New J. Phys.* **2009**, *11*, 115015;
b) K.-M. Chang, S.-H. Huang, C.-J. Wu, W.-L. Lin, W.-C. Chen, C.-W. Chi, J.-W. Lin, C.-C. Chang, *Thin Solid Films* **2011**, *519*, 5114.
- [163] A. Loesch - Zhang, A. Geissler, M. Biesalski, *Plasma Process. Polym.* **2023**, *20*, e2300016.
- [164] W. Viöl, M. Bellmann, C. Ochs, M. Harms, WO 2017/157975 AI, **2017**.
- [165] M. Bellmann, C. Ochs, M. Harms, W. Viöl, *Jahresmagazin Werkstofftechnik* **2019**, 60.
- [166] F. Massines, C. Sarra-Bournet, F. Fanelli, N. Naudé, N. Gherardi, *Plasma Process. Polym.* **2012**, *9*, 1041.
- [167] M. Bellmann, A. Loesch - Zhang, D. M. J. Möck, J. Appelt, A. Geissler, W. Viöl, *Plasma Process. Polym.* **2024**, *21*, e202300224.
- [168] a) F. I. Altuna, V. Pettarin, R. J. J. Williams, *Green Chem.* **2013**, *15*, 3360; b) G. Wuzella, A. R. Mahendran, U. Müller, A. Kandelbauer, A. Teischinger, *J. Polym. Environ.* **2012**, *20*, 1063.
- [169] a) K. Bouaziz, M. Ayadi, N. Allouche, A. Chemtob, *Eur. J. Lipid Sci. Technol.* **2017**, *119*, 1700003; b) J. Samuelsson, M. Jonsson, T. Brinck, M. Johansson, *J. Polym. Sci. A Polym. Chem.* **2004**, *42*, 6346.
- [170] Y. H. Zhao, D. Vuluga, L. Lecamp, F. Burel, *Prog. Org. Coat.* **2016**, *101*, 216.
- [171] K. Bandara, C. Ekanayake, T. K. Saha, P. K. Annamalai, *IEEE Trans. Dielect. Electr. Insul.* **2016**, *23*, 246.
- [172] a) K. J. Rapp, C. P. McShane, J. Luksich in *2005 IEEE International Conference on Dielectric Liquids. ICDL 2005*, Coimbra, Portugal, **2005**, pp. 387–390; b) L. Yang, R. Liao, S. Caixin, M. Zhu, *IEEE Trans. Dielect. Electr. Insul.* **2011**, *18*, 692.
- [173] T. A. Dankovich, Y.-L. Hsieh, *Cellulose* **2007**, *14*, 469.
- [174] a) C.-A. Teacă, D. Roşu, F. Mustaţă, T. Rusu, L. Roşu, I. Roşca, C.-D. Varganici, *BioResources* **2019**, *14*, 4873; b) M. Humar, B. Lesar, *Int. Biodeterior. Biodegrad.* **2013**, *85*, 223.
- [175] J. Mertens, J. Baneton, A. Ozkan, E. Pospisilova, B. Nysten, A. Delcorte, F. Reniers, *Thin Solid Films* **2019**, *671*, 64.



9. Appendix

List of abbreviations

1,8-ODT	1,8-Octanedithiol
AFM	Atomic Force Microscopy
AKD	Alkyl Ketene Dimer
APPJ	Atmospheric Pressure Plasma Jet
ASA	Alkenyl Succinic Anhydride
ATR-FTIR	Attenuated Total Reflectance-Fourier Transform Infrared
CL	Cotton Linters
CLSM	Confocal Laser Scanning Microscopy
CSE	Cellulose Stearoyl Ester
DBD	Dielectric Barrier Discharge
DCSBD	Diffuse Coplanar Surface Barrier Discharge
DSC	Differential Scanning Calorimetry
EGDS	Ethylene Glycol Distearate
FTIR	Fourier Transform Infrared
GC-MS/FID	Gas Chromatography-Mass Spectrometry/Flame Ionization Detector
HMDSO	Hexamethyldisiloxane
NMR	Nuclear Magnetic Resonance
PECVD	Plasma-Enhanced Chemical Vapor Deposition
PP	plasma-polymerized
SEM	Scanning Electron Microscopy
T_g	Glass Temperature
UV	Ultraviolet
WCA	Water Contact Angle
XPS	X-Ray Photoelectron Spectroscopy

Declarations – Erklärungen

Erklärungen laut Promotionsordnung

§8 Abs. 1 lit. c der Promotionsordnung der TU Darmstadt

Ich versichere hiermit, dass die elektronische Version meiner Dissertation mit der schriftlichen Version übereinstimmt und für die Durchführung des Promotionsverfahrens vorliegt.

§8 Abs. 1 lit. d der Promotionsordnung der TU Darmstadt

Ich versichere hiermit, dass zu einem vorherigen Zeitpunkt noch keine Promotion versucht wurde und zu keinem früheren Zeitpunkt an einer in- oder ausländischen Hochschule eingereicht wurde. In diesem Fall sind nähere Angaben über Zeitpunkt, Hochschule, Dissertationsthema und Ergebnis dieses Versuchs mitzuteilen.

§9 Abs. 1 der Promotionsordnung der TU Darmstadt

Ich versichere hiermit, dass die vorliegende Dissertation selbstständig und nur unter Verwendung der angegebenen Quellen verfasst wurde.

§9 Abs. 2 der Promotionsordnung der TU Darmstadt

Die Arbeit hat bisher noch nicht zu Prüfungszwecken gedient.

Darmstadt, den 09.09.2024

Amelia Lösch-Zhang

Erklärung zum Eigenanteil an den Veröffentlichungen

Im Folgenden ist aufgelistet, mit welchem Anteil ich an den Veröffentlichungen beteiligt war.

Mein Anteil an der folgenden Veröffentlichung beträgt 90%:

A. Loesch-Zhang, C. Cordt, A. Geissler, M. Biesalski, **A Solvent-Free Approach to Crosslinked Hydrophobic Polymeric Coatings on Paper Using Vegetable Oil**, *Polymers* **2022**, *14*, 1773.

Mein Anteil an der folgenden Veröffentlichung beträgt 90%:

A. Loesch-Zhang, T. Meckel, M. Biesalski, A. Geissler, **Enhancing Hydrophobic Properties in Olive Oil-Coated Papers through Thermal Treatment**, *Coatings* **2024**, *14*, 364.

Mein Anteil an der folgenden Veröffentlichung beträgt 45% (geteilte Erstautorenschaft):

M. Bellmann, A. Loesch-Zhang, D. M. J. Möck, J. Appelt, A. Geissler, W. Viöl, **Hydrophobic glass and paper coatings based on plasma-polymerized vegetable oils using a novel atmospheric pressure plasma concept**, *Plasma Process. Polym.* **2024**, *21*, e2300224.

Mein Anteil an der folgenden Veröffentlichung beträgt 85%:

A. Loesch-Zhang, M. Bellmann, K. Lachmann, M. Biesalski, A. Geissler, **Plasma Polymerization of Vegetable Oils onto Paper Substrates of Varying Porosity for Improved Hydrophobicity**, *Adv. Mater. Interfaces* **2024**, 2400507.

Mein Anteil an der folgenden Veröffentlichung beträgt 95%:

A. Loesch-Zhang, A. Geissler, M. Biesalski, **Plasma polymerization of biogenic precursors**, *Plasma Process. Polym.* **2023**, *20*, e2300016.

Darmstadt, den 09.09.2024

Amelia Lösch-Zhang

Erklärung zur Begutachtung der Veröffentlichungen

Prof. Dr. Markus Biesalski

Referent

Prof. Dr. Annette Andrieu-Brunsen

05.09.2024

Co-Referentin

Datum

Weder Referent (Prof. Dr. Markus Biesalski) noch Co-Referentin (Prof. Dr. Annette Andrieu-Brunsen) der vorliegenden kumulativen Doktorarbeit waren an der Begutachtung nachstehender Veröffentlichungen beteiligt:

- (1) A. Loesch-Zhang, C. Cordt, A. Geissler, M. Biesalski, **A Solvent-Free Approach to Crosslinked Hydrophobic Polymeric Coatings on Paper Using Vegetable Oil**, *Polymers* **2022**, *14*, 1773.
DOI: 10.3390/polym14091773
- (2) A. Loesch-Zhang, T. Meckel, M. Biesalski, A. Geissler, **Enhancing Hydrophobic Properties in Olive Oil-Coated Papers through Thermal Treatment**, *Coatings* **2024**, *14*, 364.
DOI: 10.3390/coatings14030364
- (3) M. Bellmann, A. Loesch-Zhang, D. M. J. Möck, J. Appelt, A. Geissler, W. Viöl, **Hydrophobic glass and paper coatings based on plasma-polymerized vegetable oils using a novel atmospheric pressure plasma concept**, *Plasma Process. Polym.* **2024**, *21*, e2300224.
DOI: 10.1002/ppap.202300224
- (4) A. Loesch-Zhang, M. Bellmann, K. Lachmann, M. Biesalski, A. Geissler, **Plasma Polymerization of Vegetable Oils onto Paper Substrates of Varying Porosity for Improved Hydrophobicity**, *Adv. Mater. Interfaces* **2024**, 2400507.
DOI: 10.1002/admi.202400507
- (5) A. Loesch-Zhang, A. Geissler, M. Biesalski, **Plasma polymerization of biogenic precursors**, *Plasma Process. Polym.* **2023**, *20*, e2300016.
DOI: 10.1002/ppap.202300016

Datum: 05.09.2024

Referent
(Prof. Dr. Markus Biesalski)

Co-Referentin
(Prof. Dr. Annette Andrieu-Brunsen)